"BUBBLES IN A GAS FLUIDISED BED"

BY

WAHAB MOJTAHEDI

B.Sc., M.Sc.

Thesis presented for the Degree of Doctor of Philosophy

University of Edinburgh

December, 1983.

TO ANITA

for her patience and understanding

ACKNOWLEDGEMENTS

The author would like to express his gratitude to the following people who have contributed to the successful completion of this manuscript:

1. Dr. D. H. Glass, for his advice, encouragement and help at all times during the course of the work.

2. Dr. C. Theobald of the Department of Statistics for his help with the statistical analysis of the experimental data.

3. Dr. R. Mackie of the Wolfson Microelectronics Research Institute for invaluable help in setting up the Bubble Flow Monitor.

4. Mr. D. Ketchin and his workshop staff for their assistance in the construction of experimental equipment.

5. Mrs. M. Donaldson for typing the present manuscript.

ABSTRACT

The compound fibre-optic probe technique developed for use in gas-liquid systems has been modified for use in a freely-bubbling three-dimensional gas-fluidised bed. Statistics relating to bubble properties such as rise velocity, size and frequency distributions have been measured at various superficial gas flowrates and positions within the bed.

Two different gas distributor plates, one made from sintered metal and one a simple perforated plate, were used and results compared under identical fluidising conditions.

Under the usual experimental conditions the sampling system collected only a small proportion of the bubbles encountered but, in some experiments, an alternative mode of operation was employed to give a much more accurate estimate of bubble frequency.

Part of the work was devoted to an investigation of the effect on the above parameters of a solid obstacle in the form of a horizontal tube-bundle immersed in the bed. Results were compared under identical operating conditions in the presence and the absence of the tube-bundle.

In the course of this investigation, more extensive information has been gained as to the size distributions, rising velocities and spatial distributions of bubbles in fluidised beds and also their interactions with immersed solid obstacles.

TABLE OF CONTENTS

CHAPTER 1

Introduction

Fluidisation is defined (61) as the operation by which fine solids are transformed into a fluid-like state through contact with a gas or a liquid. Pass a fluid upward through a bed of fine particles, at a low flow rate, fluid merely percolates through the void spaces between stationary particles. With an increase in flow rate, particles move apart and a few are seen to vibrate and move about in restricted regions.

At a still higher velocity, a point is reached when the particles are all just suspended in the upward flowing gas or liquid. At this point the frictional forces between a particle and fluid counterbalance the weight of the particle, the vertical component of the compressive force between adjacent particles disappears and the pressure drop through any section of the bed about equals the weight of the fluid and particles in that section per unit area. Bed is said to be incipiently fluidised. If the flow rate is increased above the minimum required to produce a fluidised bed, one of two things will occur. Either the bed will continue to expand, so that the average distance between the particles will become greater or the excess fluid will pass through the bed in the form of bubbles, giving rise essentially to a two-phase system. These two types are referred to as "particulate" and "aggregative". In general, particulate fluidisation occurs with liquid-solid systems (with gas-solid systems when particles are very fine, and then over a very limited range of velocities).

Aggregative fluidisation occurs with all other gas-solid systems, and sometimes with liquid-solid systems when solids are of high density. At very high velocities the particles will be transported from the system in the fluid stream.

Fluidisation has proved uniquely attractive during the past four decades. Although the history of the development of fluidised solid technology and its industrial application goes back to pre-war years, the use of fluidised beds in large-scale industrial operations dates from the closing years of the second world war. At this time large quantities of naptha were cracked to gasoline using the Fluid Bed Catalytic Process, in order to meet the demand for aviation spirit. Fluidised beds have gained prominence in many process industries (including chemicals, petroleum, metallurgy, food and pharmaceuticals) as a means of bringing particulate solids into contact with gases and/or liquids. Many fluidised bed operations are physical in nature (e.g. drying, coating and granulation). Other operations involve chemical reactions including the aforementioned catalytic cracking of hydrocarbons, the manufacture of phthalic anhydride, the roasting of metallurgical ores and regeneration of spent catalysts.

In recent years fluidised beds have been of special interest because of their potential as the central component in new processes for utilising coal as a source of energy notably in coal combustion and gassification processes.

The fluidised bed offers a number of advantages over most other methods of cont acting solids and fluids, in particular high rates of heat transfer, temperature uniformity and solids mobility. In fact one of the main reasons for the ever increasing application of fluidisation in industrial processes is this high rate of heat and mass transfer obtainable in fluidised systems. The burning of coal

in fluidised beds is one example of a relatively efficient method of generation of heat. It is believed that the good mixing characteristic of a fluidised bed is the main reason why the heat transfer coefficient may be many times higher than in an equivalent packed bed.

Practical applications have diversified the academic research on fluidisation in recent years. Heat and mass transfer properties of gas fluidised beds as well as the performance of fluid bed catalytic reactors are largely determined by the bubble characteristics, e.g. in the case of a catalytic reaction the bypass of gas in the bubble phase limits the yield of reaction and in the case of bed-to-wall heat transfer the local bubble size and frequency governs the surface renewal process at the heat transfer surface.

Hence bubble characteristics, the bubble flow pattern and coalescence have received much attention among researchers. Despite much research, there are still a number of questions to be answered in these areas.

Combustion and gas ification are at the centre of many investigations today. One of the most effective mechanisms of heat removal from a fluidised bed is the use of tube arrays immersed in the bed.

Several years of research in this department led to the development of a probe technique for the simultaneous measurement of bubble velocity, shape and size, and its distribution in fluidised beds. The present work was undertaken to extend such a technique to the measurement of bubble properties in a three-dimensional, freely-bubbling gas fluidised bed.

Solid obstacles, in the form of a tube-bank were immersed in the bed to investigate the effect of the presence of a tube-bank on the said bubble characteristics and the dynamics of a gas fluidised bed.

Finally, the bubble characteristics in turn are influenced by the design of the gas distributor. A multiorifice distributor was designed to study the bubbling behaviour and flow pattern of the bubble phase for a stream of bubbles rising from such a distributor, as well as a porosint plate distributor, with the view to investigating the influence of the distributor design on the said bubble characteristics.

CHAPTER 2

Survey of the Literature

2.1 Bubble Rise Velocity

2.1.1 Bubble Rise Velocity in Isolation

Dumitrescu (26) theoretically derived the expression:

$$U_b = 0.35\ g^{\frac{1}{2}}\ D^{\frac{1}{2}} \qquad (2.1)$$

for the velocity of a large 3-D bubble (bubble diameter almost equal to tube diameter) rising in isolation in a liquid of small viscosity. Later Davies and Taylor (24) gave similar results with a slightly different value of the empirical constant. But Davies and Taylor's work was for bubbles small compared with the apparatus dimensions.

For a bubble rising in a large volume of liquid where the width of the bubble is small compared to the vessel diameter, Rippin (89) gave the equation:

$$U_b = 0.914\ (g\ D_e)^{\frac{1}{2}} \qquad (2.2)$$

where D_e is the diameter of sphere that has the same volume as the bubble. Davies and Taylor (24) from their experimental observations found that bubble rise velocity can be approximated by

$$U_b = 0.71\ (g\ D_e)^{\frac{1}{2}} \qquad (2.3)$$

Davidson et al (22) in 3-D beds of small diameter and later Harrison and Leung (53) in a bed of bigger diameter measured bubble rise velocity. Bubbles of different volumes were injected near the bottom of the bed, which was kept at or near incipient fluidisation condition. By measuring the time taken by bubbles to reach the surface of the bed they gave the following expression for the bubble rise velocity

$$U_b = k_b\ g^{\frac{1}{2}}\ V_b^{\ 1/6} \qquad (2.4)$$

Applying the wall correction factor 'm' of Uno and Kintner (109) they obtained the value of the numerical coefficient k_b for a bubble rising in an infinite medium to be equal to 0.71. Hence the equation becomes

$$U_{b\infty} = 0.71\ g^{\frac{1}{2}}\ V_b^{1/6} \qquad (2.5)$$

Many authors have measured bubble rise velocity in isolation in both 2-D and 3-D beds. Table (2.1) summarises such data for 3-D beds only. It is seen from table 2.1 that the value of coefficient lies close to 0.71 in the range 0.66 to 0.74. Davidson and Harrison (21) have suggested that the difference between the predictions of equations (2.3) and (2.5) is insignificant and applied equation (2.3) to fluidised beds. Most authors (Leva and Wen (63), Potter (83)) have adopted equation (2.3) to calculate bubble rise velocity in fluidised beds.

Observations suggest that velocity of a bubble does not remain constant as predicted by these equations. Rowe and Partridge (97), Rowe and Matsuno (94), Chiba et al (11) report that there is considerable fluctuation in the velocity of an individual bubble. The variation is supposedly a result of shedding of particles from the wake. Rowe and Partridge (97) Row and Matsuno (94) indicate that the wake of a bubble appears to be continuously fed by a boundary layer of particles and periodic shedding maintains an average size.

TABLE 2.1

SUMMARY OF THE DATA ON BUBBLE VELOCITY IN ISOLATION IN THREE-DIMENSIONAL BEDS

C : Bed of circular cross-section
S Bed of square cross-section
R Bed of rectangular cross-section

d: particle diameter
GS: Glass spheres
S: Sand ac: alumina catalyst
c: coke
ss: swede seeds

AUTHORS		BED SIZE cm	PARTICLE SIZE	MEASURING TECHNIQUE	GIVEN RELATION
Davidson et al* (22)	C S	7.6 15.2	d_{GS} = 150μ d_S = 400μ d_{ss} = 170μ	Capacitance probe	$U_{b\infty} = 0.79\, g^{\frac{1}{2}} V_b^{\frac{1}{6}}$
Harrison & Leung* (53)	S	61.0	S,60-150 B.S. Mesh.	Capacitance probe	$U_{b\infty} = 0.71^{\frac{1}{2}} V_b^{\frac{1}{6}}$
Rowe & Partridge (95)	C	14.0	d_{GS} = 50μ	Dissection of the bed	$U_b = 0.67\, g^{\frac{1}{2}} D_e^{\frac{1}{2}}$
Toei et al* (106)	C S	7.6 10.0	GS,80-100# GS,16- 24# S,80-120# S,35- 48# PVC,80-100#	X-ray Photography and Capacitance probe	$U_{b\infty} = 0.74\, g^{\frac{1}{2}} V_b^{\frac{1}{6}}$
Park et al+ (79)	C	10.0	d_c = 344μ d_c = 154μ d_c = 86μ	Electro-resistivity probe	$U_{b\infty} = 0.706\, g^{\frac{1}{2}} V_b^{\frac{1}{6}}$
Rowe & Matsuno (94)	R	29.5x14.4	d_{GS},300-400μ	X-ray Photography	$U_b = 0.717\, g^{\frac{1}{2}} V_b^{\frac{1}{5.76}}$
Donsi et al (25)	C	35.0	d_{ac},170-350μ	Photography	$U_b = 0.77\, (gD_b/2)^{\frac{1}{2}}$

* These authors used wall correction factor 'm' from Uno and Kintner (109) to calculate $U_{b\infty}$.

\+ Measured bubble rise velocity in a freely bubbling bed and determined the value of the coefficient k_b using $U_b - (U - U_{mf}) = U_{b\infty}$.

2.1.2 Bubble Rise Velocity in Freely Bubbling Beds

In a case where bubbles are continuously generated at a gas distributor the velocity of each bubble is greater than the velocity with which a bubble of the same size would rise in isolation. Nicklin (76) was first to study such a case theoretically and experimentally for slugs in a gas-liquid system. He gave the following relation for bubbles rising in a swarm

$$U_a = U_{b\infty} + G_b/A \qquad (2.6)$$

where G_b is the gas flow rate. If the postulate (Toomey and Johnstone (108)) that the additional gas flow above the amount required for incipient fluidisation forms bubbles in a bed, the above equation could be used for bubbles rising in freely bubbling fluidised beds. Davidson and Harrison (21) and Orcutt, Davidson and Pigford (78) applied the above equation to a fluidised bed. Equation (2.1) could be rewritten for fluidised bed as follows:

$$U_a = U_{b\infty} + (U - U_{mf}) \qquad (2.7)$$

Several workers have measured bubble rise velocity in freely bubbling three-dimensional fluidised beds. Observations were made either by submerging probes in the bed (Yasui and Johanson (125), Kobayashi et al (59), Whitehead and Young (120), Park, Kang, Capes and Osberg and Kobayashi (59), Chiba et al (11), Burgess and Calderbank (6), Pereira (81)), or by taking photographs of bubbles visible at the wall of the bed (Godard and Richardson (41). These observations show that bubbles do travel faster in bubbling fluidised beds than in isolation.

Results of only one author (Kobayashi, Arai and Chiba (59)) show the opposite effect. The reason is that slugging conditions prevailed in this system.

In most cases it is difficult to make a quantitative comparison of the experimental data with equation (2.7). Godard and Richardson (41) and Chiba et al (11) fitted their data to an equation of the type $U_b = K_b (g D_b)^{\frac{1}{2}}$. Yasui and Johanson (125) reported bubble rise velocity as a function of height above the distributor. Whitehead and Young (120) plotted their results in the form of bubble rise velocity as a function of gas flow rate. However Park et al (79) fitted their data to equation (2.7) and gave the following relation

$$U_a = 0.706 (g D_e)^{\frac{1}{2}} + (U - U_{mf}) \qquad (2.8)$$

which compare well with Nicklin's prediction.

Masson and Jottrand (67), using a light probe in 3-D bed reported that the relationship between the velocity and the size of the bubbles at a given point is linear and that the bubble flow at a given point increases linearly with the fluidisation velocity.

2.1.3 Effect of Tube Wall on Bubble Rise Velocity

When the size of bubbles in fluidised beds is small compared to the tube diameter ($D_e/D < 0.1$) the rise velocity with respect to the bed ahead of the bubble is determined by the volume of the bubble. If such is the case for bubbles in a freely bubbling bed or in a section of it close to the distributor, then the bed or that section is said to be operating in the "bubbling regime". The bubbles grow in size because of coalescence and when the ratio H/D is high enough slugs are formed. The velocity of a slug is determined by the diameter of the tube rather than by the volume of each slug. The part of the bed where slugs are formed is said to have entered into the "slugging regime". The transition from the bubbling regime to the slugging regime is slow and gradual and in all continuously slugging beds there exists a region where bubbles are partially influenced by the tube wall and their velocity is approximated by some function of bubble volume and tube diameter. This section of the bed is said to be operating in the "transition region" and in this text it is always referred to by this name.

Uno and Kintner (109), Collins (18), Collins (19), showed that the velocity of a bubble is reduced when the ratio De/D is greater than about 0.1. Uno and Kintner (109) measured rise velocities of bubbles in the transition region ($De/D > 0.1$) in liquids contained in tubes of various diameters. Based on their observations they gave a wall correction factor 'm' which is defined as follows:

$$m = \frac{U_b}{U_{b\infty}} = \left[\frac{1}{b}\left(1 - \frac{De}{D}\right)\right]^{0.765} \qquad (2.9)$$

where b, the constant, is a function of tube size and surface tension of the liquid.

Collins (18) solved the equation for the flow of a uniform stream past a circular body (18) and later on (19) gave the equivalent three-dimensional solution. He derived the following equation for the effect of tube wall on rise velocity of a spherical cap bubble:

$$U_b = 2(g r_b)^{\frac{1}{2}} \; (R/r_b) \; T_{1,2} \; (C/R) \qquad (2.10)$$

$$\text{where:} \quad T_{1,2} \; (C/R) = \frac{\sum^{n} [k_n \exp(-k_n \, C/R)] J_o^2 (k_n)}{\sum^{n} [k_n^2 \exp(-k_n \, C/R)] J_o^2 (k_n)}$$

The summations are taken over all positive values of k_n for which $J_1(k_n) = 0$. The symbols J_o and J_1 are the Bessel functions and the symbol C has the same meaning as in Collins' (1967) paper, (19) To support the theory Collins measured bubble rise velocity in gas-water systems and obtained a fairly good agreement between his theory and the experiments. Bubbles of different sizes were injected by Donsi et al (25) at different radial positions in a bed kept at near incipient fluidisation conditions. They used the equation for bubble rise velocity in a fluid as predicted by the wave theory (Mendelson (71)) to fit their data

$$\frac{U_b}{U_{b\infty}} = \left\{ \tanh \left[0.71 \, \frac{D_b + b_o}{D_b} \right] \right\}^{\frac{1}{2}} \qquad (2.11)$$

where b_o is the distance between the bubble and the tube wall defined as follows: If viewed from the top of the bed, bubble boundary could be drawn as a small circle off-centred in a bigger circle of diameter equal to that of the bed, then b_o is the shortest distance between the circumferences of the two circles.

2.2 Particle Motion Caused by Rising Bubbles

As a bubble rises in a fluidised bed it causes an originally horizontal layer of particles to be drawn up into a peak behind it. The shape of the peak formed is similar to that of a drift profile caused by a solid sphere rising in a liquid. Observations in two-dimensional beds (Gabor (32), Singh et al (102)) and three-dimensional beds (Rowe et al (98), Woolard and Potter (122)) show that this drift effect causes virtually no net upward flow of particles, and that the volume of particles drawn up is approximately equal to the downflow of solids in the surrounding dense phase. Rowe and Partridge (95) report that the total upward displacement of particles is approximately equal to half the bubble volume. Woolard and Potter (122) gave a slightly smaller figure. They report that the drift volume is equal to about $\frac{1}{3}$ of the volume of the bubble. Measured drift profiles could also be used to determine the horizontal distance from the bubble within which particle motion is caused by a rising bubble. Measurements made by Rowe (91), Gabor (32), Woolard and Potter (122) and Singh et al (102) show that particle motion is caused in a narrow region extending horizontally a distance equal to 1.5 - 2.0 times the width (D_b) of the bubble.

Jin Yong et al (57) investigated the movement of particles in a gas-fluidised bed using a laser technique. They found that, under the same superficial gas velocity, the intensity of particle circulation was different at different heights and at higher levels more intensified circulations were observed.

2.3 Bubble Formation at a Single Orifice

By balancing the buoyancy force and rate of change of upward momentum of the liquid surrounding the bubble, Davidson and Schuler (23) gave the following expression for the volume of a gas bubble formed at an orifice in a gas liquid system:

$$V_{bo} = 1.378 \quad \frac{G_b^{6/5}}{g^{3/5}} \qquad (2.12)$$

where G_b is the gas flow rate through the orifice. Davidson and Harrison (21) using a slightly different expression for the upward momentum of the liquid gave a value of the numerical coefficient equal to 1.138. Davidson and Schuler (23) in gas-liquid systems and Harrison and Leung (52) in fluidised beds operating at near incipient conditions, measured the volume of bubbles formed at a single orifice and found that the predicted V_{bo} by the above equation is in very good agreement at low gas rates through the nozzle. At higher gas rates they found that the equation overestimates the volume of the primary bubbles. Harrison and Leung (52) observed that for a wide range of gas rates with orifices in the range of 0.5 - 2.5 cm diameter, the frequency of bubble formation at a single nozzle remains within 18 - 21 bubbles per second. They also mentioned that during the formation of a bubble gas leakage to the continuous phase is not more than 15% of the volume of bubble and usually it is much less than this.

Vakhrushev and Basov (110) derived different equations for the estimation of the volume of bubbles formed at a single orifice under different operating conditions. For a case where gas leakage is considerable they gave a fairly complicated equation (which is not presented here). In a situation where gas leakage is small compared to the bubble volume, and can be ignored, this gave the following two equations for large and small primary bubbles respectively

$$V_{bo} = 0.890 \frac{G_b^{6/5}}{g^{3/5}} \qquad (\text{for } V_{bo} > 3.4\ cm^3) \qquad (2.13)$$

$$V_{bo} = 0.52\ G_b^{3/4} \left[\frac{28.7\ \nu_g}{g\ \varepsilon_D P}\right]^{3/4} \qquad (2.14)$$

where ε_D is the porosity of the dense phase, ν_g is the kinematic viscosity of the fluidising gas and P is a constant. They compared predictions made by their equations and by the following equations derived by other authors with the experimental data collected in fluidised beds reported in literature

$$V_{bo} = 1.138\ G^{6/5} / g^{3/5} \qquad (21) \qquad (2.15)$$

$$V_{bo} = 0.976\ G^{6/5} / g^{3/5} \qquad (85) \qquad (2.16)$$

$$V_{bo} = 0.806\ G_b^{6/5} / g^{3/5} \qquad (2.17)$$

On the plot of V_{bo} versus G_b the predicted lines drawn using the above equations lay close to each other. Each equation showed a region of gas flow rate through the nozzle within which it duplicated the experimental data very well whereas the other equations in that region either under or over estimated the bubble volume.

Chiba et al (10), assuming that the velocity of a bubble as it is formed at the orifice is given by: $U_b = k_b \sqrt{g\ D_{bo}}$, gave the following equations for the volume of a primary bubble:

$$V_{bo} = \frac{1}{K_b^{6/5}} \left(\frac{6}{\pi} \right)^{1/5} \left(\frac{G_b^{6/5}}{g^{3/5}} \right) \qquad (2.18)$$

They compared their predictions with the measurements made in a 2-D bed.

2.4 Bubble Size at the Distributor

Miwa et al (73) and Watson and Harrison (112) used equation (2.15)(i.e. $V_{bo} = 1.138\ G^{6/5} / g^{3/5}$ to predict the size of bubbles formed at a distributor. Miwa et al gave the following equations: (in C.G.S. units)

$$D_{bo} = 0.347 \left\{ A\ (U - U_{mf})/n_o \right\}^{2/5} \text{ for perforated plates.} \quad (2.19)$$

$$D_{bo} = 0.00376\ \ (U - U_{mf})^2 \qquad \text{for porous plates.} \quad (2.20)$$

Equation (2.20) is also applicable to perforated plates when the gas-rate is greater than the critical flow rate above which bubbles coalesce with neighbouring bubbles as they are formed.

Watson and Harrison (112) proposed the equations:

$$D_{bo} = (36\ G_o{}^2 / \pi^2 g)^{1/5} \quad (2.21)$$

$$D_{bo} = g \left\{ \frac{\pi D^3}{12 G_o} + \frac{t_d}{2} \right\}^2 \quad (2.22)$$

$$D_{bo} = g\ T_d{}^2 + 2(U_{bc} - g t_c) t_c\ \ell n \left(T_d / t_o\right) \quad (2.23)$$

where:

U_{bc} = velocity of the combined bubble, cm/sec

t_c = time of coalescence, in this case, time of contact of two bubbles from neighbouring orifices

t_d = delay between operation of two neighbouring orifices

t_o = time for bubble to grow to diameter D_{bc} from a single orifice

T_d = time of detachment equal to $\frac{\pi}{12 G_o} (D^3 - D_{bc}^3) + t_c$

D_{bc} = diameter of the combined bubble, cm.

Equation (2.21) gives the size of bubbles at a distributor when they are formed separately at each orifice without any interference from the other orifices. Equation (2.22) applies to a situation where a forming bubble grows to such a size that it overlaps the adjacent orifice and then grows at the expense of both of them, and equation (2.23) gives the size of bubbles which form independently at separate orifices and combine into one when their perimeter touch.

Leung (62) applied equation (2.15) to calculate bubble size at the distributor, assuming uniform gas distribution, to develop a method for distributor design.

2.5 Bubble Shape

Rowe and Partridge (97) noted from X-ray studies that single bubbles in fluidised beds have characteristic lengths which are associated almost exclusively with a spherical frontal surface and spherical cap shape, usually with an indented near surface. However, Harrison (50) postulated that reduced particle size could lead to greater bubble eccentricity because of a decrease in the apparent bed viscosity. Examination of Rowe and Partridge's data for 3-D bubbles reveals that for a particle size of 100 μm as used here, the wake angle θ_w should be almost 150^o with the wake fraction approaching 0.40.

Unlike bubbles in gas-liquid systems, where bubble shapes range from spheres through oblate spheroids, irregular ellipsoids to spherical caps, as reported by several workers (58, 65), the bubble shape depending on its volume, bubbles in fluidised beds present a single shape independent of volume (81). Bubble shapes in fluidised beds are generally spherical with an indented rear surface, which comprises a wake of particles travelling with the bubble.

The best description of bubble shape in fluidised beds was given by Rowe and Partridge (97) analysing three dimensional bubbles in fluidised beds of different materials, using X-ray photography.

Fig. (2.1) presents an idealised description of their findings. The wake angle, θ_w, was found to increase with diminishing particle size. For glass spheres they found $\theta_w = 134^o$ at $d_p = 550\ \mu m$ and $\theta_w = 151^o$ at $d_p = 60\ \mu m$.

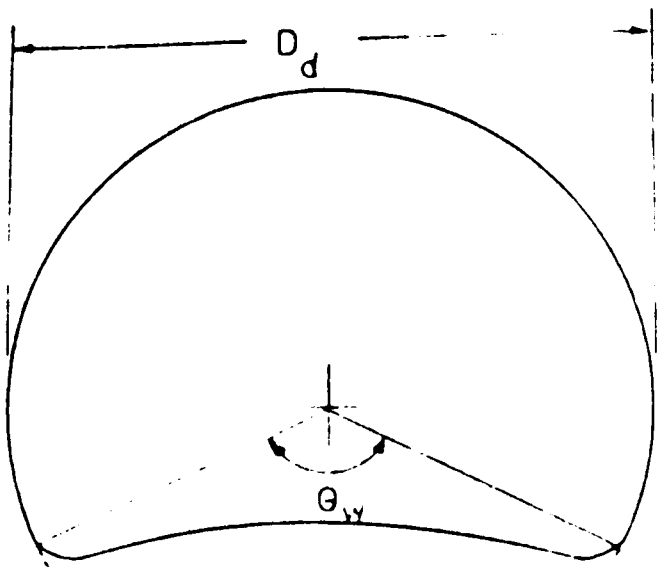

Ideal gas-fluidised bed bubble.

Figure 2.1 (after Rowe and Partridge (97))

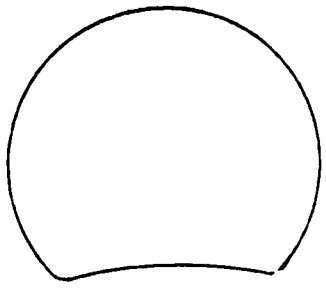

crushed coal

410 μm

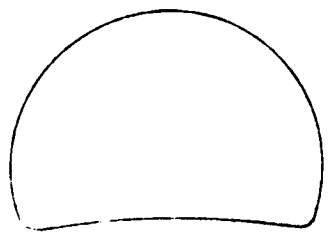

Magnesite

240 μm

acrylic granules

121 μm

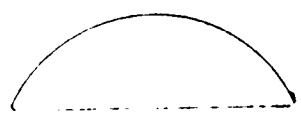

synclyst catalyst

52 μm

Figure 2.2 Bubble shapes in various materials

(after Rowe and Partridge (97))

Fig. (2.2) shows the bubble outlines as obtained by Rowe and Partridge 97 for different materials.

The variation of the wake angle with particle size was analysed by Harrison (50) by considering the variation of the bed viscosity with particle size. This has been measured by Kramers (60) and Matheson et al (69), who found that the bed viscosity decreases with decreasing particle size. Thus, as particle size decreases bubbles in fluidised beds will tend to have the same shape as the idealised shape proposed by Davies and Taylor for bubbles in inviscid liquids, a trend which is reflected in Fig. (2.2).

Observations in 2-D beds (Rowe (91)), Rowe and Partridge (95), Rowe et al (99), Toei et al (106), Singh (101) using photographic techniques and in 3-D beds (Harrison and Leung (53), Rowe and Partridge (97), Toei et al (106), Rowe and Matsuno (94) using visual observations at the wall or employing X-ray photography, show that bubbles have a nearly circular or spherical cap with a concave base line. Burgess and Calderbank (6) developed a compound (5-channel) electrosensitivity probe which was capable of detecting the bubble shape in gas-liquid systems. Pereira (81) developed a similar compound probe but used light-guides (fibre-optic) to measure the bubble eccentricity in froth regimes. Figure (2.3) below exhibits the generally observed shape.

Fig. 2.3

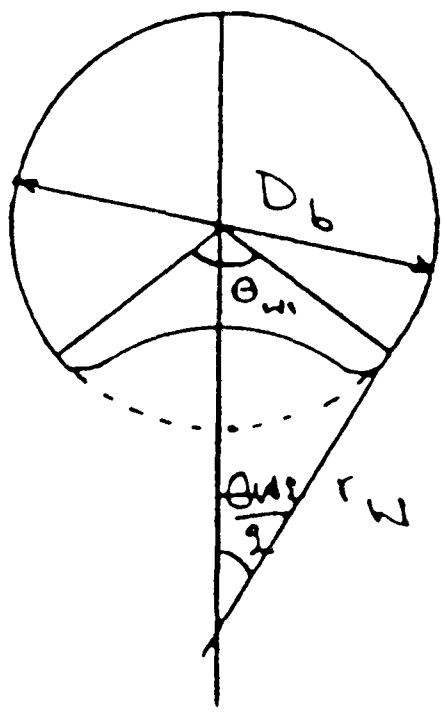

In most cases, the bubble occupied more than half the volume of the sphere of which the cap is part. The wake angle θ_{w1}, in most cases, remained less than or equal to 160^{o}C. Rowe and Partridge (97), Singh (101) suggest that the angle θ_{w1} increases with decrease in average particle diameter.

Studies by Rowe and Matsuno (94), Rowe and Everett (93), Werther (115) and Rowe and Widmer (100), indicate that bubbles, as they grow in size tend to become somewhat flatter in shape and carry a relatively large wake.

Rowe and Matsuno (94) and Harrison and Leung (53) used the following equations respectively to correlate the volume of a bubble with its shape.

$$V_b = \pi\, r_b^{\,3} \left\{ \frac{2}{3} + \cos\left(\frac{\theta_{w1}}{2}\right) - {}^1/3 \cos\left(\frac{\theta_{w1}}{2}\right) \right\} - \pi\, r_w^{\,3} \left\{ \frac{2}{3} - \cos\left(\frac{\theta_{w2}}{2}\right) + {}^1/3 \cos\left(\frac{\theta_{w2}}{2}\right) \right\} \qquad (2.24)$$

$$V_b = \pi\, r_b^{\,3} \left\{ \frac{2}{3} - \cos\,(180 - \theta_{w1}) + {}^1/3 \cos^3\,(180 - \theta_{w1}) \right\} \qquad (2.25)$$

Rowe and Widmer (100) recorded the shapes of numerous bubbles in fluidised beds of differing materials using X-ray photography. They found that for all materials the ratio of bubble volume V_B to the volume V_S of a sphere of the same radius was related to radius R by

$$\frac{V_B}{V_S} = 1 - e^{-0.114R} \qquad \begin{cases} V_B, V_S \text{ in } Cm^3 \\ R \text{ in } Cm \end{cases} \qquad (2.26)$$

Burgess and Calderbank (6) suggested

$$V_b = \frac{\pi}{3} L_b \left(3 a_c^2 + 4 L_b^2 \right) \qquad (2.27)$$

for an idealised bubble shape with a flat base and 50^o angle between its rim and polar axis, shown below, (Fig. 2.4):

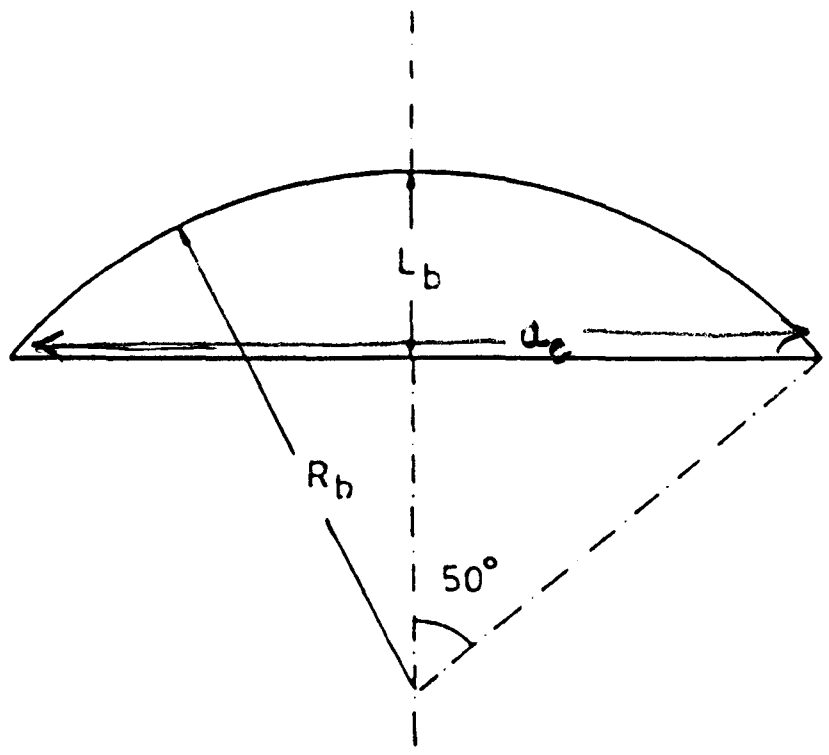

Bubble volume $V_b = \frac{\pi}{3} L_b (3a_c^2 + 4L_b^2)$

a_c = Bubble horizontal semi-axis length

L_b = Bubble vertical semi-axis length

Figure 2.4 Idealised bubble shape with a flat base and a 50^o angle between its rim and polar axis.

2.6 Variation of Bubble Size and Frequency with Height: Single Orifice

Behaviour of bubbles rising continuously from a single nozzle placed near the bottom of a bed of incipiently fluidised particles has been observed by several workers in both two- (Toei and Matsuno (105) Singh (101) and three-dimensional fluidised beds, (Harrison and Leung (54), Botterill et al (7) Orcutt and Carpenter (77)).

Such a chain of bubbles provides a good means of studying bubble coalescence in a vertical line, and the change in bubble properties as a function of bed height in its simplest form. Observations made in two-dimensional (Toei and Matsuno (105), Singh (101)) and three-dimensional (Botterill et al (7)) fluidised beds show that as a result of coalescence bubble frequency at a given height decreases approximately exponentially with increasing height above the nozzle, and that frequency is almost independent of gas flow rate through the nozzle. Their results show that bubble frequency at about 3 cm above the injection point lies in the range 10 - 12 per second and decreases to about 3 per second at approximately 20 cm above the nozzle. Only two authors (105, 77) measured bubble frequency higher up in the bed. They report an approximate figure of 2 bubble/second at a bed height of equal to 50 - 60 cm above the orifice. Botterill et al (7) gave the following empirical equation for the variation of bubble frequency with bed height

$$F_b = 34\, z^{-0.76} \qquad (2.28)$$

where y = vertical distance above the bubbling nozzle.

Observations of bubble size (Harrison and Leung (54), Botterill et al (7), Toei and Matsuno (105) show that the average bubble diameter at a given level in a bed increases with increasing bed height and increasing gas flow rate through the nozzle.

Results reported in literature show that bubble properties vary as a function of bed height only up to a certain level in the bed and at higher levels bubble properties remain almost constant. This infers that bubble coalescence is completed within a certain height above the orifice. Observations made by different experimenters show a different value of the height beyond which bubble properties remain constant. Results of Harrison and Leung (54) in a 15 cm bed, Botterill et al and Singh show that coalescence is complete within approximately 30 cm above the orifice, while observations made by Harrison and Leung (54) in a 61 cm bed, Toei and Matsuno (105) show bubble properties remaining independent of bed height at levels higher than 60 - 70 cm above the orifice.

2.7 Bubble Behaviour in Freely-Bubbling Beds

2.7.1 Bubble Size as a Function of Bed Height

Many authors have reported measurements of bubble size in freely bubbling three-dimensional fluidised beds. Different measuring techniques such as capacitance probes, electroresistivity probes, photography, X-rays etc., were used and different bubble size parameters, convenient to the technique employed, were measured. For example, experimenters who used probes for their study measured the average height of bubbles, whereas workers who employed photographic techniques gauged the average bubble diameter at different heights. In cases where probes were used no allowances were made for the probability of the probe not recording the height at the centre of the bubble. This is shown in Fig. (2.5). Sizes of fluidised beds used by different workers cover a wide range. The smallest bed used was 7.0 cm in diameter and the biggest was 122 x 122 cm bed of square cross-section. The range of gas flow rates covered is $U - U_{mf} \leqslant 42.0 Cm/Sec$.

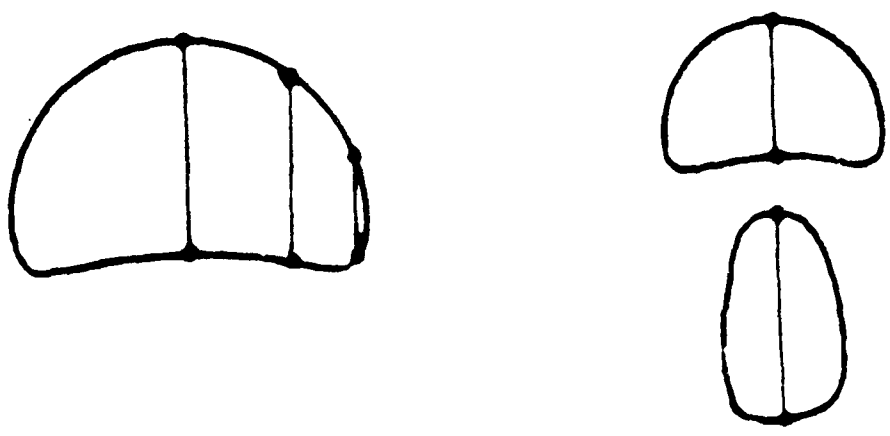

Figure 2.5

Examples of uncertainties involved in measuring bubble size by the length of pulses produced by a probe immersed in a bed.

Observations of bubble size in freely bubbling axi-symmetric beds show that at a given level bubbles of different sizes are present and that average bubble size at a given height increases with increasing height above the distributor and increasing gas flow rate. Most authors have indicated that average bubble size increases linearly with bed height whereas some authors have reported a slight decrease in bubble growth rate with increasing bed height. From the observations reported in the literature one could conclude to some extent that at a constant gas flow rate bubble growth rate is high near the distributor, because of very rapid coalescence in that region, decreases slightly with increasing height and then remains constant for the larger portion of the bed. However if the bed is fairly tall, slugging conditions might be approached and a slight decrease in growth rate could be observed. Details of the systems used by different workers and conclusions made by them are summarised in chronological order in table (2.2).

TABLE 2.2

Summary of the measurements of bubble size made by different workers in freely-bubbling three-dimensional fluidised beds

B_c ..... Bubble caps
P_e ..... Perforated plate
P_o ..... Porous plate
T ..... Tuyeres

C ..... Bed of circular cross-section
S ..... Bed of square cross-section
R ..... Bed of rectangular cross-section

NR ..... Quantity not reported in the paper.

AUTHORS	MEASURED	MEASURING TECHNIQUE	FLUIDISED BED Shape	Size (cm)	DISTRIBUTOR	PARTICLE NAME	d_p μm	U_{mf} cm/sec	RANGE OF $(U - U_{mf})$ cm/sec	RELATION GIVEN
Yasui & Johanson (125)	D_b'	Light detecting probe	C	(i) 10.2 (ii) 15.2	P_o	Glass beads Olivine Coal Resin Mag. Catalyst FCC Catalyst	41-242 42-150 450 81 70 12	NR	=7.5-12.5	$\frac{\bar{D}_b/y}{\rho_p \bar{d}_p} = a\left[\frac{U-U_{mf}}{U_{mf}}\right]^b$
Kobayashi et al (59)	D_b'	Light detecting probe	C	10.0	P_o d_o 0.05 δ NR n_o NR	Silica Gel	60-80 mesh	2.85	5.7-28.5	$\frac{\bar{D}_b'}{y} = 1.4(\bar{d}_p \rho_p)\frac{U}{U_{mf}}$
Toei et al (106)	D_b	Capacit-ance probe & X-ray photo-graphy	C S	7.6 10 x 10	NR	Glass beads Sand PVC	NR	NR	=2.0-15.0	

Whitehead[+] & Young (120)	D_{er}	Cine Photo-Graphy	S	(i) 61x61 (ii) 122x122	T δ n_o (i) 30.5 4 15.2 16 (ii) 30.5 16 15.2 64	Silica Sand	NR	2.5	<15.0	$\bar{D}_{er}=0.45\,(nU_{mf}^{0.54}(0.33y^{0.54})$ $\bar{D}_e=0.34\,(nU_{mf}^{0.54}(0.33y^{0.54})$
Geldart[*] (34)	D_{er}	Manually using a ruler	C	30.8	P_e d_o δ n_o 0.32 0.51 3100	Sand	144 160 318	1.37 1.4 5.6	<7.0	
Park et al (79)	D_b'	Electro-resistivity probe	C	10.0	P_o	Coke	344 154 86	6.8 1.83 0.63	3.4-13.6 0.9-16.5 1.9-3.2	$\frac{\bar{D}_b'}{y}=33.3d_p^{0.77}-1.5\left[\frac{U-U_{mf}}{U}\right]$
Geldart[**] (35)	D_b	Cine Photo-graph of bed surface	C	30.8	P_e d_o δ n_o 0.32 0.51 3100	Sand	128	1.2	0.3-8.0	$\bar{D}_b=\left[8\,\frac{(U-U_{mf})}{F_b \times \pi}\right]^{1/3}$
Argyriou (3)	D_b	Cine Photo-graph of bed surface	C	29.2	P	Glass beads Cat-alyst	85-470 59	NR	1.5-6.5	
McGrath & Streatfield[††] (68)	D_{er}	Manually with a ruler	R	30.5x15.2	P_e d_o 0.159 1.198 0.238 0.278 $n_o=1330$ $\delta=0.635$	Sod. Alumin-ate	1500	55.0	<42.0	

Geldart** (36)	D_{er}	Cine film of bed surface	C	30.8	P_e $d_o = 0.32$ $\delta = 0.51$ $n = 3100$	Rounded Sand Angular Sand	100 128 175 275 75 250 470	1.37 1.2 3.1 5.6 1.0 7.4 25.4	1.0-8.0	$D_b=0.915(U-U_{mf})^{0.4}$ $+0.027y(U-U_{mf})^{0.94}$ (POROUS PLATE) $\bar{D}_b=1.4(\frac{U-U_{mf}}{n_o})^{0.4}$ $\frac{1}{g^{0.2}}+0.027y$ $(U-U_{mf})^{0.94}$ (PERFORATED PLATE)
Miwa et al (73)	D_b'	Capacit-ance probe	C	7.0 15.0	P_e $d_o = 0.3$	Sand	NR	NR	5-12.5	-
Rowe & Everett (93)	D_b	X-ray photo-	S R	30x30 30x20	P_o	Alumina Carbon Quartz Glass beads Glass powder	210 296 135 323 268	2.54 8.0 2.75 8.0 5.5	1.3-3.8 2.4-5.6 3.3-15.4 4.8-11.2 4.1-9.6	$\bar{D}_b=-P_1+P_2y+P_3(U/U_{mf})^2+$ $P_4y(U/U_{mf})+P_5(U/U_{mf})^2$
Chiba+ et al (11)	D_b'	Light detecting probe	C	10.0 20.0	P_e	Silica gel Catalyst	89 210 67 443	0.53 2.85 0.28 6.7	5.0-22.3	$\bar{D}_e=D_{bo}(2^{7/6}-1)$ $(y-y_{bo})/D_{bo}+1)^{2/7}$
Tomita & Adachi (107)	D_b	Capacit-ance probe	C	21.4 37.8 59.9	P_e d_o δ n_o 0.1 1.5 504 0.1 1.5 1571 0.1 1.5 3946	Sand	202	4.0	6.0-21.0	-

33.	Fryert (31)	D_{er}	Cine photo-graph of bed surface	C	22.9	B_c δ n_o 2.78 61	Sand	71	1.7	0.7-10.4	$D_b = D_{bo} + 2.05 \times 1$ U $D_{bo} = 1.08 (U-U_m$
	Werther (115)	D_b'	Capacit-ance needle probe	C	20.0 100.0	P_o	Quartz Glass beads	= 80 =175	1.8 3.9	9.0-11.7	$D_b' \sim y^{0.82}$
	Mori & Wen (74)	USED DATA FROM OTHER WORKERS									$\frac{D_{max}-\bar{D}_e}{D_{max}-D_{bo}} = e^{0.}$ $D_{max} = (0.347)$ (1.87) $\left[(A(U-U_{mf})\right]^{2.5}$

* Authors assumed that eruption diameter D_{er} is equal to D_b.

** Authors used $D_b = 2/3\ D_{er}$ to calculate D_b based on Botterill's et al (7) results.

\+ Authors used $D_e = 0.75\ D_{er}$ to calculate D_e.

++ Authors calculated D_b from the measured $\bar{\varepsilon}_b$.

† Authors used their own data and data from other workers.

†† Authors did not report the value of n_o, it was calculated from their information using the equation, $n_o = \frac{2A}{\sqrt{3\delta^2}}$, obtained from Miwa et al (73).

2.8 Bubble Frequency as Function of Bed Height

The term "bubble frequency" has been used rather liberally in the literature. Bubble properties such as F_b, number of bubbles passing a certain height per unit time, f_b, number of bubbles striking a probe per unit time and f'_b, average number of bubbles present in a given volume, are sometimes referred to as bubble frequency. Although the above quantities are numerically different from each other, they are closely inter-related and show a similar variation with bed height and with gas flow rate.

Several authors have measured one of the above mentioned bubble properties in freely-bubbling three-dimensional fluidised beds. Conditions under which measurements were made are summarised in Table (2.3). It is fairly established (Yasui and Johanson (125), Hamilton (49), Geldart (35), Argyriou, List and Shinnar (3), McGrath and Streatfield (68), Rowe and Everett (93), Tomita and Adachi (107), Werther (115), Fryer (31)) that bubble frequency in bubbling fluidised beds decreases approximately exponentially with increasing bed height.

Allahwala (1) using a computer model simulating a three-dimensional, freely-bubbling gas-fluidised bed showed that there is good agreement between the experiments of Hamilton (49) and the predictions of his simple model.

The variation of bubble frequency with $(U - U_{mf})$ is not very clearly known. Observations made by Geldart (35) show that frequency decreases almost linearly with increasing gas rate, whereas McGrath and Streatfield report that bubble frequency first increases with increasing $(U - U_{mf})$, reaches a maximum value, and then decreases with increasing $(U - U_{mf})$.

TABLE 2.3

Resume of the published data on bubble frequency & related properties in freely-bubbling three-dimensional fluidised beds

B_c - Bubble Caps
P_e - Perforated plate
P_o - Porous plate

C - Bed of circular cross-section
S - Bed of square cross-section
R - Bed of rectangular cross-section

NR - Quantity not reported in the paper.

AUTHORS	MEASURED	MEASURING TECHNIQUE	FLUIDISED BED SHAPE size (cm)	DISTRIBUTOR	NAME	PARTICLE SIZE (μm)	U_{mf} ($\frac{cm}{sec}$)	RANGE OF $U-U_{mf}$ $cm.sec^{-1}$
Yasui & Johanson (125)	f_b	Light Detecting probe	C (i) 10.2 (ii) 15.2	P_o	Glass beads Olivine Coal Resin Mag. Catalyst FCC Catalyst	41-242 42-150 450 81 70 12	NR	=7.5-12.5
Toei et al (106)	F_b	X-ray photography and capacitance probe	C 7.6 S 10 x 10	NR	Glass beads Sand PVC	NR	NR	=2.0-15.0
Geldart (34)	Number of bubble tracks	Visual Counting	C 30.8	P_e d_o δ n_o 0.32 0.51 3100	Sand	144 160 318	1.37 1.4 5.6	<7.0
Park et al (79)	f_B	Electro-resistivity probe	C 10.0	P_o	Coke	86 154 344	0.63 1.83 6.80	3.1-5.7 1.8-9.2 6.8-20.4
Hamilton (49)	F_b	Cine film of bed surface	S 30.5x30.5 C 30.5 S 30.5x30.5	B_c δ=2.7 n_o= 121 B_c δ=3.0 n_o = 100 T δ=10.2 n_o = 9	Glass beads	75-142 75-116 75, 97	0.7-2.4 0.7-1.7 0.7,1.2	0.7-9.9 0.8-6.7 1.2-8.6

Geldart (35)	F_b	Cine Film of bed surface	C	30.8	P_e d_o δ n_o 0.32 0.51 3100	Sand	128	1.2	0.3-8.0
Argyriou et al (3)	F_b	Cine film of bed surface	C	29.2	P_o	Glass beads C.Catal-yst	85-470 59	NR	1.5-6.5
McGrath & Streatfield* (68)	F_b	Visual Counting	R	30.5x15.2	F_e d_o δ 0.159 0.198 0.238 0.635 1330 0.278	Sodium Aluminate	500	55.0	<42.0
Rowe & Everett (93)	f_b'	X-ray photo-graphy	S R	30x30 30x20	P_o	Alumina Carbon Quartz Glass beads Glass powder	210 296 135 323 268	2.5 8.0 2.8 8.0 5.5	1.3-3.8 2.4-5.6 3.3-15.7 4.8-11.2 4.1-9.6
Matsen (70)	f_b	capacitance probe	C	61.0	Single Orifice d_o=5.1 multi orifice d_o δ n_o 2.5 30.5 4	Coke	(= 90 = 150)	< 1.5	<59.4

Tomita & Adachi (107)	f_b	Capacitance probe	C (i)21.4 (ii)37.8 (iii)59.9	P_e d_o δ n_o 0.1 1.5 504 0.1 1.5 1571 0.1 1.5 3946	Sand	202	4.0	6.0-21.0
Werther (115)	f_b	Capacitance needle probe	C (i)20.0 (ii)100.0	P_o	Quartz Glass beads	= 80 = 175	1.8 3.9	9.0-11.7
Fryer (31)	F_b	Cine film of bed surface	C 22.9	B_c δ n_o 2.78 61	Sand	71	1.7	0.7-10.4

* Authors did not report the value of n_o, it was calculated from their information using the equation,

$n_o = \frac{2A}{\sqrt{3}\delta^2}$, obtained from Miwa et al (73).

2.9 Bubble Frequency Distribution

Observations of bubble frequency distributions in freely-bubbling fluidised beds (Whitehead and Young (120), Grace and Harrison (46), Park et al (79), Singh (101), Tomita and Adachi (107), Werther (115), Watson and Harrison (112), Burgess and Calderbank (6), show that at heights not in the vicinity of the gas distributor, bubbles tend to follow preferred tracks and as a result the distribution of bubbles becomes non-uniform. Observations made by the above authors could be summarised as follows: At heights close to the distributor the distribution of bubbles across the bed cross-section remains fairly even, this suggests a homogeneous bubbling at the gas distributor. The bubble frequency distribution as one moves upwards from the distributor first shows a region of relatively higher bubble frequency, near the tube wall. This region then moves towards the centre of the bed with increasing height above the distributor and increasing flow rate. Watson and Harrison (112) in their paper plotted peakedness, a measure of non-uniformity in bubble distribution at a given height, as a function of bed height. They showed that these non-uniformities in fluidised beds first increase with bed height, then decrease slightly, inferring a slight redistribution of bubbles and starts increasing again with increasing height above the distributor. Tomita and Adachi (107) also report a slight redistribution of bubbles with increasing bed height. Burgess and Calderbank (part II 6) defined bubble size distribution as the number fraction of bubbles of a given size existing in the entire volume of the dispersion; a spatial definition. They later (part III, 6) used this definition to measure the bubble size distribution in a freely-bubbling fluidised bed of circular cross-section. They reported that at

the top of the bed, bubbles exist preferentially at the bed centre-line, which from their enhanced velocity may be recognised as the position of upward emulsion phase movement. Conversely, smaller bubbles exist in the region of downward emulsion movement near the vessel walls. They also showed that at the bottom of the bed the opposite trend obtains with the bubbles near to the wall being larger than those near to the centre. They concluded that larger bubbles exist in regions of upward emulsion phase movement and vice-versa.

Masson and Jottrand (_67) reported that the bubble fraction at a given point varies proportionally to the difference $U - U_{mf}$ and the bubble flow changes linearly with the fluidisation velocity.

Yoshida et al (126) measured bubble size distributions using laser beams. Their results showed that the distributions had a bi-nodal form differing from the distributions previously reported.

Farrokhalaee and Clift (29) developed a model for predicting bubble behaviour and their results are generally in agreement with the measurements of Werther (115). They reported that some discrepancy arose from non-uniform bubble formation caused by solids circulation. Their model predicts that the size and spatial distribution of bubbles at any level above the distributor is dependent on the bed depth above that level.

2.10 Division of Gas Between Bubble and Dense Phases

The relation between bubble flow rate, G_B, and gas flow rate in a fluidised bed can be given as:

$$U_{GB} = G_B/A = U - k_d\, U_{mf} \qquad (2.29)$$

The simple two-phase theory of Toomey and Johnstone (108) predicts that $k_d = 1$. Lockett, Davidson and Harrison (66) considered the effect of volume fraction occupied by bubbles, ε_B, and of gas flow through the bubbles. They gave:

$$k_d = 1 + \varepsilon_B \qquad \text{in 2-D beds}$$

$$k_d = 1 + 2\varepsilon_B \qquad \text{in 3-D beds}$$

Observations made by several workers, tabulated in Table 2.6, show that the value of k_d differs from system to system and that within a given system at a given height k_d increases with increasing gas flow rate and decreases with increasing height above the distributor. It is seen from the table (2.4) that in most cases the value of k_d lies between 1.1 - 6.0. Grace and Clift (44) extended the theory of Lockett et al (66) incorporating the variation of ε_B with height. They proposed:

$$\Delta\, U_{GBab} = U_{mf}\, k_d\, (\varepsilon_{Ba} - \varepsilon_{Bb}) \qquad (2.30)$$

where a and b are levels in the bed.

TABLE 2.4

Resume of the Experimental Investigations of the Division of Gas between the Bubble and Dense Phases

AUTHORS	MEASURING TECHNIQUE	BED SHAPE	BED SIZE cm	PARTICLES TYPE	d_p μm	U_{mf} cm/sec	RANGE OF $(U - U_{mf})$ cm/sec	HEIGHT ABOVE DISTRIBUTOR cm	$\frac{U-G_B/A}{U_{mf}}$
Baumgarten and Pigford (4)	Gamma-rays	R	7.6 x 15.2	Cracking cat	41	0.7	5-21	20	8.27
					74	0.7	1-21	20	2-18
				Glass beads	116	1.1	5-20	20	5.11
					119	1.6	1-23	20	1.5-7.5
					234	5.2	4-25	20	1.6-4.5
Pyle and Harrison (84)	Photo-graphy	2D	1 x 24.2	Glass beads	100	1.2	1.7-10.5	20-100	1.0-6.6
					370	14.7	1.0-27.0	10-100	1.0-2.3
				Iron shot	180	14.7	3-26	20-96	1.2-2.2
Whitehead and Young (120)	Light detecting probes	S	122 x 122	Silica Sand	-	2.5	$\leqslant$ 17.0	85,206	2.1-5.8
Geldart (34)	Manually with a ruler	C	30.8	Sand	318	5.6	1-7	5-20	1.1-1.3
Grace and Harrison	Photo-graphy	2D	1.9 x 45.7	Magnesite	274	8.1	5.24	15.60	1.1-3.0
Singh (10)	Photo-graphy	2D	1.1 x 45.7	Glass Beads	97	1.2	3.4-27.8	10-52	1.0-14.0
			1.1 x 91.4		292	8.5	7.7-57.5	15-75	1.2-3.7
Geldart (35)	Cine film of bed surface photo-	C	30.8	Sand	128	1.2	0.3-8	10-60	1.5-4.8
		2D	1.3 x 68.5	Sand	128	1.5	0.3-8	10-80	1.5-4.5

McGrath & Streatfield (68)	Manually with a ruler	R	15.2 x 30.5	Sodium Aluminate	1500	55	⩽ 42.0	2.6-13.3	1.1-1.4
Werther & Molerus (117)	Capacit-ance needle	C	10 20 45 1000	Sand	83	1.8	⩽ 7.1	5-30	1.0-3.1
Rowe & Everett (93)	X-rays	S	30 x 30	Alumina	210	2.5	1.3-3.8	20-70	Average value of 1.5
		R	30 x 20	Carbon	296	8.0	2.4-5.6	12-60	
				Quartz	135	2.8	3.3-15.7	20-70	
				Glass beads	323	8.0	4.8-11.2	15-45	
				Glass powder	268	5.5	4.1-9.6	15-60	

2.11 Coalescence

2.11.1 Vertically Aligned Bubbles

Studies in fluidised beds show that in most cases only two bubbles are involved in the process of coalescence. When the two bubbles are nearly vertically aligned to each other one bubble (called the following bubble) is accelerated, enters into the wake of the other (referred to as the leading bubble) and coalesces with it. During the process of coalescence bubbles deform and this deformation follows a rather standard sequential pattern. The influence of the leading bubble is such that the front edge of the following bubble is accelerated more than its rear edge, resulting in elongation of the following bubble. The shape of the leading bubble is not affected until the following bubble is fairly close to it whereupon its base flattens out. When the two bubbles are about to become one, the front of the following bubble starts to extend sideways in order to be able to fit into the back of the leading bubble. On coalescence the thin film of particles which held the two bubbles separate, breaks and some particles are thrown inside the leading bubble. The above model of bubble coalescence summarises the observations made by most workers (Harrison and Leung (54), Botteri 11 et al (7), Toei and Matsuno (105), Godard and Richardson (41), Clift and Grace (12), Singh (101)).

Some contradictory results have been reported in the literature. Most authors (54), (41), (101), (101), observed that during bubble coalescence in fluidised beds the velocity of leading bubble remains constant. However (12, 14, 45) from their theoretical and experimental analysis are of the opinion that the leading bubble accelerated, but only slightly, and that the acceleration of the leading bubble is significant in 2-D beds only. They (12) gave the following expression for the velocity of the leading and the trailing bubbles respectively:

$$U_{b_1} = U_{b_{1\infty}} + \frac{U_{b_2}\, r_{b_2}}{(h' + r_{b_1})} \qquad (2.31)$$

$$U_{b_2} = U_{b_{2\infty}} + \frac{U_{b_1}\, r_{b_1}}{(h' + r_{b_2})} \qquad (2.32)$$

where $\frac{U_{b_2}\, r_{b_1}}{(h' + r_{b_1})}$ and $\frac{U_{b_1}\, r_{b_1}}{(h' + r_{b_2})}$ are the particle velocities at the noses of leading and the following bubbles respectively. Singh (101) reports that velocity of the following bubble can be approximated by the expression:

$$U_{b_2} = U_{b_{2\infty}} + 2\, U_{b_1}\left(1 - \frac{h}{2\, D_{e_1}}\right) \qquad (2.33)$$

The subscripts 1 and 2 stand for the leading and following bubbles respectively.

(54), (105) and Singh from their observations support the idea that there exists a critical distance behind the leading bubble beyond which the effect of the leading bubble is not felt by the following bubble. (Harrison and Leung (54) and Singh (101) observed that this critical distance is approximately equal to one bubble diameter. Toei and Matsuno (105) report that the critical distance is equal to $(D_{b_1} + D_{b_2})/2.0$. Clift and Grace

and Lin (64) suggest that equal sized bubbles will always coalesce regardless of their initial spacing provided that the bed is tall enough and that critical distance only exists when the following bubble is smaller than the leading one.

Toei and Matsuno (105) observed a slight deceleration of the rear bubble just before coalescence occurs. No such effect has been reported by any other worker. Singh (101), Grace (43), Grace and Venta (48) found that when two bubbles coalesce the volume of the newly formed bubble is about 10 - 15% greater than the sum of the two volumes of the two parent bubbles. Also during coalescence gas leakage from the trailing bubble to the leading bubble and vice-versa is reported (Grace (43) and Grace and Clift (45) to take place only rarely. The phenomenon is relatively more frequent when the bubbles are different in size.

2.11.2 Bubbles not in Vertical Alignment

When two bubbles are travelling upwards, side by side in the same horizontal line, they seldom coalesce with each other, but maintain their relative positions. However, when one of the bubbles lies obliquely below the other, the velocity of the lower bubble is influenced by the presence of the leading bubble and coalescence does occur. At this stage the leading bubble is hardly affected by its trailing counterpart.

When ϕ, the angle between the vertical line passing through the centre of the leading bubble and line joining the noses of the two bubbles, is large, the lower bubble experiences a retarding effect and as a result the distance between the two bubbles becomes larger and angle ϕ becomes smaller. As the angle ϕ gradually decreases the velocity of the following bubble gradually increases, exceeds the velocity of the upper one and it coalesces with the leading bubble. During coalescence the bubbles deform and follow roughly the same sequential pattern as described for the vertically aligned bubbles except for the fact that instead of the following bubble being elongated in the vertical direction it becomes stretched obliquely in the direction of the leading bubble. The picture of coalescence described above is in accordance with the observations made by Toei and Matsuno (105), Singh (101), Clift and Grace (14), , and Grace and Clift (45).

Two authors (Toei and Matsuno (105), Singh (101)) measured the time taken for the two obliquely aligned bubbles to become one big bubble. Their observations show that the time for coalescence

increases with increase in the angle ϕ. Toei and Matsuno (105) report that the time for coalescence of bubbles aligned with the angle ϕ equal to 45^{o} and 57^{o} is twice and thrice respectively, the time for coalescence of the same sized vertically aligned bubbles. Singh (101) gave the following equation for the velocity of the trailing bubble:

$$U_{b2} = U_{b2\infty} + 2\,U_{b1}\,\left(1 - \frac{h}{2\,D_{e1}}\right)\,(1 - \mathrm{Sin}\,(\phi)) \qquad (2.34)$$

and found a tolerable agreement with his experimental data.

Darton, Lanauze, Davidson and Harrison (20) investigating bubble growth due to coalescence in fluidised beds gave the following equation for the bubble diameter.

$$D_e = 0.54\,(U - U_{mf})^{0.4}\,(h + 4\sqrt{A_o})^{0.8}/g^{0.2} \qquad (2.35)$$

where h = height above the distributor

A_o = is the "catchment area" for the bubble stream at the distributor plate, which characterises different distributors.

The basis of their theory is that bubbles tend to rise in preferred paths and that the distance travelled by two neighbouring bubbles before coalescence is proportional to their lateral separation. With the empirical constant 0.54, the above equation agrees quite well with the most of the literature data on bubble size, provided bubble growth is not limited by the presence of fine particles.

Werther (115) developed a statistical model of bubble coalescence in freely bubbling beds using the mechanism of bubble coalescence put forward by Clift and Grace (12 , 13), with a porous plate distributor in 1 m diameter bed. He proposed an empirical correlation for bubble growth:

$$d_v = 0.853\ (1 + 0.272\ (U - U_{mf}))^{1/3} + (1 + 0.0689h)^{1.21} \qquad (2.36)$$

d_v = diameter of sphere with a volume equal to the local average bubble volume, cm

h = height above distributor, cm

U, U_{mf} are in cm/sec.

2.12 Bubble Splitting

Observations of bubbles in fluidised beds (Rowe et al (99), Rowe and Partridge (97), Botterill et al (7), Rowe and Matsuno (94), Clift and Grace (16) have indicated that bubbles have a tendency to split into more than one daughter bubbles. Their results can be summarised as follows: Bubbles splitting takes place when a small knife-edge of particles descends from the roof of the bubble, grows while moving down through the bubble and eventually divides the bubble. It is quite typical that one of the daughter bubbles is considerably smaller than the other and in some cases the smaller bubble moves round behind the larger counterpart and recoalesces with it. Observations show that the phenomenon of bubble splitting does not take place very frequently in fluidised beds. Rowe (92) has shown that more than 50% of the bubbles in a fluidised bed do not split and about 25% of the split bubbles immediately recoalesce with each other.

2.13 Behaviour of Gas Distributors

Whitehead and Dent (118) determined U_I, the superficial gas velocity required to initiate operation of all the tuyeres in a gas distributor, and found that U_I is of the order of 5 U_{mf}. They also measured U_M, a critical minimum gas velocity at which a distributor could function without any tuyere becoming momentarily non-operative. They gave the following empirical equation:

$$\frac{U_M}{U_{mf}} = 0.7 \left[0.49 + \frac{3.23 \times 10^{-7} \, n_o^{0.22} \, K_D^2 \, \rho_p H}{U_{mf}^2} \right]^{\frac{1}{2}} \qquad (2.36)$$

where H and ρ_p are in (ft) and (lb/ft^{-3}) respectively. Flow factor K_D is equal to 60 $U\Delta p_D^{-0.5}$ where Δp_D is the pressure drop across the distributor (in of H_2O).

Fakhimi and Harrison (28) derived an expression relating the number of orifices operating at any time in a distributor with gas flow rate. They proposed:

$$\frac{n_w}{n_o} = \frac{\left[\frac{U}{U_{mf}} - 1 \right]}{\left[1 + \frac{2 \phi^2}{\rho_f . U_{mf}^2} \Delta p_{b,mf} - \Delta p_s \right]^{\frac{1}{2}} - 1} \qquad (2.37)$$

where n_w is the number of orifices operating at a certain gas flow rate, and Δp_s is the pressure drop across the preferential gas path through the bed.

Whitehead and Dent (118) and Fakhimi and Harrison (28) have also pointed out that it is important to know whether a particular fluidising flow-rate has been reached by increasing or decreasing the gas supply. Fakhimi and Harrison (28) obtained a good

agreement between their predictions and experiments when n_w was measured by decreasing the gas supply. However, when n_w was measured by increasing the gas rate, equation (above) agreed with the experiments only up to when $nw/n_o = 0.7 - 0.85$.

Werther (114) investigated the influence of distributor design on the local bubble characteristics. Eight different distributor plates, including multihole, nozzle and tuyere-type distributors were used. He developed a method which permitted the prediction of bubble growth as a function of height above the distributor, excess gas velocity and distributor design. His model predicts local average bubble sizes which are in good agreement with measurements for all the distributors used and also with the results of Whitehead and Young (120). Yue and Kolaczkowski (127) proposed a method for the design of a multiorifice distributor for a fluidised bed. They proposed the following:

$$\left(\frac{A_T}{Na_o}\right)^2 \left(\frac{\rho_f}{2g_c C_D^2}\right)(U - U_{mf}) = \Delta p_{Bmf}\left(\bar{e}_B + 0.363\,\frac{hs}{H_{mf}}\right) \qquad (2.38)$$

where N = total number of orifices,

A_T = total area of fluidised bed (m^2)

h_s = height of spout or jet (m)

$\bar{e}_B$ = average bubble voidage,

H_{mf} = bed height at minimum fluidisation.

To determine the superficial gas velocity at which all the orifices become active, they proposed the following equation

$$U = \left[\Delta p_{Bmf}\left(\bar{e}_B + 0.363\,\frac{hs}{H_{mf}}\right)\left(\frac{2gC_D^2\,\phi^2}{\rho_f} + U_{mf}^2\right)\right]^{\frac{1}{2}} \qquad (2.39)$$

where $\phi = \frac{N a_o}{A_T}$, the orifice density

a_o = area of orifice

C_D = coefficient of discharge of orifice

They found that the bed height affects the performance of the distributor, except in the case of very deep beds. Hsiung and Grace (56) experimenting with a bed of rectangular cross-section (8 x 10 cm) concluded that for low pressure drop orifices, the frequency of bubble formation depends on the volume of chamber feeding the orifice. As the flow rate through the orifice increases the bubble frequency levels off at a constant value between about 19 and 25 Hz. They also reported that at low flow rates bubble formation tends to be very regular. With increasing flow rate, they observed coalescence before detachment and irregular bubble formation.

Yacono and Angelino (124) examined bubble behaviour in a 3-D air fluidised bed fitted with "ball distributors" and found that the results were qualitatively similar to the results obtained with a standard porous distributor. They observed quantitative differences in that the bubble size was larger and the bubble concentration smaller with a "ball distributor" than with a porous plate. Wen et al (113) used 2-D and 3-D fluidised beds to investigate dead zones near the distributor region. Their results from the 3-D bed confirmed the importance of the orifice pitch and they found that the behaviour of the 2-D bed cannot be readily extrapolated quantitatively to 3-D cases.

2.14 Effect of an Immersed Object on Fluidisation Behaviour

Glass and Harrison (40) and Glass (39) Gelperin et al (38), Botterill et al (7) Cloete (17), Morgan (72), Harrison and Grace (51), Newby and Keairns (75), Xavier and Davidson (123), Staub and Canada (104), Andeen et al (2), Richardson et al (86), Catipovic et al (8), Wood et al (121), Zabrodsky et al (128), Chandran (9), and others have studied the effect of the presence of solid obstacles on the flow pattern, hydrodynamics and the heat transfer in 2-D and 3-D gas fluidised beds. Of all the different types of solid obstacles reported in the literature, this section will deal with the horizontal tube (or array of tubes) only. Immersed horizontal tubes have been a common feature of fluidised beds to which heat is supplied or removed. Glass and Harrison (40) used a photographic investigation of the flow patterns of particles and of the fluidising gas near a horizontal tube in 2-D fluidised bed. They found that below the tube there was a thin film or cushion of air of variable thickness. Above the tube there was apparently a defluidised region, the extent of which decreased by increasing the gas flow rate. At either end of the horizontal diameter of the tube irregular chains of bubbles formed. Glass (39) also studied the pattern of gas flow near a tube in the air-fluidised bed by using nitrogen dioxide tracer technique developed by Wace and Burnett (111). He found that at higher flow rates than 0.5 U_{mf} the streamlines are increasingly disrupted by indigenous bubbles. However, there was evidence of slight convergence of gas streamlines towards the tube at flow rates near incipient fluidisation. Morgan (72) photographed

the surface of gas fluidised bed of 20.3 cm square cross-section. Air flow rate was increased from 0.4 - 2.0 U_{mf}, while the bed height was kept constant. He showed that a horizontal tube is able to initiate bubbling at flow rates considerably lower than that at incipient fluidisation. Of course in a deeper bed these "premature bubbles" do not have a long life at those flow rates, for they soon leak away into the general interstitial flow. His photographs show that in a deeper bed, a greater flow rate is needed to generate premature bubbling on a large enough scale for bubbles to reach the bed surface before they become fully dissipated into an air-fluidised particulate phase. At higher flow rates and bed heights the immersed tube continues to have a marked influence on the behaviour of the bed; the bubbling appears chiefly at the surface directly above the sides of the tube, and between these two bubbling regions the surface is not broken by erupting bubbles, although there is some particle movement. Fakhimi (27) used a capacitance technique to detect the initiation of fluidisation at the sides of an immersed tube by measuring the time-average voidage fraction near a tube in an air-fluidised bed.

2.14.2 An Array of Tubes

Glass (39) observed the effect of thirteen 1 cm diameter cylinders mounted in three horizontal rows (4 - 5 - 4) on a 2 cm square pitch on the behaviour of a 2-D air-fluidised bed. When rising air bubbles met this tube array, they generally passed right through it unchanged, commonly on a diagonal path. Bubble splitting was not

often observed, except when bubbles larger than the tube-size made direct collisions with the tubes. However, when this occurred bubble coalescence usually made good the damage in a short distance above the tube array, and thus, with regard to size and number, the bubbles above the array were not noticeably different from those below it. This observation strongly suggests that unless the array of tubes almost fills the bed the influence it has on the average bubble size is small. However several authors have reported that the presence of a tube-array in a fluidised bed has the effect of reducing the bubble sizes.

Whitehead et al (119) reported that incorporating a bundle of horizontal tubes in a fluidised bed has the effect of markedly reducing the bubble size compared to the bubble size at corresponding conditions in an open bed. They calculated that the presence of tube bundle produced a much more uniform bubble distribution, indicating a reduction in the axial mixing of gas and solids.

Grace and Harrison (51) reported that surfaces which are inclined to the horizontal encourage the channelling of gas on their under-sides and particle defluidisation on their top-sides, both effects detrimental to good gas-solid contacting and good bed-surface heat exchange.

Chandran (9) experimented with a single horizontal tube immersed in freely-bubbling 3-D gas fluidised bed as well as a 10-row tube-bundle. One of the tubes in the bundle was instrumented and was placed at two different positions within a ten-row bare tube

bundle. Capacitance probe measurements on the surface of horizontal tubes showed that local bed-surface contact dynamics depended strongly upon gas flow-rate and circumferential position. In general, it was observed that at low flow rates close to minimum fluidisation conditions, the top portion of the tube remained covered by a dense emulsion, the sides of the tube experience a renewal type of contact with alternating voids and dense packets, and the bottom portion of the tube tends to be continuously washed by a gaseous medium with some entrained particles. These circumferential differences were seen to diminish with increasing flow rate.

The values of the dense phase residence time and the fractional contact time of the bubble phase were observed to vary significantly with gas flow rate and circumferential position. The data indicated that the contact characteristics are complex in the bubbly flow regime but become more ordered in the slug and turbulent flow regimes, as the flow rate is increased.

Chandran also concluded that the dense phase contact occurred more often for a tube at the inner-row position than for a tube in the bottom-row of the bundle.

Newby and Keairns (75) studied bed-to tube heat transfer rates within compact tube-bundles and heat transport rates by bed mixing between parallel, horizontal tube-bundles. Their results showed that the compact tube-bundles improved bubble distribution in the air-fluidised bed of 80 μm magnesia powder at velocities up to 30 U_{mf}.

Rooney (90) studied particle movement around an immersed horizontal tube by photographic and capacitance techniques. The former studies were performed by cine-filming an inclined mirror inside a transparent tube, while a segmented electrode on the tube surface was used for the capacitance method.

Bubble frequency could not be measured from a frame by frame analysis of the film (i.e. photographic method), as the bubbling did not give rise to discrete events. But the following general features were observed:

(a) There was often no clear distinction between the bubble phase and the particulate phase.

(b) Bubbling was highly irregular and disordered - unlike bubbles in a freely bubbling bed.

(c) "Fingers" of particles extended into the bubbles.

(d) Particles from the defluidised cap resting on the upper surface of the tube cascaded down over the sides of the tube as a bubble moved past the tube.

(e) There was considerable lateral movement, both of bubbles and of particles, along the axis of the tube in either direction.

(f) Between the limits investigated (tube diameter from 30 mm to 80 mm), tube diameter did not seem to have a strong effect on the general pattern of flow as a function of gas velocity.

(g) At U = 0.5 U_{mf}, fluidisation was initiated at the sides of the tube.

(h) As the gas velocity increased to nearly minimum fluidising, the fluidised band became continuous and wider.

(i) From film taken of the top of the tube, the defluidised cap was seen to be mobile, even at low fluidising velocities. Bulk shifting of the cap was seen at 1.25 U_{mf}, and particle residence times at the surface of the tube were estimated to be of the order of a few minutes. At 1.75 U_{mf}, particles were shifted across the top of the tube into the path of rising bubbles, so that the residence time was reduced to the order of seconds. At 2 U_{mf}, occasional bubbles swept right across the top of the tube, entirely displacing the defluidised cap. At 2.5 U_{mf}, the cap was swept off regularly from either side.

She extended this investigation to consider the effect of a tube bundle submerged in a three-dimensional bed. The bundle consisted of seven tubes in a centred hexagonal arrangement, with the inter tube spacing being equal to the tube diameter (= 37 mm). She reported that the main differences measured for a tube in a bundle as compared with a single tube, were at low gas velocities. At low velocities, the bubble chains left the tube at a greater angle from the vertical, so that interference between the tubes was most likely.

The effect of the tube bundle was to decrease the stability of the defluidised cap. The voidage at the top of the tube was higher at a given flow rate for the tube bundle than for a single tube. At higher gas velocities ($\sim 4\ U_{mf}$), if the tubes were close enough together, the particle contact at the sides of the tube could become very poor; bubbles generated by one tube could come into contact with the adjacent tubes.

Heat transfer studies on a single tube and tubes in bundles have suggested that the tubes do not interact until spacing is less than about two tube diameters. So, for the arrangement used by Rooney, interaction is to be expected.

CHAPTER 3

Experimental Apparatus and Procedure

3.1 Apparatus

3.1.1 The Bed

A schematic diagram of the fluidised bed is shown in Fig. 3.1 and a photograph of the assembled apparatus in Fig. 3.2. It consists of a three-dimensional bed of rectangular cross-section 48 x 28 cm. The bed depth can be increased to about 100 cm above the distributor and readings taken with the probe up to 70 cm. Air from a compressor is passed through a humidifier (to reduce electrostatic effects), a rotameter (to measure the volume flowrate) is finally introduced to the calming section of the bed (height 16 cm) below the distributor plate.

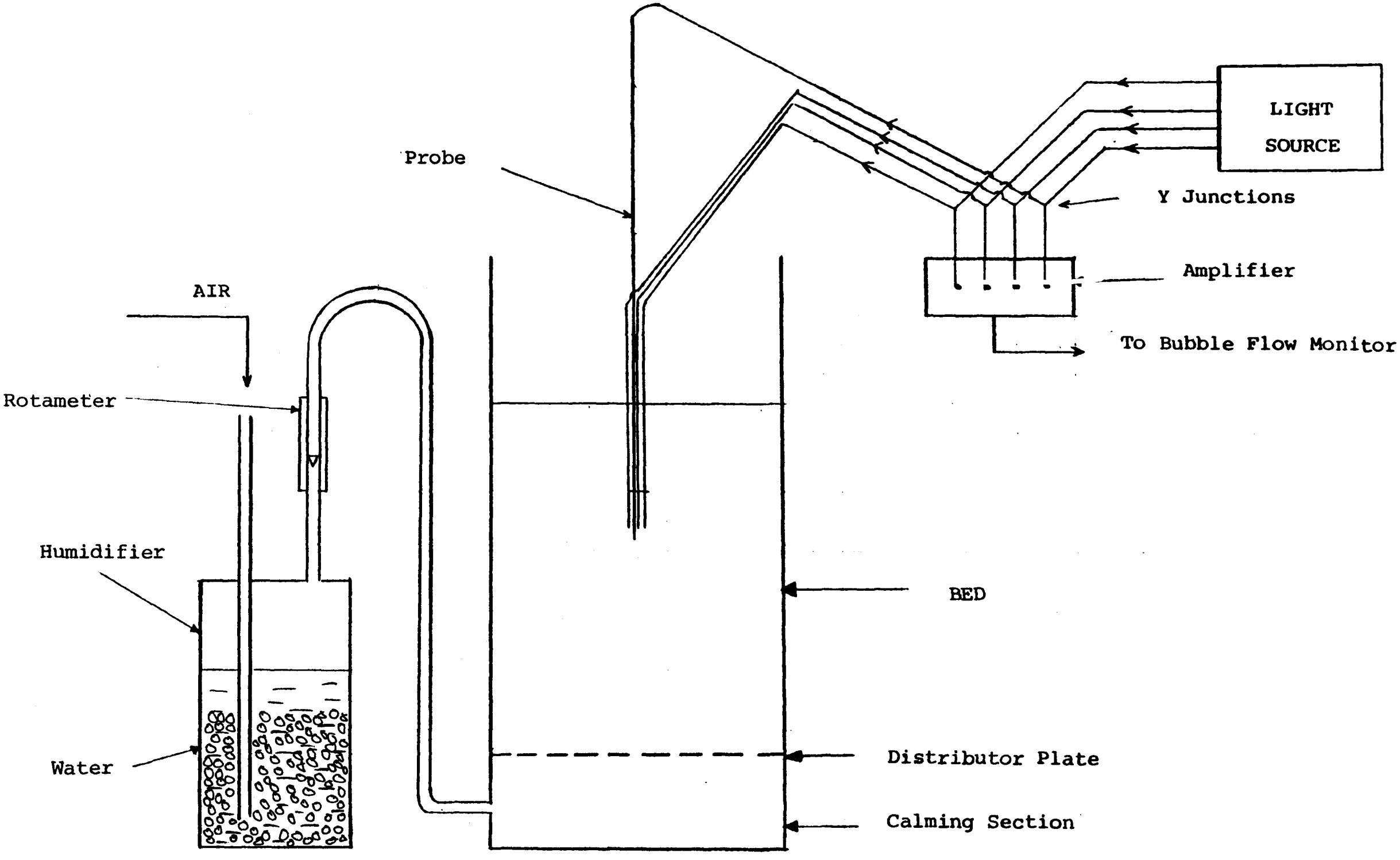
LIGHT
SOURCE
Probe
Y Junctions
Amplifier
To Bubble Flow Monitor
AIR
Rotameter
Humidifier
Water
BED
Distributor Plate
Calming Section

Figure 3.1

Fig. 3.2 The photograph of the assembled apparatus

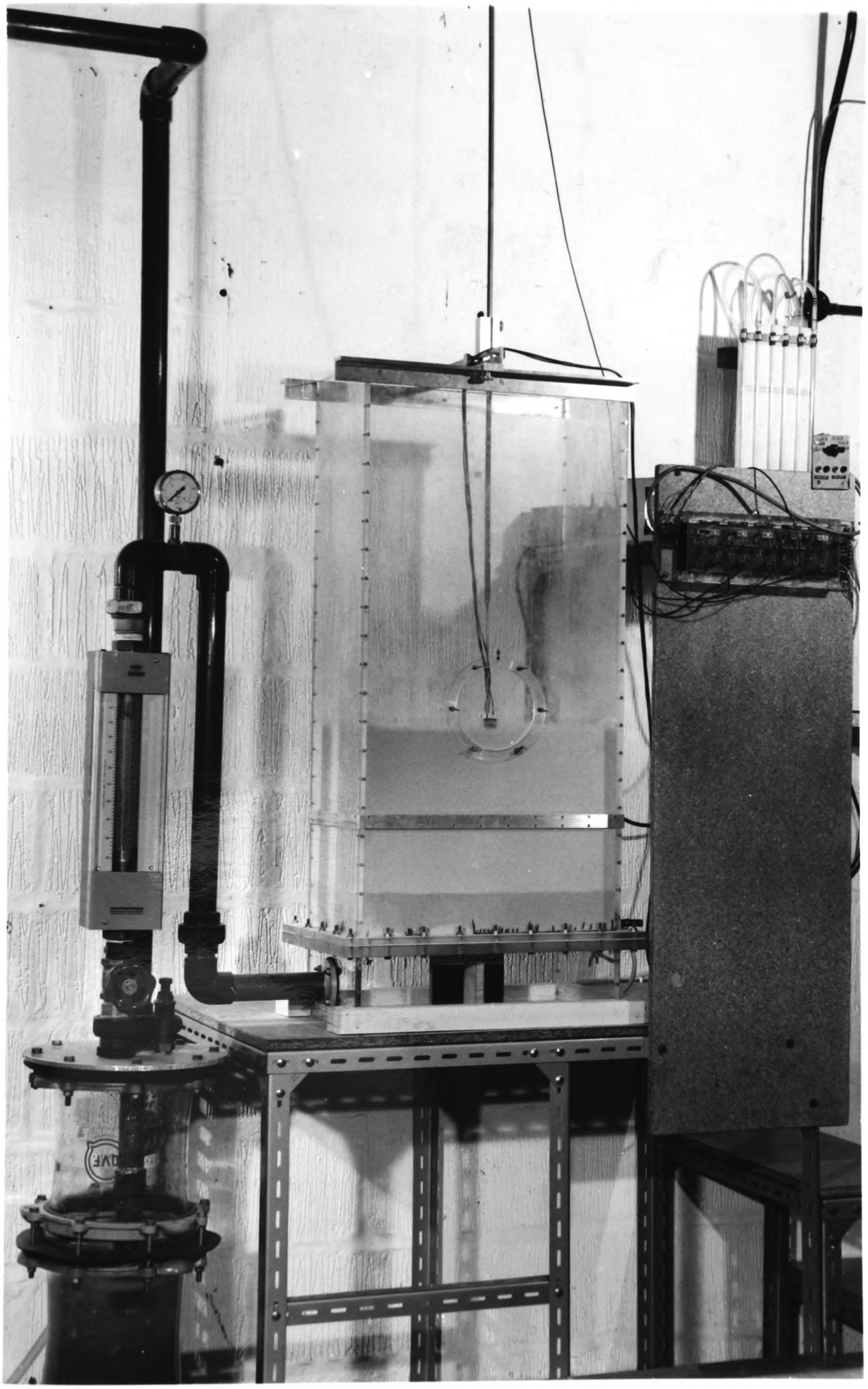

Two distributor plates were used. One was a porosint sheet 5 mm thick and of pore size 30 - 40 μm. The other, a multiorifice distributor made of 5 mm thick mild steel, had 66 perforations, each 3.2 mm in diameter, symmetrically distributed on a 12 x 7 cm grid as shown in Fig. 3.3, below.

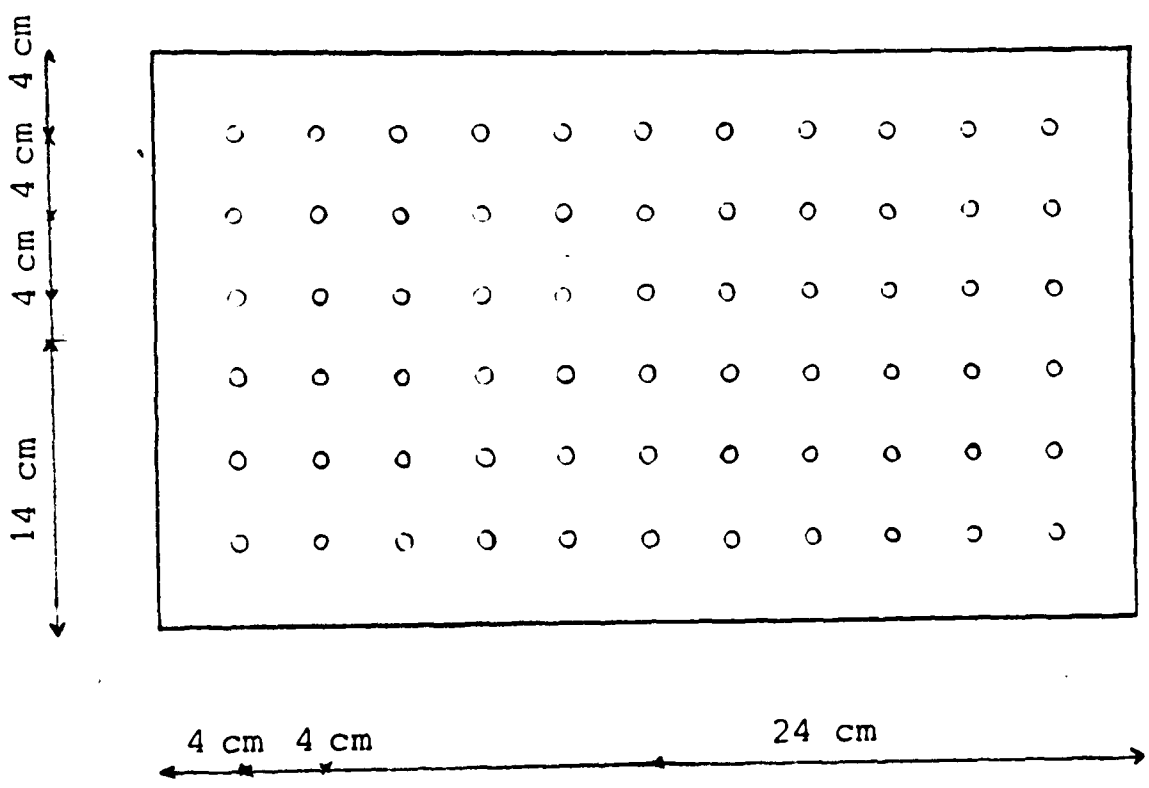

Fig. 3.3 Multiorifice Distributor

The distributor plate was supported by a flange at the top of the calming section. Two pressure tappings, 5 mm below and one 5 mm above the distributor plate enabled the pressure drop readings to be taken, the latter being used to determine the minimum fluidisation velocity. The bed pressure was measured by water manometers.

The fluidised material in these experiments was a round sand of density 2.50 g/cm^3, a minimum fluidising velocity of 0.95 cm/sec. (Figs. 3.4 and 3.5), and the size distribution given in Table 3.1 below.

Sieve Aperture μm	Weight % Retained
250	1.8
210	1.7
180	1.8
150	35.4
125	36.2
105	10.3
90	7.3
75	2.9
45	1.6
-45	1.1

TABLE 3.1

Fig. 3.4

Δp - U Relationship for

Porosint Distributor

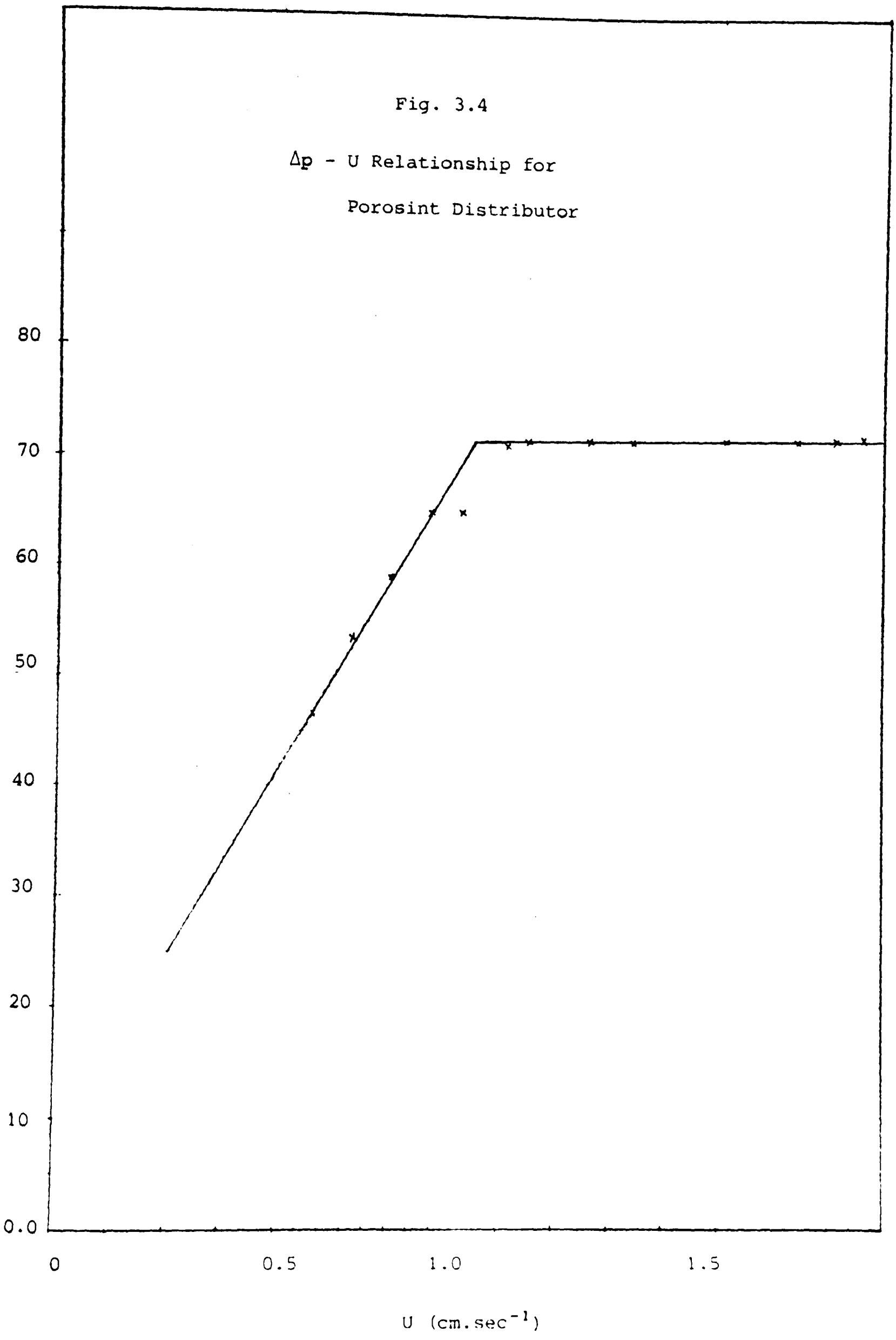

Fig. 3.5

Δp - U Relationship for Multiorifice Distributor

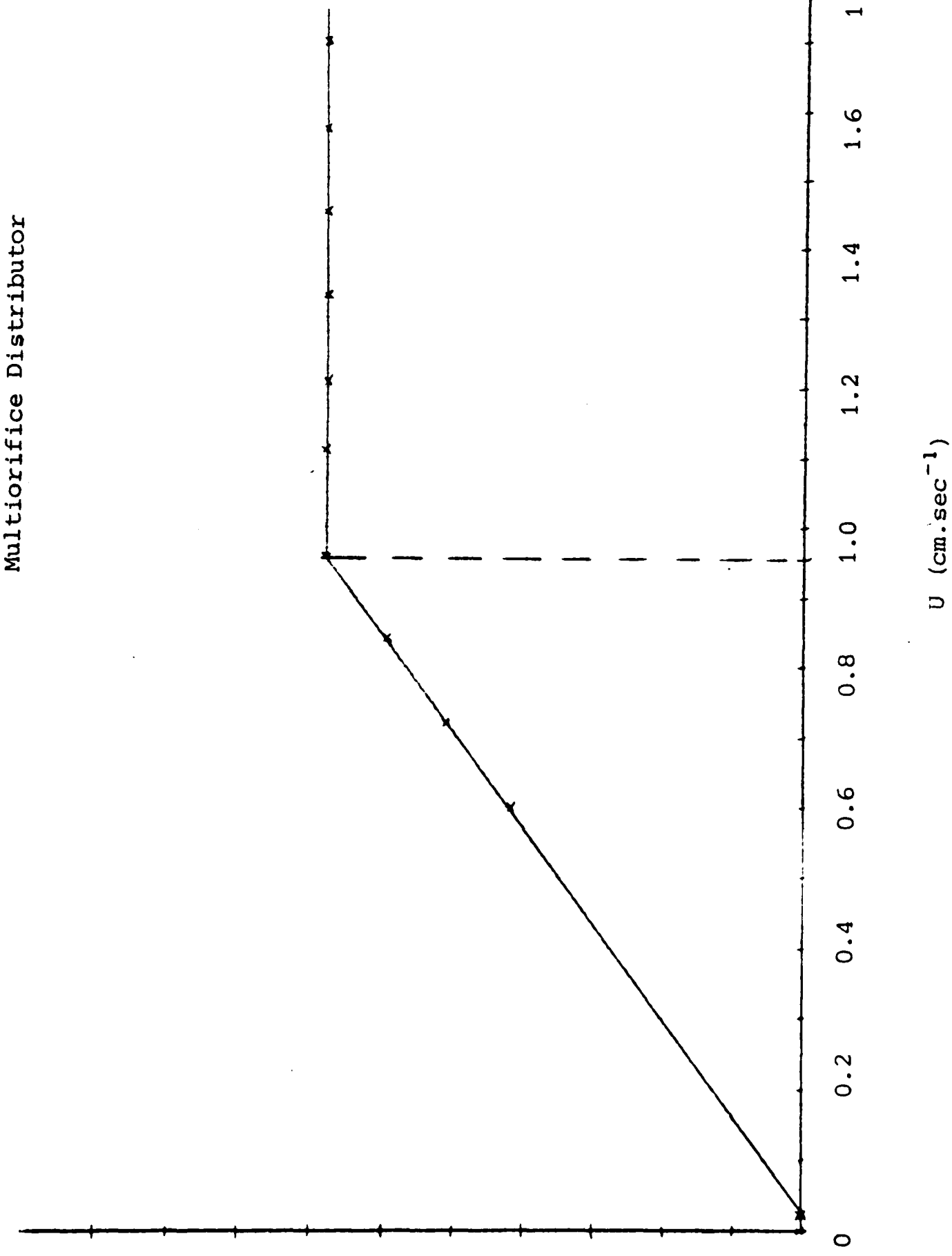

The mean diameter of the sand particles was found to be 144 μm. The minimum fluidisation velocity is measured by the bed pressure-drop technique, it being defined by the intersection of the graphical asymptotes of the two sections of the $\Delta p - U$ curve during the increase and/or decrease in gas flow rate, as is shown in Figures 3.4 and 3.5.

Minimum fluidisation velocity for this material was measured using this procedure, in both beds described above and in a 150 mm diameter bed of round cross-section, 250 mm deep and with a porous paper distributor. The result (U_{mf} = 9.5 mm. sec^{-1}) was exactly the same in both determinations, (increasing flowrate).

The operating air flow rate was varied between 2 X and almost 4 X the minimum * required to fluidise the bed. These resulted in the following superficial fluidising velocities:

Gas Flow Rate Lit/min.	Superficial Fluidising Velocity $cm.sec^{-1}$
155	1.87
200	2.41
250	3.01
300	3.61

* (Minimum fluidisation velocity = 0.95 $cm.sec^{-1}$)

Some experiments were carried out at a low superficial fluidising velocity of 13.6 $mm\,s^{-1}$. However, results collected under these conditions (particularly the bubble rise velocities) were very irreproducible. Higher superficial velocities were therefore used in most of the experimental work.

3.1.2 Probe

Park (80) and Rigby et al (88) developed a two-element resistivity probe to examine two and three-phase fluidisation mechanics, while Werther and Molerus (116) used a similarly designed capacitance probe in non-conducting systems. In these cases, lack of information about the point of impact of the probe on the bubbles frontal surface leads to uncertainties in the size and velocity distributions.

Burgess and Calderbank (6) designed a five-channel resistivity probe which was able to measure the local bubble interface angle as well as size and velocity. This was coupled via a high-speed analogue-digital converter to a digital computer. Pereira and Calderbank (82) developed a compound fibre-optic bubble sensor which was used to investigate bubble properties in gas-liquid froths. Its advantages were judged to be applicability to a wider range of systems than a resistance probe, together with a small size which made it less obtrusive than many designs of capacitance probe. This probe was modified and used in gas-solid fluidised beds.

3.1.3 Compound Optical Probe and Bubble Flow Monitor

The use of fibre-optic probes to detect the presence of bubbles in liquids was described by Geake and Smalley (33). These consist of a fibre light-guide which conveys light to a specially-shaped terminal (Figure 3.6). If the probe is in a gas of low refractive index the light is totally internally reflected and returned through the guide to a sensor. If, however, it is immersed in a liquid of high refractive index the light is transmitted and dissipated. The

transition from one mode to the other produces a step-change in reflected light intensity which is used to detect the passage of a bubble boundary.

Such probes are also effective in fluidised beds, although here the polarity of the signal is reversed. Light is reflected back up the guide when its end is immersed in reflective particles but is dissipated when the terminal is in a particle-free void.

The compound probe consists of a leading sensor surrounded by three coplanar trailing probes, as shown in Fig. 3.7. A bubble is judged to be co-axial with the leading probe if it is later sensed at the same time by each of the three upper probes. The time delay between making the lower and upper contacts is used to calculate the bubble rising velocity, while the time between making and breaking the leading contact is used to calculate the nose-to-floor height of the bubble. The smallest height which can be measured is thus limited by the vertical separation of the leading and coplanar probes.

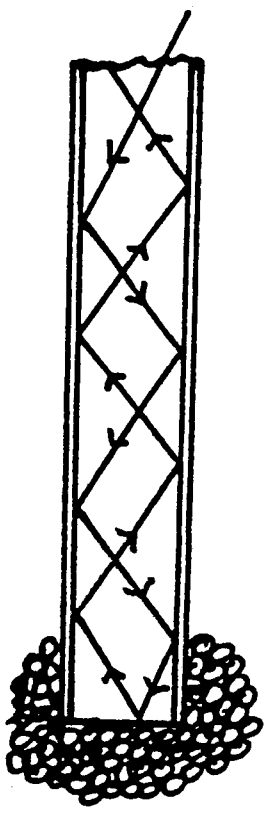

In particles -
light reflected back

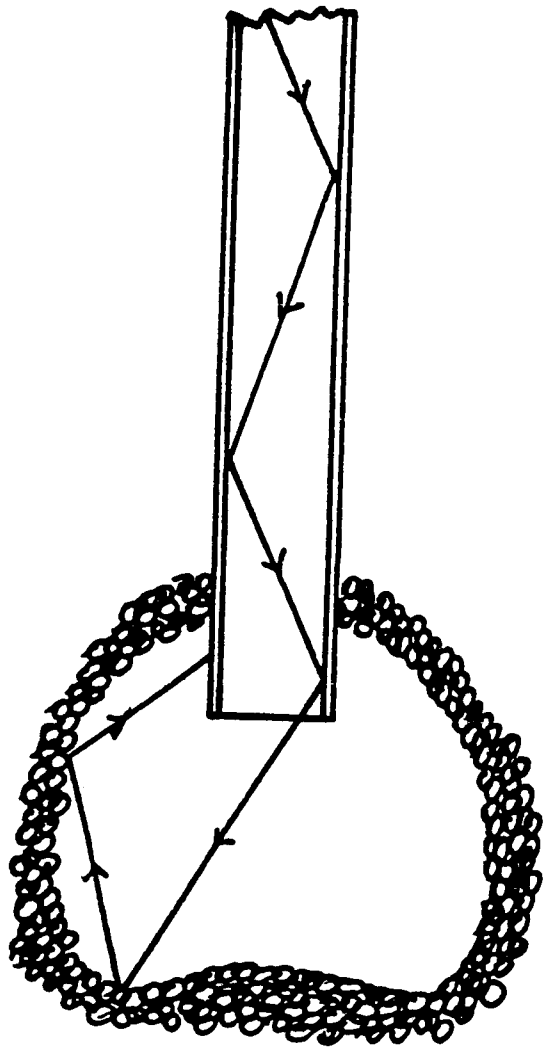

In void - light
transmitted and
dissipated.

Fig. 3.6 Operation of fibre-optic light probe.

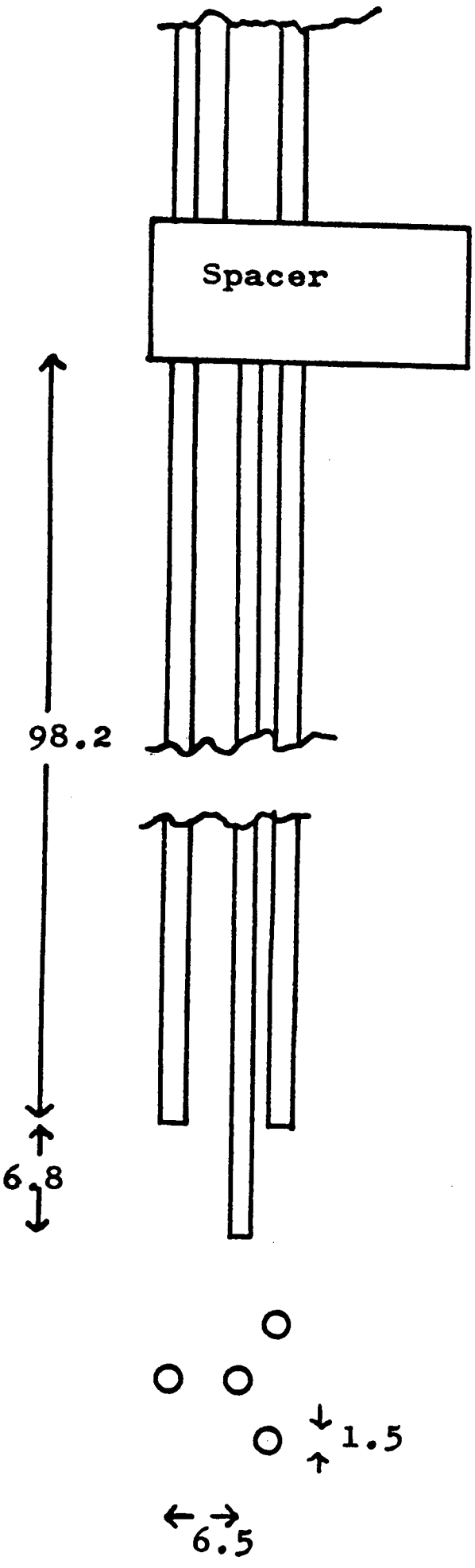

Fig. 3.7
Compound 4-sensor optical probe.
Dimensions in mm.

Pulses from the four channels are fed to a microprocessor-based bubble flow monitor, developed in cooperation with the Wolfson Microelectronics Research Unit of Edinburgh University. This tests pulse sequences for the following criteria:

(a) that all channels are initially in the same "break" mode;

(b) that all the lower and the three upper probes "make" contact in that order and then "break" it in the same order;

(c) that the three upper probes all "make" contact within some arbitrary short-time interval;

(d) that all probes return to the same "break" mode.

These tests ensure that all sampled bubbles hit the probe squarely and free from interference from other bubbles. Since only bubbles which are coaxial with the probe are counted, the results are a true sample of the bubble population at a given point in the bed and any bias towards counting larger bubbles is eliminated. The measured bubble size is thus the nose-to-floor height along the central axis of the bubble. If the bubble should break up in the period of measurement, this sequence of events would not be satisfied and the bubble would not be sampled.

The following elapsed times are recorded:

T_1 : delay between leading and upper contacts.

T_2 : time of immersion of leading probe.

Jitter: time between first and last contacts at the three upper coplanar probes.

All these times are fed as 4-bit nibbles (half a byte) to the microprocessor system. Sampling is immediately recommenced. The microprocessor uses the stored value of the vertical probe separation ℓ to calculate the rising velocity $U_a = \ell/T_1$ and the height $h = \ell.T_2 /T_1$ for each bubble. It forms in its memory a histogram of bubble size with smallest height ℓ and 100 slots of width $\ell/4$. Any bubble with a size outside this range is discarded. Each slot is assigned a mean bubble rising velocity. After each run, the histogram of bubble sizes and rise velocities is transferred to paper tape via a teletype, in the form of hexadecimal numbers.

Jitter is the time between the first arrival of a bubble at one of the three coplanar probes and the subsequent complete immersion of all three of them. The hardware measures the jitter time in units 32 coarser than the current timing range and also compares the actual jitter time with the maximum allowable jitter (entered during the keyboard preamble) for both leading and trailing edges of the bubble signals. The result of this comparison is made available to the microprocessor so that the invalid events (jitter too great) can be discarded. The units of jitter time as entered via the keyboard (and as displayed) are 0.1% of the current timing range. The maximum jitter which can be preset is 124 (12.4% of the current timing range). The timing range selection character has the following significance.

Range Characteristic	Range Selected	Basic Time unit
1	0 - 65 ms	1 μs
2	0 - 325 ms	5 μs
3	0 - 650 ms	10 μs
4	0 - 1300 ms	20 μs

During the keying procedure, the characters entered are displayed in the right hand half of the front panel display for reference. The coding of the input parameters is as follows:

PARAMETER	CHARACTERS KEYED 1	2		LAST	DEFAULT VALUES
N (event count)	B	0	1 - 9999	*	1000
1 (probe separation)	B	1	length in μm	*	
V_S (superficial gas velocity)	B	2	velocity in mm/sec	*	
JM (maximum jitter)	B	3	1 - 124	*	50
R (timing range)	B	4	1, 2, 3 or 4	*	1
K (system constant)	B	5	in $mm^2\ sec^{-\frac{1}{2}}$	*	
SW (slot width)	B	6	1 - 10	*	4
PS (probe selection)	B	7	1 or 4	*	1

The maximum number of characters in any one input line is seven. Before 'B' mode can be entered, parameters ℓ, V_S and K must be entered.

The bubble flow monitor was initially made to calculate the rising velocity of gas bubbles in liquids (froth regimes) as well as various other parameters (such as gas hold-up, shape factor etc). Some of the experimental parameters entered via the keyboard (such as V_S and K), essential for those calculations, are not necessary for the purpose of our experiment. The bubble flow monitor was modified to meet the necessary requirements of this work; namely gas bubbles rising in a particulate phase, thus some of the calculations done by the monitor are not required.

3.1.4 'B' and 'C' Modes

A summary of the procedure for recording bubbles in B mode and the calculations of U_a and h were given in section 3.1.3, above. The bubble selection (and collection) in B mode are subject to two constraints imposed by the software as well as the hardware. The constraint imposed by the software (i.e. $T_1 < T_2$) ensures that bubbles greater than a fixed size, ℓ (the probe separation length), are recorded. The second constraint, imposed by the hardware, is the jitter time selection which ensures that bubbles co-axial with the probe axis are collected. The imposition of these two restrictions causes the rejection of a large proportion of small bubbles and therefore, an accurate picture of bubble frequency distributions across the bed cross-sectional area cannot be obtained. To measure the bubble frequency, free of any constraints, there is another mode of timing provided by the microprocessor, namely 'C' mode.

Starting from the condition where the leading probe (or any one of four probes) is in the emulsion phase, the measuring cycle is started when a bubble first arrives at this probe. The following elapsed times are then recorded:

T'1 : This is the time that the next bubble first arrives at the selected probe.

T'2 : This is the time that the selected probe spends immersed in the first bubble.

If n = number of C mode events,

$$F_C = \frac{10\ n}{\sum_1^n T'1} \qquad (0.1\ \text{Hz}) \qquad 3.1$$

where F_C = bubble frequency in C mode.

C mode can be entered without any experimental parameter entry. Each recorded bubble yields a T1 and T2, and during data collection the microprocessor merely keeps a running total of the number of events and T'1 and T2' in seconds.

It was found that the frequencies measured in this mode give a more realistic picture of frequency distributions in the bed.

T'2 is used in calculating the gas hold-up by time, H* defined by:

$$H^* = 1000\ \frac{\sum_1^n T'2}{\sum_1^n T1'} \qquad (0.1\%) \qquad 3.2$$

This calculation is, obviously not required in our experiments.

Fixed rails at the top of the bed permit the probe to be moved in two horizontal directions as well as vertically, giving almost complete coverage of the whole bed volume.

The light source was a Swiss-made Intralux 500-H modified to run from a stabilised 24-volt D.C. power supply to eliminate 100 cycle ripples. The bed, light source, probe and Bubble Flow Monitor are shown in Fig. 3.2.

3.2 Experimental Procedure

The vertical separation of the leading and coplanar probes was measured using a travelling telescope before starting each run and keyed into the microprocessor system. This opportunity was also used to check that the three upper probes were coplanar. The bed was fluidised and then defluidised (to ensure a flat surface), the probe was positioned in the bed (x, y and z co-ordinates of the sampling point carefully measured and adjusted), and the bed was fluidised again to the desired velocity.

Figure 3.8 shows the sampling points across the bed cross-section with reference to the perforations of the multiorifice distributor.

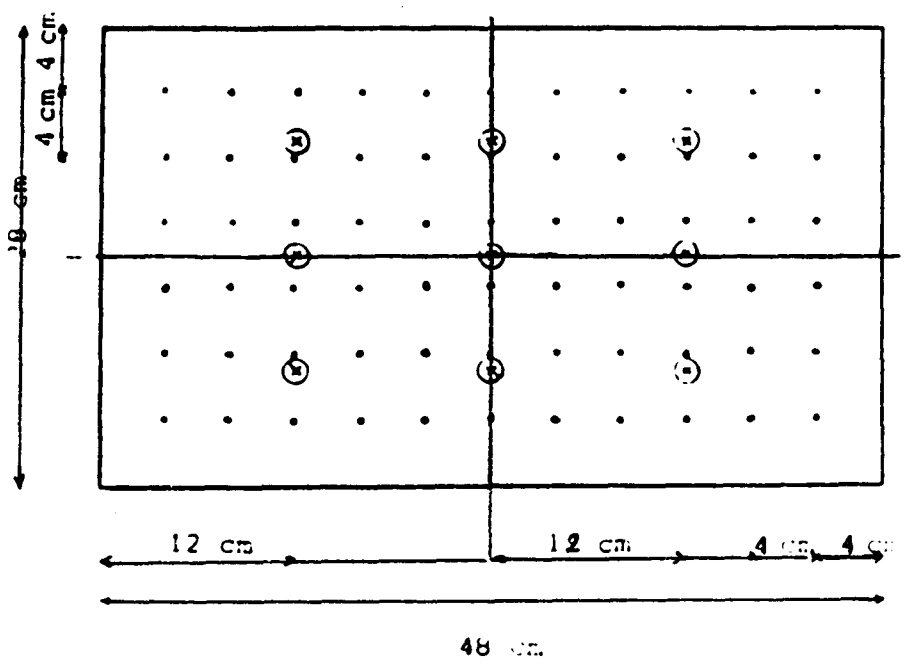

Fig. 3.8

These nine symmetrically distributed points were used for positioning of the probe tip at six different planes, 20, 30, 40, 50, 60 and 70 cm above the distributor plate.

When the probe was in position, the power source and the light source were switched on and the microprocessor initialised. A

prolonged period of data collection was commenced and when a sufficient number of bubbles (as indicated on the monitor display) had been collected the run was terminated. Data was transferred to paper tape, fed to an index file and analysed using the Edinburgh University's main computer.

3.3 Tube Bank

Heat removal from gas fluidised beds may be carried out by the use of tubes, containing a circulating coolant. Since the mobile particles surrounding the tubes are solid and have a high heat capacity, a heat transfer coefficient of about five times greater than for gas/solid contacting can be obtained.

A tube bank, shown in Figure 3.9 was assembled and was immersed in the bed to study the effect on the bubble formation, coalescence and various bubble statistics.

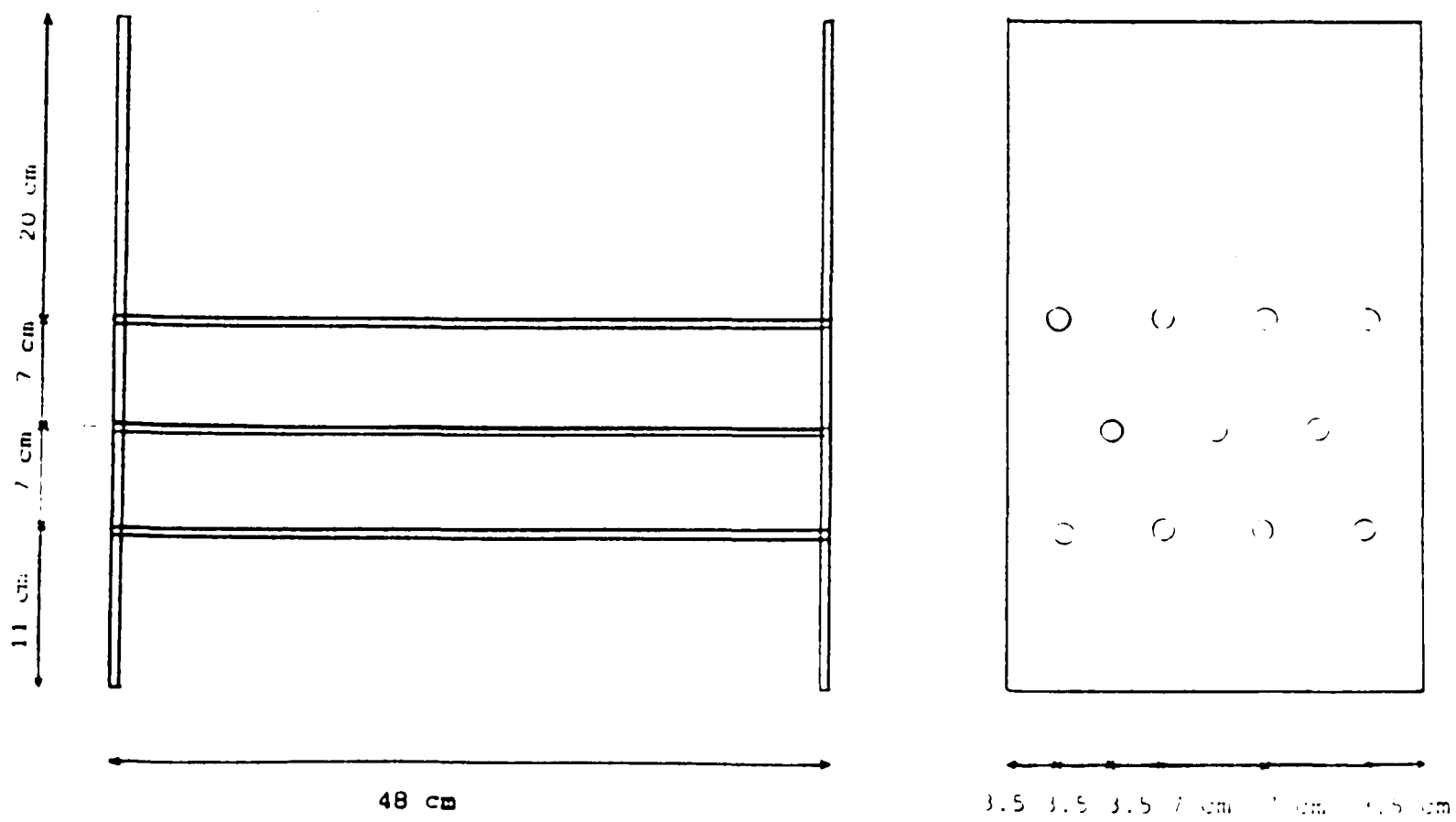

Fig. 3.9 Tube-Bank

A staggered-array of wooden tubes 1.9 cm in diameter, in 7 cm x 7 cm pitch was constructed which could be lowered down to rest ∿11 cm above the distributor plate, (Figure 3.9).

The tubes are fixed into chip-board which is 2 cm thick, thus narrowing the bed slightly. A horizontal tube arrangement was chosen since this is used in coal combustion fluidised bed furnaces.

Skinner (103) reported that a pitch/diameter ratio of 2 to 8 is used over a wide range of industrial applications.

For tube diameter of 35 mm, a decrease in pitch/diameter ratio (over the range investigated), decreased the heat transfer coefficient by 15 - 20%. A pitch/diameter ratio of 3.5 was therefore used in these experiments, as representing common industrial practice with heat transfer tubes in fluidised beds. Three rows of 2 cm diameter tubes were used.

CHAPTER 4

The Relationship of Bubble Rise Velocity to Bubble Size

4.1 Bubble Rise Velocity

For each bubble encountered, the microprocessor system records T1 (time delay between signals from the leading probe and the three coplanar probes) and T2 (time of immersion of the leading probe). It uses these measurements to calculate the bubble rise velocity $U_a = \frac{\ell}{T1}$ and the bubble nose-to-floor height $h = U_a.T2$ (ℓ = vertical separation of leading and coplanar probes). The bubbles are sorted into 100 intervals of vertical height h and a mean rise velocity is calculated for each interval. This permits study of the relationship between bubble size and rise velocity.

4.2 Porosint Plate Distributor

Bubble rise velocities have been measured at nine symmetrically distributed points on a 12 x 7 cm grid (Fig. 3.8) and at three superficial fluidising velocities of 1.87, 2.41 and 3.01 $cm.sec^{-1}$. At certain points, however, a very low velocity of 1.36 cm/sec, and at some others a very high gas velocity of 3.61 $cm.sec^{-1}$ were also investigated.

The points of reference used in this chapter (e.g. the position of the gas inlet), are shown in Figure 3.1, in chapter 3.

Since at low heights above the distributor and low superficial fluidising velocities, the number of bubbles large enough to be detectable by the probe is negligible, a reasonable sample could not be collected in all these 162 runs.

4.2.1 Variation of Rise Velocity with Superficial Fluidising Velocity

Fig. 4.1 shows the variation of U_a with bubble size at a height of 40 cm above the distributor plate, on the bed vertical centre line, for three different superficial fluidising velocities. The results seem not to lie on a single curve and this is possibly due to the enhancement of the rise velocity of bubbles rising in clouds compared with that of a single isolated bubble.

According to the two-phase theory of fluidisation, the rise velocity U_b of an isolated bubble is related to U_a by:

$$U_a = U_b + k\ (U - U_{mf}) \qquad 4.1$$

where U and U_{mf} are the superficial fluidising and minimum fluidising velocities. There is little agreement in the literature about the value of constant k but some authors (29) suggest 1.0.

The second term in equation (4.1) represents the fact that a bubble rises relative to the particulate phase around its nose. The latter has a velocity of its own due to the displacement of bubbles rising in a cloud.

Rowe (92), resorting to the analogy with bubbles in liquids, showed that there were adequate data for the velocity of bubble swarms and that a simple and commonly accepted relationship (Davidson and Harrison, 21) could be adapted to the fluidised bed situation . Equation 4.1 with k = 1.0 could be used. He concluded that this equation implied that the bubble velocity is augmented by an upward flow of the solids equal to the total bubble flow rate. He concluded that, although various authors (Davidson and Harrison, 21) have discussed various other equations, equation (4.1) is probably the most useful relationship in calculating the bubble rise velocity.

In extensive fluidised beds (such as the one used in these experiments), the displacement of rising bubbles can give rise to stable circulatory patterns so that k will be positive in some parts of the bed and negative in others. Burgess and Calderbank (6) showed the variation of the emulsion phase velocity vector with radial position in a cylindrical bed. Their results were in good agreement with the circulation theories of Hills (55), Freedman and Davidson (30) and Rietema and Ottengraf (87).

$$U_E = U_b - (0.71(g\,d_e)^{\frac{1}{2}} + (U - U_{mf}))$$

Figure (4.2) shows the data from Fig. (4.1) plus one set at a higher velocity, replotted using equation (4.1) in the form of U_b VS bubble size h. The points for the different fluidising velocities are rather closer together but there still seem to be systematic differences.

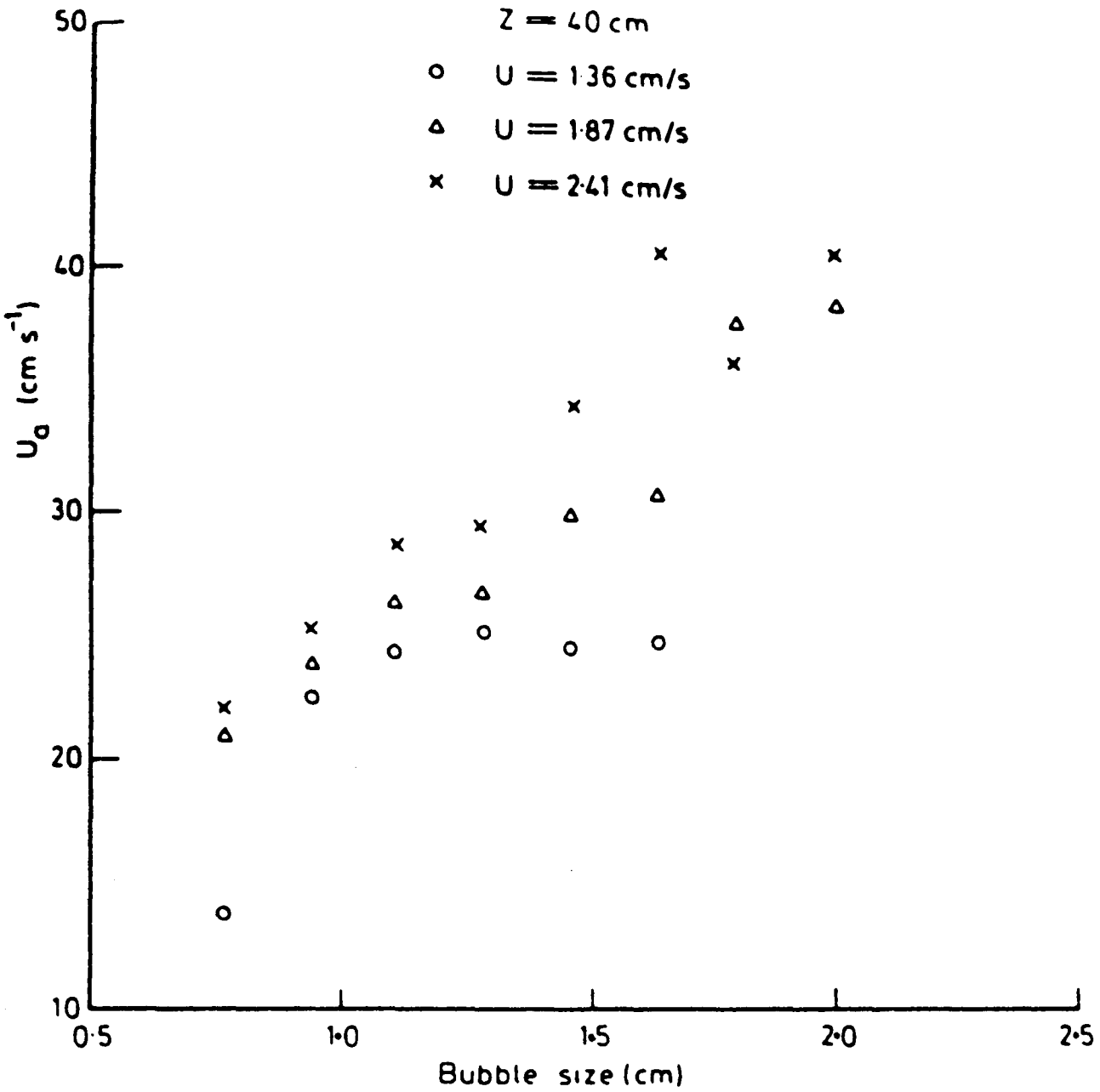

Figure 4.1 Variation of absolute bubble rise velocity U_a with bubble size h.

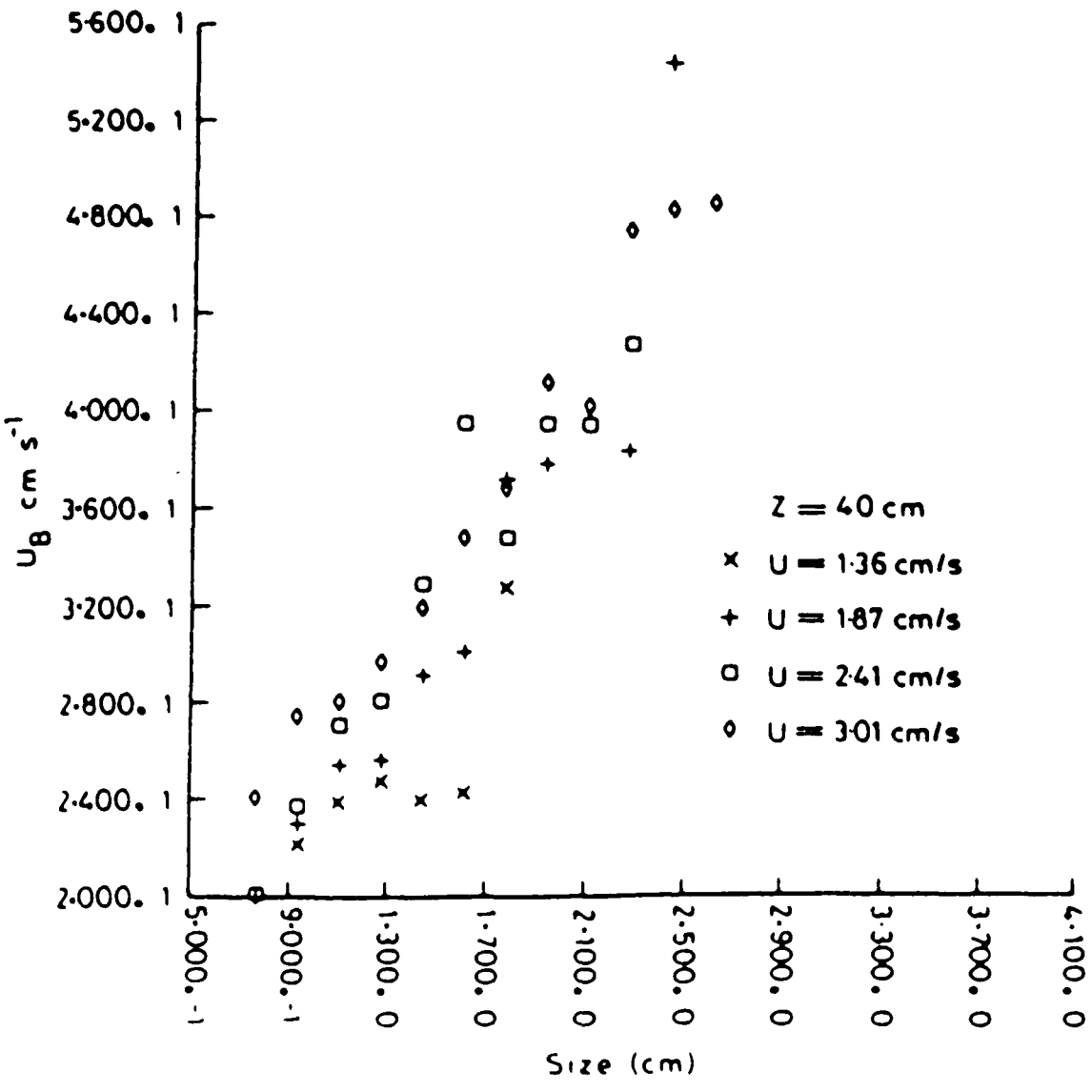

Figure 4.2 Bubble rise velocity U_B versus bubble size, h.

The data of Figure (4.2) are plotted on logarithmic axes in Figure (4.3) and a linear regression analysis has been used to fit equations of the form

$$\log (U_b) = \alpha + \beta \log (h) \qquad 4.2$$

to the data. This corresponds to a relationship of the form

$$U_b = C h^{\beta} \qquad 4.3$$

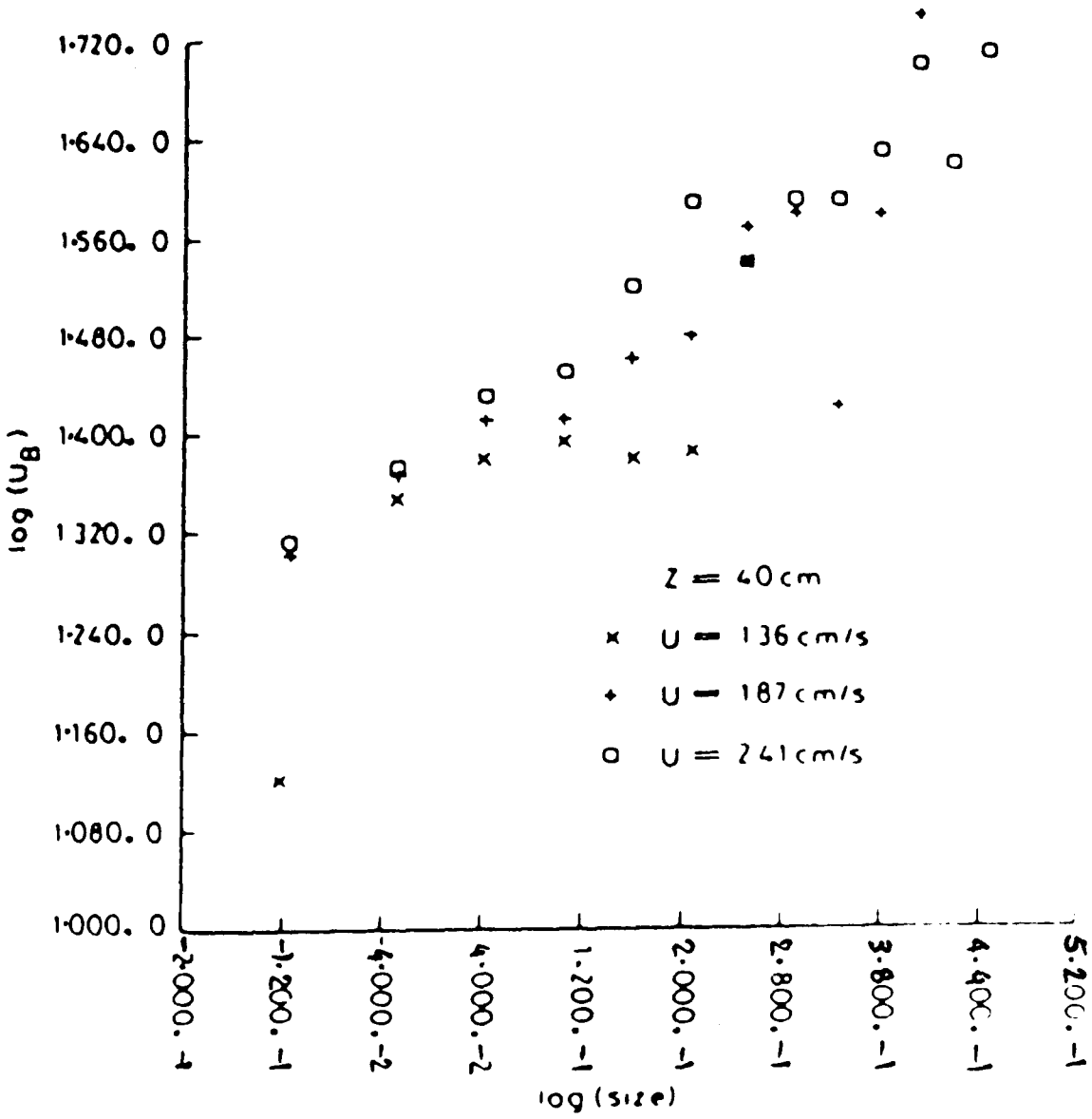

Figure 4.3 Log U_B versus log h.

The results of the regression analysis are shown in Table 4.1 below:

U cm/s	α	C	β	Correlation Coefficient
1.36	1.29	19.59	0.76	0.82
1.87	1.37	23.25	0.64	0.83
2.41	1.39	24.89	0.66	0.97
All points	1.35	22.40	0.67	0.89

TABLE 4.1

Relationship between bubble rise velocity and size at 40 cm above distributor plate

Analysis of the variance of the data (see Appendix B) suggests that the regression lines are parallel but not identical, i.e. that the "constant" C is a function of superficial fluidising velocity.

Similar calculations for 30 and 70 cm above the distributor plate give similar results: the regression lines are parallel (with slopes of 0.64 and 0.65) but not identical. (These calculations are given in Appendix C).

Figure (4.4) shows the absolute rise velocity variation with nose-to-floor height of the bubbles, at a point with co-ordinates X = 36 cm, Y = 7 cm and Z = 50 cm. Measurements were taken at this point because at these elevations the measured bubble rate on the bed centre line was too low for accuracy.

FIG. 4.4

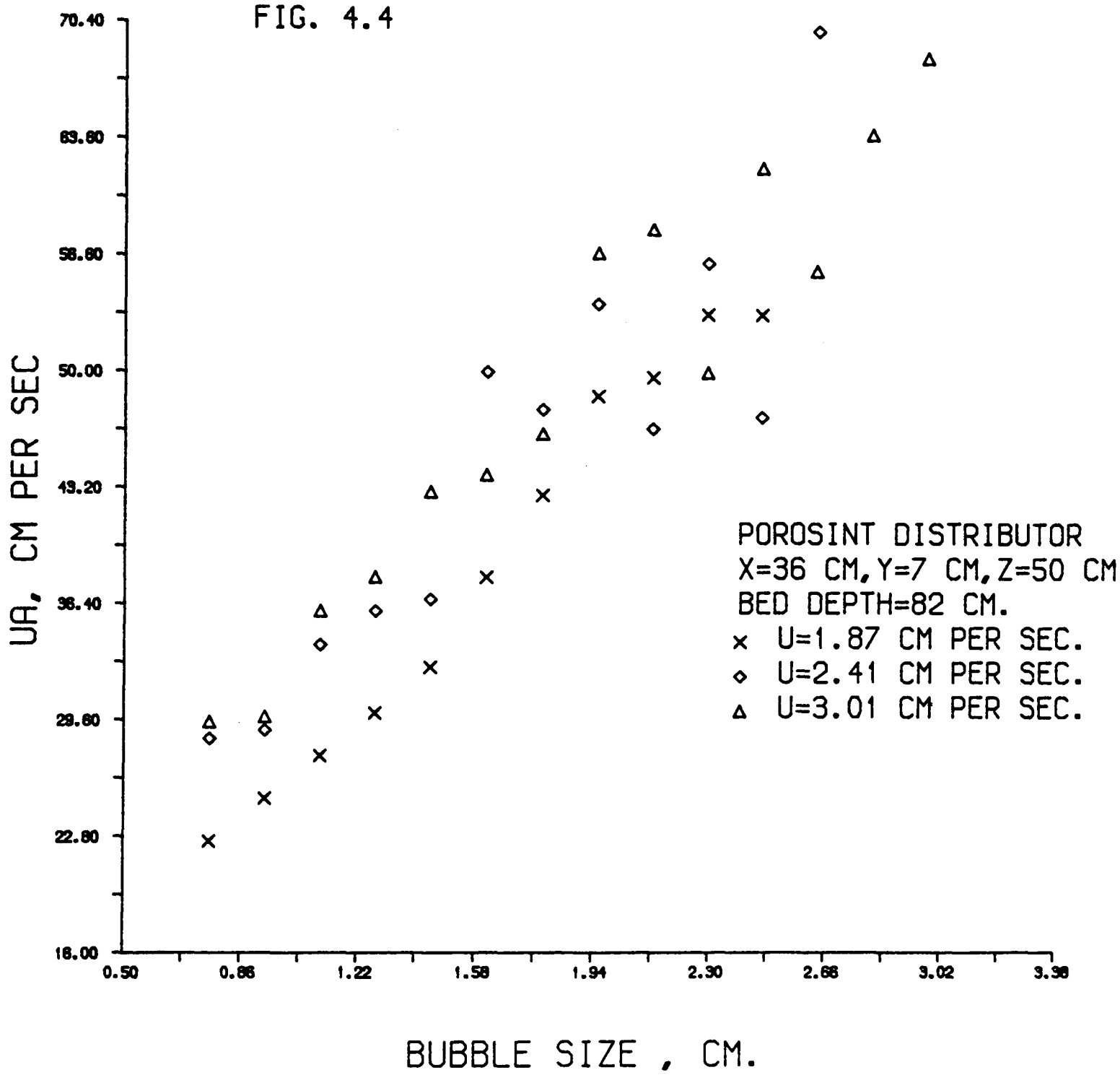
70.40
63.80
56.80
50.00
43.20
36.40
29.60
22.80
16.00
0.50
0.86
1.22
1.58
1.94
2.30
2.66
3.02
3.38
UA, CM PER SEC
BUBBLE SIZE , CM.
POROSINT DISTRIBUTOR
X=36 CM, Y=7 CM, Z=50 CM
BED DEPTH=82 CM.
× U=1.87 CM PER SEC.
◇ U=2.41 CM PER SEC.
△ U=3.01 CM PER SEC.

Three superficial fluidising velocities (1.87, 2.41 and 3.01 cm/sec) were investigated and the bed depth is 82 cm when fluidised. The rise velocity increases with the bubble size and the higher the superficial fluidising velocity the higher the rise velocities recorded, for each interval of bubble height.

Absolute rise velocities between 21 $cm.sec^{-1}$ and 70 $cm.sec^{-1}$ have been measured at this point. Equation 4.1 is used to calculate U_b from the data in Fig. (4.4) and these are plotted against the bubble size in Fig. (4.5).

Graphs show less scatter for the smaller bubbles. In Figure (4.6), the U_b - size relationship is shown for a point at Z = 60 cm above the distributor plate. The other operating conditions are maintained.

The rise velocity recorded, for each bubble size at Z = 60 cm is greater than the corresponding value measured for Z = 50 cm. This comparison is further extended to an elevation of 70 cm in Figure (4.7), where U_b - size variation is shown, for a point with X = 36 cm, Y = 7 cm and Z = 70 cm co-ordinates. The bed depth is maintained at 82 cm and the same three gas velocities are used.

A comparison of these three graphs (4.5, 4.6 and 4.7) shows the rise velocity increasing with the superficial velocity and the higher the elevation, the greater the rise velocity recorded, for each interval of bubble height.

Rise velocities of up to 80 $cm.sec^{-1}$ have been measured at the high elevation of 70 cm above the distributor plate.

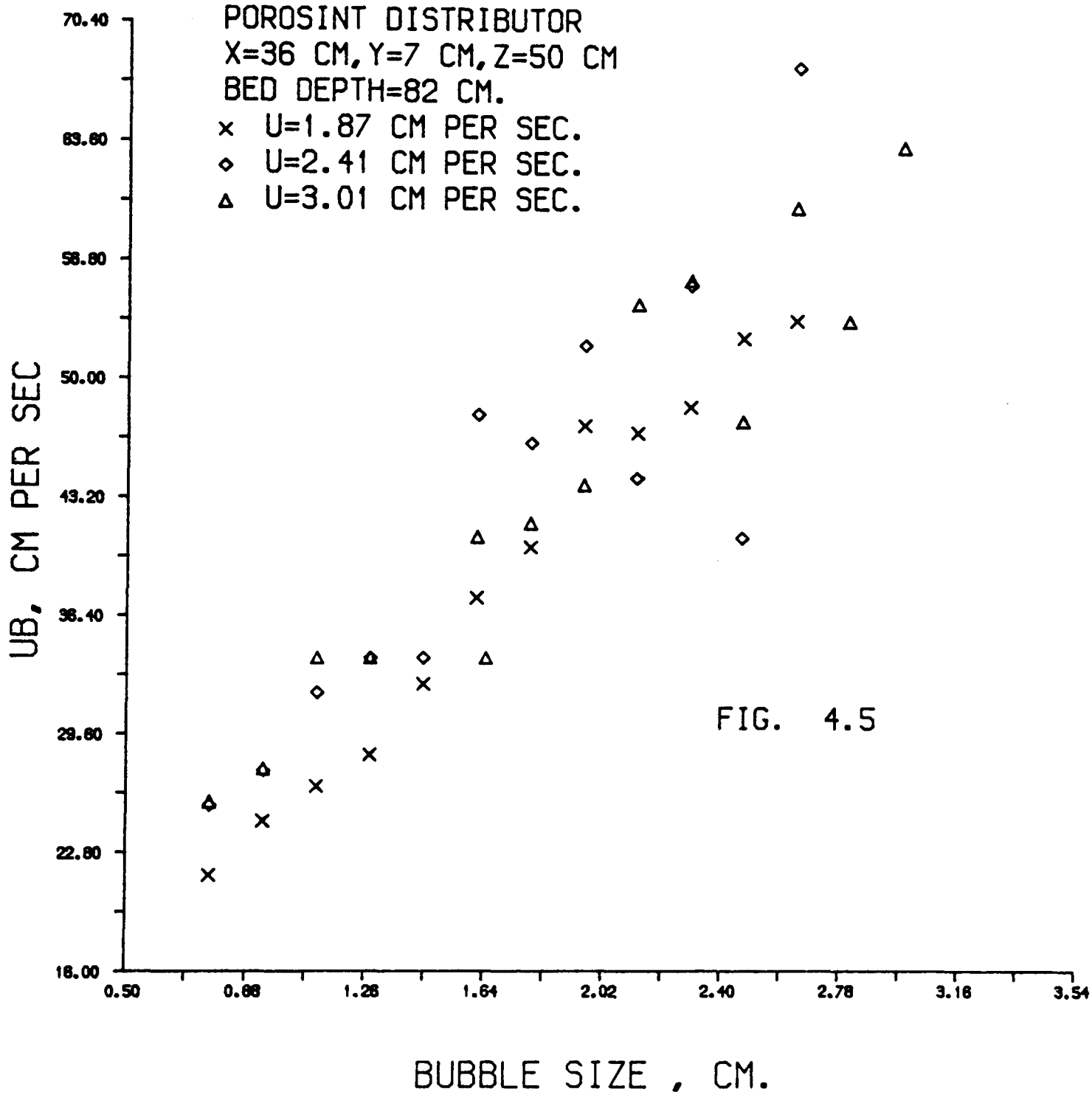
POROSINT DISTRIBUTOR
X=36 CM, Y=7 CM, Z=50 CM
BED DEPTH=82 CM.
× U=1.87 CM PER SEC.
◇ U=2.41 CM PER SEC.
△ U=3.01 CM PER SEC.
UB, CM PER SEC
70.40
63.60
56.80
50.00
43.20
36.40
29.60
22.80
16.00
0.50
0.88
1.26
1.64
2.02
2.40
2.78
3.16
3.54
BUBBLE SIZE , CM.

FIG. 4.5

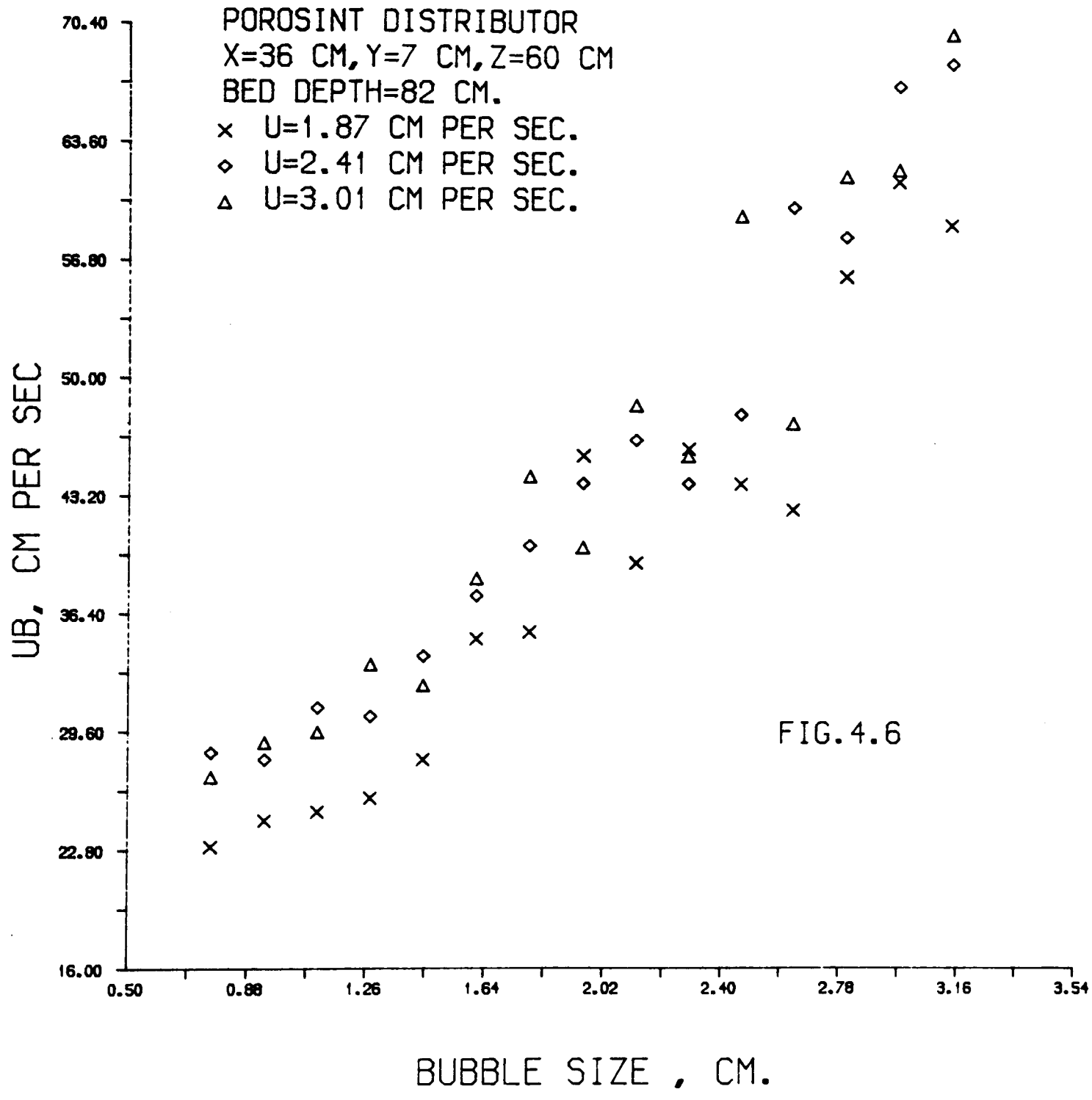
POROSINT DISTRIBUTOR
X=36 CM, Y=7 CM, Z=60 CM
BED DEPTH=82 CM.
× U=1.87 CM PER SEC.
◇ U=2.41 CM PER SEC.
△ U=3.01 CM PER SEC.
70.40
63.60
56.80
50.00
43.20
36.40
29.60
22.80
16.00
UB, CM PER SEC
0.50
0.88
1.26
1.64
2.02
2.40
2.78
3.16
3.54
BUBBLE SIZE , CM.

FIG.4.6

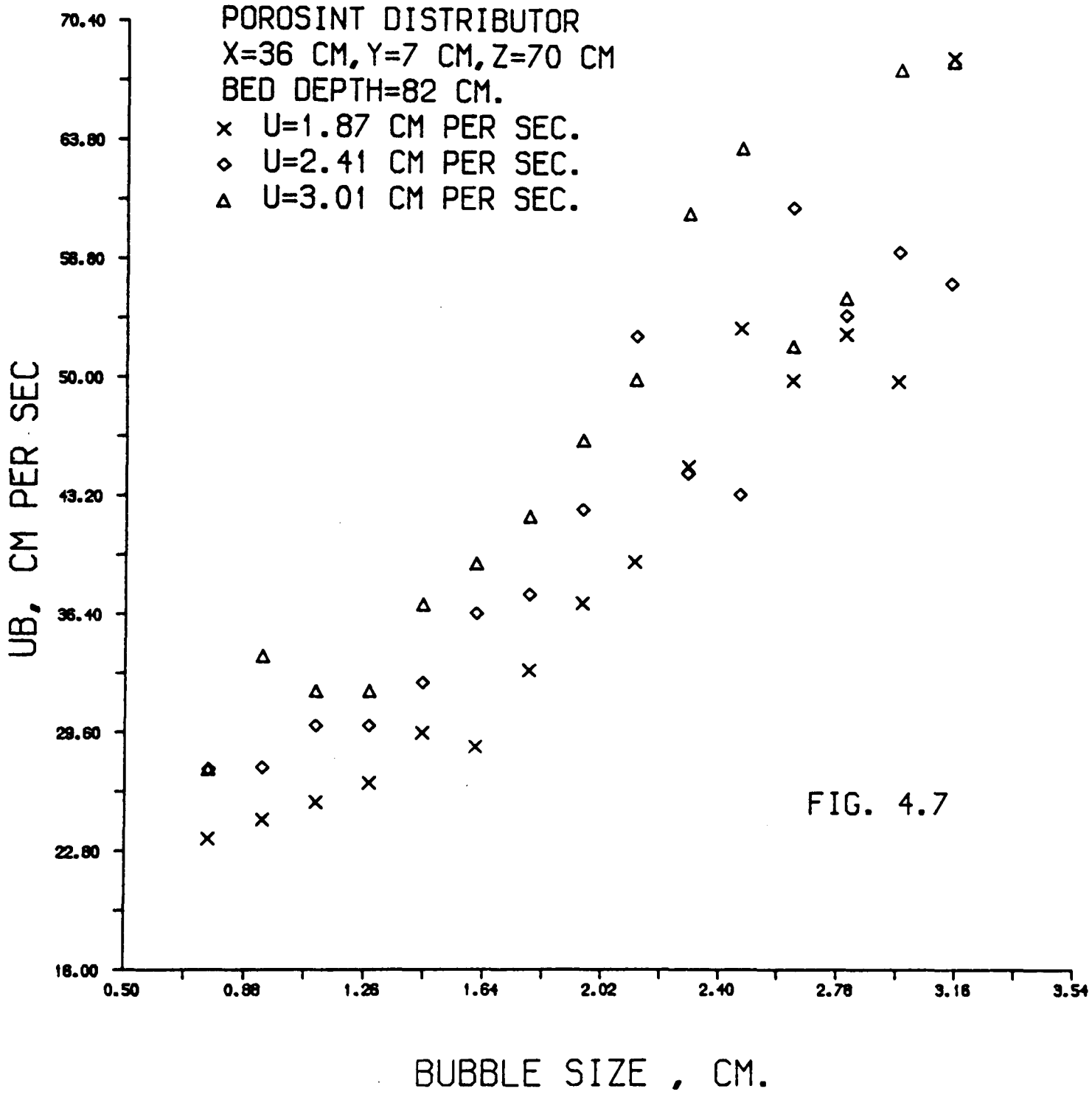
POROSINT DISTRIBUTOR
X=36 CM, Y=7 CM, Z=70 CM
BED DEPTH=82 CM.
× U=1.87 CM PER SEC.
◇ U=2.41 CM PER SEC.
△ U=3.01 CM PER SEC.
UB, CM PER SEC
70.40
63.80
56.80
50.00
43.20
36.40
29.60
22.80
16.00
0.50
0.88
1.26
1.64
2.02
2.40
2.78
3.16
3.54
BUBBLE SIZE , CM.

FIG. 4.7

4.2.2 Variation with Height above Distributor Plate

Figure (4.8) shows the variation of U_a with bubble size at a superficial fluidising velocity of 1.87 $cm.sec^{-1}$ and elevations of 30, 40, 50 and 70 cm above the distributor, on the bed vertical centre line. The relative rise velocity U_b, calculated using equation (4.1) with k = 1.0, is shown as a function of bubble size in Figure (4.9), while the data is replotted on logarithmic axes in Fig. (4.10). Once more, straight lines are fitted to the individual sets of data and a summary of the results is shown in Table (4.2) below.

z cm	α	C	β	Correlation Coefficient
20	1.34	21.79	0.70	0.91
30	1.41	25.81	0.75	0.99
40	1.36	23.15	0.65	0.83
50	1.30	20.06	0.85	0.99
70	1.45	28.56	0.68	0.96
All points	1.37	23.56	0.72	0.89

TABLE (4.2)

Relationship between bubble rise velocity and size at a superficial fluidising velocity of 1.87 cm/s.

Analysis of the variance of these results (Appendix D) suggests that all the lines have a common slope but that they are not identical, i.e. that there is a significant variation of "constant" C with height in the bed.

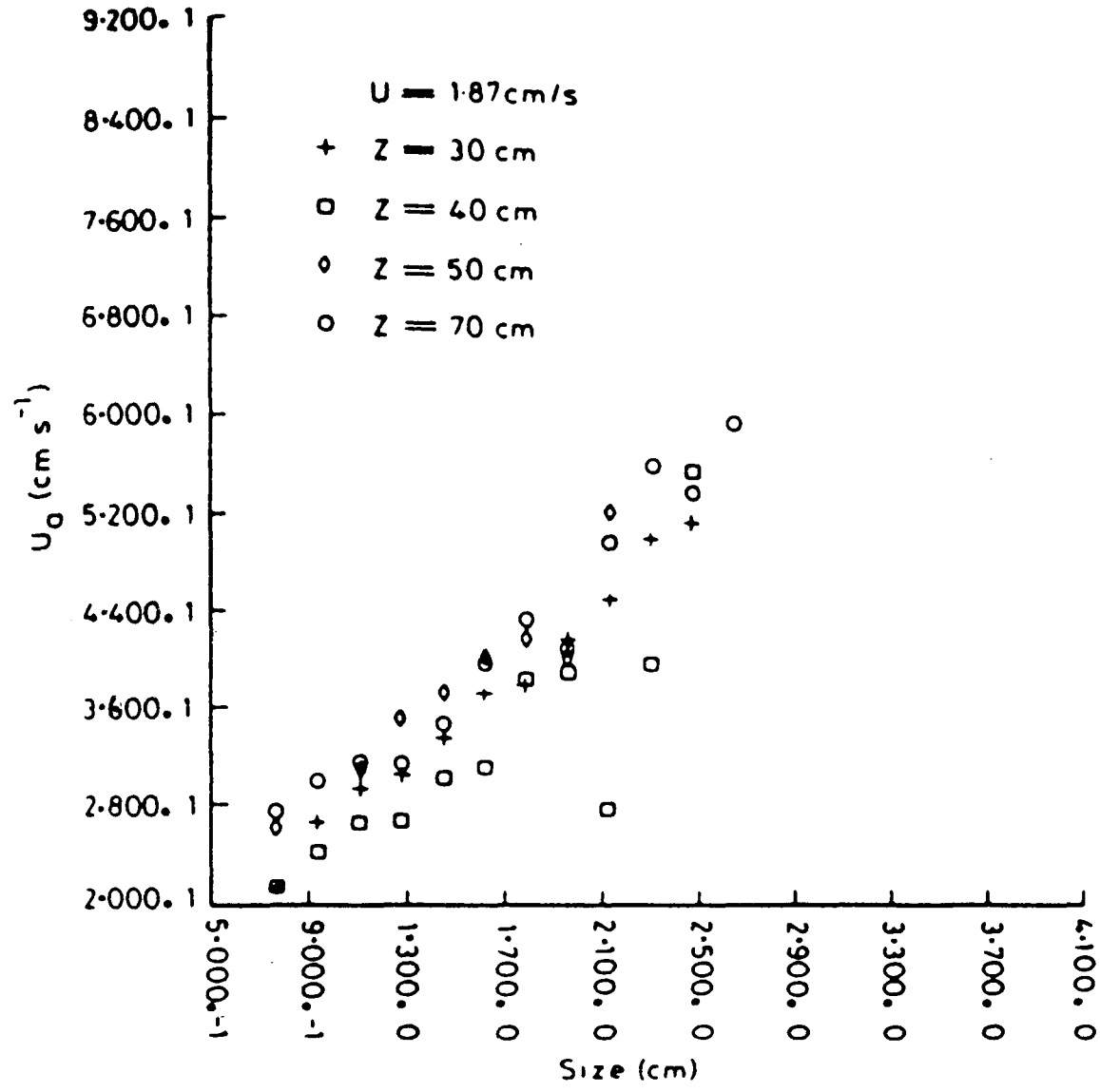

Figure 4.8 Variation of absolute bubble rise velocity U_a with bubble height h.

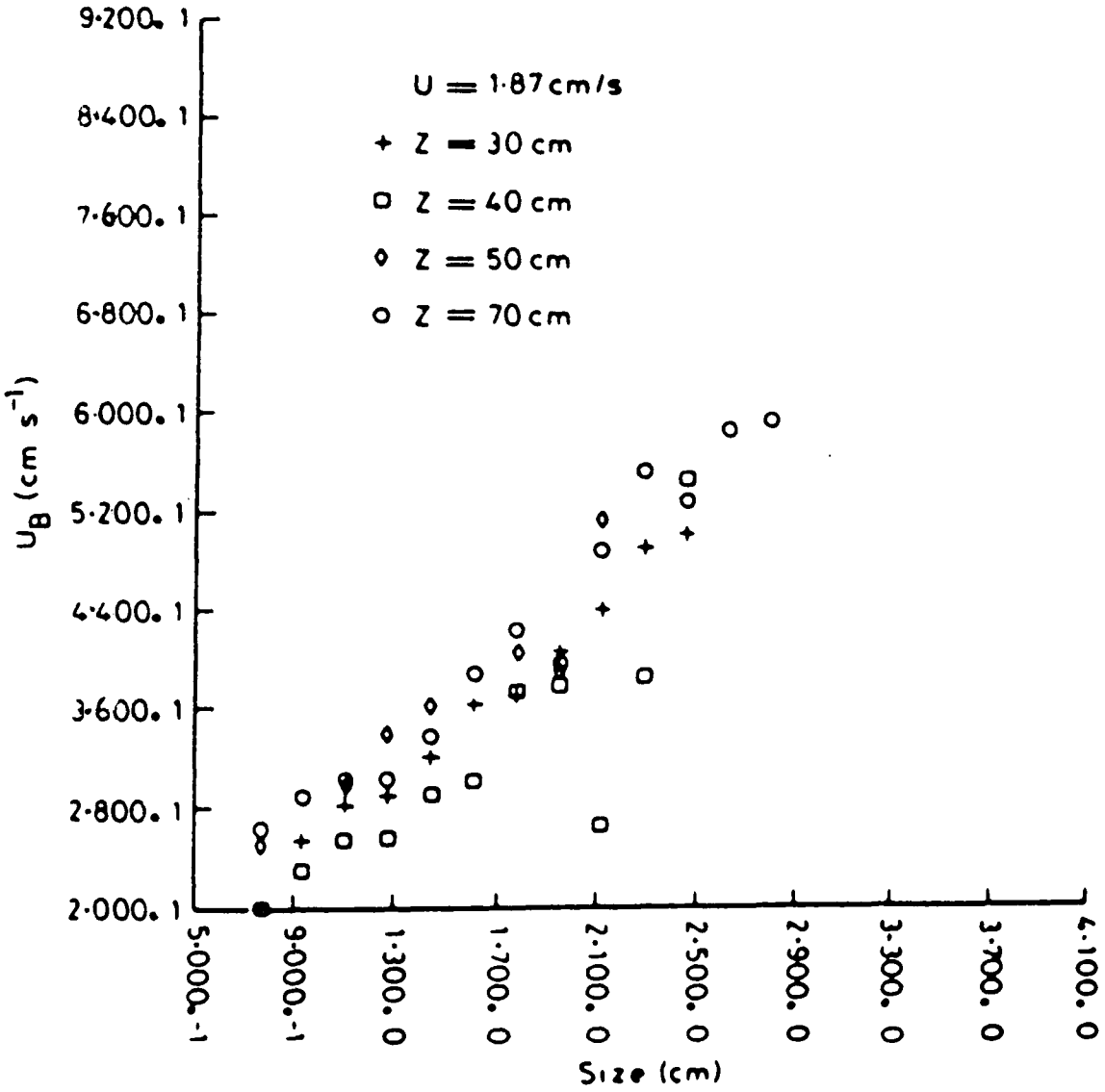

Figure 4.9 Variation of relative bubble rise velocity U_B with bubble height h.

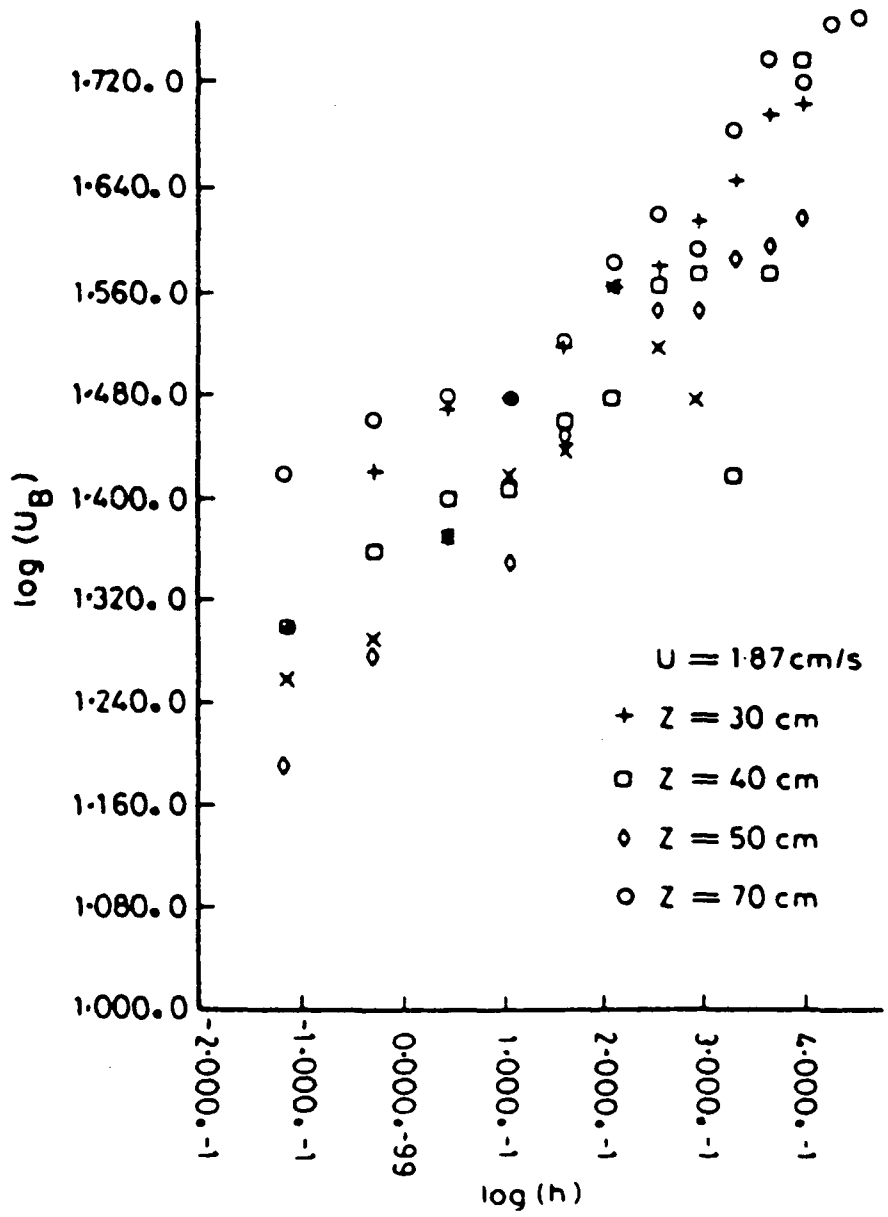

Figure 4.10 Log U_B versus log h.

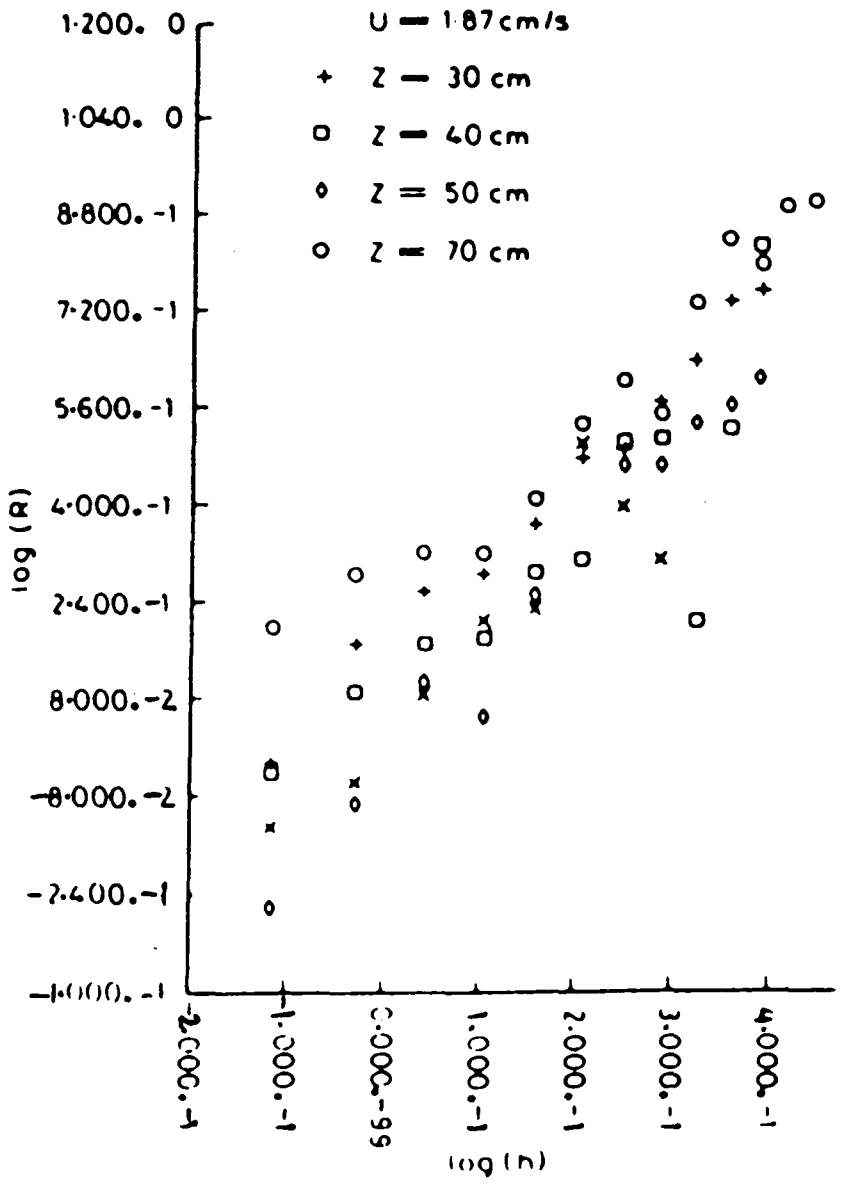

Figure 4.11 Log R versus log h

4.2.3 Implications for Bubble Shape

The results for bubble rise velocity may be summarised in the form

$$U_b = C\,h^{\beta}$$

where h is the nose-to-floor height of the bubble and β is a constant between 0.6 and 0.8. Values of C range from 20 to 28. The Davies-Taylor (24) equation suggests that for a spherical-cap bubble U_b varies with the square root of the radius of curvature. Rowe (92) correlated bubble rise velocities and horizontal diameters, both measured using X-ray cine photography, by the equation

$$U_b = 1.0 \sqrt{\frac{g d_B}{2}}$$

Since β differs from 0.5, it seems that the relationship between h and d_B or R, the radius of curvature, is not independent of size.

To investigate this phenomenon, the data for U = 1.87 $cm.sec^{-1}$ were used to calculate R by means of the Davies-Taylor equation

$$R = 9\,\frac{U_b^2}{4g} \qquad 4.4$$

The results are shown on Fig. (4.11). It may be seen that, as expected, R increases more rapidly than does h. A linear regression analysis on the data suggested that

$$R \propto h^{1.447} \quad \text{or} \quad h \propto R^{0.691} \qquad 4.5$$

Rowe and Widmer (100) recorded the shapes of numerous bubbles in fluidised beds of differing materials using X-ray photography. They found that for all materials the ratio of bubble volume V_B to the volume V_S of a sphere of the same radius was related to radius R by

$$\frac{V_B}{V_S} = 1 - e^{-0.114R} \qquad 4.6$$

V_B, V_S in Cm^3

R in Cm

Making the assumption (Figure 4.12) of a bubble, radius R, with a spherical indent also of radius R protruding a distance of 2δ

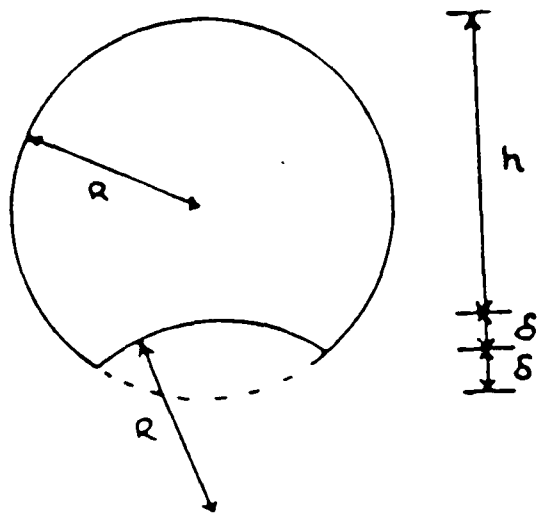

Figure 4.12

from the base of the circumscribed sphere, it can be shown (see Appendix A) that:

$$\frac{V_B}{V_S} = 1 - \frac{3}{2} \left(\frac{\delta}{R}\right)^2 \left[1 - \frac{1}{3} \left(\frac{\delta}{R}\right)\right] \qquad 4.7$$

The relationship between δ and R obtained by equating 4.6 and 4.7, namely

$$\frac{V_B}{V_S} = 1 - e^{-0.057 d_B} = 1 - \frac{3}{2} \left(\frac{\delta}{R}\right)^2 \left(1 - \frac{1}{3} \left(\frac{\delta}{R}\right)\right)$$

is not explicit. However, an approximate power relationship fitted to numerical values of R and $h = 2(R - \delta)$, (shown in Table (4.3) below), gives:

$$h = 1.342\ R^{0.86} \qquad 4.8$$

δ/R	V_B/V_S	$e^{-0.057 d_B}$	d_B (cm)	h(cm)
0.05	0.003687	0.9963	0.0648	0.0616
0.10	0.01450	0.9855	0.2562	0.2306
0.15	0.03206	0.96794	0.5717	0.4859
0.20	0.0560	0.9440	1.0110	0.8089
0.25	0.08594	0.9141	1.5765	1.1824
0.30	0.1215	0.8785	2.2726	1.5908
0.35	0.1623	0.8377	3.1069	2.0195
0.40	0.2080	0.7920	4.0911	2.4546
0.45	0.2582	0.7418	5.2399	2.8819
0.50	0.3125	0.6875	6.7536	3.3768

TABLE 4.3

In Figure (4.13), some measured values of h are compared to the predicted values from the power relationship.

The exponent 0.86 is rather larger than the one given in equation (4.5). Nevertheless, the results obtained in this work agree with those of Rowe and Widmer in predicting a progressive flattening of bubbles with increasing bubble size in the bed. As the mean bubble size increases with height in the bed, therefore a progressive flattening of bubbles is observed with increasing elevation above the distributor plate.

Figure (4.14) shows the absolute rise velocity - size variation at three points, 50, 60 and 70 cm above the distributor plate respectively. They are all on the X = 24 and Y = 7 cm plane, the bed depth is 82 cm and the superficial fluidising velocity is fixed at 1.87 $cm.sec^{-1}$.

The rise velocity increases with increasing bubble size and the highest velocities correspond to Z = 70 cm elevation.

The relative rise velocities, U_b, are calculated using equation 4.1 and are plotted against the bubble size in Figure (4.15). There is much less scatter for smaller bubbles. The relative rise velocity, for each interval of bubble height, is greater for 70 cm elevation than the corresponding values for Z = 60 cm. Similarly rise velocities measured at the point where Z = 60 cm are greater than those recorded at Z = 50 cm.

Fig. 4.13

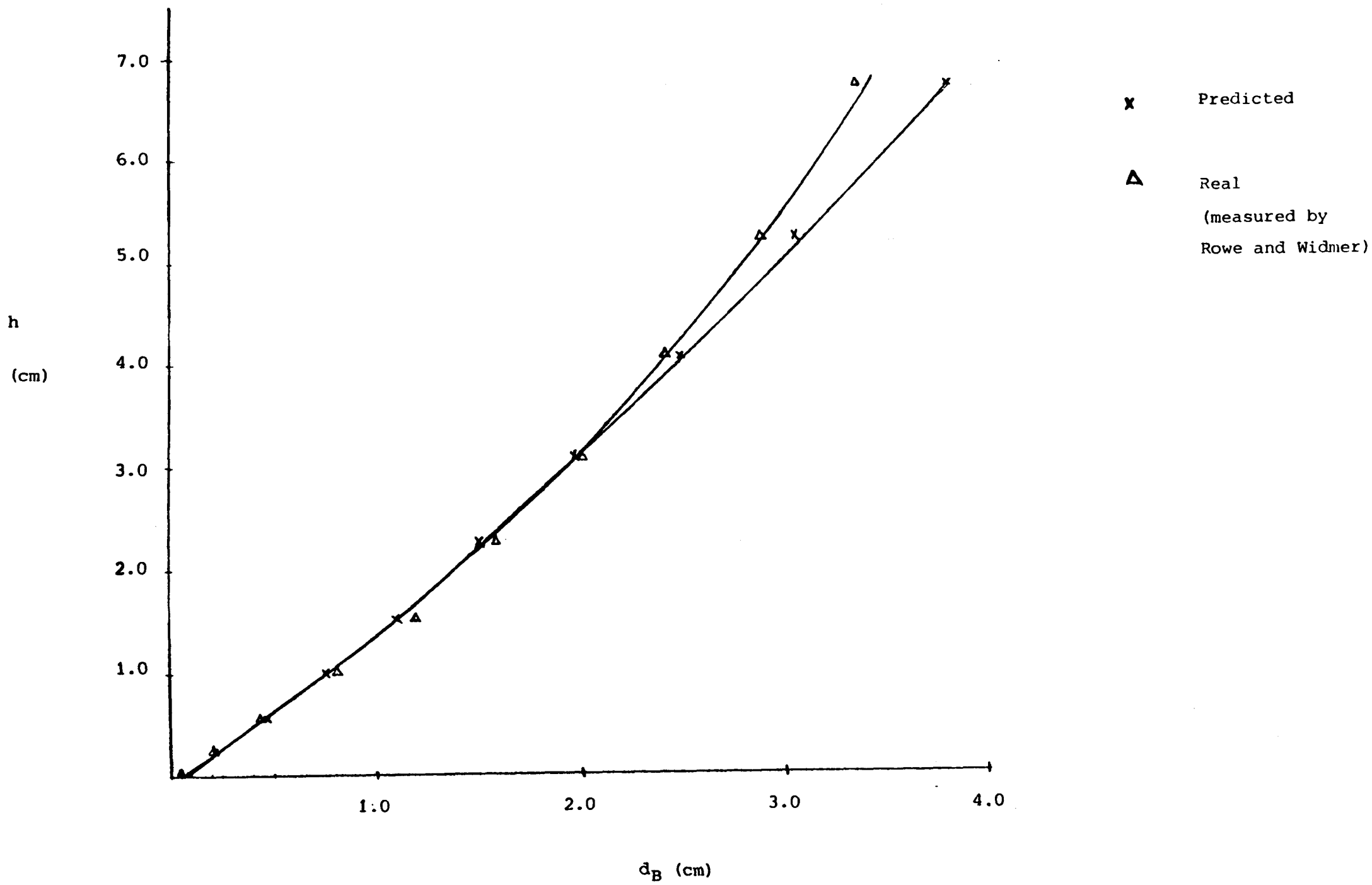
7.0
6.0
5.0
h
(cm)
4.0
3.0
2.0
1.0
1.0
2.0
3.0
4.0
d_B (cm)
Predicted
Real
(measured by
Rowe and Widmer)

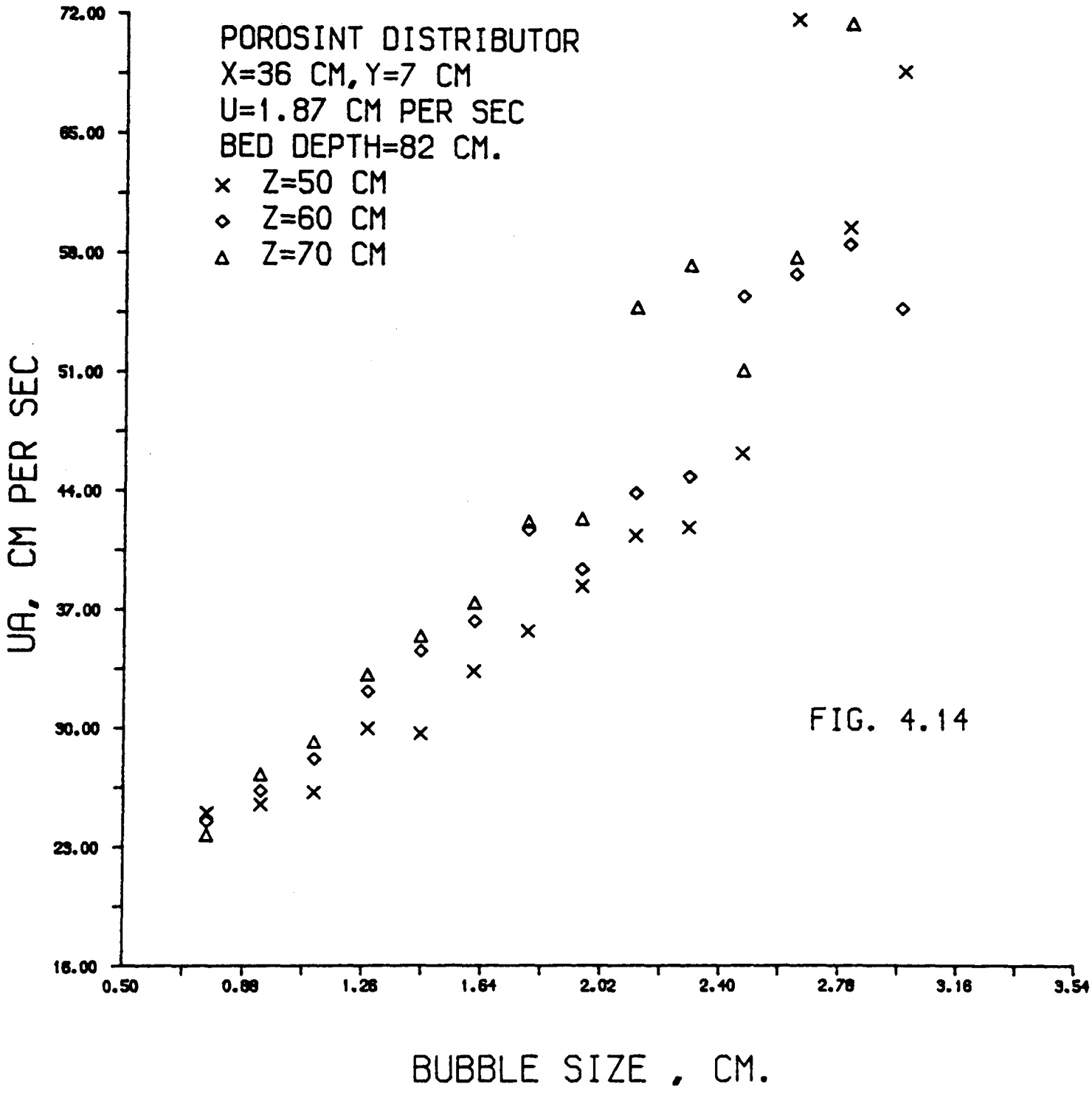
POROSINT DISTRIBUTOR
X=36 CM, Y=7 CM
U=1.87 CM PER SEC
BED DEPTH=82 CM.
× Z=50 CM
◇ Z=60 CM
△ Z=70 CM
UA, CM PER SEC
72.00
65.00
58.00
51.00
44.00
37.00
30.00
23.00
16.00
0.50
0.88
1.26
1.64
2.02
2.40
2.78
3.16
3.54
BUBBLE SIZE , CM.

FIG. 4.14

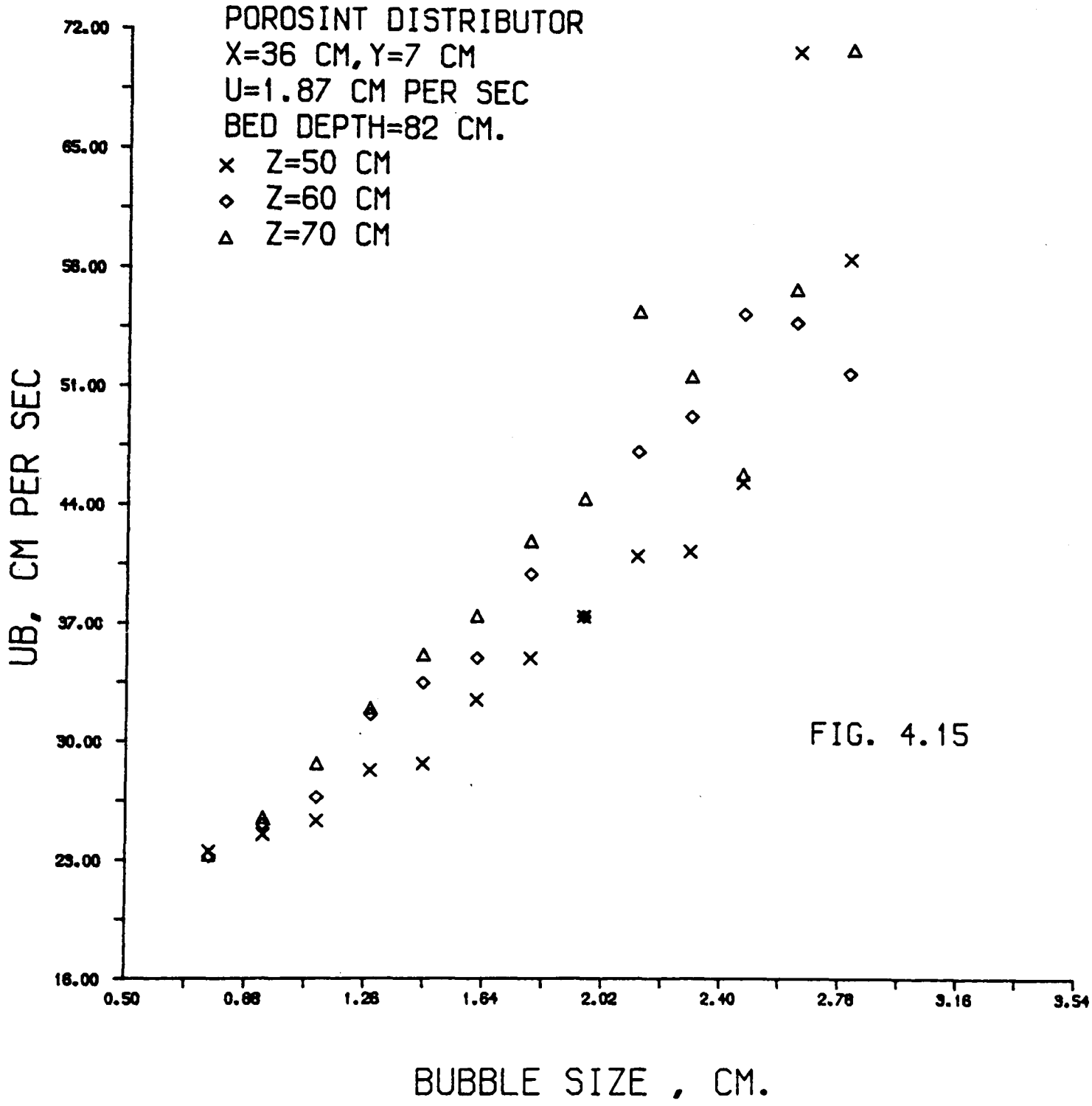
POROSINT DISTRIBUTOR
X=36 CM, Y=7 CM
U=1.87 CM PER SEC
BED DEPTH=82 CM.
× Z=50 CM
◇ Z=60 CM
△ Z=70 CM
72.00
65.00
58.00
51.00
44.00
37.00
30.00
23.00
16.00
CM PER SEC
UB,
0.50
0.88
1.26
1.64
2.02
2.40
2.78
3.16
3.54
BUBBLE SIZE , CM.

FIG. 4.15

Figure (4.16) shows the U_b size relationship for the same three points (as Figure 4.15) and under identical operating conditions, except that the superficial fluidising velocity is increased to 3.01 $cm.sec^{-1}$. The bubble rise velocity measured at this higher gas velocity, for each interval of bubble height, is greater than the corresponding values, measured when U = 1.87 $cm.sec^{-1}$. But, otherwise a similar pattern of the rise velocity increasing with the bubble size prevails.

In Figure (4.17), the U_b - size variation with elevation above the distributor plate is studied at three different points, all three with X = 36 cm and Y = 7 co-ordinates. The same superficial fluidising velocity, (U = 3.01 $cm.sec^{-1}$), and the same bed depth (82 cm) as Figure (4.16) are maintained. It is intended to compare the rise velocity, for each interval of bubble height, corresponding to these points (Figures 4.16 and 4.17).

Greater velocities are recorded at the three heights in Figure (4.17), for corresponding bubble sizes. The only difference in conditions prevalent in these two sets of experiments, is the different X co-ordinate of the two vertical axes on which the points are located. The marked difference in the magnitude of the rise velocities, recorded at these two locations is possibly due to the effect of particulate phase circulation patterns which exist in the bed.

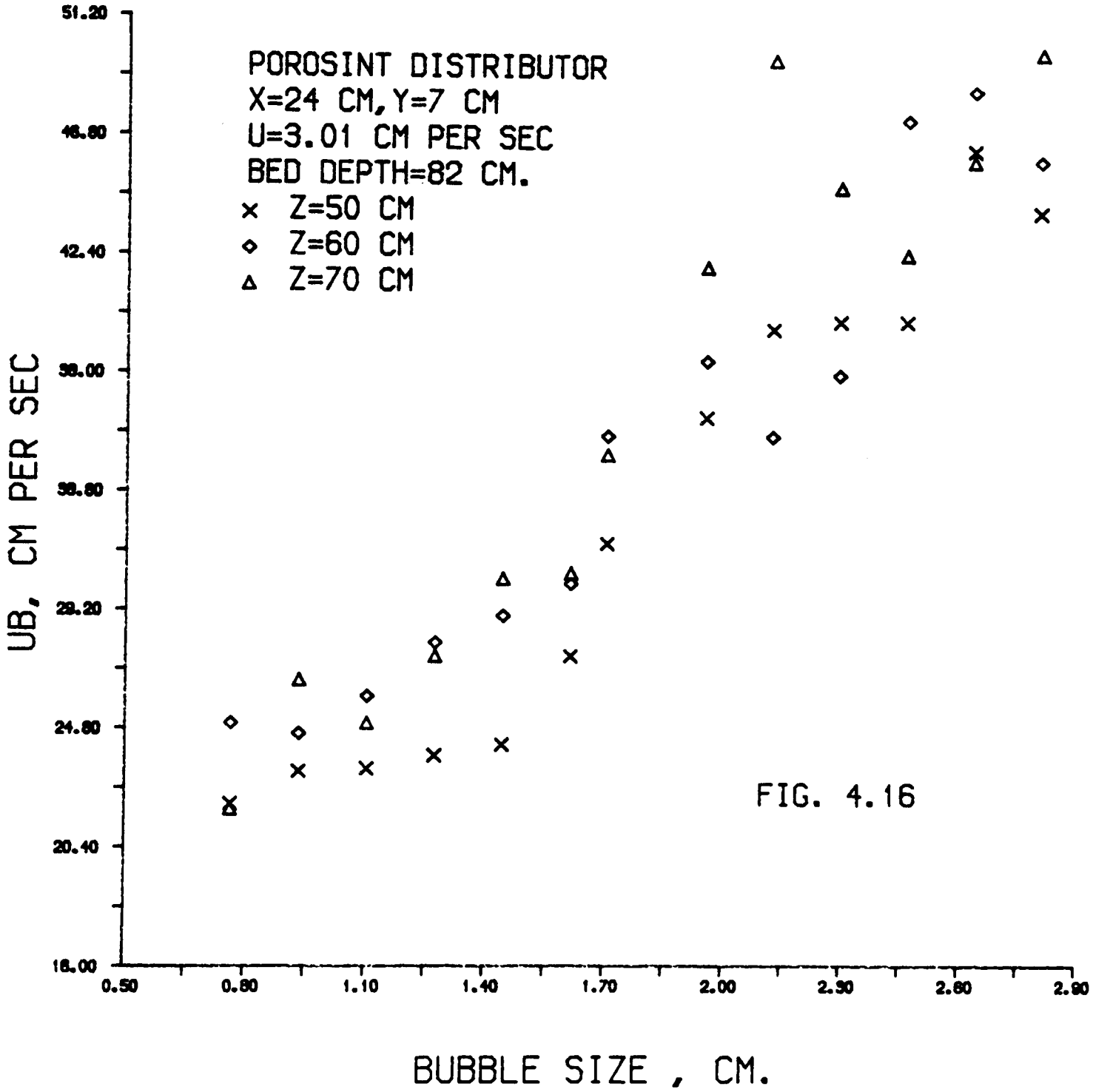
POROSINT DISTRIBUTOR
X=24 CM, Y=7 CM
U=3.01 CM PER SEC
BED DEPTH=82 CM.
× Z=50 CM
◇ Z=60 CM
△ Z=70 CM
UB, CM PER SEC
51.20
46.80
42.40
38.00
33.60
29.20
24.80
20.40
16.00
0.50
0.80
1.10
1.40
1.70
2.00
2.30
2.60
2.90
BUBBLE SIZE , CM.

FIG. 4.16

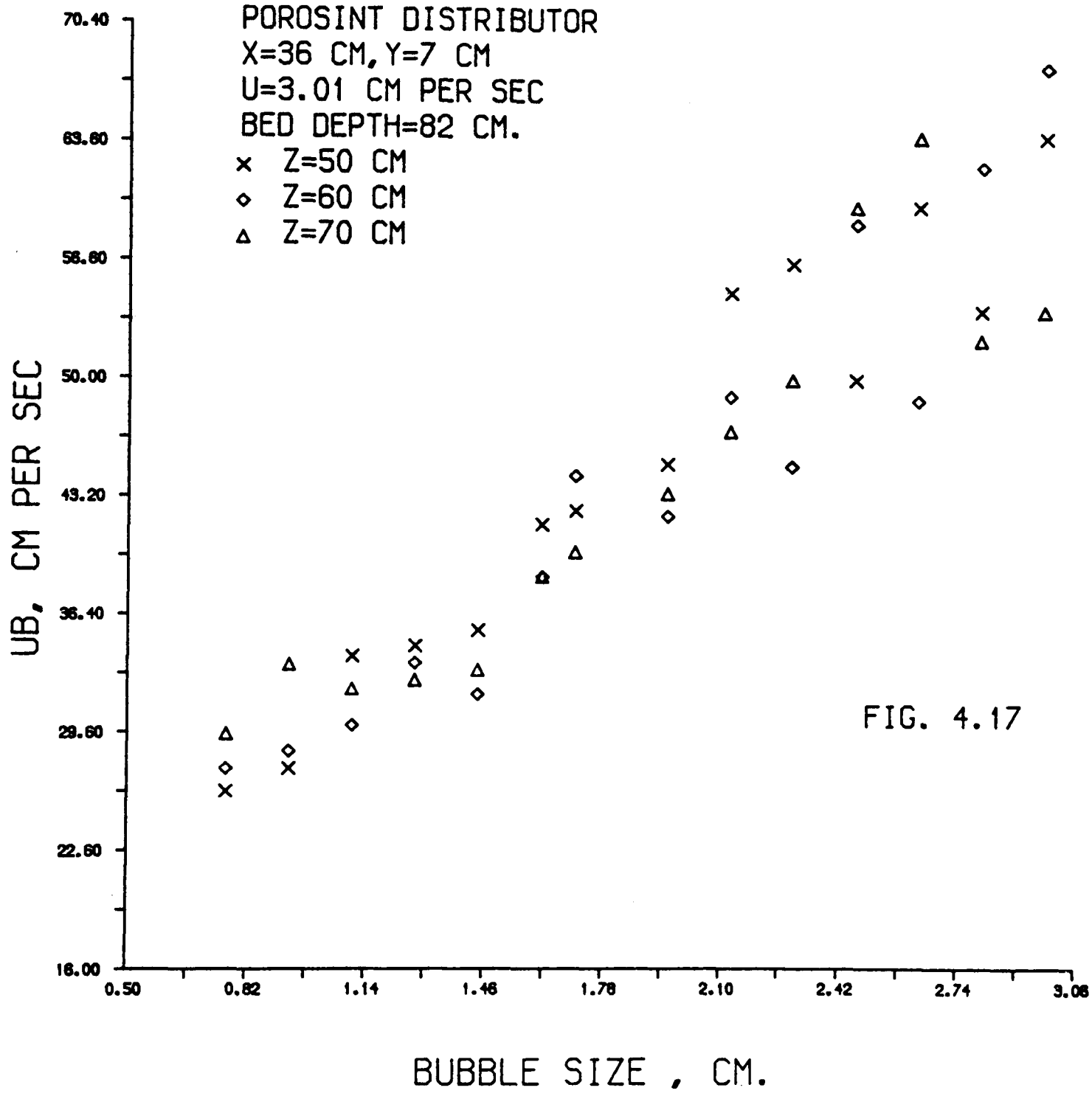
POROSINT DISTRIBUTOR
X=36 CM, Y=7 CM
U=3.01 CM PER SEC
BED DEPTH=82 CM.
× Z=50 CM
◇ Z=60 CM
△ Z=70 CM
UB, CM PER SEC
70.40
63.80
56.60
50.00
43.20
36.40
29.60
22.60
16.00
0.50
0.82
1.14
1.46
1.78
2.10
2.42
2.74
3.06
BUBBLE SIZE , CM.

FIG. 4.17

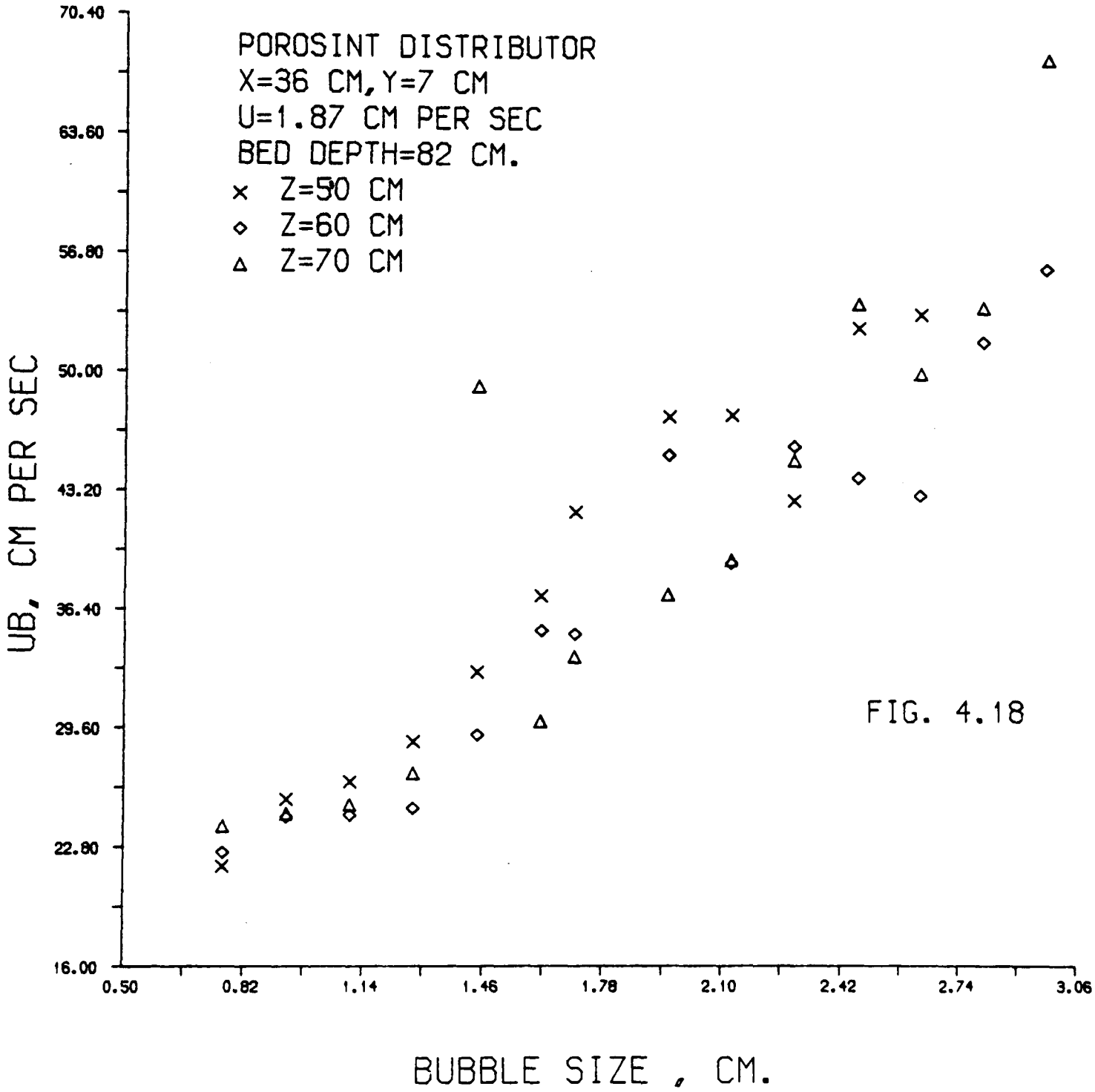
POROSINT DISTRIBUTOR
X=36 CM, Y=7 CM
U=1.87 CM PER SEC
BED DEPTH=82 CM.
× Z=50 CM
◇ Z=60 CM
△ Z=70 CM
UB, CM PER SEC
70.40
63.60
56.80
50.00
43.20
36.40
29.60
22.80
16.00
0.50
0.82
1.14
1.46
1.78
2.10
2.42
2.74
3.06
BUBBLE SIZE , CM.

FIG. 4.18

Finally, Figure (4.18) shows the U_b - size relationship for the same three points as in Figure (4.17), but at a lower gas velocity of 1.87 cm.sec^{-1}. The bed depth and X and Y co-ordinates of the points are identical in the two graphs.

In Table (4.4) the rise velocities shown in Figures (4.17) and (4.18) are tabulated against bubble size, for better comparison.

Bubble Size (cm)	Z = 50 cm		Z = 60 cm		Z = 70 cm	
	U = 1.87	U = 3.01	U = 1.87	U = 3.01	U = 1.87	U = 3.01
0.765	21.529	26.395	22.820	27.125	23.536	29.290
0.935	24.197	27.642	24.493	28.897	24.563	33.077
1.105	26.363	34.134	24.891	29.940	25.569	31.941
1.275	28.936	34.417	25.179	33.760	26.836	31.973
1.445	32.879	35.228	29.141	31.905	29.817	32.896
1.615	37.488	41.387	35.457	38.843	28.919	37.217
1.785	42.234	42.066	35.726	45.132	33.482	39.878
1.955	47.654	44.752	45.852	41.778	36.829	42.027
2.125	47.190	54.961	38.855	48.111	39.832	46.265
2.295	37.093	56.094	46.238	45.694	44.920	49.219
2.465	52.830	47.974	44.876	59.312	53.304	60.235
2.635	53.650	59.800	42.742	47.745	50.140	63.453
2.805		53.448	56.487	61.939	53.221	52.120
2.975		63.624	61.360	61.749	50.052	54.463
3.145			58.767	69.034	69.559	68.995

TABLE 4.4

As expected, the velocity for each interval of bubble height is less, for the lesser of the two superficial fluidising velocities. Figure (4.18) can also be compared to Figure (4.15), as the experimental conditions are identical for both graphs.

The difference in the magnitude of the rise velocities is not so pronounced at this low gas velocity ($U = 1.87$ cm.sec^{-1}), between these two sets of data (4.15 and 4.18).

4.3 Multiorifice Distributor

Bubble rise velocities have been measured at the same nine points across the bed cross-sectional area (Figure 3.8), at the same superficial fluidising velocities (1.87, 2.41 and 3.01 cm.sec^{-1}) and the same elevations above the distributor plate, (20, 30, 40, 50, 60 and 70 cm). In fact, some of these experiments are duplicated, as far as possible, under identical conditions to the porosint plate distributor, to make possible comparison of the rise velocities of bubbles in the two cases. The same equations are used to calculate the relative rise velocity and the radius of curvature. It must be noted that experiments are also carried out, with this distributor, when the bed is initially filled to a maximum depth of 82 cm and then the rise velocities are measured at the six elevations mentioned above.

4.3.1 Variation with Superficial Fluidising Velocity

Figure (4.19) shows the variation of U_a with bubble nose-to-floor height at a point 20 cm above the distributor plate, on the bed vertical centre line, for three different superficial fluidising velocities.

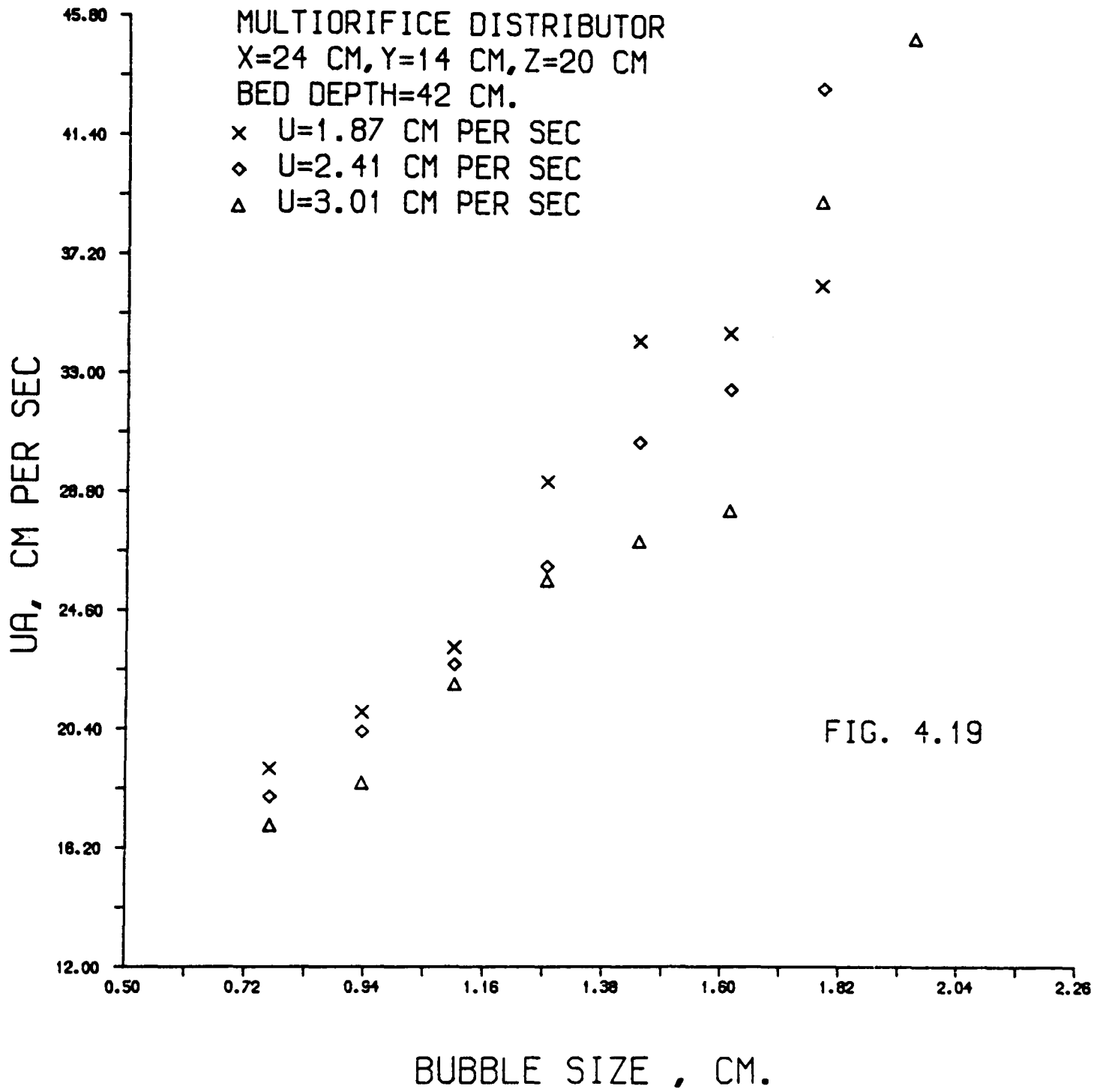
MULTIORIFICE DISTRIBUTOR
X=24 CM, Y=14 CM, Z=20 CM
BED DEPTH=42 CM.
× U=1.87 CM PER SEC
◇ U=2.41 CM PER SEC
△ U=3.01 CM PER SEC
UA, CM PER SEC
45.80
41.40
37.20
33.00
28.80
24.60
20.40
16.20
12.00
0.50
0.72
0.94
1.16
1.38
1.60
1.82
2.04
2.26
BUBBLE SIZE , CM.

FIG. 4.19

The experimental points show less scatter for smaller bubble sizes. Equation (4.1) is used to calculate the relative bubble rise velocities, U_b, and these are plotted against bubble size in Figure 4.20.

The rise velocity at each interval of bubble height is greater for U = 1.87 $cm.sec^{-1}$ than the corresponding value for U = 2.41 $cm.sec^{-1}$. Similarly, bubble rise velocities measured with the superficial fluidising velocity U = 2.41 $cm.sec^{-1}$ are greater than the measured values for U = 3.01 $cm.sec^{-1}$. It seems, at this point in the bed, increasing the superficial fluidising velocity has a negative effect on the bubble rise velocity.

Figure (4.21) shows the variation of the absolute rise velocity with bubble nose-to-floor height at a point 30 cm above the distributor on the vertical centre line. Again the data show much less scatter in the lower size ranges.

The rise velocity at each interval of bubble height is greater than the corresponding value measured at Z = 20 cm above the distributor plate.

In Figure (4.22), the relative rise velocities, U_b, calculated using equation (4.1), are plotted against bubble size for the same point as in Figure (4.21).

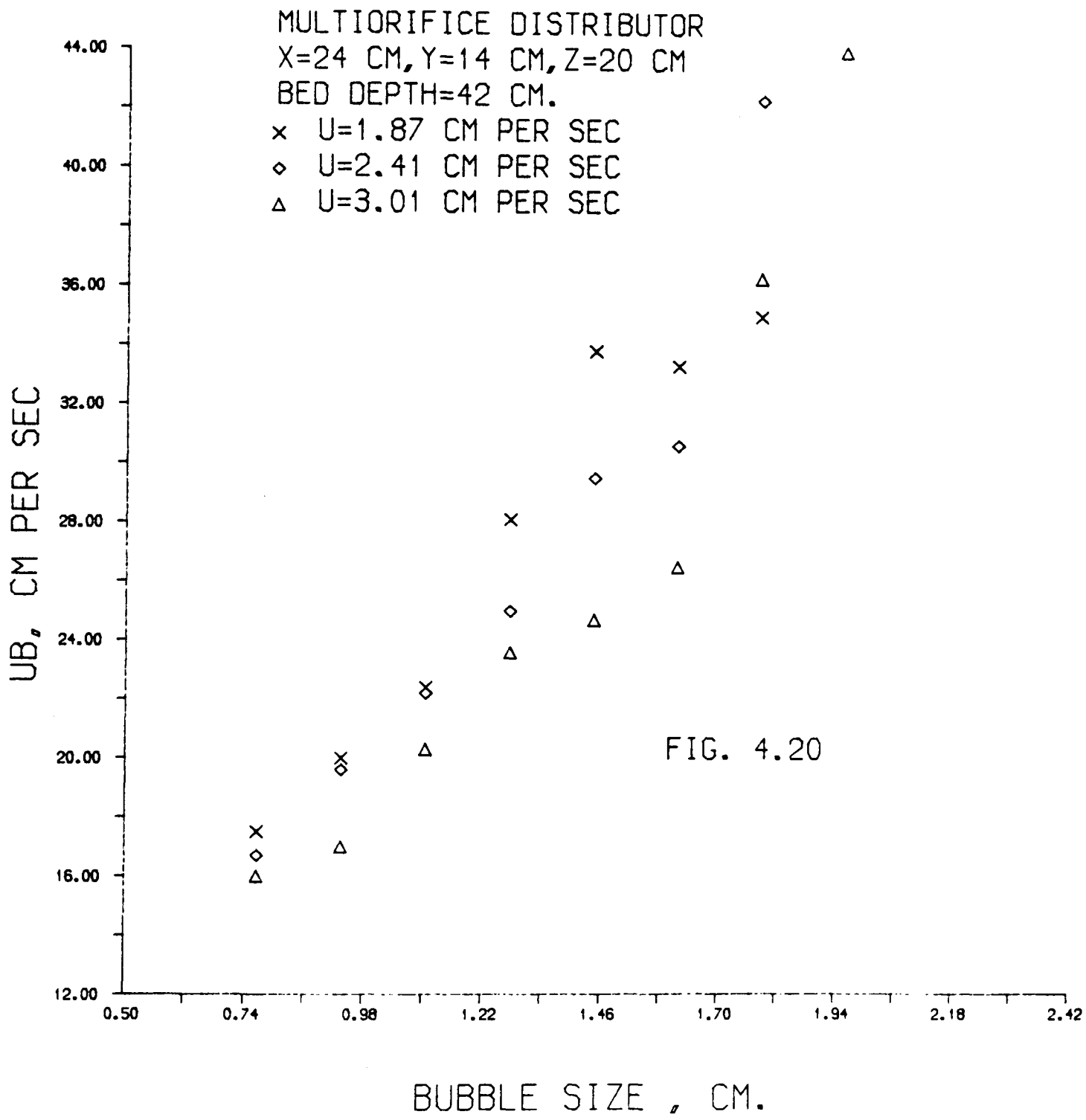
MULTIORIFICE DISTRIBUTOR
X=24 CM, Y=14 CM, Z=20 CM
BED DEPTH=42 CM.
× U=1.87 CM PER SEC
◇ U=2.41 CM PER SEC
△ U=3.01 CM PER SEC
UB, CM PER SEC
44.00
40.00
36.00
32.00
28.00
24.00
20.00
16.00
12.00
0.50
0.74
0.98
1.22
1.46
1.70
1.94
2.18
2.42
BUBBLE SIZE , CM.

FIG. 4.20

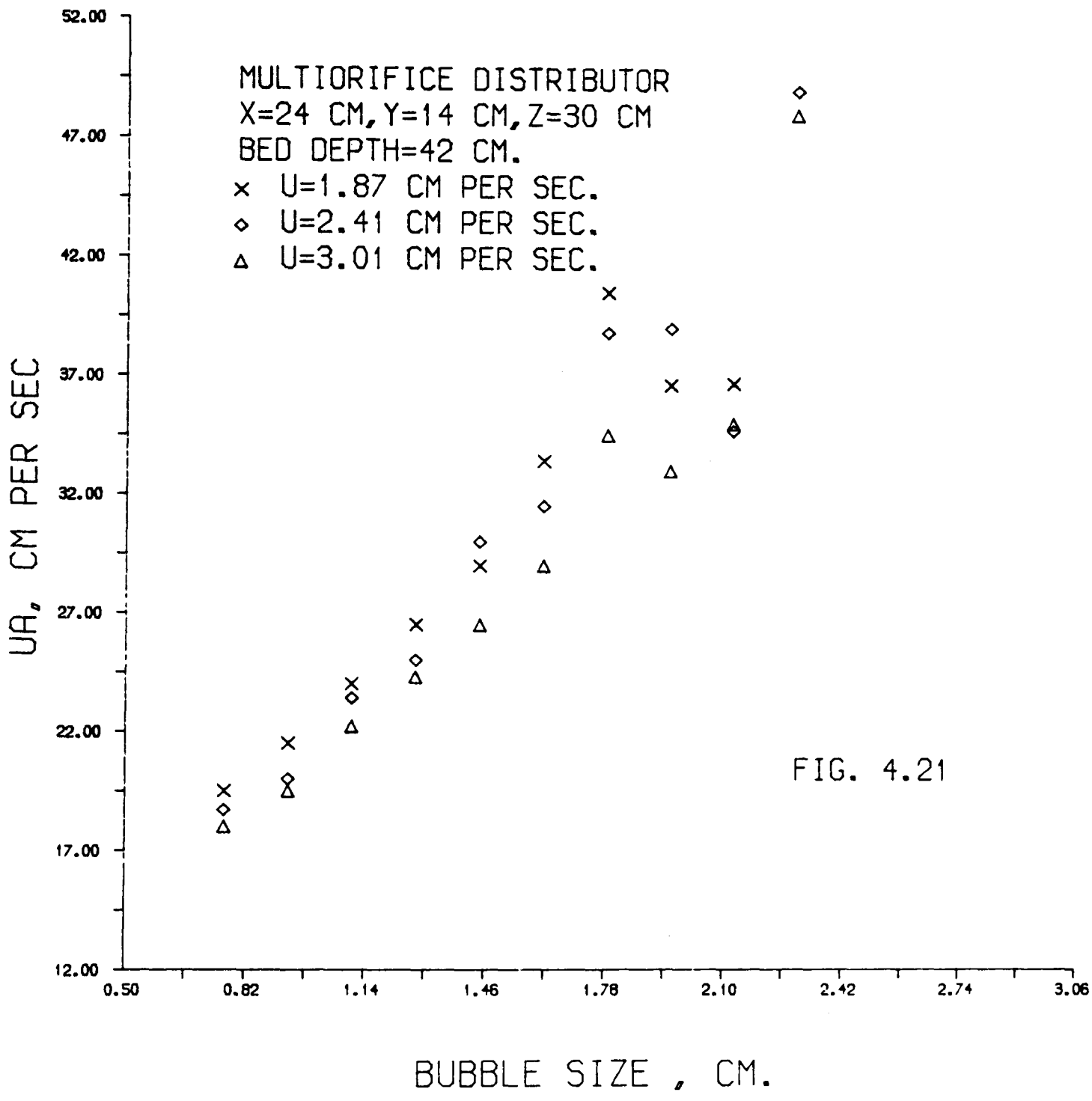
MULTIORIFICE DISTRIBUTOR
X=24 CM, Y=14 CM, Z=30 CM
BED DEPTH=42 CM.
× U=1.87 CM PER SEC.
◇ U=2.41 CM PER SEC.
△ U=3.01 CM PER SEC.
CM PER SEC
52.00
47.00
42.00
37.00
32.00
27.00
22.00
17.00
12.00
0.50
0.82
1.14
1.46
1.78
2.10
2.42
2.74
3.06
BUBBLE SIZE , CM.

FIG. 4.21

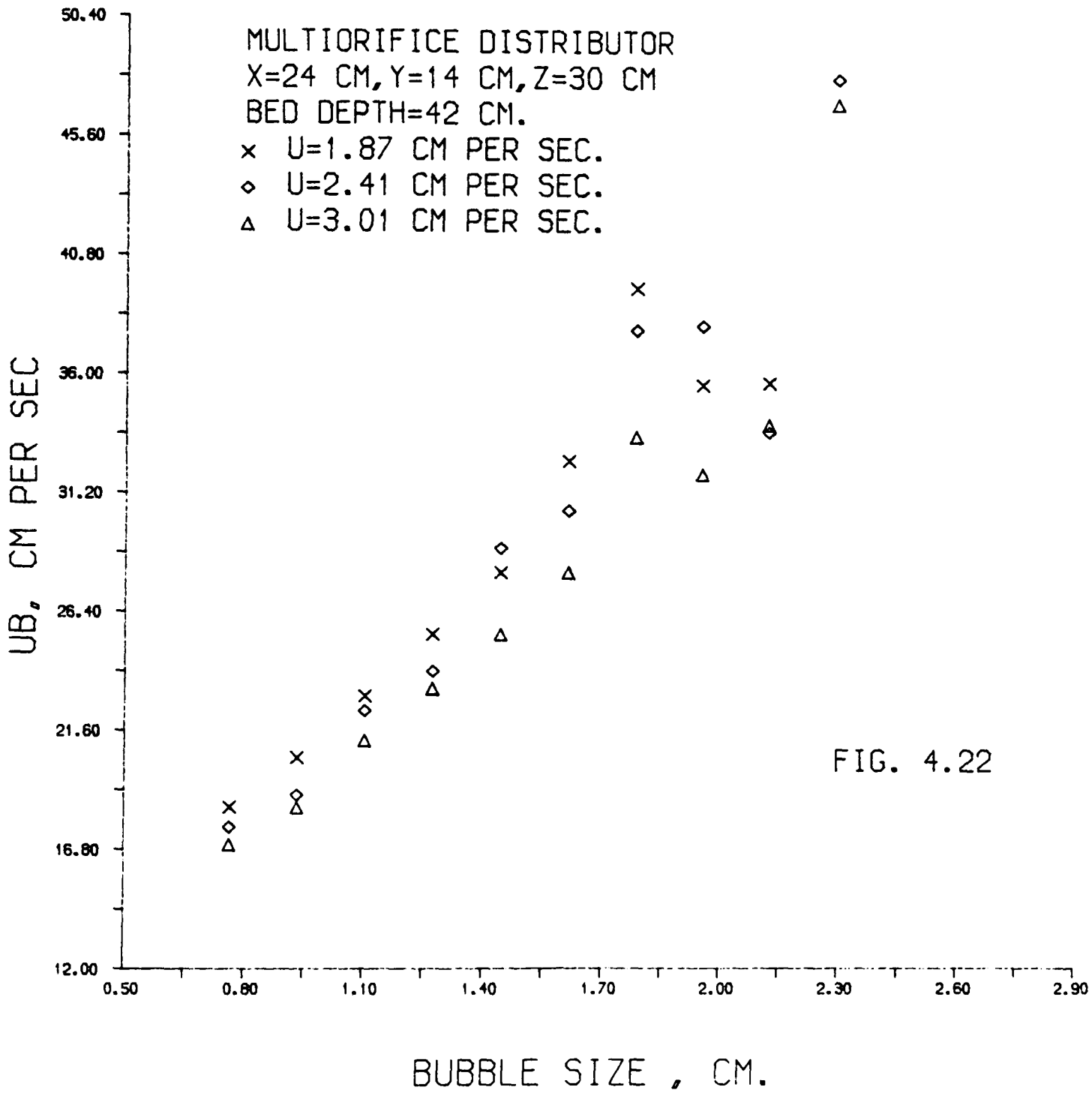
MULTIORIFICE DISTRIBUTOR
X=24 CM, Y=14 CM, Z=30 CM
BED DEPTH=42 CM.
× U=1.87 CM PER SEC.
◇ U=2.41 CM PER SEC.
△ U=3.01 CM PER SEC.
UB, CM PER SEC
50.40
45.60
40.80
36.00
31.20
26.40
21.60
16.80
12.00
0.50
0.80
1.10
1.40
1.70
2.00
2.30
2.60
2.90
BUBBLE SIZE , CM.

FIG. 4.22

Table (4.5) below, shows the absolute rise velocities at each interval of bubble height, for the two gas distributors employed.

Bubble Size (cm)	U = 1.87		U = 2.41		U = 3.01	
	P.P.D.	Multiorifice	P.P.D.	Multiorifice	P.P.D.	M.O.D.
0.765	21.965	19.186	22.117	19.354	27.627	19.771
0.935	22.700	21.445	26.492	21.230	29.915	20.178
1.105	24.937	23.613	30.461	24.163	29.590	23.645
1.275	25.859	26.287	33.301	26.067	29.299	25.330
1.445	30.122	29.155	36.694	31.077	32.261	28.052
1.615	29.951	33.477	35.386	32.417	37.639	30.942
1.785	32.434	40.645	41.543	38.557	37.842	35.330
1.955	36.116	36.238	39.634	40.015	38.135	34.199
2.125	38.000	36.414	42.344	34.907	40.649	36.982
2.295	42.422		43.770	49.639	47.241	49.912
2.465			57.178	42.402	40.137	47.041
2.635			64.531		56.064	55.293
2.805			59.087		50.986	
2.975			52.739		56.172	
3.145						
3.315						

TABLE 4.5

Bed Depth = 42 cm

X = 24 cm, Y = 14 cm, Z = 30 cm

The rise velocity at each interval of bubble height is greater when the porosint plate distributor is employed, at this elevation of Z = 30 cm. Presumably, this reflects the mechanism of bubble generation by the two gas distributors.

The porosint plate distributor generates a much larger proportion of small bubbles than the multiorifice distributor; the enhancement of rise velocity in the former case may reflect the fact that a greater proportion of bubbles is actually in the process of coalescence (and therefore with increased velocity) at the point of measurement.

It is also worthwhile pointing out that, in the case of the porosint plate distributor, the bubble rise velocity is significantly enhanced by the increases in superficial fluidising velocity.

For the porosint distributor, the average value of k in

$$U_a = U_b + k\ (U - U_{mf})$$

appears to be 1.44.

Figure (4.23) shows the variation of U_a with bubble nose-to-floor height at a point 20 cm above the multiorifice distributor plate, for four different superficial fluidising velocities. This point has X = 36 cm and Y = 21 cm co-ordinates, shown overleaf.

Fig. 4.23

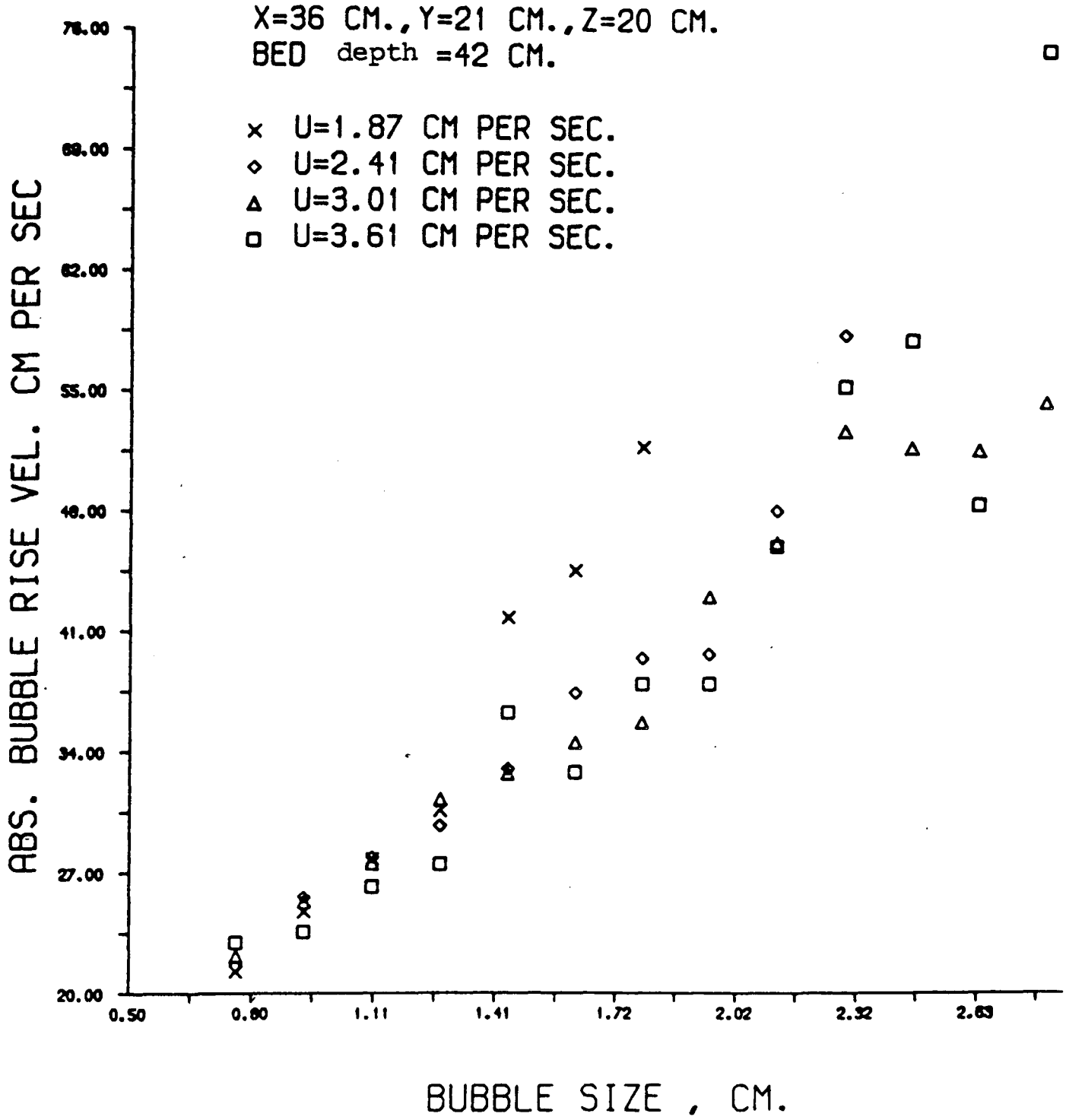
X=36 CM., Y=21 CM., Z=20 CM.
BED depth =42 CM.
× U=1.87 CM PER SEC.
◇ U=2.41 CM PER SEC.
△ U=3.01 CM PER SEC.
□ U=3.61 CM PER SEC.
ABS. BUBBLE RISE VEL. CM PER SEC
76.00
69.00
62.00
55.00
48.00
41.00
34.00
27.00
20.00
0.50
0.80
1.11
1.41
1.72
2.02
2.32
2.63
BUBBLE SIZE , CM.

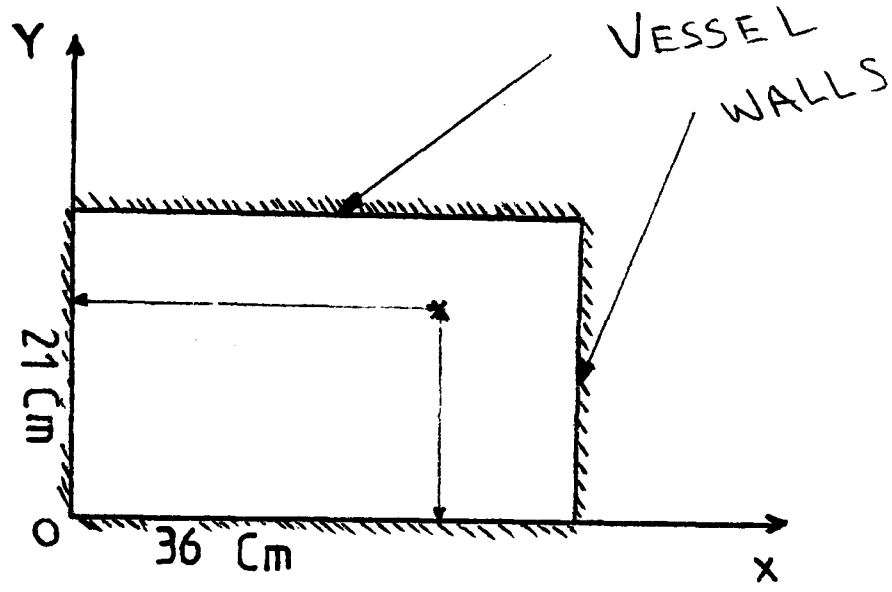

Here too, the experimental points show less scatter for smaller bubble sizes.

Equation (4.1) is used to calculate the relative bubble rise velocities, U_b, and these are plotted against bubble size in Figure (4.24).

The data of Fig. (4.24) are plotted on logarithmic axes in Fig. (4.25) and a linear regression analysis has been used to fit equations of the form (4.2) to the data. The results of this analysis are shown in Table (4.6) below.

U ($cm.sec^{-1}$)	α	C	β	Correlation Coefficient
1.87	1.41	25.58	1.11	0.97
2.41	1.39	24.33	0.79	0.99
3.01	1.38	23.87	0.78	0.99
3.61	1.34	22.16	0.92	0.94
All Points	1.39	24.11	0.86	0.95

TABLE (4.6)

Relationship between bubble rise velocity and size at a height of 20 cm above the distributor plate.

Fig. 4.24

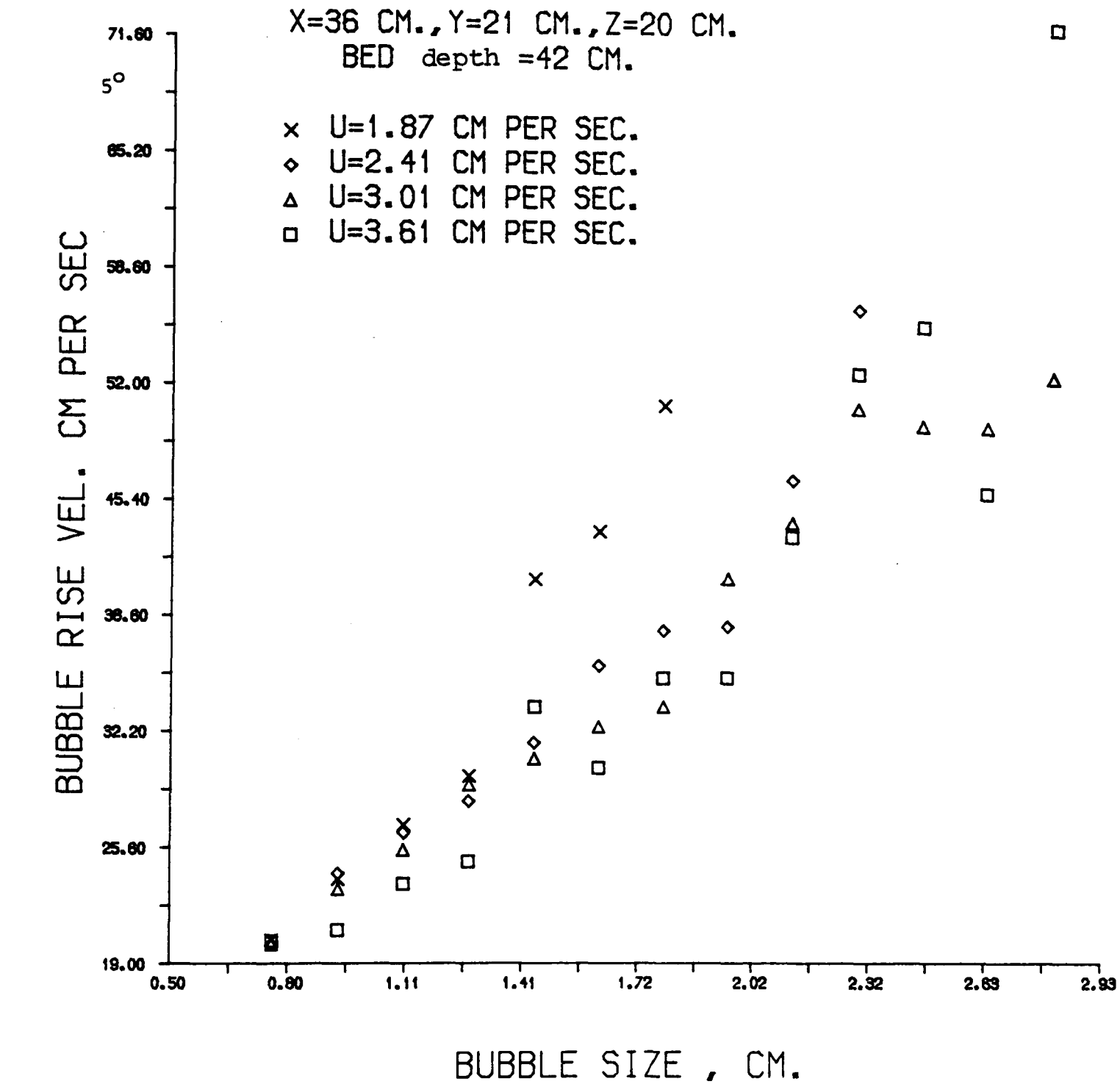
X=36 CM., Y=21 CM., Z=20 CM.
BED depth =42 CM.
× U=1.87 CM PER SEC.
◇ U=2.41 CM PER SEC.
△ U=3.01 CM PER SEC.
□ U=3.61 CM PER SEC.
BUBBLE RISE VEL. CM PER SEC
71.60
65.20
58.80
52.00
45.40
38.80
32.20
25.60
19.00
0.50
0.80
1.11
1.41
1.72
2.02
2.32
2.63
2.93
BUBBLE SIZE , CM.

Fig. 4.25

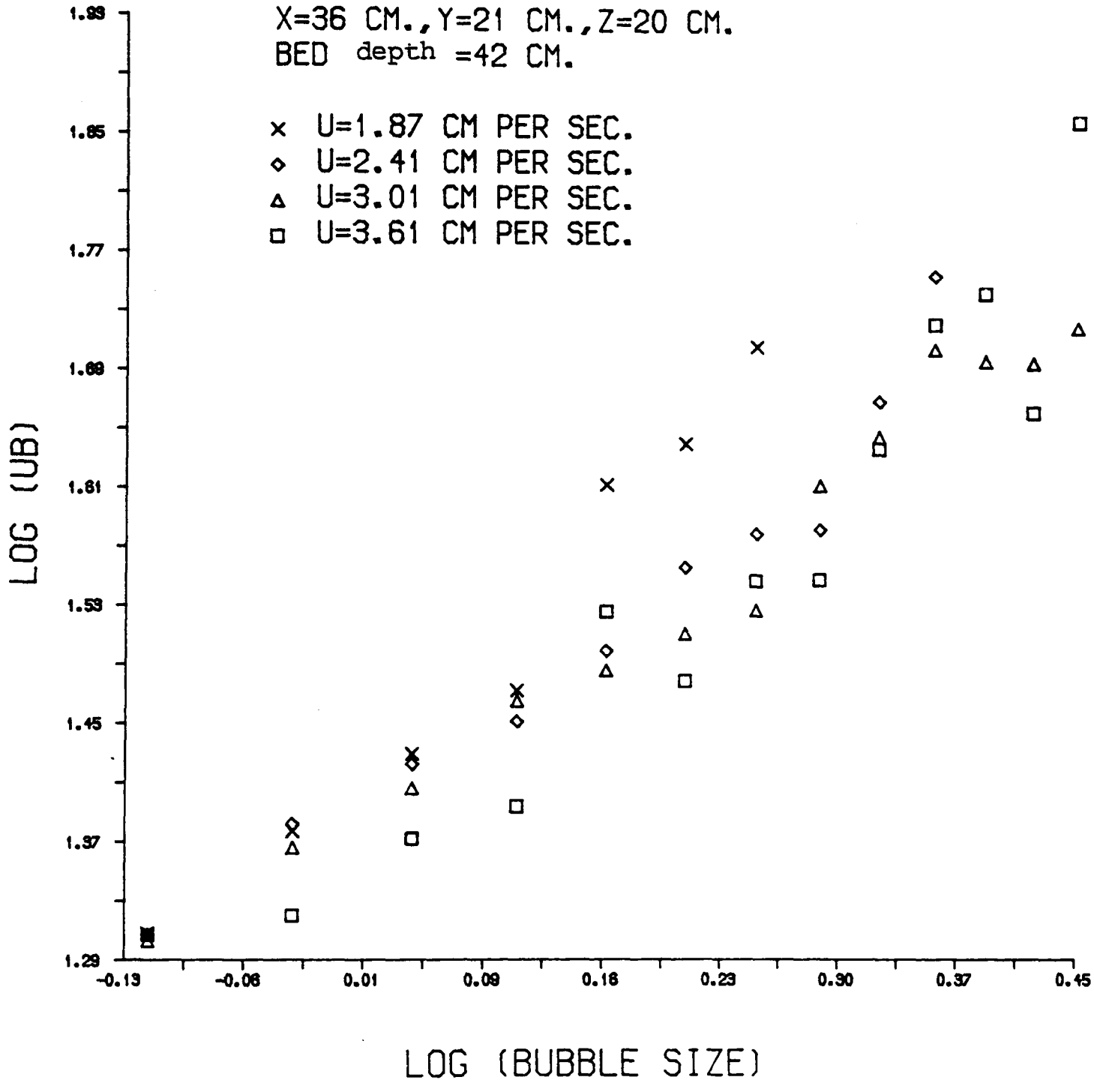
X=36 CM.,Y=21 CM.,Z=20 CM.
BED depth =42 CM.
× U=1.87 CM PER SEC.
◇ U=2.41 CM PER SEC.
△ U=3.01 CM PER SEC.
□ U=3.61 CM PER SEC.
LOG (UB)
1.83
1.65
1.77
1.69
1.61
1.53
1.45
1.37
1.29
-0.13
-0.06
0.01
0.09
0.16
0.23
0.30
0.37
0.45
LOG (BUBBLE SIZE)

The value of $\beta = 1.10$ is abnormally high compared to those of the other three lines. This is caused by the very large scatter (for a very few large bubbles) recorded at this low superificial fluidising velocity. In fact, exclusion of one experimental point, which represents as few as five bubbles would bring this value of β, down to under 1.0.

Table (4.6) shows that the "constant" C is actually decreasing with increasing superficial fluidising velocity. One possible explanation for this could be that this point is on the downward flow of the emulsion phase movement and the negative value of the circulation velocity vector is enhanced by increasing gas velocity.

Analysis of the variance of the data (Appendix E) suggests that the regression lines are parallel but not identical.

Figure (4.26) shows the variation of the absolute rise velocity with bubble nose-to-floor height at another point across the bed cross-sectional area. This point is 20 cm above the distributor plate and on the longitudinal (longer) centre line.

A comparison of Figures (4.19), (4.23) and (4.26) shows that the rise velocity at each interval of bubble height in Figure 4.23 is greater than the corresponding values measured at the points in Figures (4.19) and (4.26). Since these three points are on the same Z plane, this marked difference could be attributed to their relative position with respect to the particle circulation patterns prevalent at this height.

Fig. 4.26

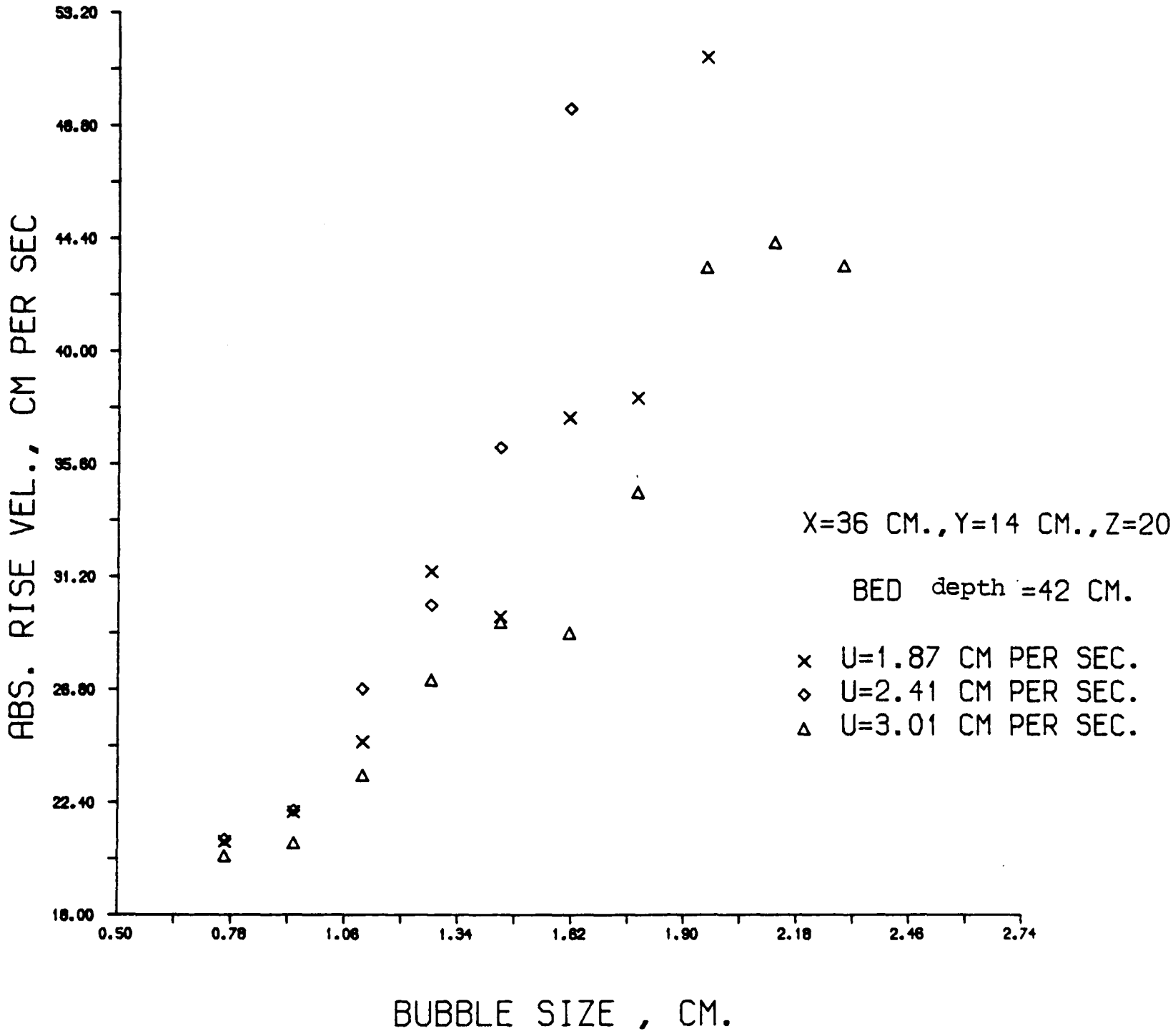
ABS. RISE VEL., CM PER SEC
53.20
48.80
44.40
40.00
35.60
31.20
26.80
22.40
18.00
0.50
0.78
1.06
1.34
1.62
1.90
2.18
2.46
2.74
BUBBLE SIZE , CM.
X=36 CM., Y=14 CM., Z=20
BED depth =42 CM.
× U=1.87 CM PER SEC.
◇ U=2.41 CM PER SEC.
△ U=3.01 CM PER SEC.

Bubble rise velocities were also measured, using the multiorifice plate distributor, with the bed filled initially to a maximum depth of 82 cm.

Figure (4.27) shows the rise velocity-size variation for three different superficial fluidising velocities, at a point 20 cm above the distributor plate. The experimental points show less scatter for smaller bubble sizes.

In Figures (4.28) and (4.29) the investigation of the rise velocity-size variation is carried further to elevations of 50 cm and 70 cm above the distributor plate. All the three experiments (Figures 4.27, 4.28 and 4.29) lie on the same vertical axis. The same three superficial fluidising velocities are used and the bed height is maintained at 82 cm for all three sets of experiments.

These three graphs can be directly compared to reveal the effect of increasing elevation on the bubble rise velocity. The experimental points show much more scatter at lower heights above the distributor plate, (Figure 4.27).

Figure (4.29), corresponding to an elevation of Z = 70 cm, shows very little scatter even for larger bubbles. The number of large bubbles, at this height, is obviously greater, due to the coalescence of smaller bubbles, as they rise up in the bed.

Fig. 4.27

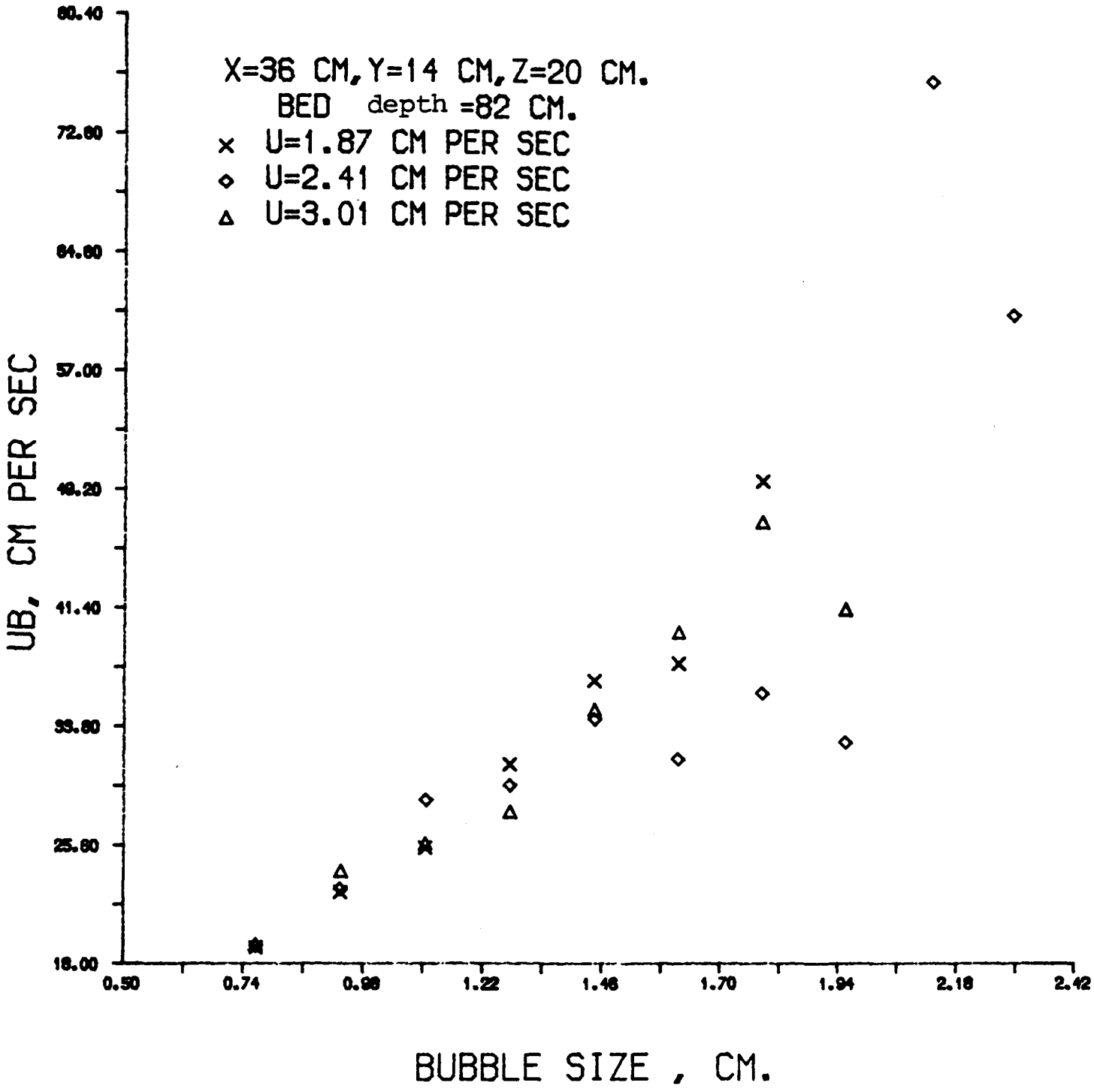
X=36 CM, Y=14 CM, Z=20 CM.
BED depth =82 CM.
× U=1.87 CM PER SEC
◇ U=2.41 CM PER SEC
△ U=3.01 CM PER SEC
UB, CM PER SEC
80.40
72.60
64.80
57.00
49.20
41.40
33.60
25.80
18.00
0.50
0.74
0.98
1.22
1.46
1.70
1.94
2.18
2.42
BUBBLE SIZE , CM.

Fig. 4.28

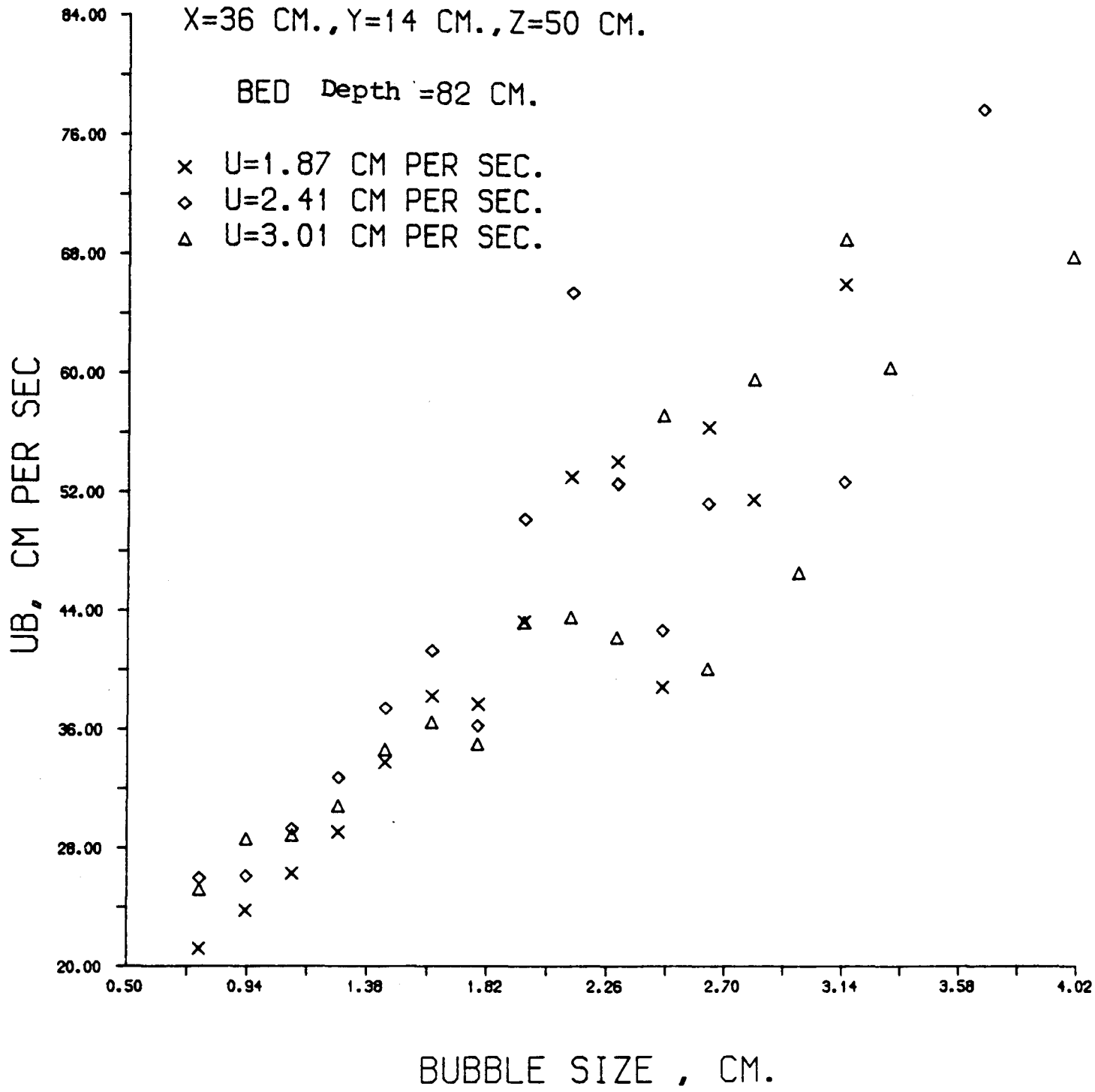
X=36 CM., Y=14 CM., Z=50 CM.
BED Depth =82 CM.
× U=1.87 CM PER SEC.
◇ U=2.41 CM PER SEC.
△ U=3.01 CM PER SEC.
UB, CM PER SEC
84.00
76.00
68.00
60.00
52.00
44.00
36.00
28.00
20.00
0.50
0.94
1.38
1.82
2.26
2.70
3.14
3.58
4.02
BUBBLE SIZE , CM.

Fig. 4.29

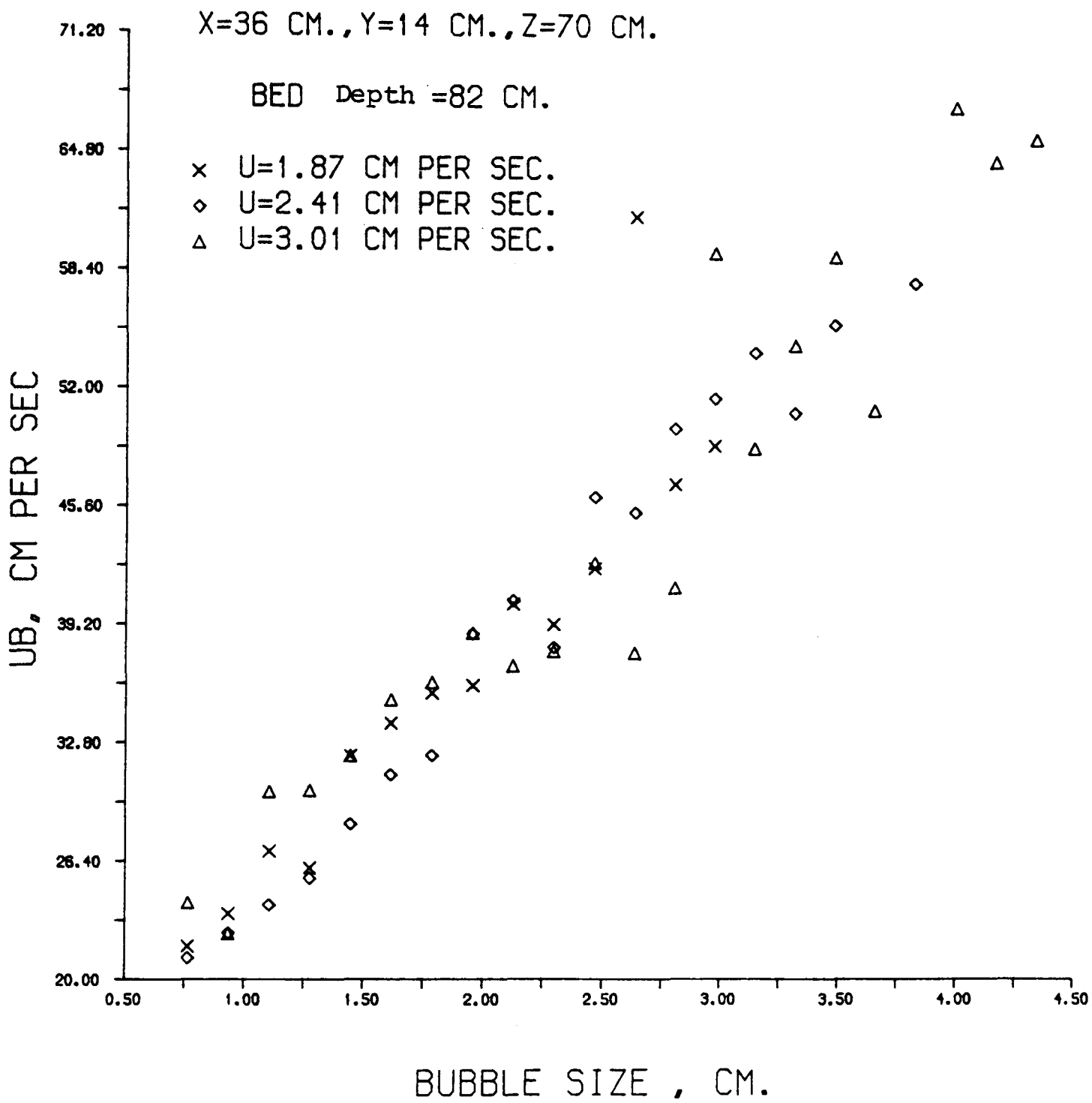
X=36 CM., Y=14 CM., Z=70 CM.
BED Depth =82 CM.
× U=1.87 CM PER SEC.
◇ U=2.41 CM PER SEC.
△ U=3.01 CM PER SEC.
UB, CM PER SEC
71.20
64.80
58.40
52.00
45.60
39.20
32.80
26.40
20.00
0.50
1.00
1.50
2.00
2.50
3.00
3.50
4.00
4.50
BUBBLE SIZE , CM.

4.3.2 Variation with Height above Distributor Plate

Figure (4.30) shows the variation of U_a with the bubble nose-to-floor height at three points on the bed vertical centre line, 20, 30 and 40 cm respectively above the distributor plate. Superficial fluidising velocity is fixed at 3.01 $cm.sec^{-1}$. The rise velocity increases with the bubble size and the higher the elevation the greater the rise velocity for each interval of bubble height recorded.

Equation (4.1) is again used to calculate the relative bubble rise velocity, U_b, and these are plotted against bubble size in Figure (4.31). In Figure (4.32) the bubble rise velocity - bubble size variation is shown for four points on the bed vertical centre line at elevations of 40, 50, 60 and 70 cm above the distributor plate. The superficial fluidising velocity is fixed at 3.01 $cm.sec^{-1}$ and the bed depth is 82 cm.

Again, we find that the bubble rise velocity is increasing with increasing bubble size, but the higher the elevation the smaller the rise velocities recorded, for most intervals.

Figure (4.33) shows the variation of the relative rise velocity, U_b, calculated using equation (4.1) and plotted against bubble size. Experimental points are very close together for the smaller bubbles but show some scatter for larger bubbles.

Figure (4.34) shows the variation of U_a with the bubble nose-to-floor height at six points, on a vertical axis with co-ordinates of X = 36 cm and Y = 14 cm. The superficial fluidising velocity is maintained at 2.41 $cm.sec^{-1}$ and the bed is initially filled to

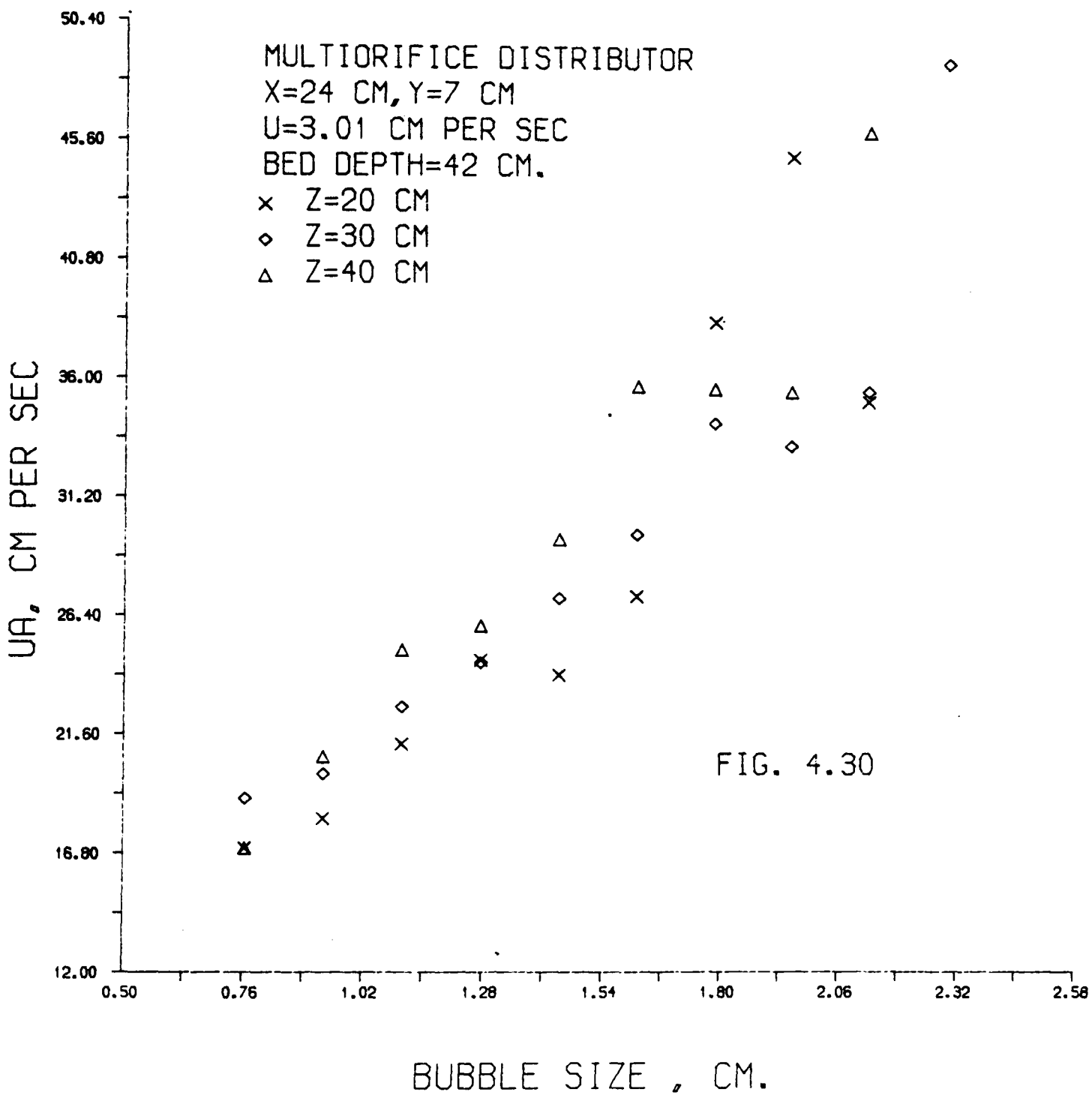
MULTIORIFICE DISTRIBUTOR
X=24 CM, Y=7 CM
U=3.01 CM PER SEC
BED DEPTH=42 CM.
× Z=20 CM
◇ Z=30 CM
△ Z=40 CM
UA, CM PER SEC
50.40
45.60
40.80
36.00
31.20
26.40
21.60
16.80
12.00
0.50
0.76
1.02
1.28
1.54
1.80
2.06
2.32
2.58
BUBBLE SIZE , CM.

FIG. 4.30

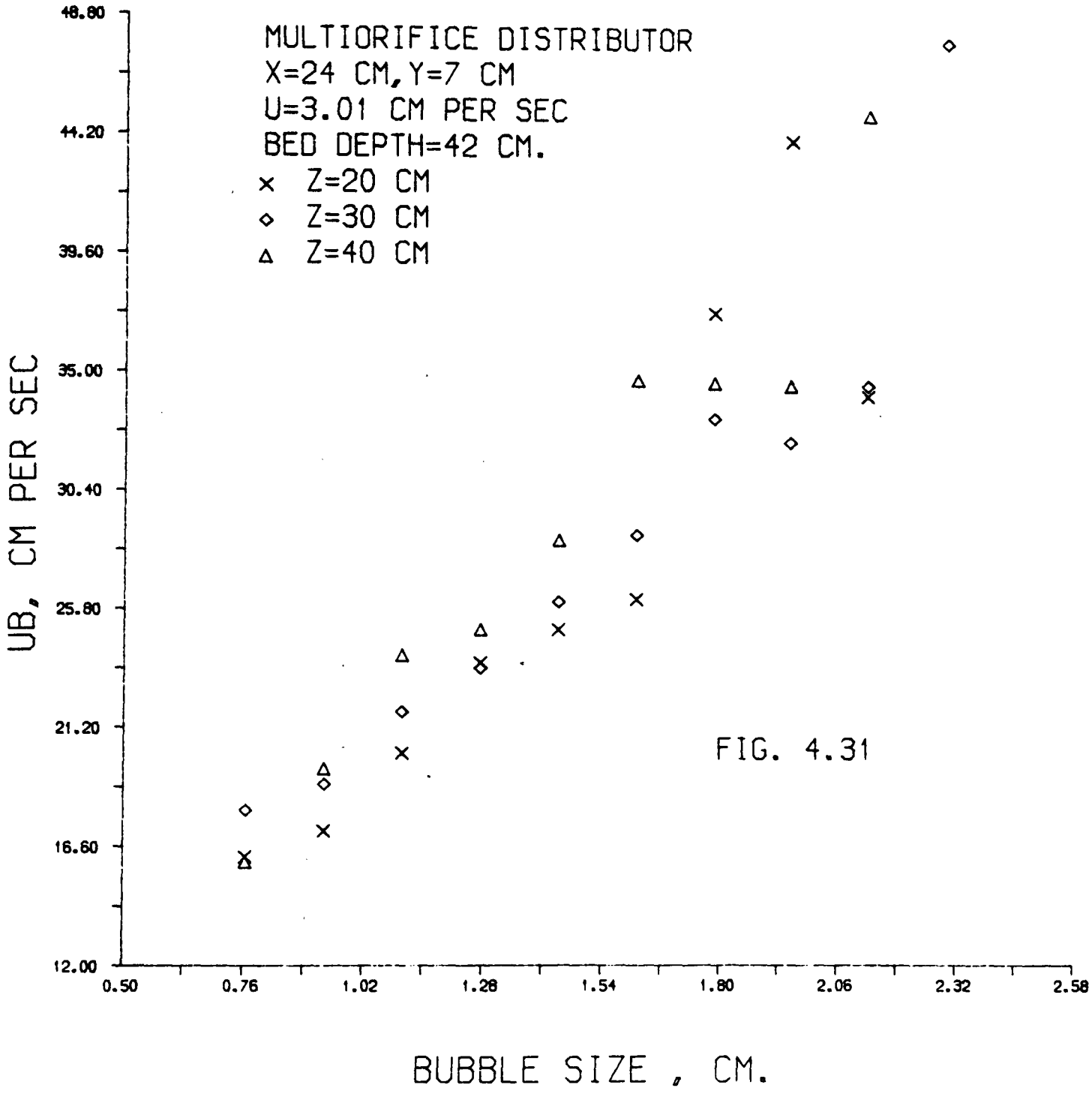
MULTIORIFICE DISTRIBUTOR
X=24 CM, Y=7 CM
U=3.01 CM PER SEC
BED DEPTH=42 CM.
× Z=20 CM
◇ Z=30 CM
△ Z=40 CM
UB, CM PER SEC
48.80
44.20
39.60
35.00
30.40
25.80
21.20
16.60
12.00
0.50
0.76
1.02
1.28
1.54
1.80
2.06
2.32
2.58
BUBBLE SIZE , CM.

FIG. 4.31

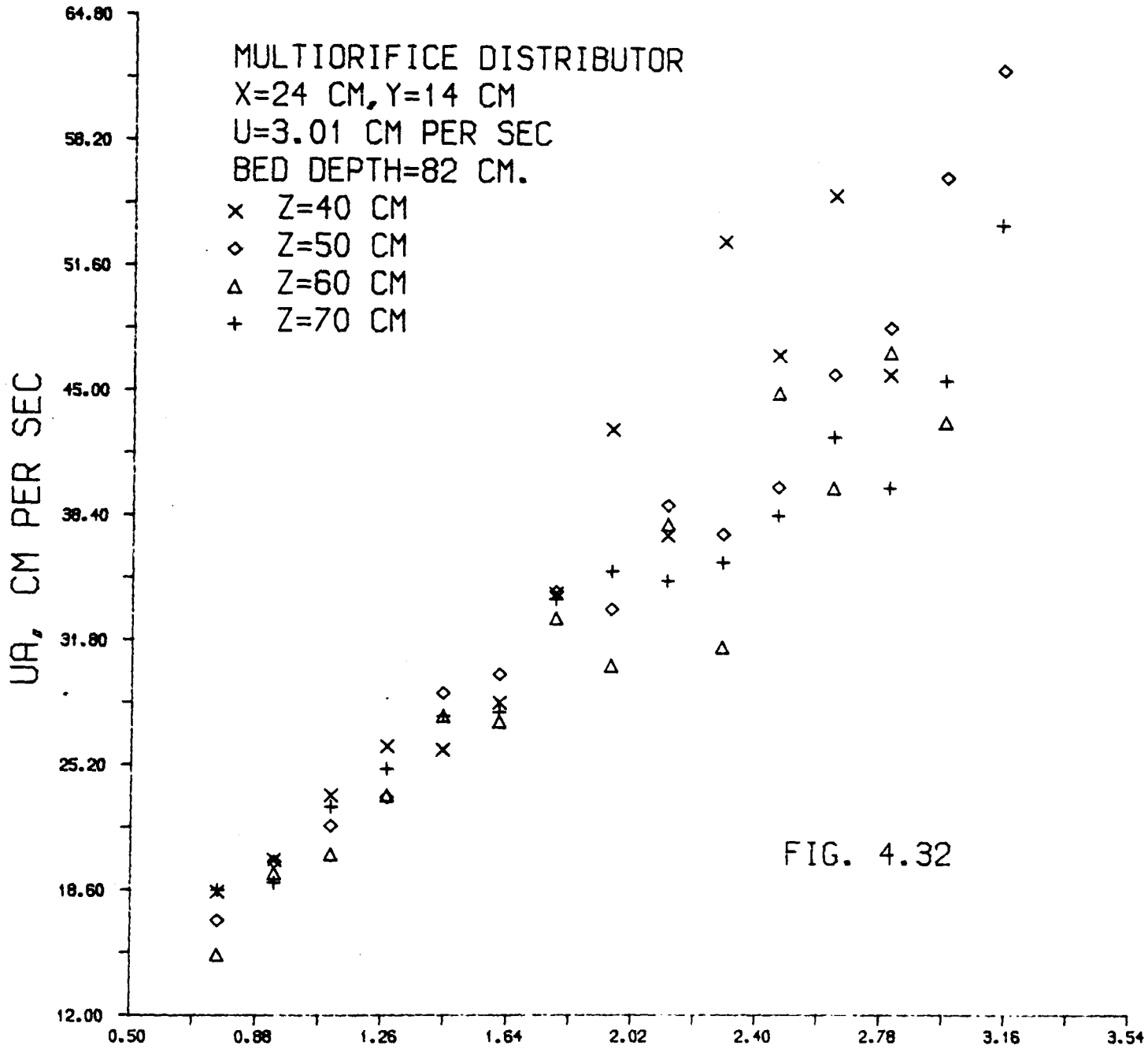
MULTIORIFICE DISTRIBUTOR
X=24 CM, Y=14 CM
U=3.01 CM PER SEC
BED DEPTH=82 CM.
× Z=40 CM
◇ Z=50 CM
△ Z=60 CM
+ Z=70 CM
UB, CM PER SEC
64.80
58.20
51.60
45.00
38.40
31.80
25.20
18.60
12.00
0.50
0.88
1.26
1.64
2.02
2.40
2.78
3.16
3.54
BUBBLE SIZE , CM.

FIG. 4.32

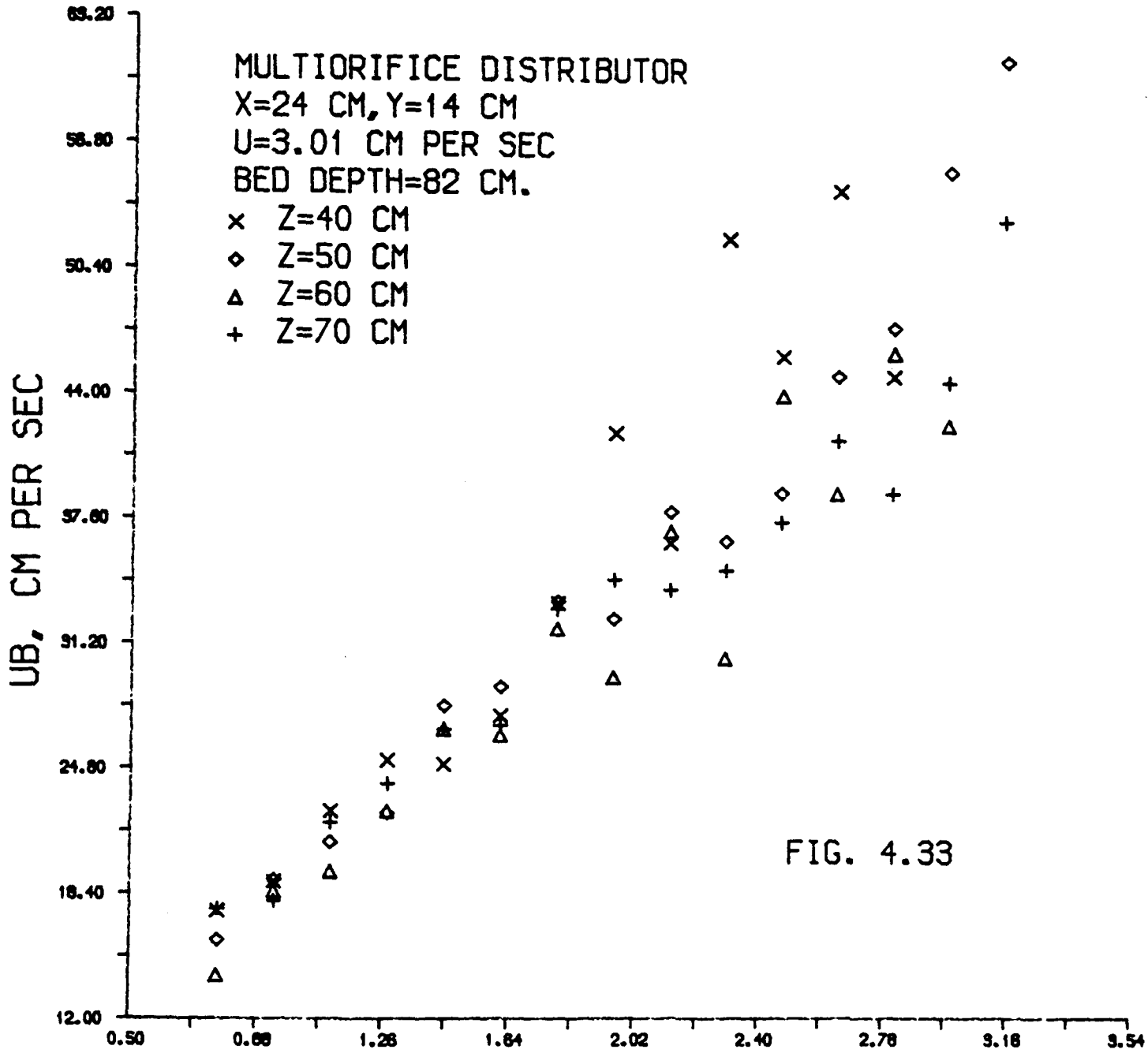
MULTIORIFICE DISTRIBUTOR
X=24 CM, Y=14 CM
U=3.01 CM PER SEC
BED DEPTH=82 CM.
× Z=40 CM
◇ Z=50 CM
△ Z=60 CM
+ Z=70 CM
UB, CM PER SEC
63.20
56.80
50.40
44.00
37.60
31.20
24.80
18.40
12.00
0.50
0.88
1.26
1.64
2.02
2.40
2.78
3.16
3.54
BUBBLE SIZE , CM.

FIG. 4.33

Fig. 4.34

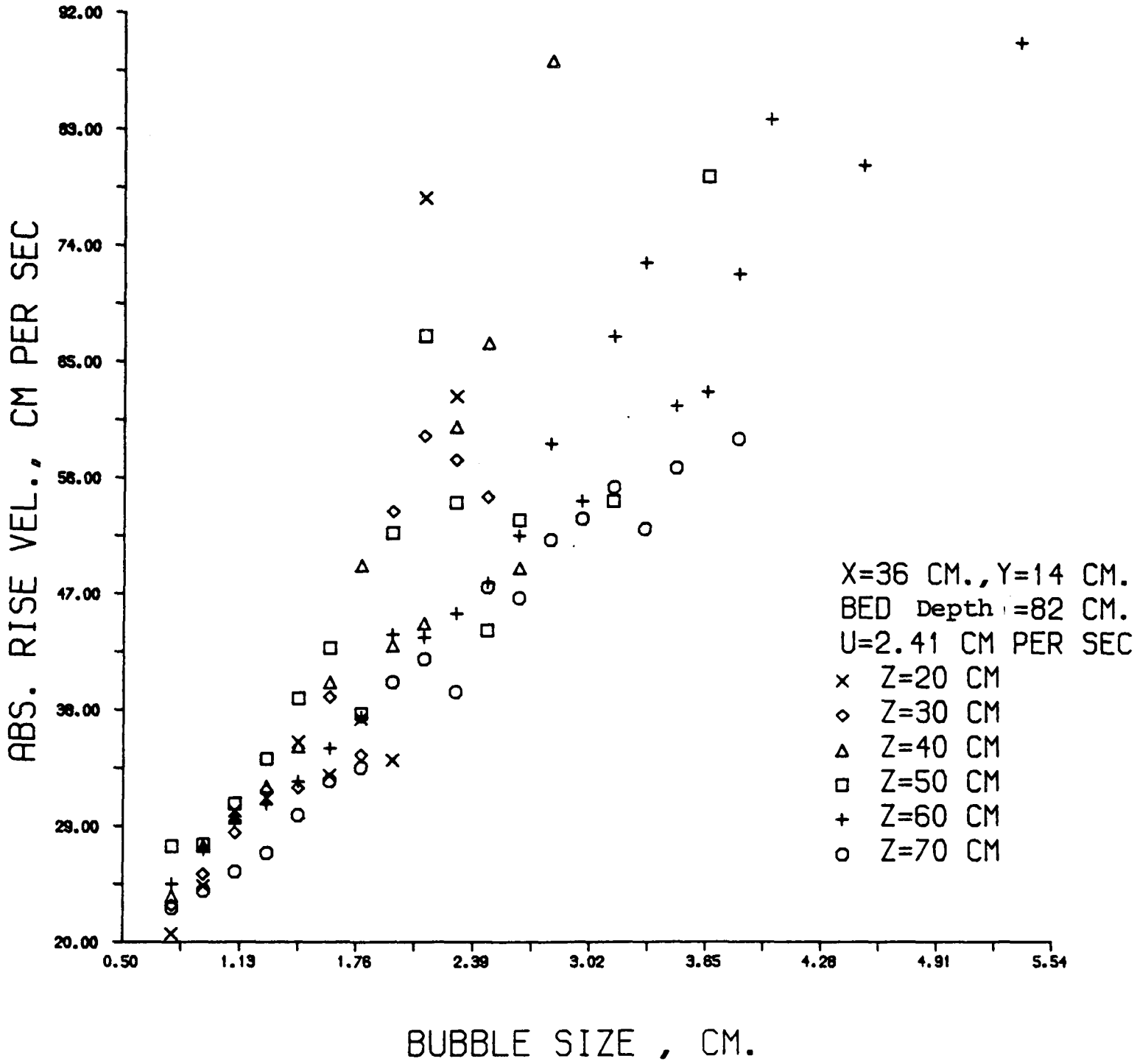
ABS. RISE VEL., CM PER SEC
92.00
83.00
74.00
65.00
56.00
47.00
38.00
29.00
20.00
0.50
1.13
1.76
2.39
3.02
3.65
4.28
4.91
5.54
BUBBLE SIZE , CM.
X=36 CM., Y=14 CM.
BED Depth =82 CM.
U=2.41 CM PER SEC
× Z=20 CM
◇ Z=30 CM
△ Z=40 CM
□ Z=50 CM
+ Z=60 CM
○ Z=70 CM

a maximum depth of 82 cm. The rise velocity, again, increases with the bubble size and the higher the elevation the greater the rise velocity recorded.

The two graphs (Figures 4.32 and 4.34) reveal two opposite trends in the U_a - bubble size variation with increasing height above the distributor plate. In one (Figure 4.32) the highest velocities recorded (for most intervals of bubble height), correspond to the lowest of the four elevations investigated; namely Z = 40 cm. In the other, Figure (4.34), conversely, the highest values of the rise velocities measured belong to an elevation of 60 cm above the distributor plate.

Points for Z = 70 cm seem anomalously low. There are not many large bubbles to be found at low heights above the distributor plate. The anomalous variation with height in (4.32) could possibly be due to the relative position of these points with respect to the particle phase circulation patterns affecting the bubble rise velocities, at these elevations. It must also be mentioned, here, that the radius of curvature of the bubbles, R, varies with h, the bubble nose-to-floor height, much more rapidly at high values of h than at low, causing in turn a much greater increase in the rise velocity, U_b.

The relative rise velocities, U_b, calculated using equation (4.1), are plotted against the bubble size in Figure (4.35), while the data is replotted on logarithmic axes in Figure (4.36).

Fig. 4.35

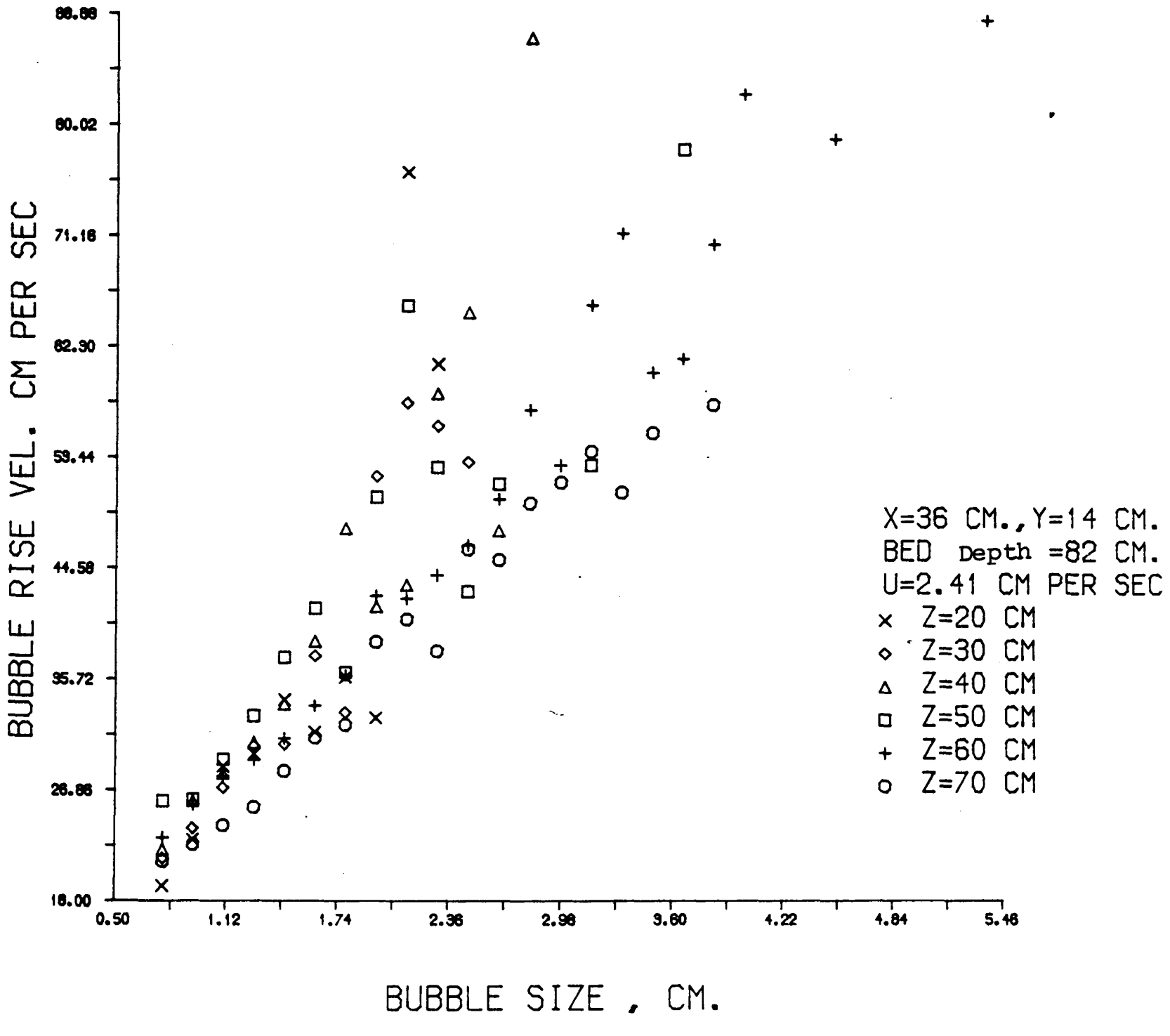
BUBBLE RISE VEL. , CM PER SEC
88.88
80.02
71.16
62.30
53.44
44.58
35.72
26.86
18.00
0.50
1.12
1.74
2.36
2.98
3.60
4.22
4.84
5.46
BUBBLE SIZE , CM.
X=36 CM., Y=14 CM.
BED Depth =82 CM.
U=2.41 CM PER SEC
× Z=20 CM
◇ Z=30 CM
△ Z=40 CM
□ Z=50 CM
+ Z=60 CM
○ Z=70 CM

Fig. 4.36

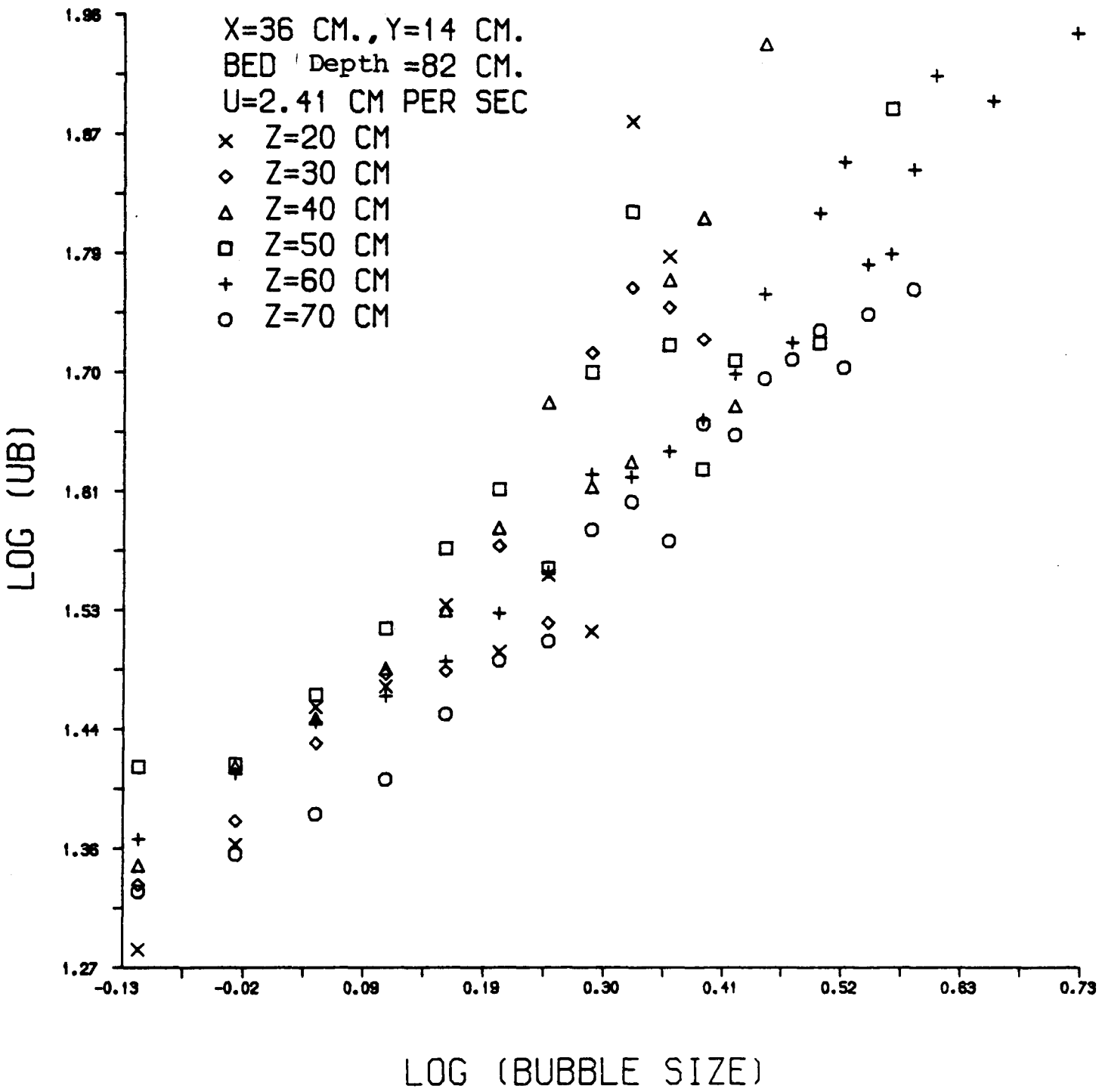
X=36 CM., Y=14 CM.
BED Depth =82 CM.
U=2.41 CM PER SEC
Z=20 CM
Z=30 CM
Z=40 CM
Z=50 CM
Z=60 CM
Z=70 CM
1.96
1.87
1.79
1.70
1.61
1.53
1.44
1.36
1.27
-0.13
-0.02
0.09
0.19
0.30
0.41
0.52
0.63
0.73
LOG (UB)
LOG (BUBBLE SIZE)

Straight lines are fitted to the individual sets of data and a summary of the results is shown in Table (4.7) below.

Z cm	α	C	β	Correlation Coefficient
20	1.38	23.79	0.98	0.85
30	1.39	24.92	0.89	0.94
40	1.42	26.11	0.88	0.93
50	1.46	28.91	0.66	0.90
60	1.40	25.23	0.75	0.98
70	1.36	23.09	0.69	0.99
All Points	1.42	25.73	0.74	0.92

TABLE (4.7)

Relationship between bubble rise velocity and size at a superficial fluidising velocity of 2.41 $cm.sec^{-1}$ and differing elevations in the bed.

$U = 2.41\ cm.sec^{-1}$

X = 36 cm

Y = 14 cm

Bed depth = 82 cm

Analysis of the variance of the data (Appendix F) suggest that the regression lines are parallel but not identical.

The "constant" C, in Table (4.7) increases with elevation above the distributor plate up to the point corresponding to Z = 50 cm and then decreases.

This change of direction, could possibly be caused by a change in the direction of the particle phase circulation patterns at around 50 cm elevation above the distributor plate.

Table (4.8) below, shows the absolute rise velocities of bubbles generated by the two distributor plates at three elevations above the plates.

Bubble Size (cm)	Z = 50 cm		Z = 60 cm		Z = 70 cm	
	P.P.Distr.	M.O.D.	P.P.D.	M.O.D.	P.P.Distr.	M.O.Distr.
0.765	26.792	22.124	24.119	24.702	25.00	22.700
0.935	29.143	24.697	23.574	27.322	24.382	24.482
1.105	30.569	27.195	26.179	27.373	27.715	27.859
1.275	36.633	29.993	25.239	30.999	30.200	26.936
1.445	38.047	34.697	28.618	30.469	30.481	33.003
1.615	45.728	39.187	33.293	35.725	34.465	34.749
1.785	44.141	38.625	35.806	32.561	36.414	36.379
1.955	50.635	44.243	36.311	44.175	42.070	36.780
2.125	54.824	54.053	42.554	47.593	39.941	41.211
2.295	58.140	55.098	37.766	44.492	43.843	40.107
2.465	49.614	39.805	39.849	51.655	61.289	43.145
2.635	52.637	57.412	43.613	52.310	47.407	62.192
2.805		52.544	52.075	59.077	40.337	47.705
2.975		67.168	54.307	61.274	68.013	49.814
3.145			54.048		49.336	
3.315			65.781			
			55.000			

TABLE (4.8)

X = 36 cm, Y = 14 cm, U = 1.87 cm.sec^{-1}, Depth = 82 cm.

The rise velocity at each interval of bubble height is greater when the porosint distributor is employed, up to elevations around 50 cm, especially for the smaller bubbles. The difference in the magnitude of the velocities is not so pronounced for the larger bubbles.

At an elevation of 60 cm (and above) the pattern is reversed and greater rise velocities are measured using the multiorifice distributor. Here too, there does not seem to be a marked difference in the greater bubble size-ranges.

Most theories assume that the only relevant parameter affecting the bubble rise velocity is the bubble size (volume) regardless of how the bubble reached that volume. Table (4.8) compares the rise velocities of bubbles of equal size. Enhanced velocity of bubbles at low elevations above the porosint plate distributor may be due to the fact that, at low elevations above the multi-orifice distributor, not all the bed is uniformly fluidised, (due to inactive orifices on the multiorifice distributor).

4.3.3 Variation across the Bed Cross-Sectional Area

Figure (4.37) shows the rise velocity-size relationship for three points, across the bed cross-sectional area, all 20 cm above the multiorifice distributor plate. The superficial fluidising velocity is fixed at 2.41 $cm.sec^{-1}$ and the bed is initially filled to a maximum depth of 82 cm.

The graph shows that the data for all three points are very close but the variation of the centre line results more irregular than the two "wall" positions.

This relationship is shown for three points, with the same X and Y co-ordinates, but on a plane 20 cm higher up in the bed, Figure (4.38). The same superficial fluidising velocity, U = 2.41 $cm.sec^{-1}$ and the same bed height of 82 cm are maintained.

The values of U_b seem to be greater in the "wall" positions, at low depths in the bed, but with an increase in height the pattern is reversed.

Figure (4.38) clearly shows that, above Z = 40 cm, the bubbles in the central zone are rising faster than near the walls of the bed. Again, the results for the two "wall" positions are very close, the centre line results differing appreciably from these.

Fig. 4.37

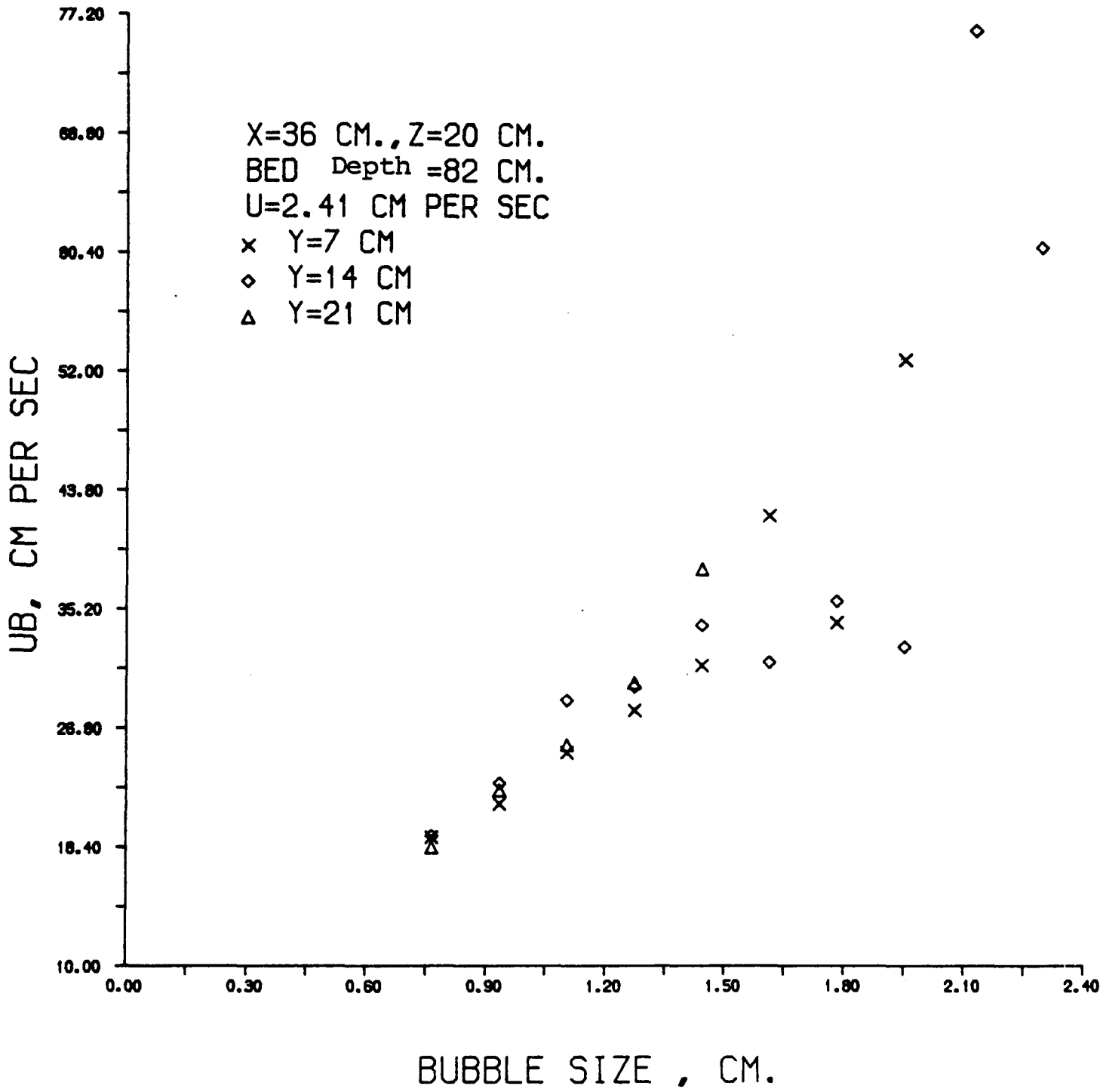
X=36 CM., Z=20 CM.
BED Depth =82 CM.
U=2.41 CM PER SEC
× Y=7 CM
◇ Y=14 CM
△ Y=21 CM
UB, CM PER SEC
77.20
68.80
60.40
52.00
43.80
35.20
26.80
18.40
10.00
0.00
0.30
0.60
0.90
1.20
1.50
1.80
2.10
2.40
BUBBLE SIZE , CM.

Fig. 4.38

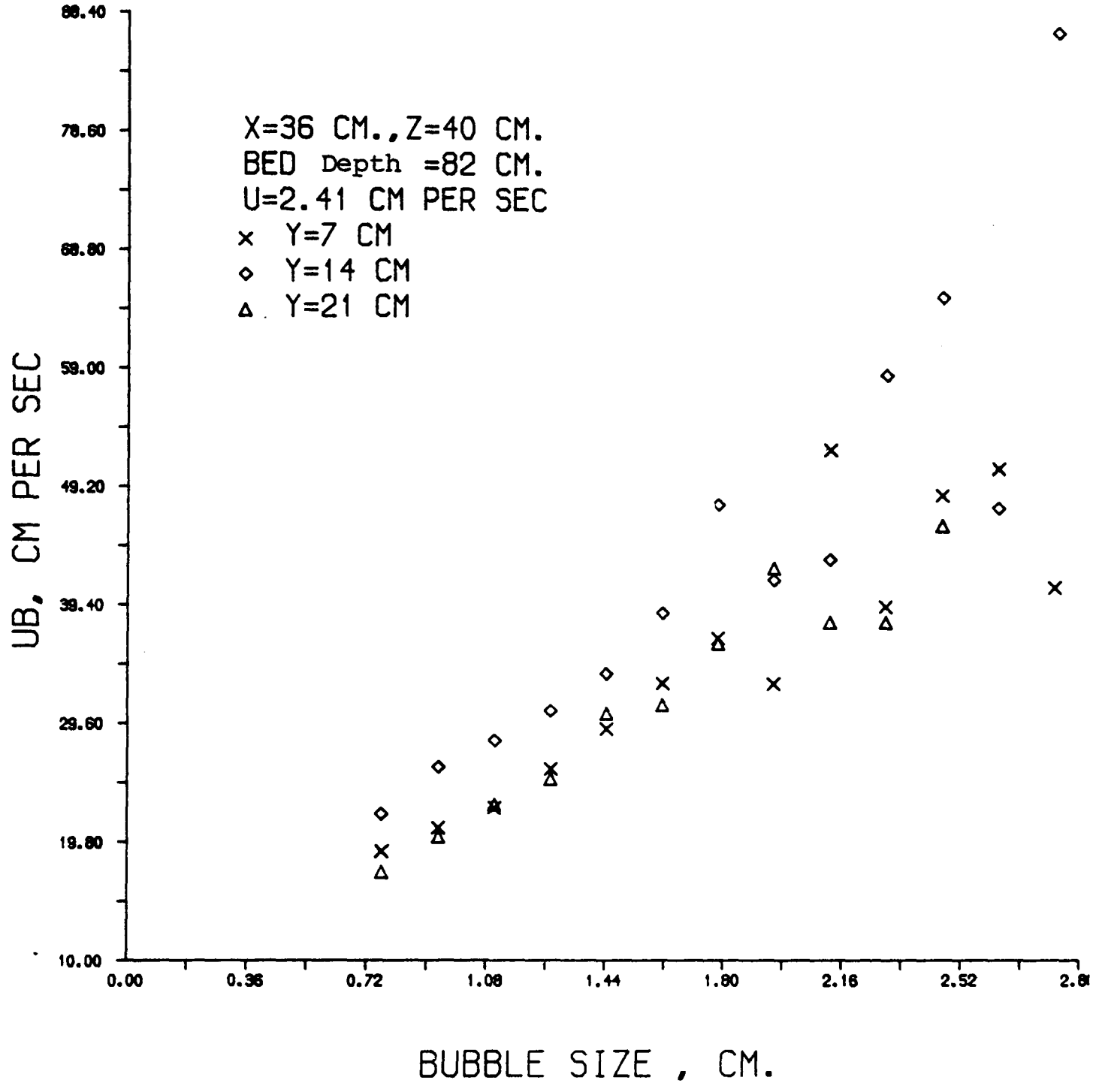
X=36 CM., Z=40 CM.
BED Depth =82 CM.
U=2.41 CM PER SEC
× Y=7 CM
◇ Y=14 CM
△ Y=21 CM
UB, CM PER SEC
88.40
78.60
68.80
59.00
49.20
39.40
29.60
19.80
10.00
0.00
0.36
0.72
1.08
1.44
1.80
2.16
2.52
BUBBLE SIZE , CM.

Figure (4.39) is a further demonstration of this phenomenon. It shows the U_b - size variation for two points, at an elevation of 60 cm above the distributor plate, but at the same superficial fluidising velocity of 2.41 $cm.sec^{-1}$. Bed height is, again, maintained at 82 cm in both experiments. The data for the centre line position show markedly greater velocities than the corresponding values for the point near the "front wall". The two points are on the same X = 36 cm plane, and only 7 cm apart.

A reasonable sample (sufficient number of bubbles) could not be collected for the third point, (i.e. Y = 21 cm). Presumably, the bubbles are swept away from this point by the particle phase circulation movements. This is further indicated when the bubble frequency distributions across the bed are studied (chapter 6). High concentrations of bubbles seem to lie near the walls at low depths in the bed, but moving towards more central positions as the elevation above the distribution is increased.

The comparison of rise velocities at different points across the bed cross-sectional area is extended to another plane (X = 24 cm). Table (4.9), below, shows the rise velocity-size variation for three different points with 7.0, 14.0 and 21.0 cm Y co-ordinates. Although the same superficial fluidising velocity (U = 2.41 $cm.sec^{-1}$) is maintained in these experiments, these results cannot be directly compared to those in Figure (4.39), the bed depth being 42 cm here. All three points are located on the Z = 20 cm plane.

Fig. 4.39

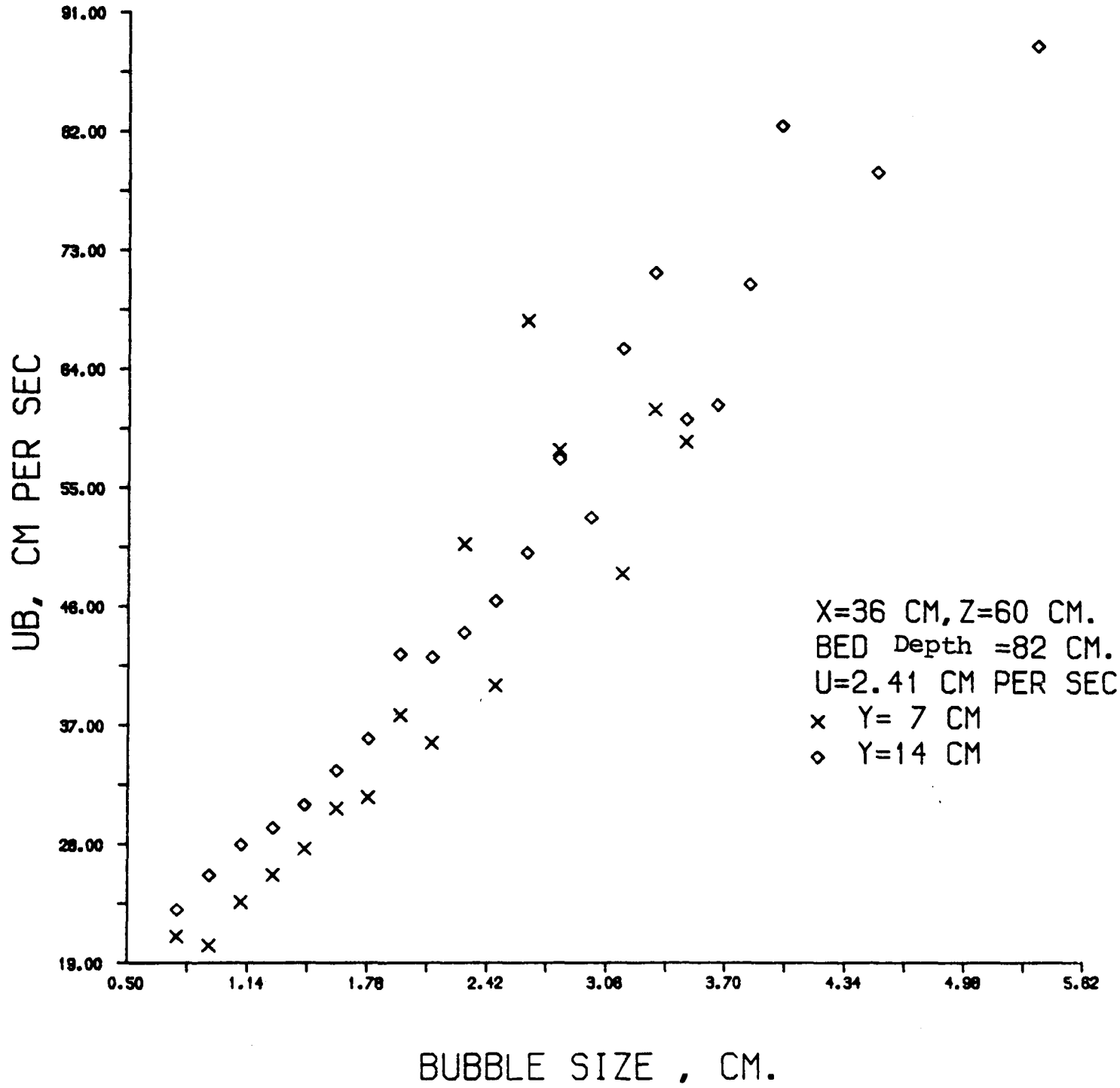
91.00
82.00
73.00
64.00
55.00
46.00
37.00
28.00
19.00
UB, CM PER SEC
0.50
1.14
1.78
2.42
3.06
3.70
4.34
4.98
5.62
X=36 CM, Z=60 CM.
BED Depth =82 CM.
U=2.41 CM PER SEC
× Y= 7 CM
◇ Y=14 CM
BUBBLE SIZE , CM.

Size (cm)	U_B (Y = 7.0)	U_B (Y = 14.0)	U_B (Y = 21)
0.765	22.468	16.770	19.67
0.935	23.923	19.844	22.707
1.105	26.606	22.212	25.315
1.275	32.859	24.790	28.586
1.485	34.575	29.341	33.071
1.615	37.278	30.493	35.693
1.785	44.912	42.642	-
1.955	40.483	-	-
2.125	67.681	-	-
2.295	64.858	-	-

TABLE (4.9)

Rise Velocity-Size Variation for three points with different Y co-ordinates, superficial fluidising velocity = 2.41 cm/sec.

Multiorifice Distributor

Z = 20 cm

U = 2.41 $cm.sec^{-1}$

X = 24 cm

Bed Depth = 42 cm

Table (4.9) shows that the central point has the lowest rise velocities for all the intervals of bubble height. It suggests strong upward currents at Y = 7 cm and to a lesser extent at Y = 21 cm. Presumably, this suggests an upward emulsion phase movement in the "wall" positions (i.e. near the walls of the bed), and downwards in the central zone. It must be remembered that the bed height is 42 cm in these experiments and therefore the emulsion phase movement would look something like Figure (4.40) below.

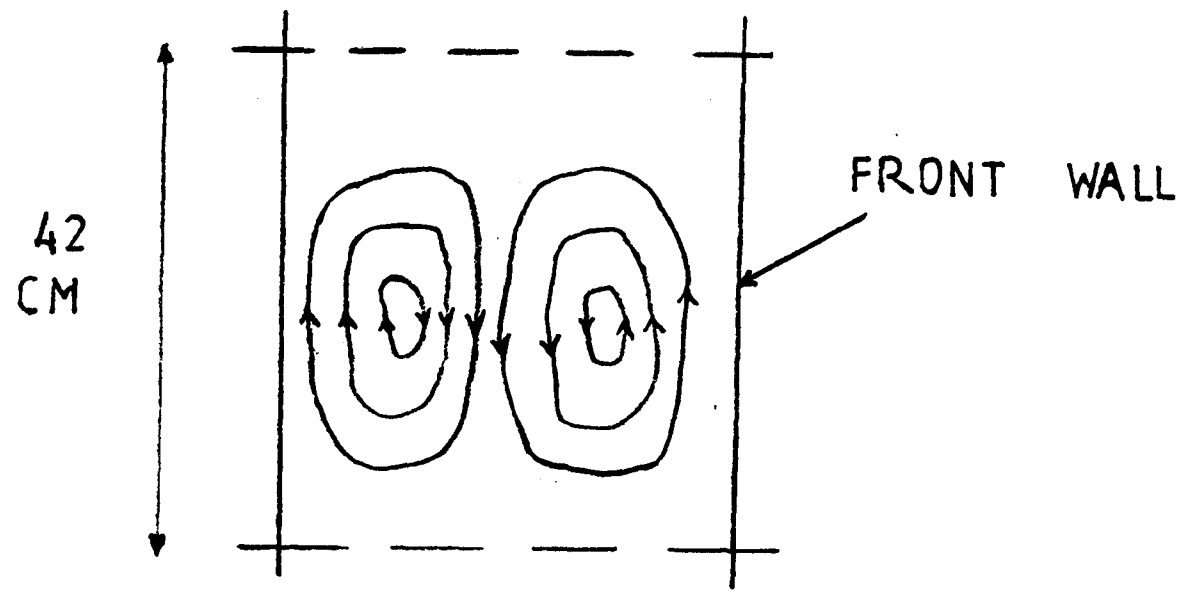

Figure (4.40)

Side-view of the bed

Table (4.10) shows the same relationship for three points at a higher elevation of 40 cm above the distributor plate.

Size (cm)	U_B (Y = 7 cm)	U_B (Y = 14 cm)	U_B (Y = 21 cm)
0.765	22.207	23.695	18.409
0.935	24.187	24.782	19.900
1.105	24.575	27.041	23.240
1.275	30.811	30.537	25.581
1.445	30.564	36.891	27.759
1.615	32.056	36.423	30.437
1.785	36.887	39.548	34.263
1.955	39.302	40.127	33.896
2.125	49.561	43.042	50.571
2.295	50.376	51.500	-
2.465	43.491	47.168	43.130
2.975	54.487	58.559	-

TABLE (4.10)

Rise Velocity-Size Variations for three points, at Z = 40 cm

U = 2.41 $cm.sec^{-1}$, X = 24 cm, Bed depth = 42.0 cm.

Multiorifice Distributor

Comparison of the data in Table (4.10) with those in Table (4.9) reveals an interesting phenomenon. When the bed depth is 42 cm, the points in Table (4.10) are all on the Z = 40 cm plane, just 2 cm below the bed surface. The central point now shows greater velocities than the value corresponding to the points on either side, for almost all the intervals of bubble height.

Table (4.11) shows the data for U_b - size variation at a still higher elevation of 50 cm above the distributor plate. Obviously the bed height is increased (to 52 cm), in this case.

The same superficial fluidising velocity and the same X co-ordinates are maintained.

Comparison of these two tables (4.10 and 4.11) with Table (4.9) reveals a reversal of pattern, in that, in these, the highest rise velocities recorded correspond to the central point, in most of the intervals of bubble height.

Size (cm)	U_B(at Y = 7)	U_B(at Y = 14)	U_B(at Y = 21)
0.765	21.519	21.987	19.810
0.935	23.691	25.361	20.791
1.105	26.064	26.255	24.155
1.275	24.941	31.118	24.333
1.455	28.096	31.860	29.922
1.615	32.624	40.269	29.231
1.785	37.808	45.244	36.145
1.955	36.943	34.365	35.366
2.215	42.051	49.351	38.232
2.295	41.841	40.688	44.956
2.465	55.498	42.261	53.101
2.635	51.079	48.774	45.942
2.805	51.050	-	56.728
2.975	-	63.315	57.388

TABLE (4.11)

Z = 50 cm

X = 24 cm

Bed Depth = 52 cm

U = 2.41 $cm.sec^{-1}$.

Multiorifice Distributor

While data in Table (4.10) can be directly compared to Table (4.9), both representing data of experiments carried out under identical conditions, a comparison of Tables (4.9) and (4.11) is not, strictly speaking, quite valid. Increasing the bed depth by 10 cm will probably change the magnitude of the particle flow patterns. But it seems unlikely to change the direction of flow at 20 cm elevation, very much. Therefore, it seems reasonable to assume that very similar particle flow patterns would exist in the bed, the radius of the circulation being somewhat greater, in the case of a bed with 10 cm greater depth. A close study of the velocities in these three tables, confirms this conclusion.

It is interesting to note that in all three tables (4.9, 4.10 and 4.11) data corresponding to the points nearer to the "front" wall show greater velocities than those corresponding to the "back" wall of the bed. Although the difference is not so marked at higher elevations it persists, even at 50 cm above the distributor plate.

In Table (4.12), the rise velocities are tabulated against the average bubble size for two points on Z = 70 cm plane. The points are 7 cm apart, but both on the X = 24 cm plane, and the same gas velocity (U = 2.41 $cm.sec^{-1}$) is applied in both experiments. The bed height is 82 cm, when fluidised.

Insufficient data is available for the third point, (i.e. Y = 21 cm) to make comparison between the three positions (Table 4.9, 4.10 and 4.11) possible.

Size (cm)	U_B (at Y = 7)	U_B (at Y = 14)	U_B (at Y = 21)
0.765	14.715	20.606	Insufficient data could be collected at this point
0.935	18.771	22.898	
1.105	21.287	24.910	
1.225	22.530	28.040	
1.445	25.293	30.457	
1.615	28.216	31.746	
1.785	29.837	34.517	
1.955	36.934	35.096	
2.125	-	41.277	
2.295	-	36.976	
2.465	-	47.508	
2.635	41.580	-	
2.805	-	56.004	
3.315	59.656	61.336	

TABLE (4.12)

Rise Velocity - Size Relationship for two points at a plane Z = 70 cm, X = 24 cm, (U = 2.41 cm/sec), Bed Depth = 82 cm. Multiorifice Distributor.

The data in this table (4.12) cannot be directly compared to any one of the three previous ones. It is thought that, when the bed depth is increased to a near maximum of 82 cm, the flow patterns which would have been present at heights of 42 or 52 cm, break up and different circulation patterns emerge.

Nevertheless, the rise velocities corresponding to the central position are greater and the difference more marked at this high elevation (70 cm) above the distributor plate.

The study of the emulsion phase movement is one aspect of this investigation which will be discussed in more detail in the next chapter.

Here, the study of U_b - size relationship is extended to include variation along the X (i.e. longitudinal) co-ordinates. In Figure (4.41) the rise velocities of bubbles at three points along the X-axis (X = 12, 24 and 36 cm) and at the Y = 7 cm plane are plotted against the average bubble size.

The point with X = 12 cm is the nearest to the point of gas inlet. The superficial fluidising velocity is 2.41 $cm.sec^{-1}$ and these three points are on the Z = 20 cm plane. The bed depth is 42 cm when the bed is fluidised. The experimental points are close and show less scatter for smaller bubbles. The data for the central position are more irregular, especially towards greater sizes.

Fig. 4.41

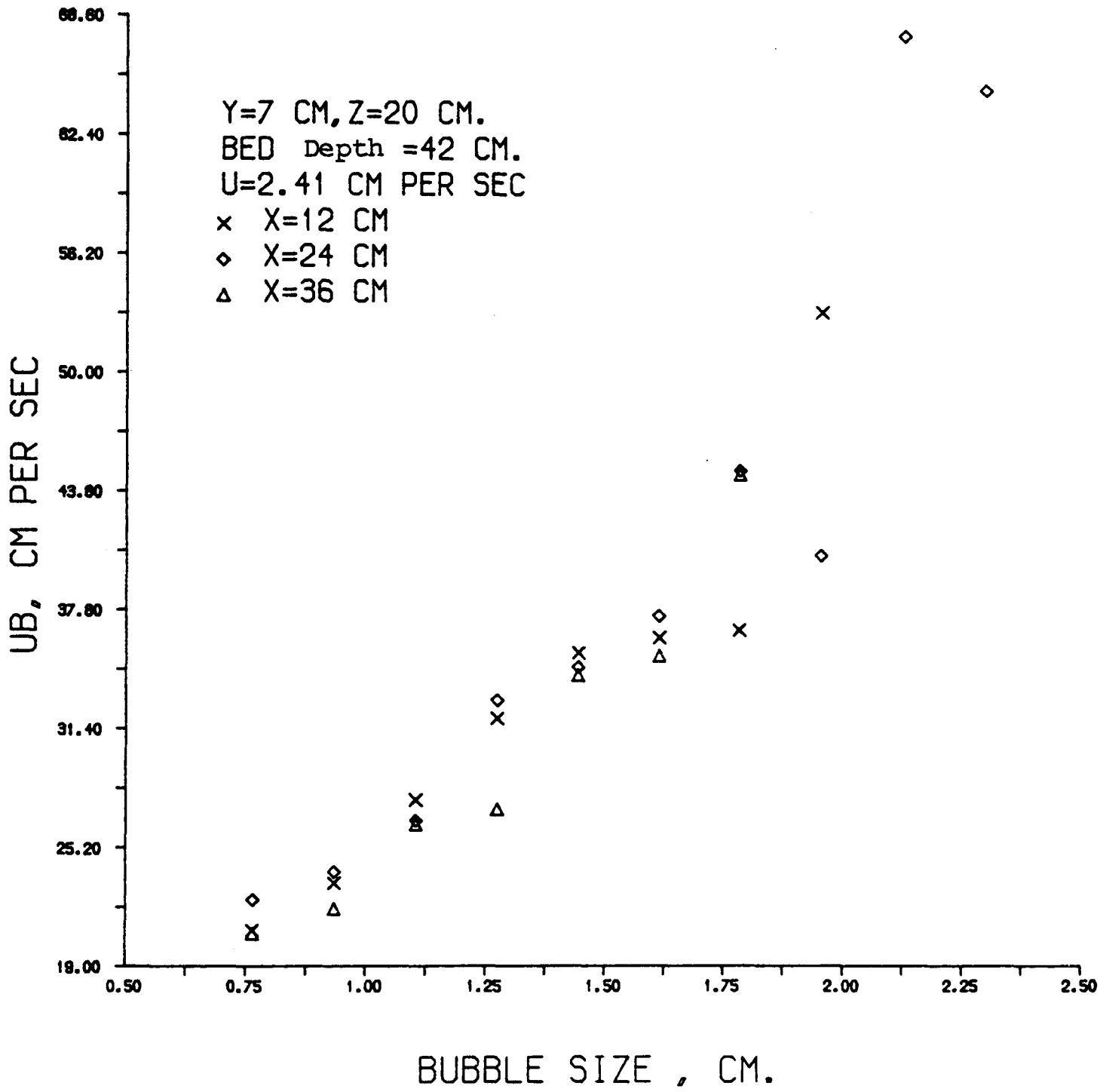
Y=7 CM, Z=20 CM.
BED Depth =42 CM.
U=2.41 CM PER SEC
× X=12 CM
◇ X=24 CM
△ X=36 CM
UB, CM PER SEC
62.60
56.20
50.00
43.80
37.80
31.40
25.20
19.00
0.50
0.75
1.00
1.25
1.50
1.75
2.00
2.25
2.50
BUBBLE SIZE , CM.

The rise velocity - size relationship, studied at a higher elevation of 50 cm, Figure (4.42), shows very little change. This graph represents points on the Z = 50 plane, the bed depth being 52 cm, at a superficial fluidising velocity of 2.41 $cm.sec^{-1}$. Again, all the points are on the Y = 7 cm plane.

It seems that no conclusion can be drawn from these two graphs (4.41 and 4.42), partly due to the fact that they are at different bed depths and partly because of the scatter of the points.

Nevertheless, a close study of these two graphs shows that the influence of the particle circulation patterns on the bubble rise velocity, experienced along the Y co-ordinates (Tables 4.9, 4.10 and 4.11), seems not to exist along this X-axis.

In Table (4.13), the rise velocity - size variation, along the X-axis (at the Y = 7 cm plane), is extended to an elevation of 70 cm above the distributor plate. The bed depth is 82 cm and the superficial fluidising velocity is fixed at 1.87 $cm.sec^{-1}$.

Here, the data corresponding to the central point, show a marked drop from the two points on either side. Experimental results for the two points (with X = 12 cm and X = 36 cm) are close and both markedly greater than the corresponding values for X = 24 cm. Unfortunately, too many parameters (e.g. bed depth, superficial fluidising velocity), being different, there is no way of comparing these results directly and meaningfully.

Fig. 4.42

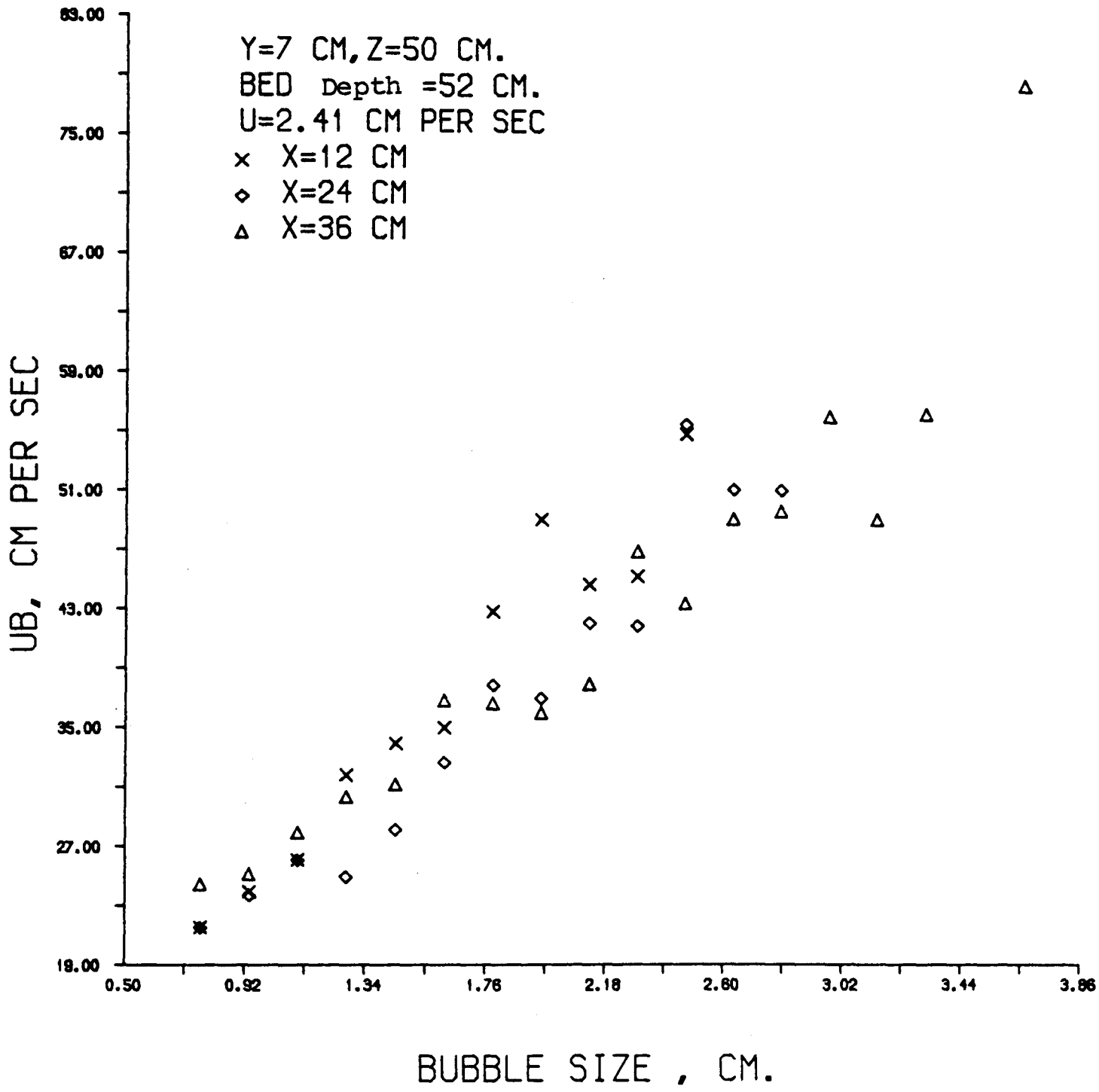
Y=7 CM, Z=50 CM.
BED Depth =52 CM.
U=2.41 CM PER SEC
X=12 CM
X=24 CM
X=36 CM
UB, CM PER SEC
83.00
75.00
67.00
59.00
51.00
43.00
35.00
27.00
19.00
0.50
0.92
1.34
1.76
2.18
2.60
3.02
3.44
3.86
BUBBLE SIZE , CM.

Size (cm)	U_B(X = 12)	U_B(X = 24)	U_B(X = 36 cm)
0.765	17.670	14.715	21.809
0.935	20.144	18.771	23.023
1.105	23.638	21.287	25.359
1.275	25.059	22.530	25.552
1.445	27.286	25.293	29.637
1.615	31.106	28.216	32.808
1.785	34.424	29.837	33.887
1.955	37.466	36.934	36.363
2.125	44.432	-	35.862
2.295	48.885	-	46.829
2.465	53.924	-	45.345
2.635	-	41.580	47.381
2.805	-	-	40.452
3.315	-	59.656	-
3.655	46.785	-	59.148

TABLE (4.13)

U_B - Size Relationship for three points (X = 12,24 and 36 cm) at Z = 70 cm, Y = 7 cm and U = 1.87 $cm.sec^{-1}$.

Multiorifice Distributor.

Bed Depth = 82 cm

In an attempt to shed some light on the bubble rise velocity - bubble size variation along the longitudinal (longer) centre line, the data for three points on this axis (Y = 14 cm), are tabulated in Table (4.14) below.

Size (cm)	U_B(X = 12 cm)	U_B(X = 24 cm)	U_B(X = 36 cm)
0.765	17.686	16.170	18.243
0.935	17.322	17.212	18.755
1.105	20.802	20.254	21.385
1.275	24.005	23.565	25.088
1.445	23.341	24.727	27.349
1.615	37.657	26.031	26.937
1.785	34.404	37.510	32.464
1.955	-	44.688	41.309
2.125	-	33.553	42.286
2.295	-	-	41.392

TABLE (4.14)

Rise Velocity - Size Variations for three points, at Z = 20 cm, U = 3.01 cm/sec, Y = 14 cm. Bed Depth = 82 cm.
Multiorifice Distributor.

Which clearly demonstrates the effect of the particle phase circulation patterns on the bubble rise velocities, at low elevations in the bed. Bubbles nearer the vessel walls are rising faster than the bubbles on the bed vertical centre line, at an elevation of 20 cm above the distributor plate.

At a higher elevation of 50 cm above the distributor, the opposite trend prevails, Table (4.15). Here, the bubbles located on the bed vertical centre line are rising faster. The operating conditions, such as the superficial fluidising velocity, the bed depth and the Y co-ordinate are identical (the same) in these two sets of experiments (i.e. Tables 4.14 and 4.15).

It is generally accepted that circulation patterns modify the bubble velocities; bubbles coinciding with the upward emulsion phase movement register greater velocities than those rising in the zones of downward flow.

Size (cm)	U_B (X = 12 cm)	U_B (X = 24 cm)	U_B (X = 36 cm)
0.765	23.284	21.585	20.777
0.935	23.948	23.118	25.799
1.105	24.573	25.879	27.647
1.275	26.932	26.266	29.141
1.445	30.137	33.902	34.468
1.615	31.226	33.865	33.877
1.785	35.565	30.423	41.114
1.955	38.272	41.495	47.940
2.125	42.149	40.670	47.535
2.295	38.506	41.804	49.376
2.465	55.855	47.320	50.040
2.635	57.042	48.961	55.816
2.805	77.452	51.793	66.143
2.975	73.262	67.916	53.536
3.315	68.331	57.901	54.161
3.485	82.198	-	-

TABLE (4.15)

Z = 50 cm, Y = 14 cm, U = 3.01 $cm.sec^{-1}$.

Bed Depth = 82 cm.

Multiorifice Distributor.

4.4 Conclusions

It has been reported that macro-circulation patterns in the bed influence the bubble rise velocities. Bubbles existing in the regions of upward emulsion phase movement have greater rise velocities than those corresponding to the downward movement of the emulsion phase. It has been an aim of this investigation to show how the bed height affects these circulation patterns which in turn enhance the bubble rise velocities, or retard the bubbles as the case may be.

Experimenting with a cylindrical bed, Burgess and Calderbank (6) reported that bubbles near the top of the bed had velocities greater than the predicted values (they used an equation similar to Equation 4.1), whilst those near the distributor had velocities below this value. They also found that the bubble velocity decreased with radial distance away from the centreline, at the top of the bed. They concluded that a downward movement of the emulsion phase was present at the centre of the bed close to the distributor. They observed that this was unstable and existed only up to about one vessel diameter above the distributor.

As in the work of Burgess and Calderbank, particle circulation patterns were detected in the present experiments by studying the variation of absolute bubble rise velocity with position on the bed cross-section and with superficial fluidising velocity.

It was found that bubbles, of identical size, had unequal rising velocities at different points on the bed cross-section. These differences were ascribed to gross circulation patterns of the particulate phase, upwards in the region of enhanced bubble velocity and downwards in the region of depressed bubble velocity.

The regions of enhanced bubble velocity also corresponded to a high rate of bubble sampling, particularly among larger bubbles. Conversely, regions of depressed bubble velocity exhibited a low bubble sampling rate, while a disproportionate fraction of those bubbles which were sampled proved to be very small. This conclusion agrees with the findings of Burgess and Calderbank for a bed of circular cross-section.

The discrepancies in bubble rise velocity were least at low values of the superficial fluidising velocity and became greater as the superficial fluidising velocity was increased. This appears to confirm the supposition that such discrepancies are caused by particulate-phase circulation cells which are in some way "driven" by the bubble flow-rate. It is hard to imagine any other hypothesis which would explain the fact that, in some portions of the bed, an increase in superficial velocity would actually reduce the bubble rise velocity.

As mentioned earlier in this chapter, two modes of filling the bed were employed, to examine the effect of the bed depth on these circulation patterns. Some of the experiments were done when the bed depth was 42 cm (a few with a bed depth of 52 cm), and more experiments when this depth was almost doubled to 82 cm.

In the former case (bed depth = 42 cm) two cells of particle circulation patterns seemed to exist in the bed, moving upwards near the wall, downwards at the centre.

At the top of the bed, the bubble rise velocities measured on the bed centreline were greater in magnitude, indicating positions of upward emulsion phase movement. When the bed is filled to a maximum depth of 82 cm, there seem to be very different particle circulation patterns in the bed. The regions near opposite walls show very different patterns of rise velocity variation along the X and Y coordinates.

Initially (i.e. at lower elevations above the distributor plate), the same picture as before prevails. But, as the height above the distributor is increased a lack of symmetry emerges along the Y-axis, (the shorter centre-plane) of the bed. The circulation patterns have an upward direction at elevations of $\sim$ 60 cm above the distributor, on the bed vertical centreline, downwards near the "front" wall.

Insufficient data prevents the extension of this comparison to the "back" wall of the bed.

It is acknowledged that the overall picture is more complicated than this simple explanation would suggest, due to the influence of many parameters suggested by various investigators, (Geldart and Kelsey (37) and Grace and Harrison (47)).

Nevertheless, our experimental results, using three different superficial fluidising velocities (1.87, 2.41 and 3.01 $cm.sec^{-1}$), show that, even at low gas flow rates, these particle circulation patterns modify the bubble rise velocities.

In the tables and the graphs in this chapter, the average bubble size is taken to be the mid-point of the segment width corresponding to that size. But the number of bubbles in each segment varies with increasing size as shown in Table 4.16, below.

Slot Width (cm)	Ave. Size (cm)	No of Bubbles	U_a $cm.sec^{-1}$
0.68 - 0.85	0.765	170	24.70
0.85 - 1.02	0.935	169	27.32
1.02 - 1.19	1.105	150	27.37
1.19 - 1.36	1.275	105	31.00
1.36 - 1.53	1.445	88	30.47
1.53 - 1.70	1.615	65	35.73
1.70 - 1.87	1.785	33	32.56
1.87 - 2.04	1.955	26	44.17
2.04 - 2.21	2.125	29	47.59
2.21 - 2.38	2.295	20	44.49
2.38 - 2.55	2.465	13	51.66
2.55 - 2.72	2.635	10	52.31
2.72 - 2.89	2.805	5	59.08
2.89 - 3.06	2.975	0	0.00
3.06 - 3.23	3.145	6	61.27
3.23 - 3.40	3.315	3	66.70
3.40 - 3.57	3.485	1	61.81
3.57 - 3.74	3.655	3	49.26
3.74 - 3.91	3.825	0	0.00

TABLE (4.16)

Table (4.16) shows a typical printout of the "results" from the microprocessor. A very large number of bubbles exists in the slots corresponding to the lower sizes while the slots of larger size contain relatively few bubbles. In this work a minimum of five bubbles in any slot was required before inclusion in the results. Nevertheless, results corresponding to larger sizes are obtained by averaging figures for relatively few bubbles and must be subject to much greater errors than those for lower sizes.

In order to draw usable conclusions at all, however, it has been necessary to assign equal weight to figures from all the bubble sizes despite the reservations expressed above.

An example is the value of $\beta = 1.1$ in Table (4.6), where an experimental point corresponding to an average size of an interval with five bubbles in it, is included.

This value of 1.1 is unreasonably higher than the other three and the exclusion of the above mentioned experimental point, would decrease this value of β to less than 1.0. Similarly in most of the U_a - "Size" (and U_b - "size") graphs, we find a very large scatter for larger bubbles. In basing arguments and drawing conclusions from these graphs, it has to be borne in mind that an equal weight is attached to points representing very few bubbles.

Finally from the results presented in this chapter the following conclusions can also be drawn:

1. There is evidence of bubbles becoming flatter in shape as they rise higher in the bed, Figures (4.8 - 4.18). These show that a bubble with a given "height" h, will have a larger radius of curvature (and hence a larger rising velocity) at higher elevations.

2. There is sufficient evidence that the larger bubbles are flatter in shape, irrespective of height in the bed. This is indicated by the fact that the bubble rise velocity is increasing faster with bubble height h, than the 0.5 power given by the Davies - Taylor equation. The coefficient β in Table (4.2) is greater than 0.5 for all heights in the bed.

3. The "constant" C varies with height in the bed, first rising and then falling and finally rising again. This phenomenon may probably be ascribed to the circulation patterns mentioned earlier. Evidence for these are the marked differences in bubble rise velocity for the same sizes and heights in the bed but:

   (a) different superficial fluidising velocities at the same position on the cross-section, Figures (4.3, 4.24), or

   (b) different positions on the bed cross-section for the same superficial fluidising velocity Figures (4.3, 4.24), Tables (4.9 - 4.15).

CHAPTER 5

Bubble Size Distribution

5.1 Bubble Size Distribution

The most widely used bubble size parameter in formulating a size distribution is the equivalent spherical diameter, defined as the diameter of a sphere with the same volume as the bubble. This is, obviously, a derived parameter and is thus subject to error due to the constraints imposed by the bubble shape assumed. In this work, since the bubble vertical height is measured independently of the bubble frequency and since it is a measure of the bubble size and volume, it was decided to use this parameter in formulating the bubble size distributions, shown in Figures (5.1 - 5.37).

While recording bubbles in B mode, the microprocessor imposes two constraints on the bubble detection and hence the collection rate. The first, which is provided in the software, (i.e. $T1 < T2$), ensures the rejection of any bubble smaller than a fixed size, ℓ, the separation length. The second constraint is the jitter time. This is the time between the first arrival of a bubble at one of the coplanar probes and the subsequent complete immersion of all three of them. This constraint, which is imposed on the trailing and well as the leading edges of the bubble, is to ensure that only bubbles which are coaxial with the probe are counted.

A comparison of the actual jitter with the maximum allowable jitter, (entered via keyboard), is made, the result of which is that the microprocessor discards the invalid events (jitter too great).

Therefore, it seems reasonable to assume that all the sampled bubbles in B mode hit the probe squarely and free from interference from other bubbles. Furthermore, since only bubbles which are coaxial with the probe are counted, the measured bubble size can be taken as the nose-to-floor height along the central axis of the bubble.

Past experience (5) shows that extremely skewed distributions of bubble size can be expected with the peak in the range of 5-10 mm. However, as discussed in chapter 3, a fundamental property of our system is the fact that the probe cannot detect bubbles below a particular size, typically 6.5 mm. This limit is imposed by the spacing of the three coplanar probes.

In these experiments, this limiting value was chosen as ℓ = 6.8 mm, the separation length between the leading and the three coplanar probes. It is therefore acknowledged that the distributions measured here are truncated, so that very small bubbles are not included.

In some of the graphs in this chapter (Figures 5.10, 5.19), an approximate method of presenting the bubble size distribution curves is used. This method is open to criticism since it does not comply with the true definition of frequency, f(h) defined by the equation

$$dn = f(h)\, d\, h$$

dn being the number of bubbles of size between h and h + dh.

In Figures (5.10, 5.19), the area in each histogram of size distribution (dn = f(h)dh), is represented as a bar at the midpoint of each slot, $(h + \frac{dh}{2})$, as shown below:

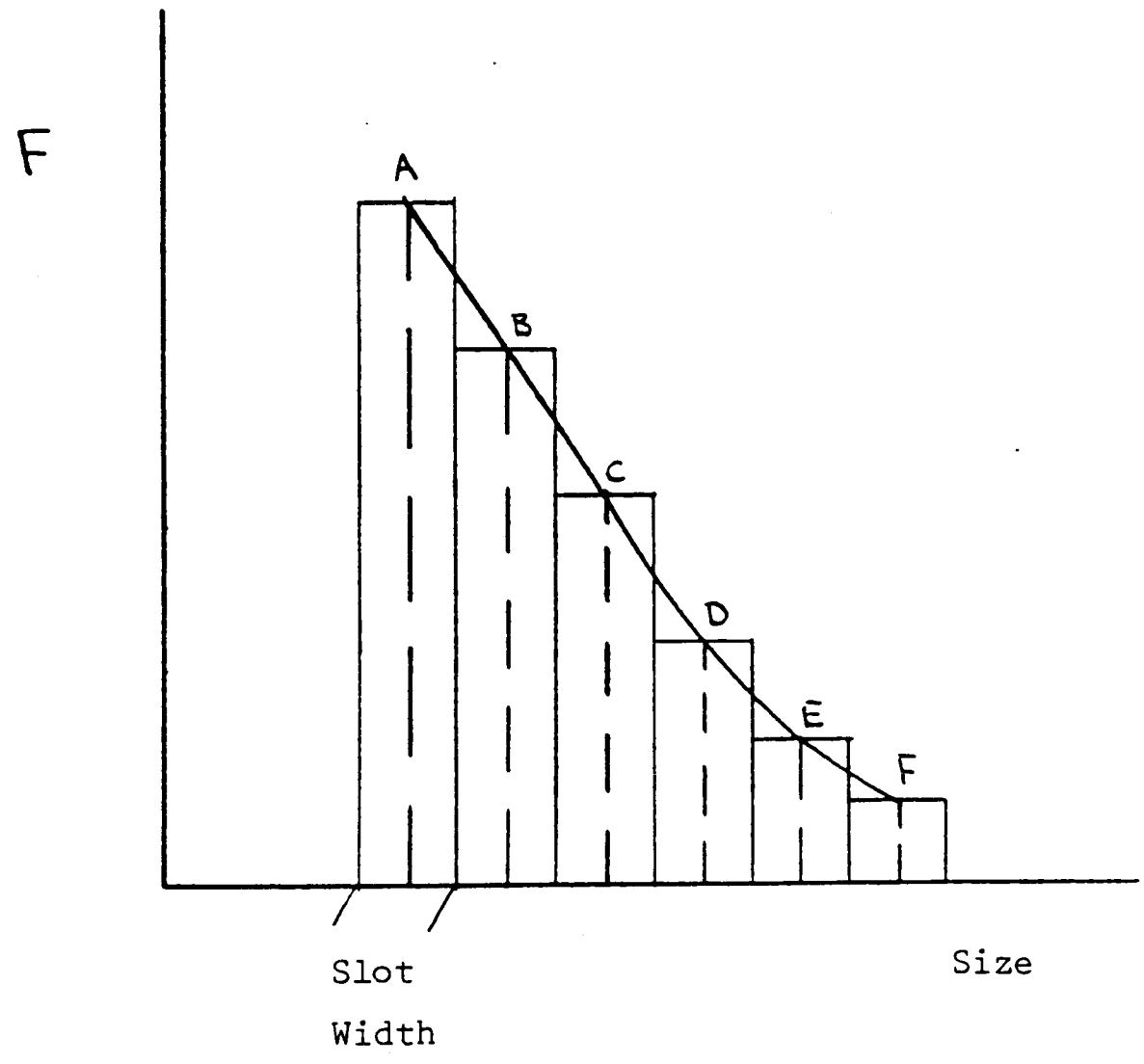

Then the points A, B, C... are joined and the resulting curve is used to represent the frequency-size relationship instead of the more accurate multi-bar charts (Figures 5.2, 5.7), or the cumulative oversize curves (Figures 5.3 - 5.5).

This method of presenting the size-frequency variation is useful when there are multiple sets of data, to be represented in one graph (e.g. Figure (5.19)). Furthermore, these curves are used as a means of comparing the bubble size distributions under different operating conditions. Therefore, it seems reasonable to assume that irrespective of the definition of frequency, this comparison is valid.

5.2 Porosint Plate Distributor

5.2.1 Variation with Superficial Fluidising Velocity

Figures (5.1) and (5.2) show histograms of bubble size distribution at fixed heights of 30 cm and 70 cm above the distributor plate. Figure (5.1) shows the bubble frequency-size relationship at a point on the vertical centreline, at two different superficial fluidising velocities of 1.36 and 2.41 cm/sec. The data for the higher superficial velocity show a smaller proportion of bubbles in the lower size-ranges. Figure (5.2) shows the influence of increasing gas velocity at a different point, 12 cm from the vertical centreline, and at three velocities of 1.87, 2.41 and 3.01 cm/sec.

Here, again, the size distributions are skewed but all three show peaks at 8 - 10 mm range. A comparison of these graphs reveals a pattern which is consistent throughout these results, (Figures (5.7, 5.9), in that at higher elevations in the bed, there seems to be a gradual decrease in frequency with increasing bubble size. At lower depths (e.g. 30 cm), the downward leg of the distribution histogram is much sharper indicating fewer large bubbles near the distributor plate.

Figure (5.3) shows size distributions at the same height above the distributor plate and at three different superficial fluidising velocities in the form of cumulative oversize curves (% of bubbles greater than a given size, plotted against the size). This is repeated for two higher elevations of 50 cm and 70 cm in Figures (5.4) and (5.5). These show that the size distribution curves are of similar shape but are displaced in the direction of greater bubble size for the higher superficial velocities.

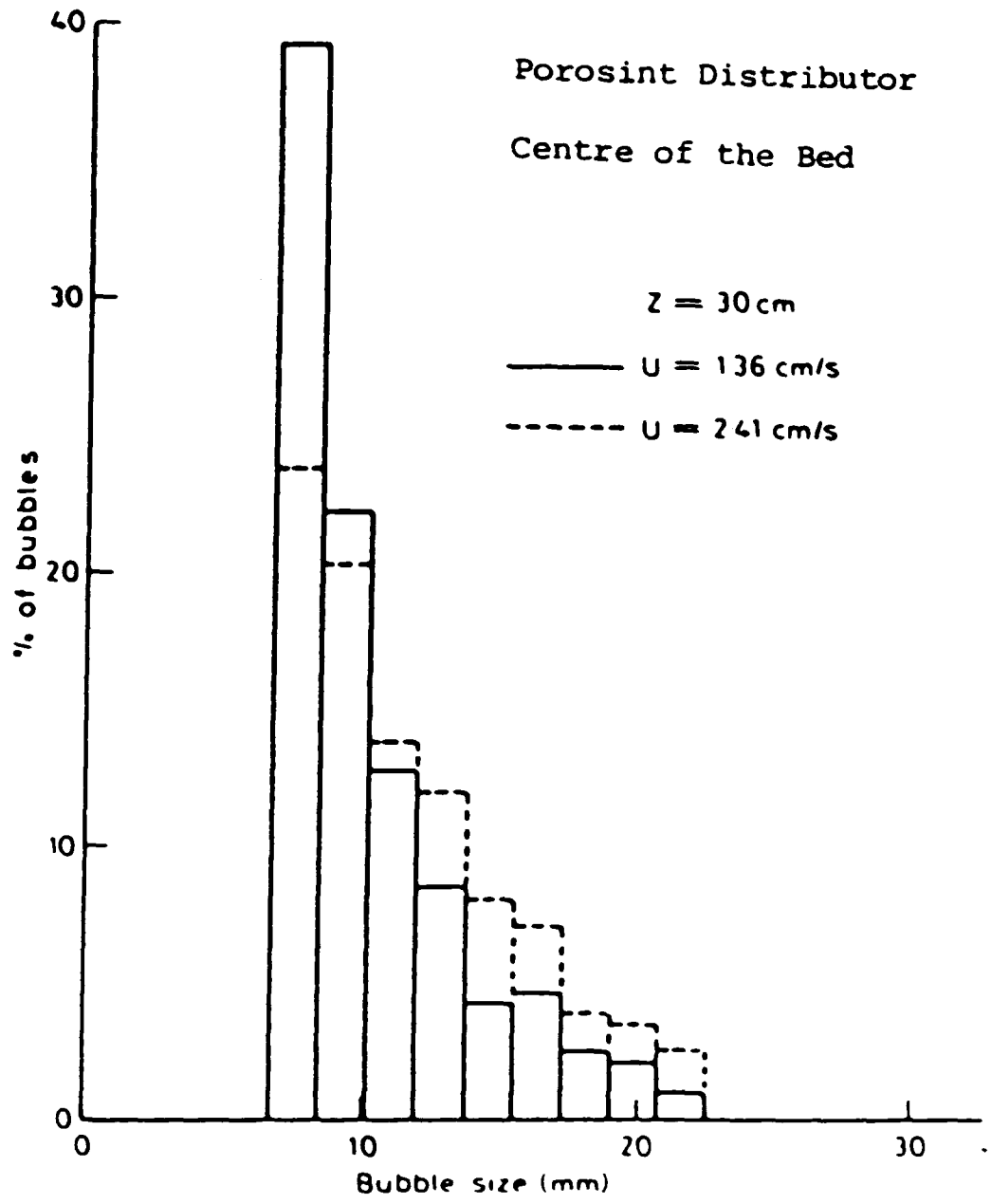

Figure 5.4 Histogram of bubble size distribution at constant height in the bed.

Fig. 5.2

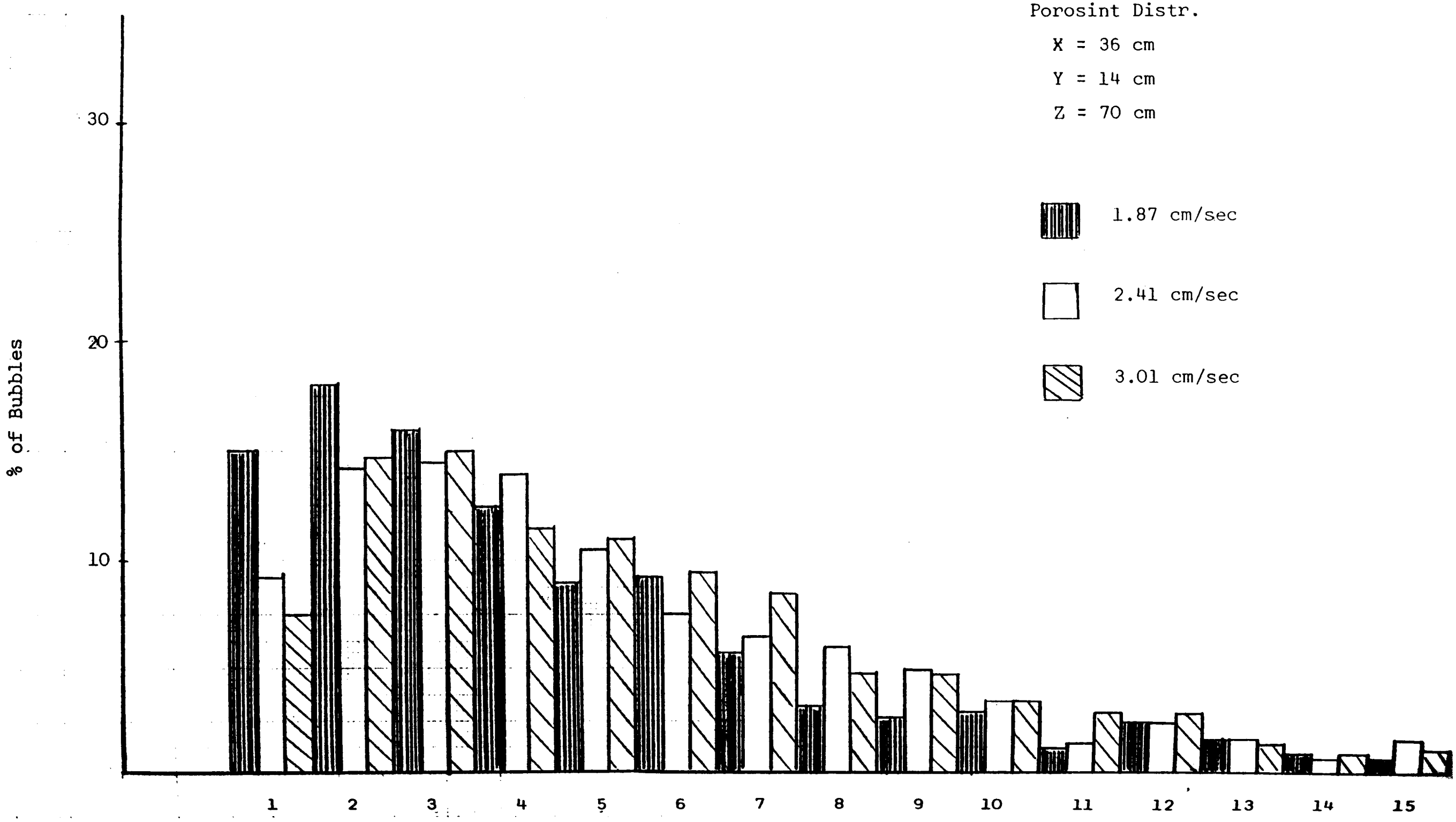
Porosint Distr.
X = 36 cm
Y = 14 cm
Z = 70 cm
1.87 cm/sec
2.41 cm/sec
3.01 cm/sec
% of Bubbles
30
20
10
1
2
3
4
5
6
7
8
9
10
11
12
13
14
15

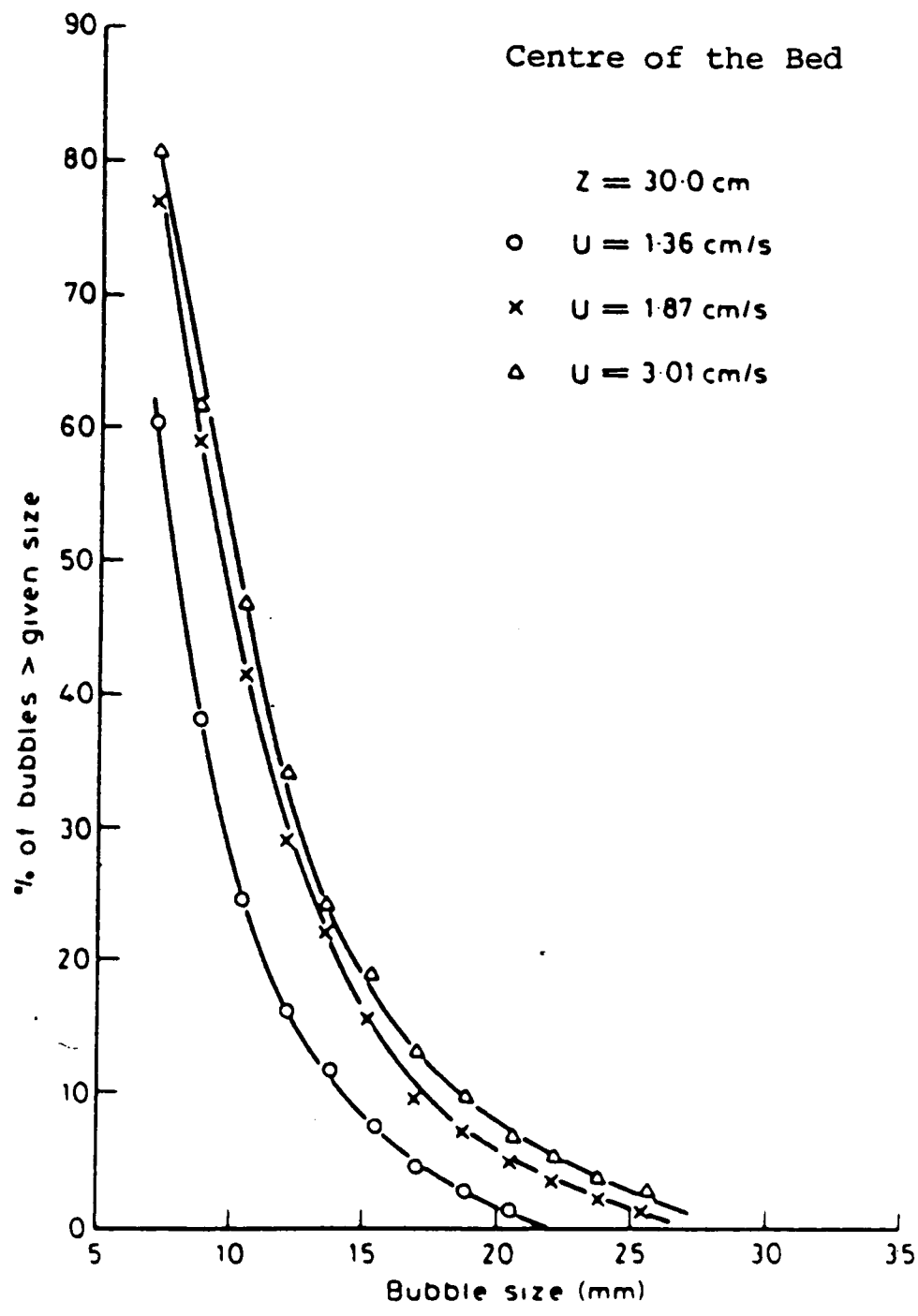

Figure 5.3 Cumulative oversize curves of bubbles at constant height in bed.

POROSINT Distributor

X = 12 cm

Y = 7 cm

Z = 50 cm

Fig. 5.4

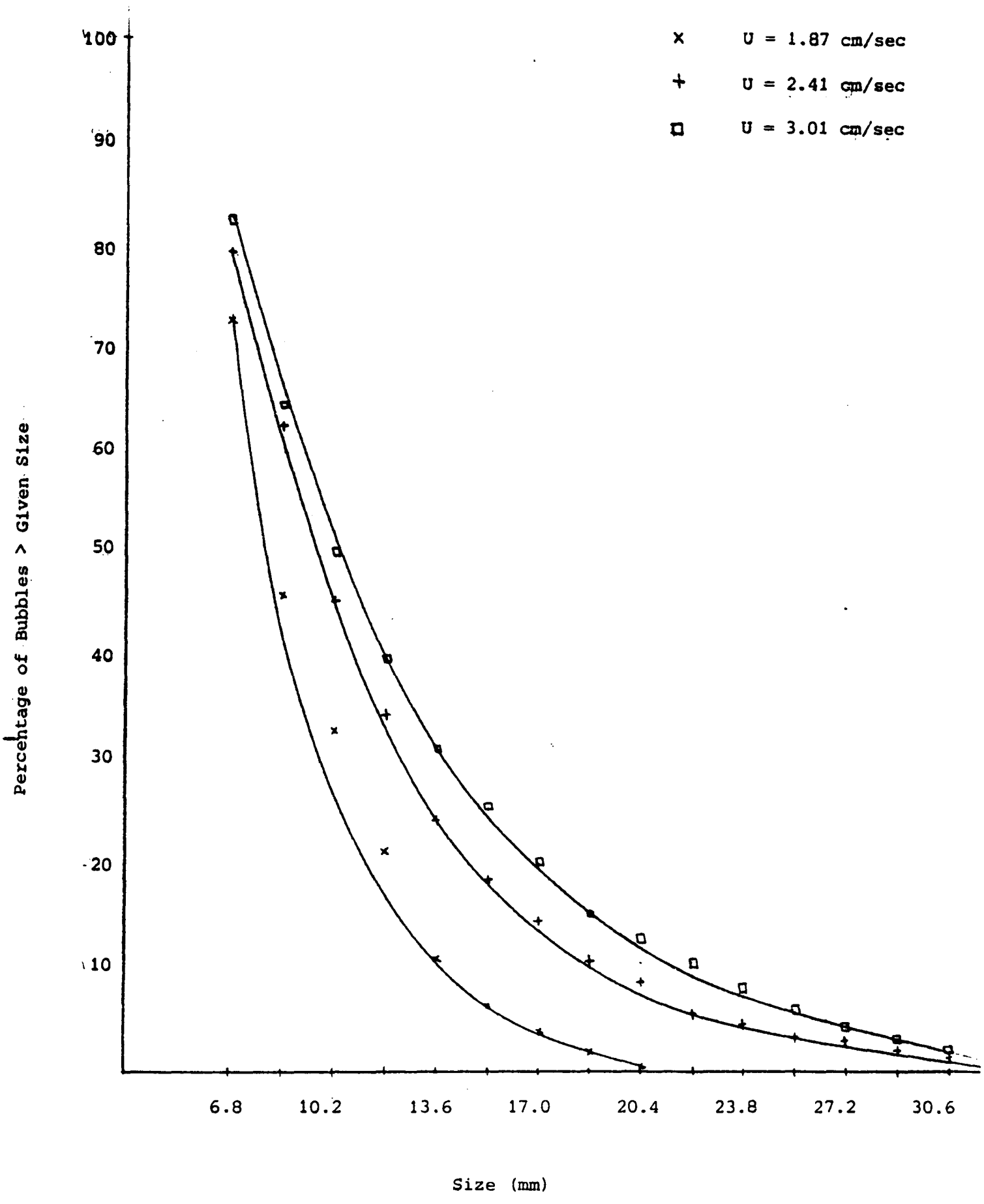

Fig. 5.5

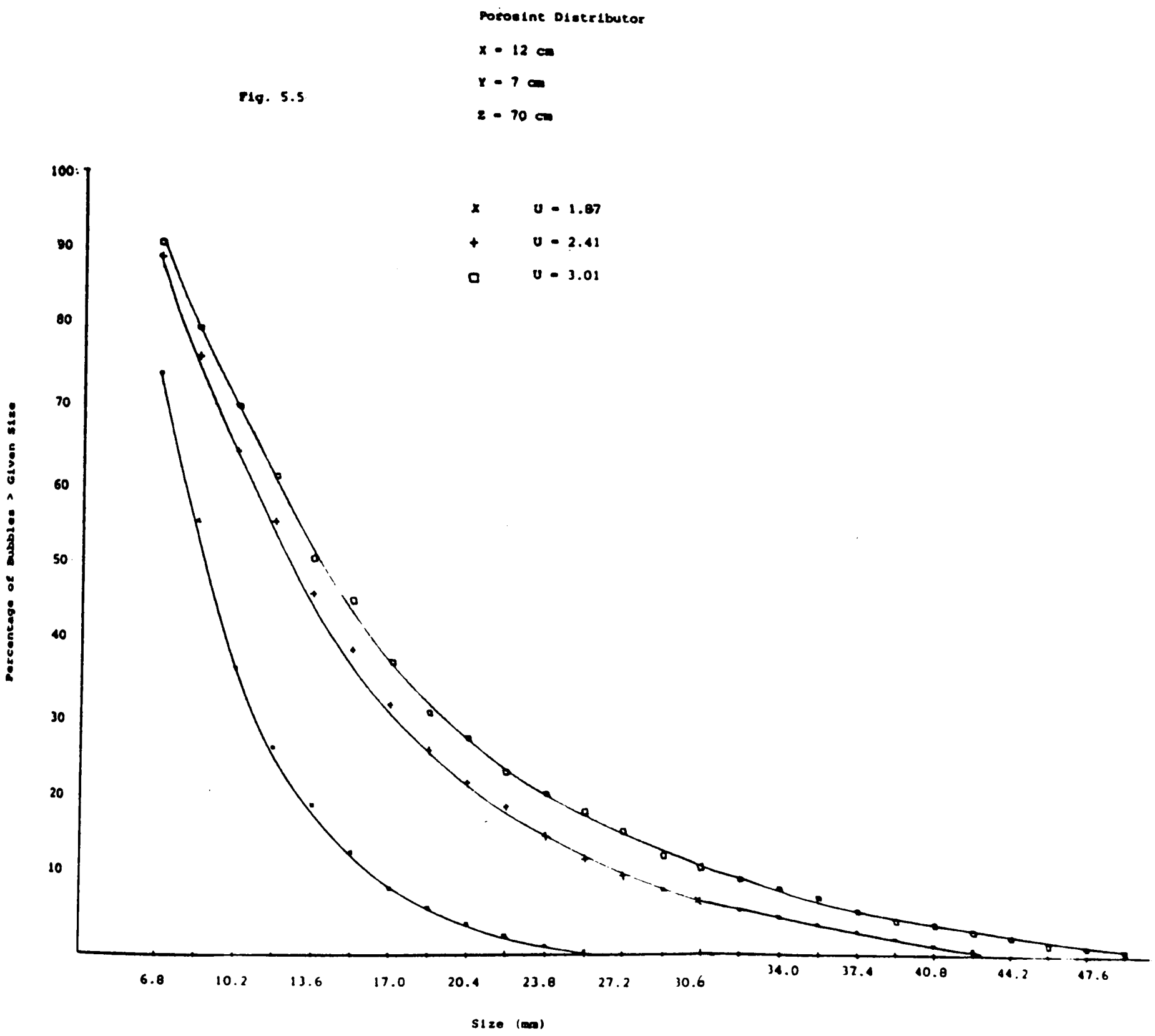
Porosint Distributor
X = 12 cm
Y = 7 cm
Z = 70 cm
X U = 1.87
+ U = 2.41
□ U = 3.01
Percentage of Bubbles > Given Size
100
90
80
70
60
50
40
30
20
10
6.8
10.2
13.6
17.0
20.4
23.8
27.2
30.6
34.0
37.4
40.8
44.2
47.6
Size (mm)

5.2.2 Variation With Height Above Distributor Plate

Figure (5.6) shows histograms of bubble size distributions at a fixed superficial fluidising velocity (2.41 cm/sec) and at two different heights above the distributor plate (20 and 40 cm). In Figure (5.7) this relationship is carried further to still higher elevations of 50, 60 and 70 cm but at a lower gas velocity of 1.87 cm/sec. Although the two graphs are for two different points in the bed, 12 cm apart, both reveal a similar pattern in that at greater heights in the bed, there is a smaller proportion of bubbles in the lower size ranges and a greater proportion in the higher size ranges.

Figure (5.8) shows cumulative oversize curves for a superficial velocity of 1.87 cm/sec and heights of 20, 50 and 70 cm above the distributor plate. The shift towards higher bubble sizes at greater heights in the bed is clearly visible but, in this case, the alteration in the shape of the curves reveals that the form of the size distribution is changing.

The shift towards larger bubbles at greater heights in the bed is attributed, among other possible causes, to coalescence of the smaller bubbles into larger ones. This should, if true, be reflected in a continuously decreasing bubble frequency as height above the distributor plate increases.

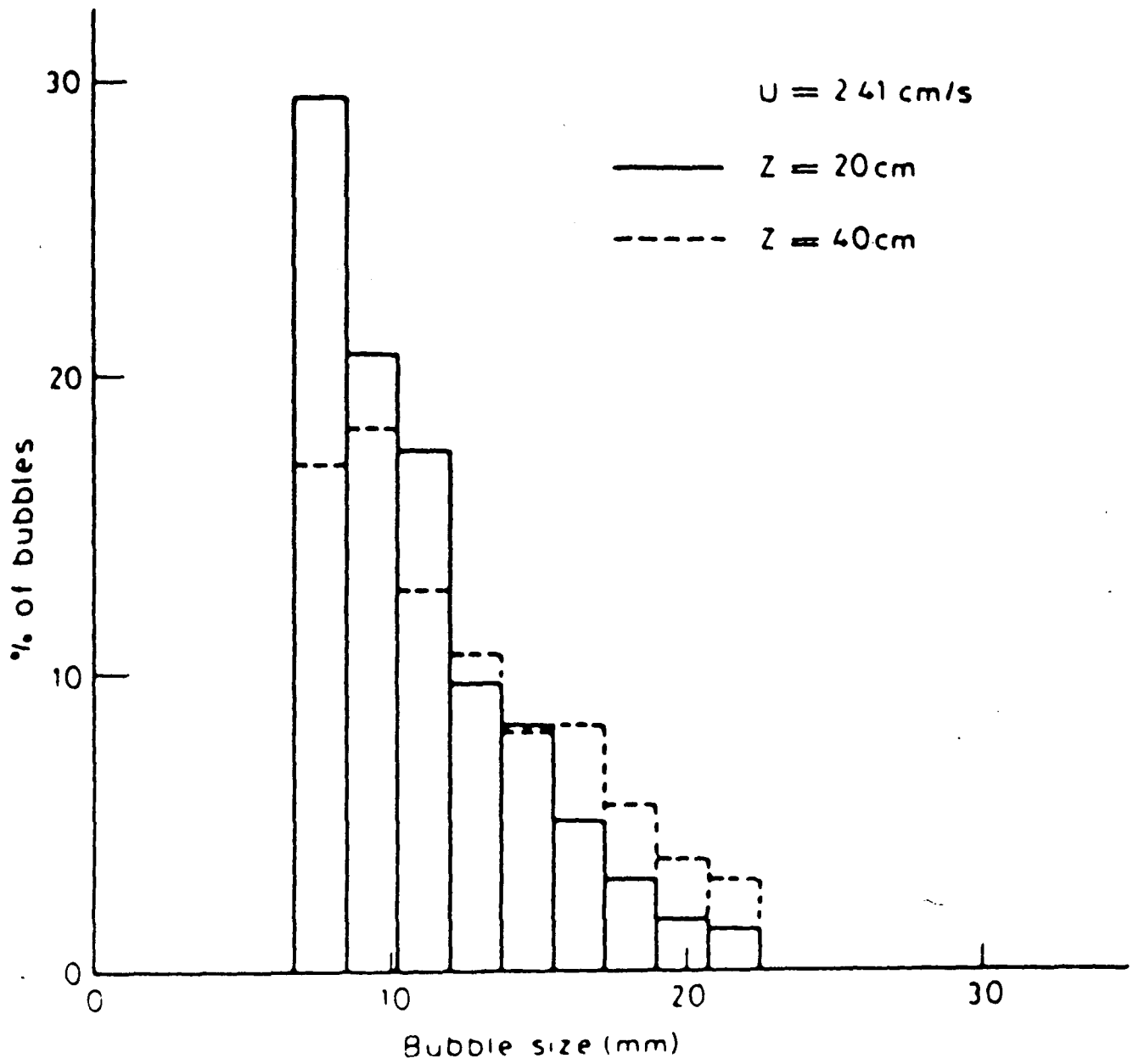

Figure 5.6 Histogram of bubble size distribution at constant superficial velocity.

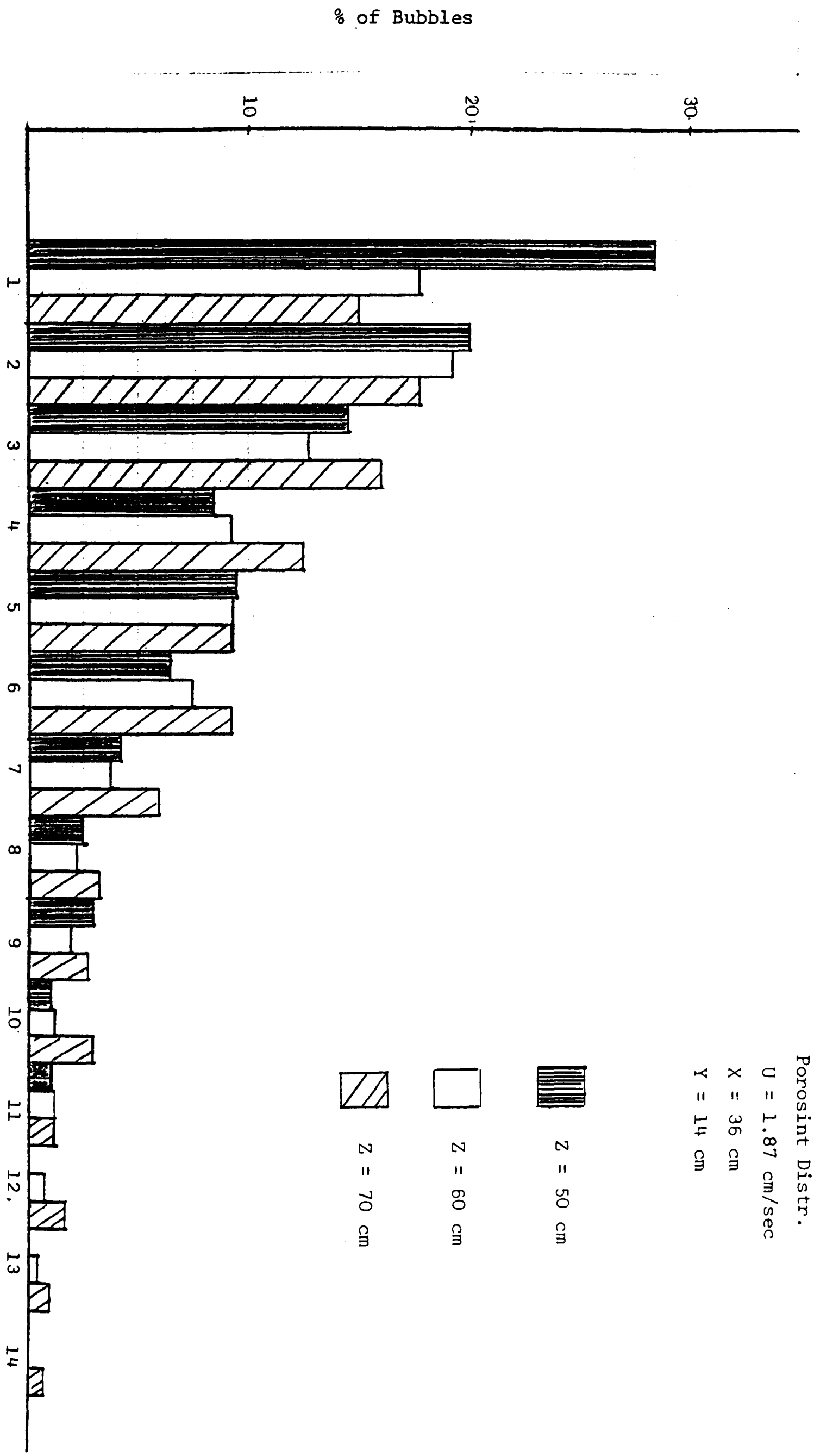
% of Bubbles
10
20
30
1
2
3
4
5
6
7
8
9
10
11
12
13
14
Slot Number
Porosint Distr.
U = 1.87 cm/sec
X = 36 cm
Y = 14 cm
Z = 50 cm
Z = 60 cm
Z = 70 cm

Fig. 5.7

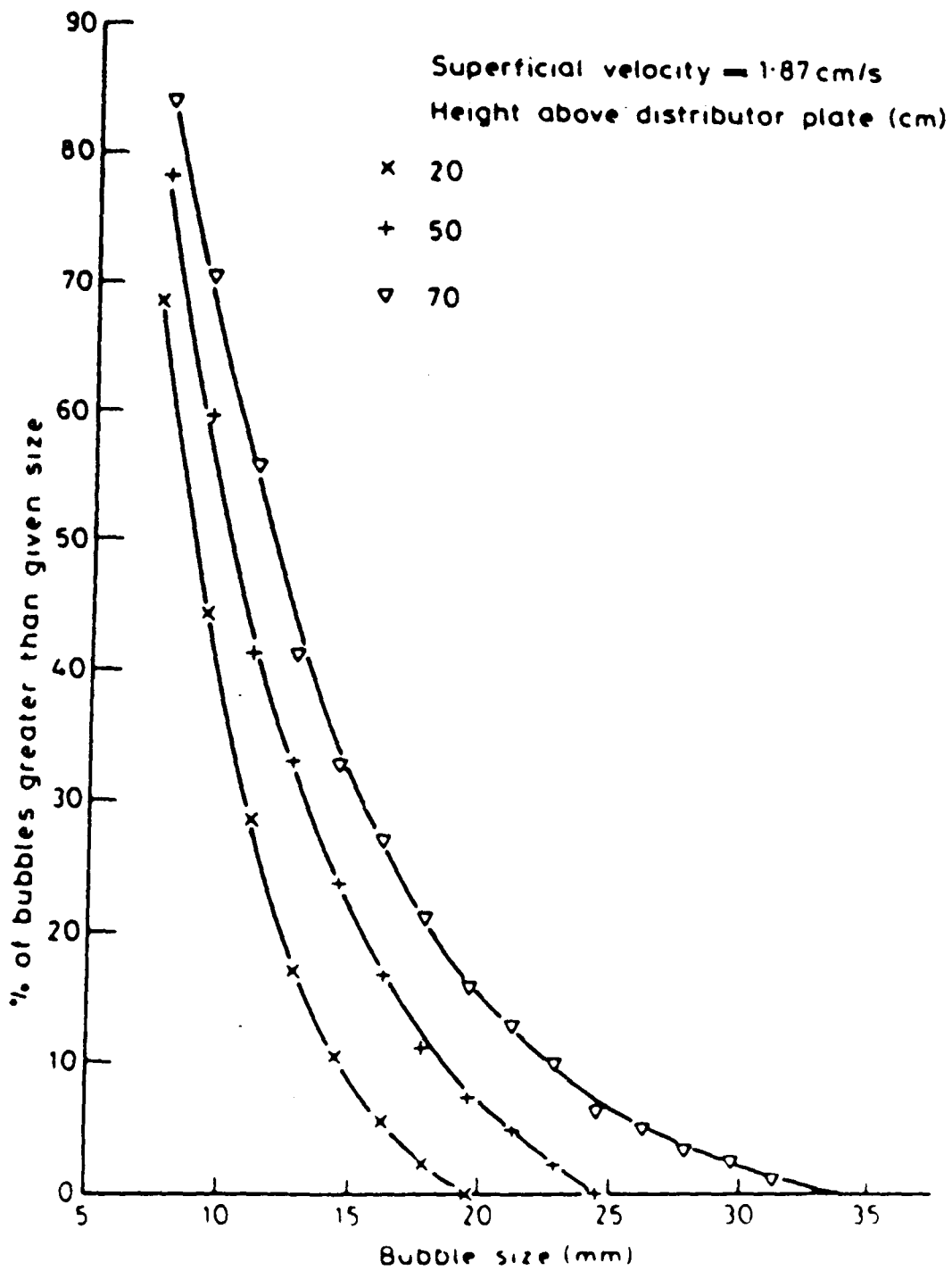
Porosint Distributor
Centre of the Bed
Superficial velocity = 1·87 cm/s
Height above distributor plate (cm)
× 20
+ 50
▽ 70
% of bubbles greater than given size
90
80
70
60
50
40
30
20
10
0
5
10
15
20
25
30
35
Bubble size (mm)

Fig. 5.8

5.2.3 Shape of the Bubble Size Distribution

Both the histograms in Figure (5.6) show a steady decrease of bubble frequency with size. The true shape of the bubble size distribution curve is in fact peaked, the peak corresponding to a most frequent bubble size. Figure (5.6) shows only truncated portions of this distribution due to the fact that very small bubbles are rejected by the microprocessor system.

With increasing height in the bed, the most frequent bubble size increases and the peaked shape of the size distribution curve is revealed. Figures (5.2) and (5.9), show this effect at two different points, (12 cm apart), but both 70 cm above the distributor plate, using various gas velocities. The peaks in these histograms are clearly visible.

Figure (5.9) shows the bubble size distribution histogram at an elevation of 70 cm above the distributor, (on the bed vertical centreline), for a superficial fluidising velocity of U = 2.41 $cm.sec^{-1}$.

At this elevation the number of large bubbles has increased so that the histogram shows a peak at 10 - 12 mm range. This is, of course expected because of the coalescence of small bubbles in the 70 cm rise in the bed.

Fig. 5.9

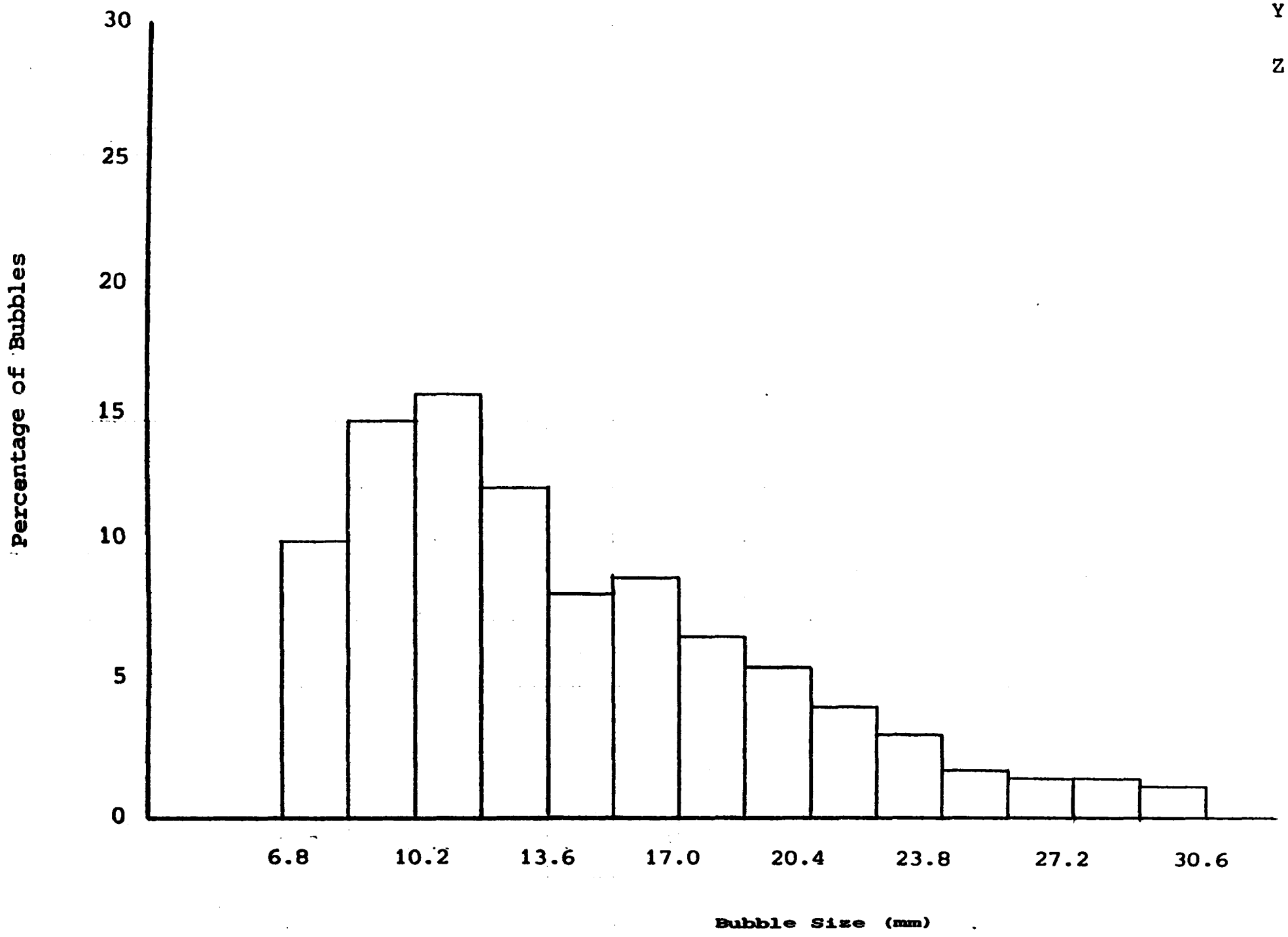
Porosint Distributor
U = 2.41 cm.sec^{-1}
X = 24 cm
Y = 14 cm
Z = 70 cm
Percentage of Bubbles
30
25
20
15
10
5
0
6.8
10.2
13.6
17.0
20.4
23.8
27.2
30.6
Bubble Size (mm)

For comparison of the bubble size distributions obtained in these experiments with the results of other investigators (6), who have used the equivalent spherical bubble diameter, d_e, as a measure of bubble size, the correlation derived in chapter 4, (4.5), is used to calculate d_e, from the measured values of the bubble height, and these are plotted in (5.10, (5.11) and (5.12).

Table 5.1 below, shows the calculated values of d_e (using the equation $h = 1.342\ R^{0.86}$) and Figure (5.13) shows the bubble frequency plotted against this 'equivalent diameter', d_e.

Slot Width	Ave. Size	d_e (cm)
0.68 - 0.85	0.765	1.04
0.85 - 1.02	0.935	1.31
0.102 - 1.19	1.105	1.59
1.19 - 1.36	1.275	1.88
1.36 - 1.53	1.445	2.18
1.53 - 1.70	1.615	2.48
1.70 - 1.87	1.785	2.79
1.87 - 2.04	1.955	3.10
2.04 - 2.21	2.125	3.41
2.21 - 2.38	2.295	3.73
2.38 - 2.55	2.465	4.06
2.55 - 2.72	2.635	4.38
2.72 - 2.89	2.805	4.70
2.89 - 3.06	2.975	5.05
3.06 - 3.23	3.145	5.38
3.23 - 3.40	3.315	5.72
3.40 - 3.57	3.485	6.07
3.57 - 3.74	3.655	6.41
3.74 - 3.91	3.825	6.76
3.91 - 4.08	3.955	7.11
4.08 - 4.25	4.165	7.46
4.25 - 4.42	4.335	7.82
4.42 - 4.59	4.505	8.18
4.59 - 4.76	4.675	8.54
4.76 - 4.93	4.845	8.90
4.93 - 5.10	5.015	9.26
5.10 - 5.27	5.185	9.63

TABLE 5.1

Figure (5.10) shows the variation of bubble frequency with measured size, as well as with the calculated "equivalent spherical diameter", d_e, at a point 70 cm above the distributor plate and a velocity of 1.87 $cm.sec^{-1}$. As would be expected the curve corresponding to the equivalent diameter, d_e, shows an enhanced dependence of bubble size on frequency, which is more pronounced towards the greater size ranges.

The relationship is plotted for the same point at a higher superficial fluidising velocity of 3.01 $cm.sec^{-1}$ in Figure (5.11) and for a point on the vertical centreline, but at a lower elevation of 30 cm above the distributor plate in Figure (5.12).

Increasing gas velocity seems to have little effect on the shape of the distribution curves (Figures (5.10) and (5.11)). Much larger size ranges are recorded when the fluidising velocity is increased to a greater value of 3.01 $cm.sec^{-1}$.

Fig. 5.10

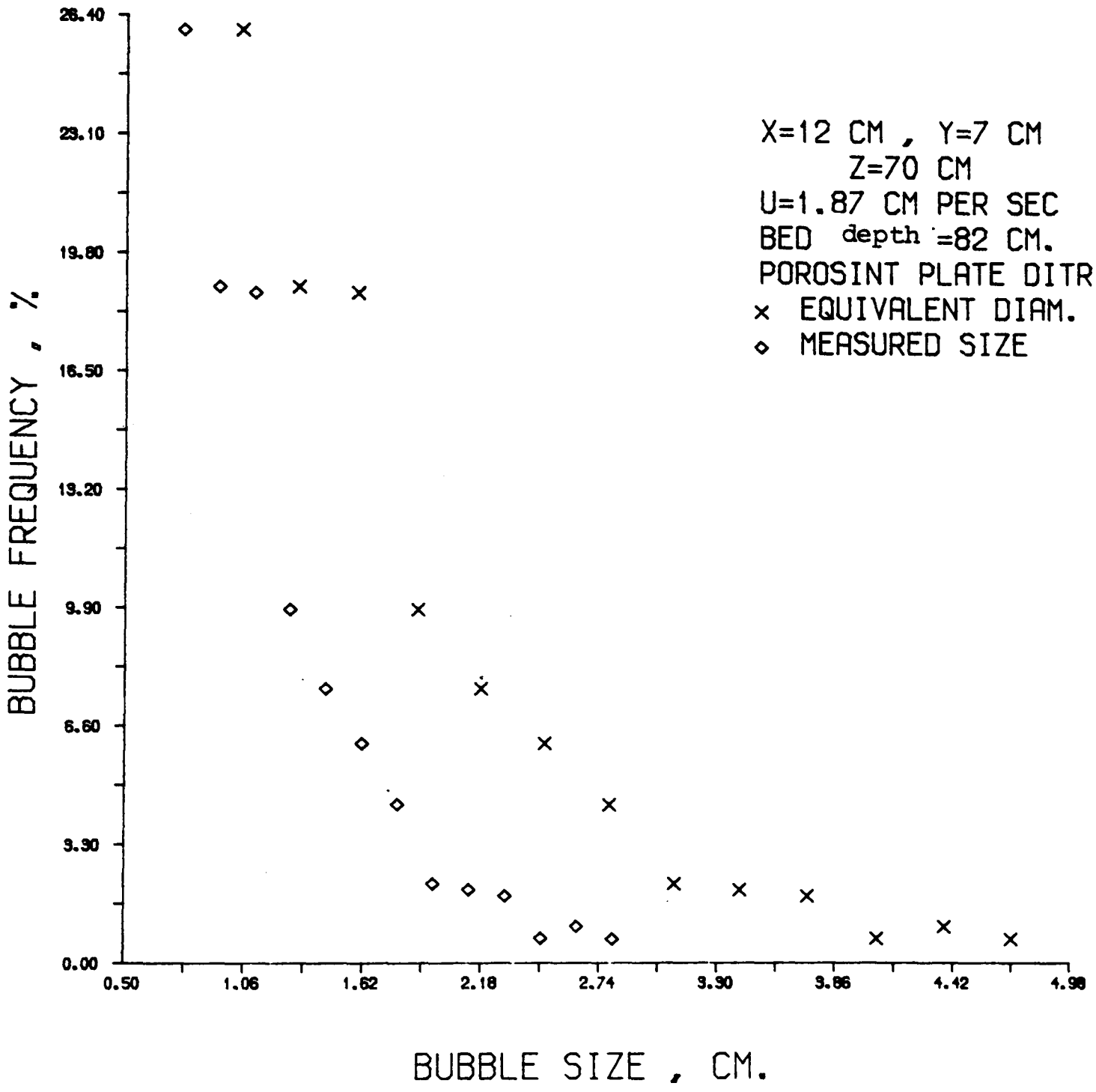
X=12 CM , Y=7 CM
Z=70 CM
U=1.87 CM PER SEC
BED depth =82 CM.
POROSINT PLATE DITR.
× EQUIVALENT DIAM.
◇ MEASURED SIZE
BUBBLE FREQUENCY , %
26.40
23.10
19.80
16.50
13.20
9.90
6.60
3.30
0.00
0.50
1.06
1.62
2.18
2.74
3.30
3.86
4.42
4.98
BUBBLE SIZE , CM.

Fig. 5.11

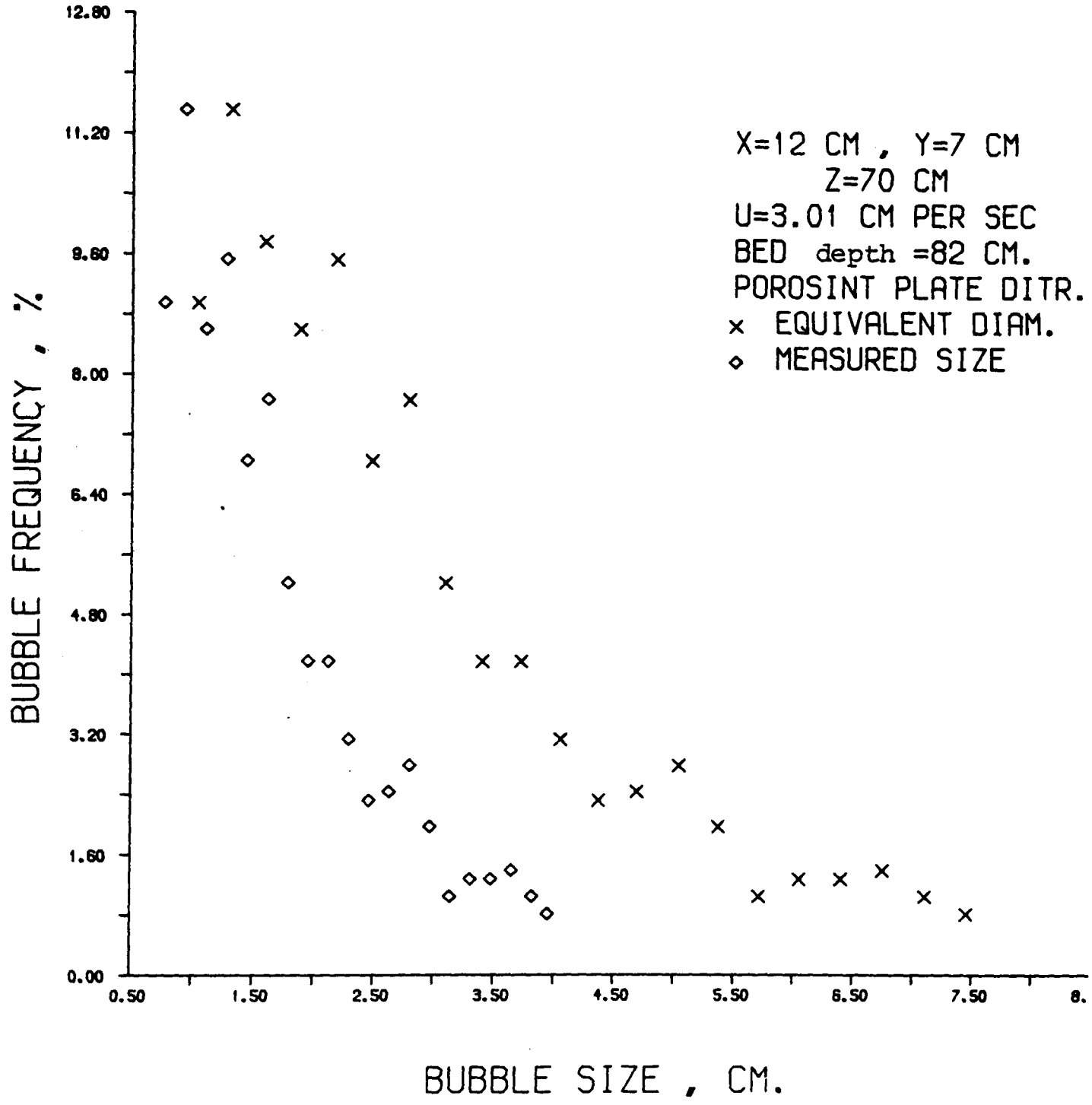
12.80
11.20
9.60
8.00
6.40
4.80
3.20
1.60
0.00
BUBBLE FREQUENCY , %
0.50
1.50
2.50
3.50
4.50
5.50
6.50
7.50
8.
BUBBLE SIZE , CM.
X=12 CM , Y=7 CM
Z=70 CM
U=3.01 CM PER SEC
BED depth =82 CM.
POROSINT PLATE DITR.
× EQUIVALENT DIAM.
◇ MEASURED SIZE

Fig. 5.12

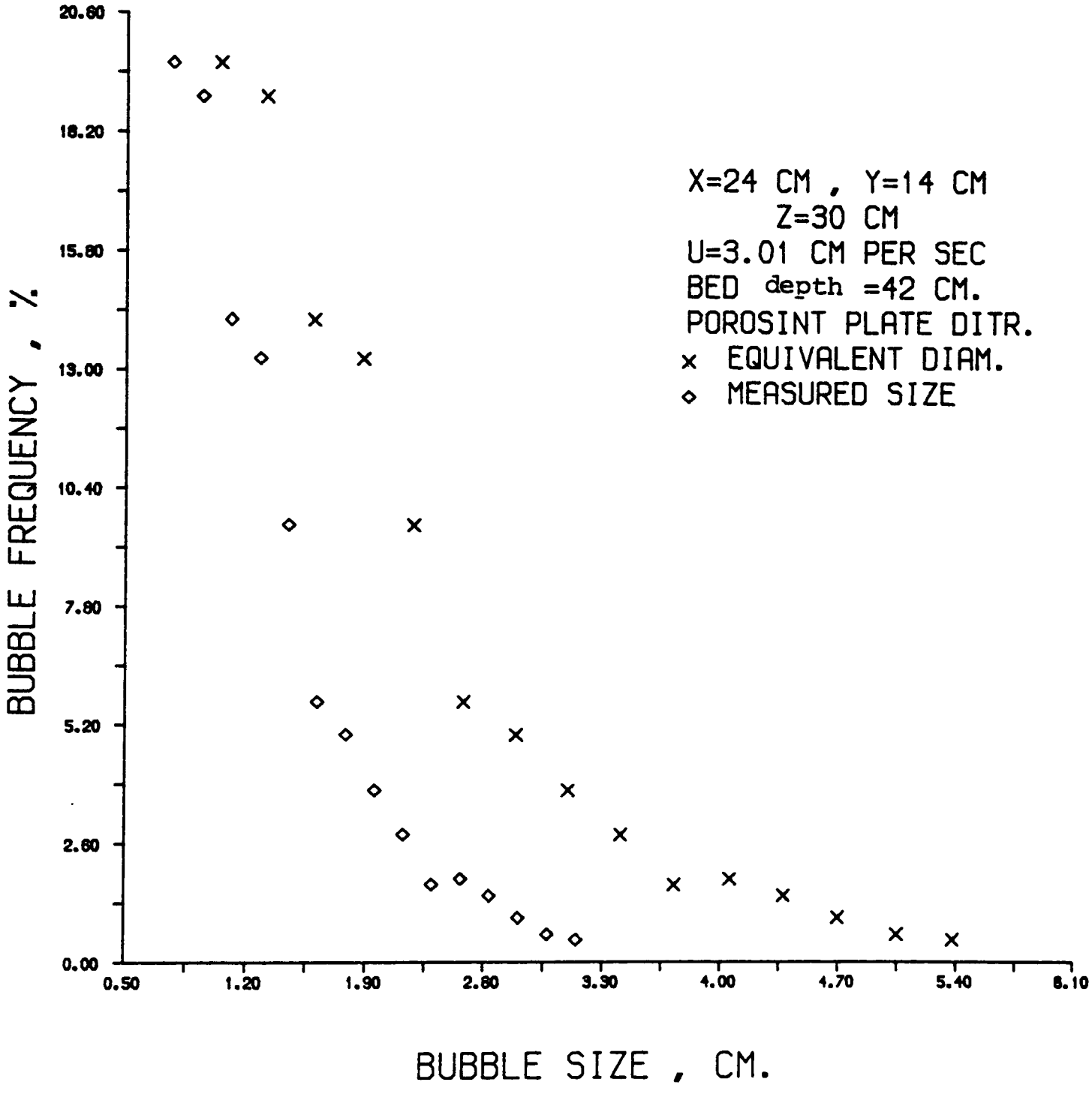
20.60
18.20
15.80
13.00
10.40
7.80
5.20
2.60
0.00
BUBBLE FREQUENCY , %
0.50
1.20
1.90
2.60
3.30
4.00
4.70
5.40
8.10
BUBBLE SIZE , CM.
X=24 CM , Y=14 CM
Z=30 CM
U=3.01 CM PER SEC
BED depth =42 CM.
POROSINT PLATE DITR.
× EQUIVALENT DIAM.
◇ MEASURED SIZE

Fig. 5.13

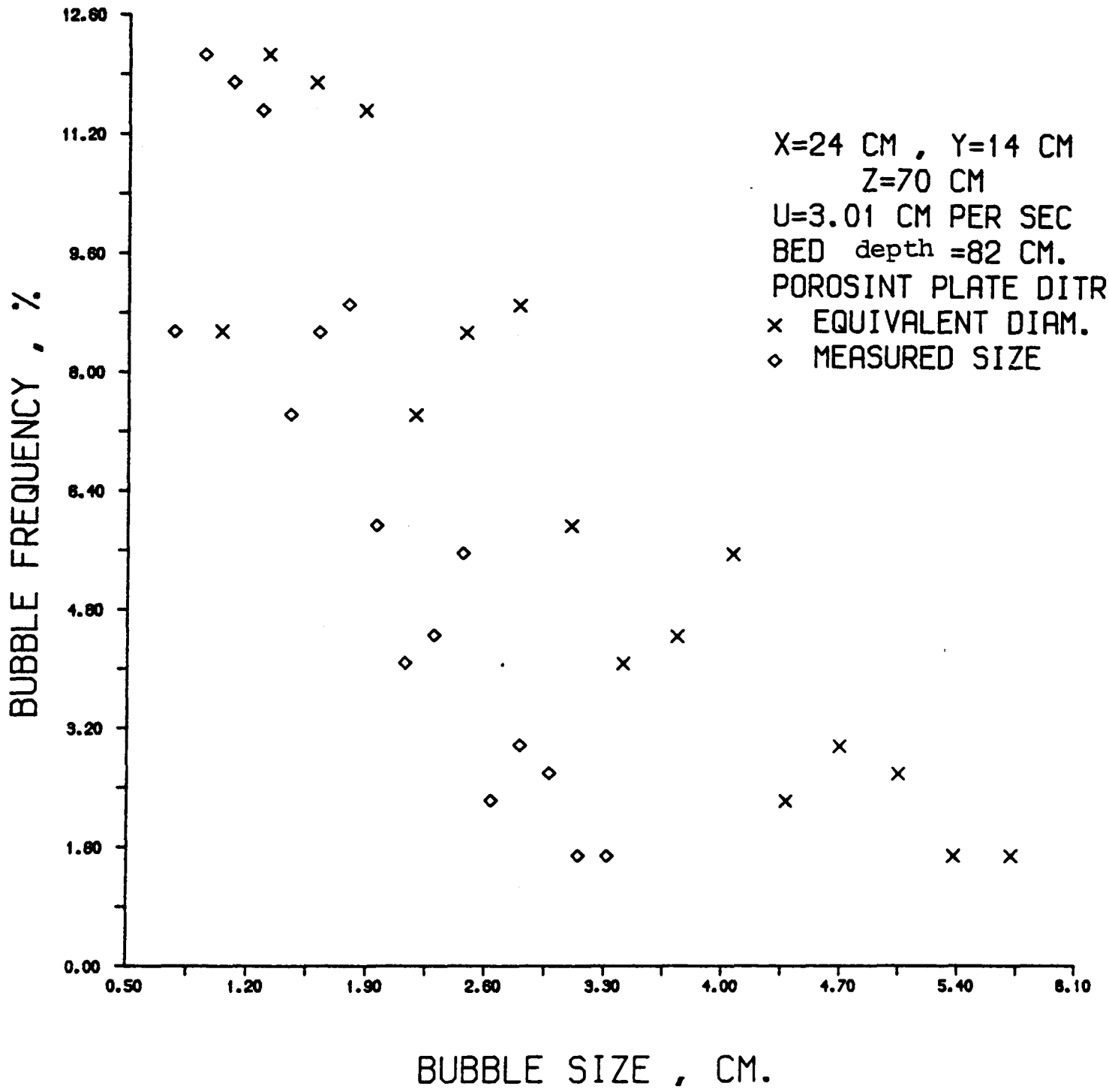
12.80
11.20
9.60
8.00
6.40
4.80
3.20
1.60
0.00
BUBBLE FREQUENCY , %
0.50
1.20
1.90
2.60
3.30
4.00
4.70
5.40
6.10
BUBBLE SIZE , CM.
X=24 CM , Y=14 CM
Z=70 CM
U=3.01 CM PER SEC
BED depth =82 CM.
POROSINT PLATE DITR.
× EQUIVALENT DIAM.
◇ MEASURED SIZE

5.3 Multiorifice Distributor

5.3.1 Variation with Superficial Fluidising Velocity

Figure (5.14) shows the variation of size distribution with superficial fluidising velocity at a fixed height of 20 cm above the distributor plate. The velocity is increased from 2 x U_{mf} to a value of almost 4 x U_{mf}. A similar pattern to that of the porosint plate distributor emerges, in that the data for the higher superficial velocity shows a smaller proportion of bubbles in the lower size ranges. Due to the fact that very small bubbles are rejected because of the discrimination exercised by the microprocessor system, all four curves are truncated.

A comparison of the relative magnitude of the frequencies corresponding to the 6.8 - 8.5 mm segment, for the four velocities, reveals an interesting pattern.

The difference between the frequencies measured, for each interval of bubble height, (with the four gas velocities), decreases as the superficial fluidising velocity is increased, which indicates a large number of small bubbles at low fluidising velocities in the bed.

Figure (5.15) shows the histograms of bubble size distributions at a fixed height of 70 cm above the distributor plate but for the same three superficial fluidising velocities of 1.87, 2.41 and 3.01 $cm.sec^{-1}$.

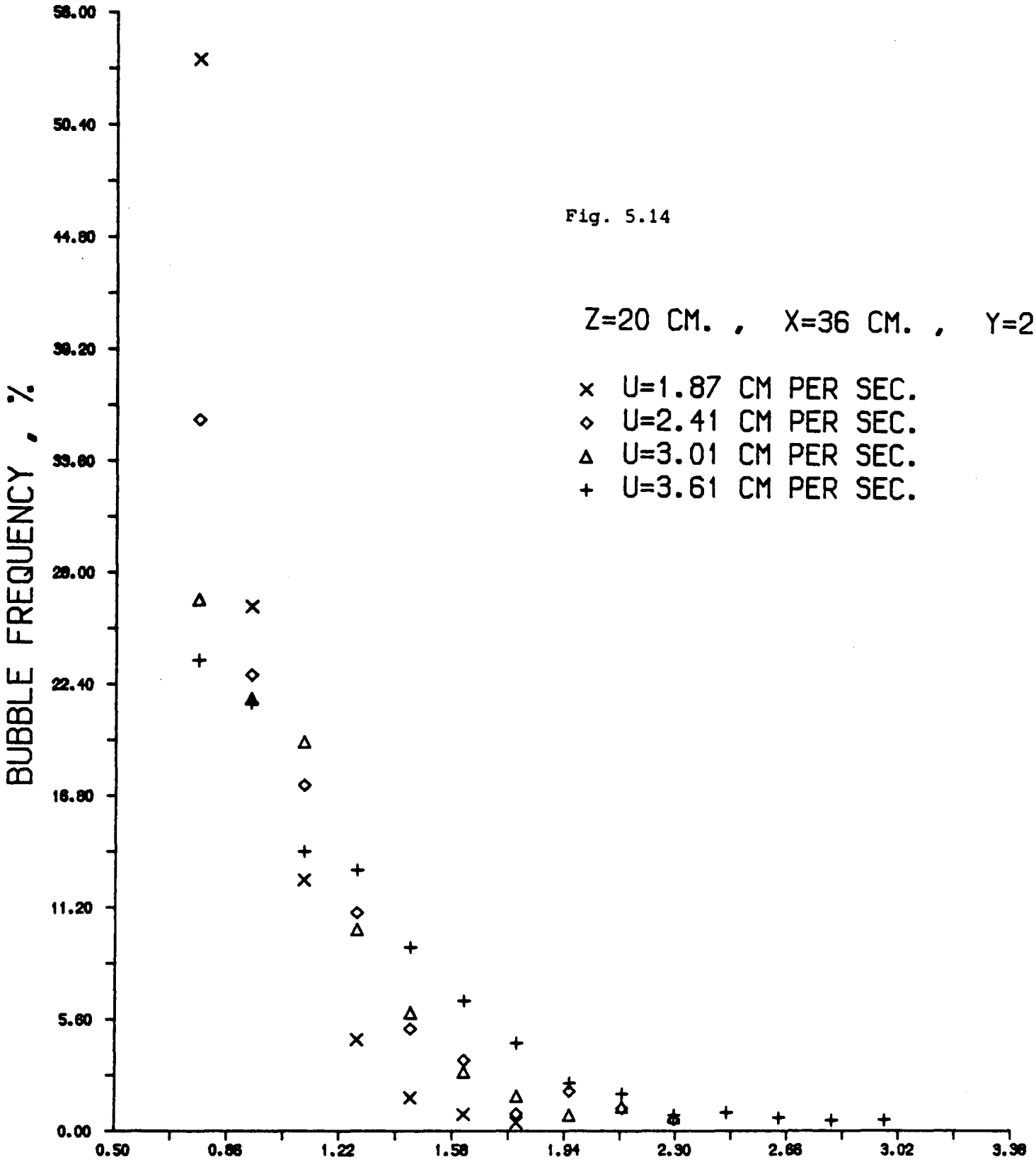

Fig. 5.14

Z=20 CM. , X=36 CM. , Y=21 CM.

× U=1.87 CM PER SEC.
◇ U=2.41 CM PER SEC.
△ U=3.01 CM PER SEC.
\+ U=3.61 CM PER SEC.

Fig. 5.15

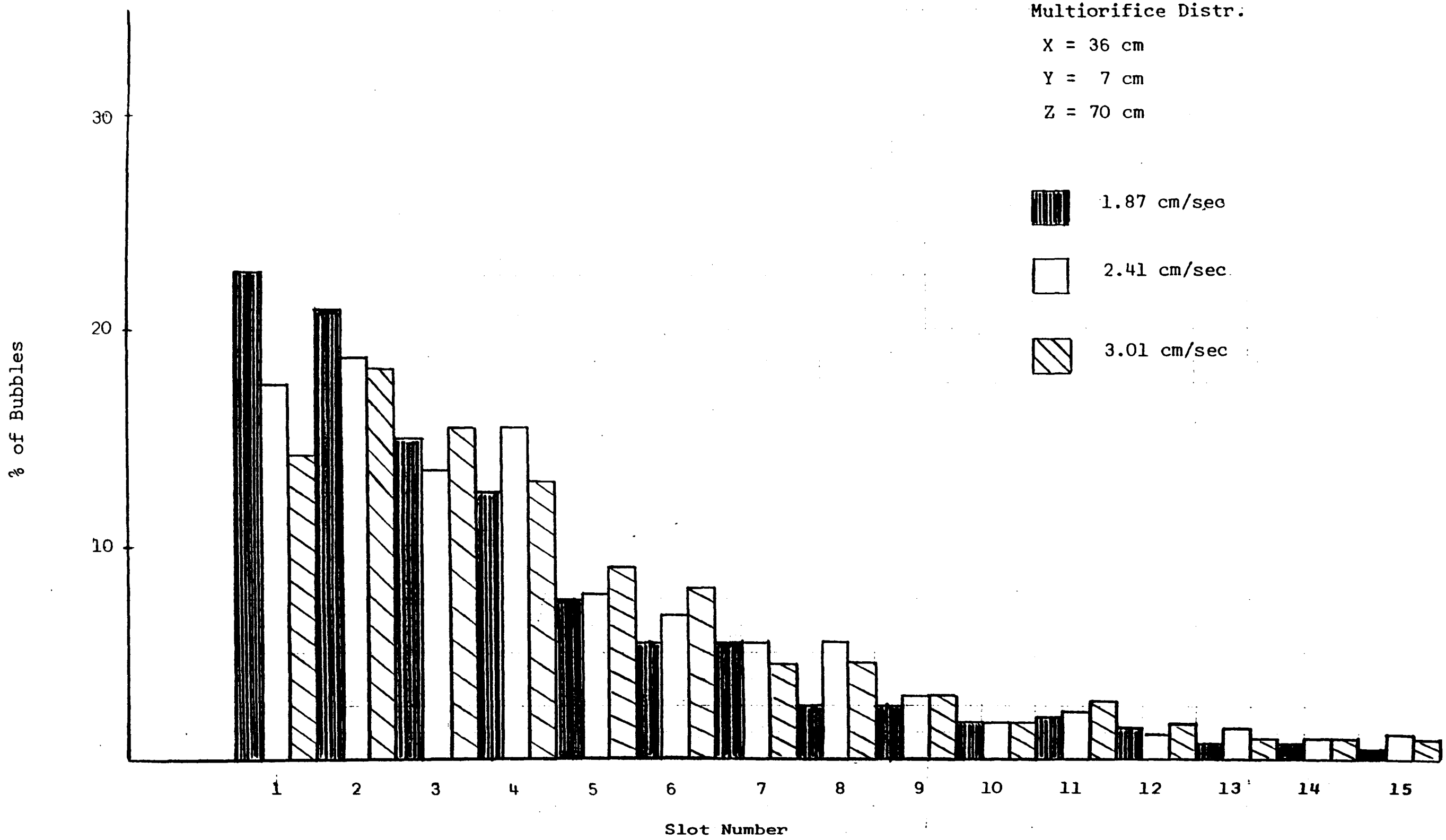
Multiorifice Distr.
X = 36 cm
Y = 7 cm
Z = 70 cm
1.87 cm/sec
2.41 cm/sec
3.01 cm/sec
% of Bubbles
30
20
10
1
2
3
4
5
6
7
8
9
10
11
12
13
14
15
Slot Number

Here, the histograms corresponding to the velocity of 2.41 and 3.01 cm.sec^{-1} show peaks in the bubble size range of 8 - 10 mm. The histogram for the 1.87 cm.sec^{-1} velocity seems to have already peaked at a bubble size smaller than 6.8 mm, which indicates the prevalence of large numbers of small bubbles generated at this low gas velocity. These small bubbles are not included in this distribution, thus making it impossible to ascertain the value of the most frequent bubble size for U = 1.87 cm.sec. At higher elevations in the bed, the bubble frequency decreases less sharply as the velocity is increased, indicating that there are fewer small bubbles higher up in the bed due to coalescence.

Figure (5.16) shows the cumulative oversize curves for the four superficial gas velocities of 1.87, 2.41, 3.01 and 3.61 cm.sec^{-1}. As with the porosint plate distributor, the curves are of similar shape but are displaced in the direction of greater bubble size for the higher superficial velocities. Cumulative oversize distribution curves for higher elevations of 40 and 70 cm are shown in Figures (5.17) and (5.18). A comparison of these three graphs, shows that the higher the elevation the greater the number of larger bubbles recorded. Although Figures (5.17) and (5.18) represent two different points, 14 cm apart, across the bed cross-sectional area the pattern, mentioned above, prevails.

These graphs reveal a pattern of decreasing bubble frequency with increasing bubble size. The lower the elevation of the sampling point, the sharper the decrease. This seems to indicate that there is a large number of small bubbles at lower elevations in

Fig. 5.16

Multiorifice Distributor

X = 36 cm

Y = 21 cm

Z = 20 cm

× U = 1.87

\+ U = 2.41

□ U = 3.01

▽ U = 3.61

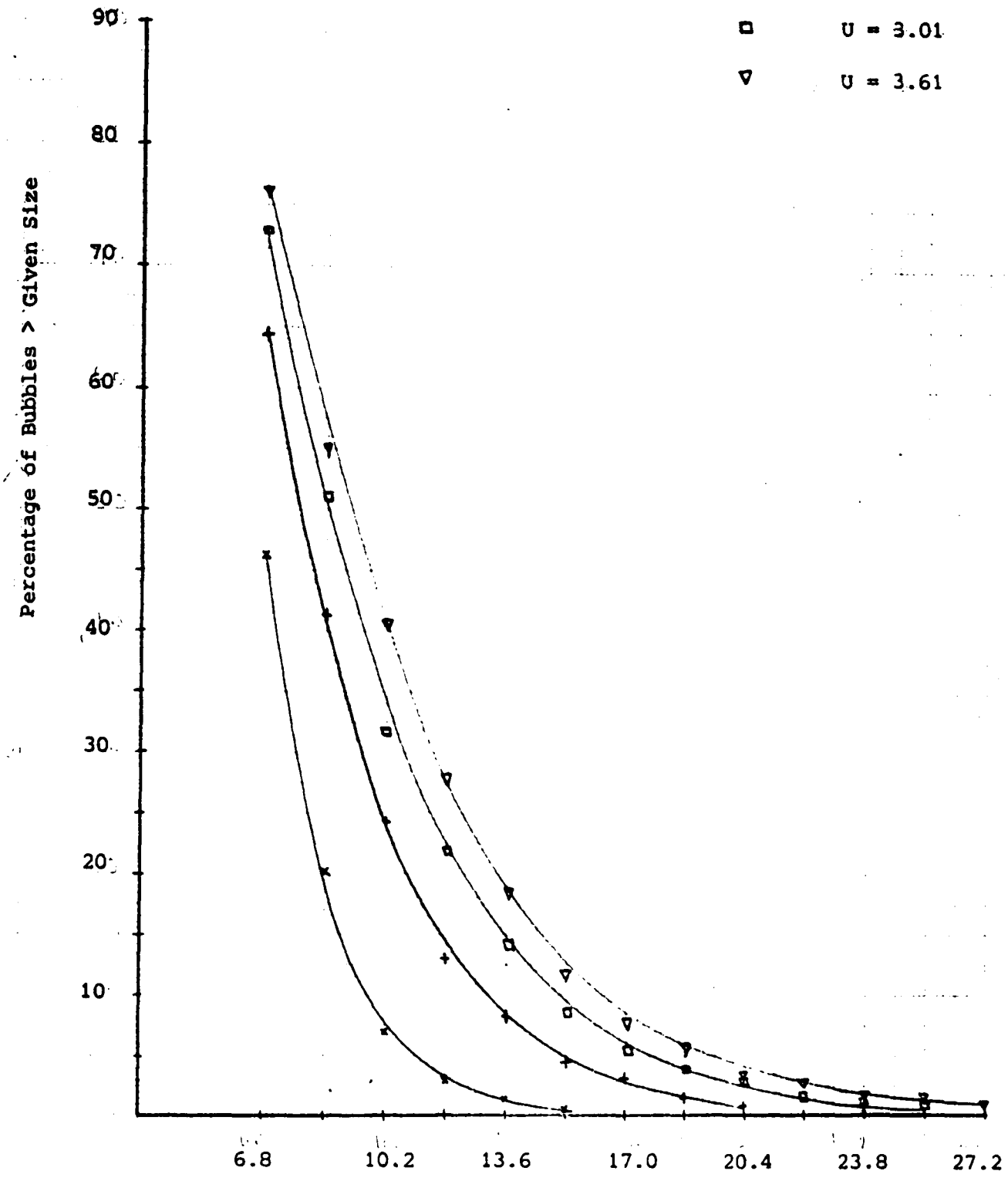

Multiorifice Distributor

X = 36 cm

Y = 21 cm

Z = 40 cm

Fig. 5.17

× U = 1.87

\+ U = 2.41

□ U = 3.01

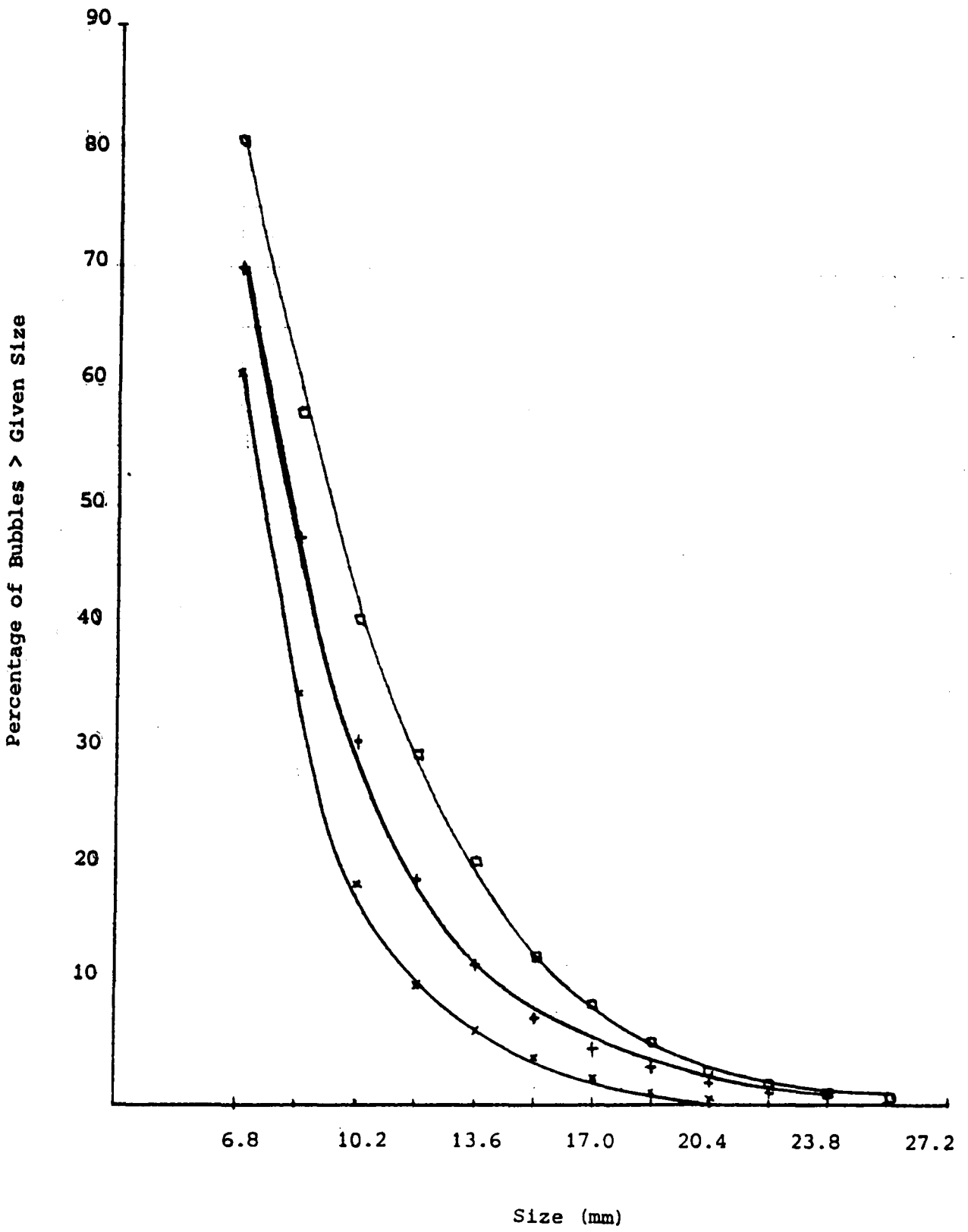

Multiorifice Distributor

X = 36 cm

Y = 7 cm

Z = 70 cm

Fig. 5.18

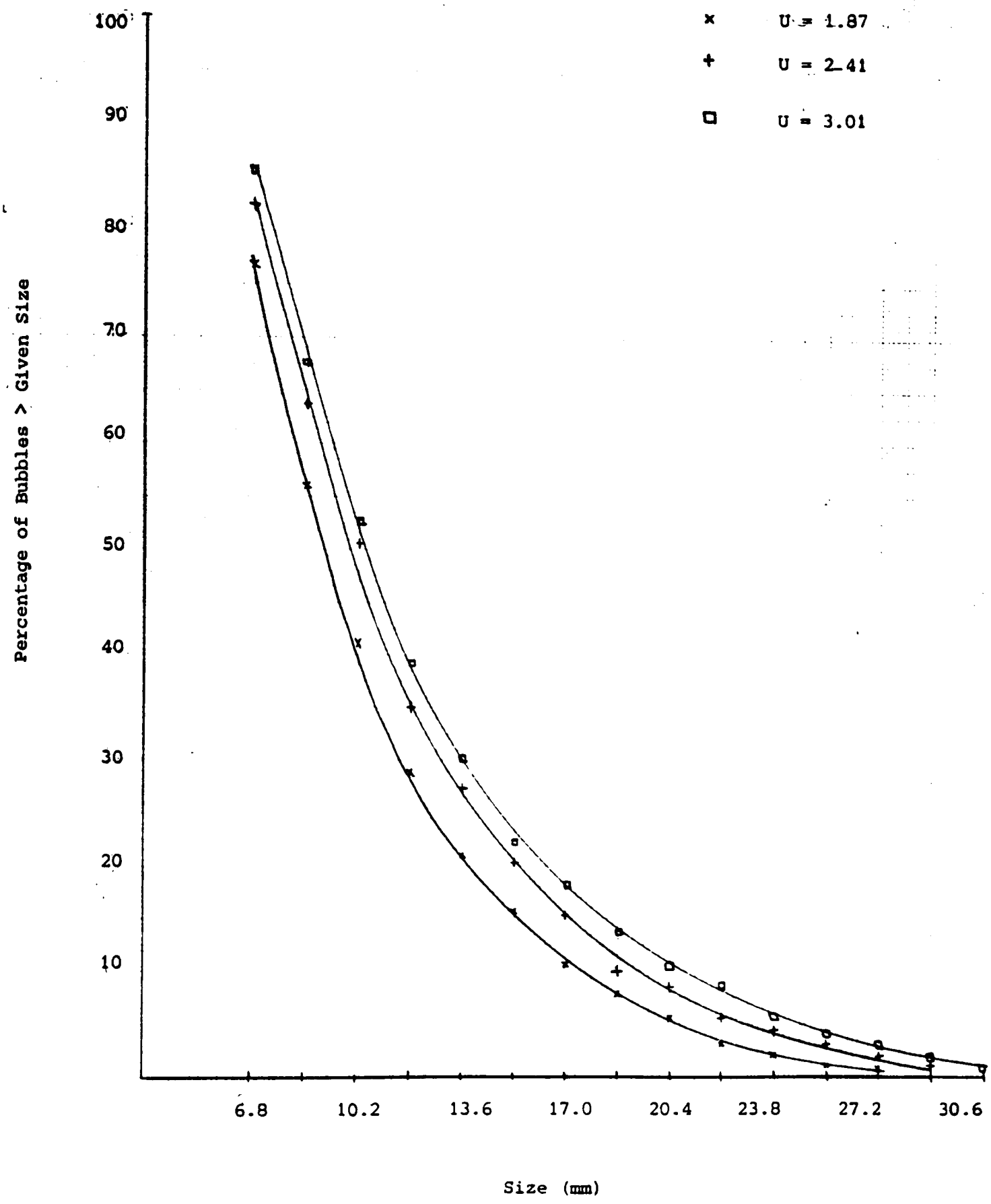

the bed. In fact there seem to be very few large bubbles (i.e. $\geqslant 2 \times \ell$) at heights around 20 cm above the distributor plate. Differences between gas flow rates diminish as elevation above the distributor increases.

5.3.2 Variation with Height above Distributor Plate

Figure (5.19) shows the variation of bubble frequency with bubble size at a fixed superficial fluidising velocity of 2.41 $cm.sec^{-1}$ and at six different heights above the multiorifice distributor plate. Bubble frequency decreases with increasing elevation in the bed. At greater elevations, there is a smaller proportion of bubbles in the lower size ranges and a greater proportion in the higher size ranges. None of the frequency distribution curves shows a peak, indicating the most frequent bubble size is less than 6.8 mm, the fixed separation length.

The variation of bubble size distribution with height above the distributor plate is shown for three points on the vertical axis defined by X = 24 cm and Y - 7 cm co-ordinates, in Figure (5.20). Here, the superficial fluidising velocity is fixed at a lower value of 1.87 $cm.sec^{-1}$ and the three elevations are 50, 60 and 70 cm above the distributor plate. The distribution histogram corresponding to the elevation of 50 cm shows a peak at 7 - 10 mm size range.

This investigation is carried to a point on the bed vertical centreline at a higher superficial fluidising velocity of 3.01 $cm.sec^{-1}$, for four elevations of 40, 50, 60 and 70 cm above the distributor plate, Figure (5.21). The shape of the bubble size distribution is very much the same regardless of height. This could be due to a rapid upward particle circulation on the bed vertical axis moving the bubbles up through the bed so fast that they have no time to coalesce.

Fig. 5.19

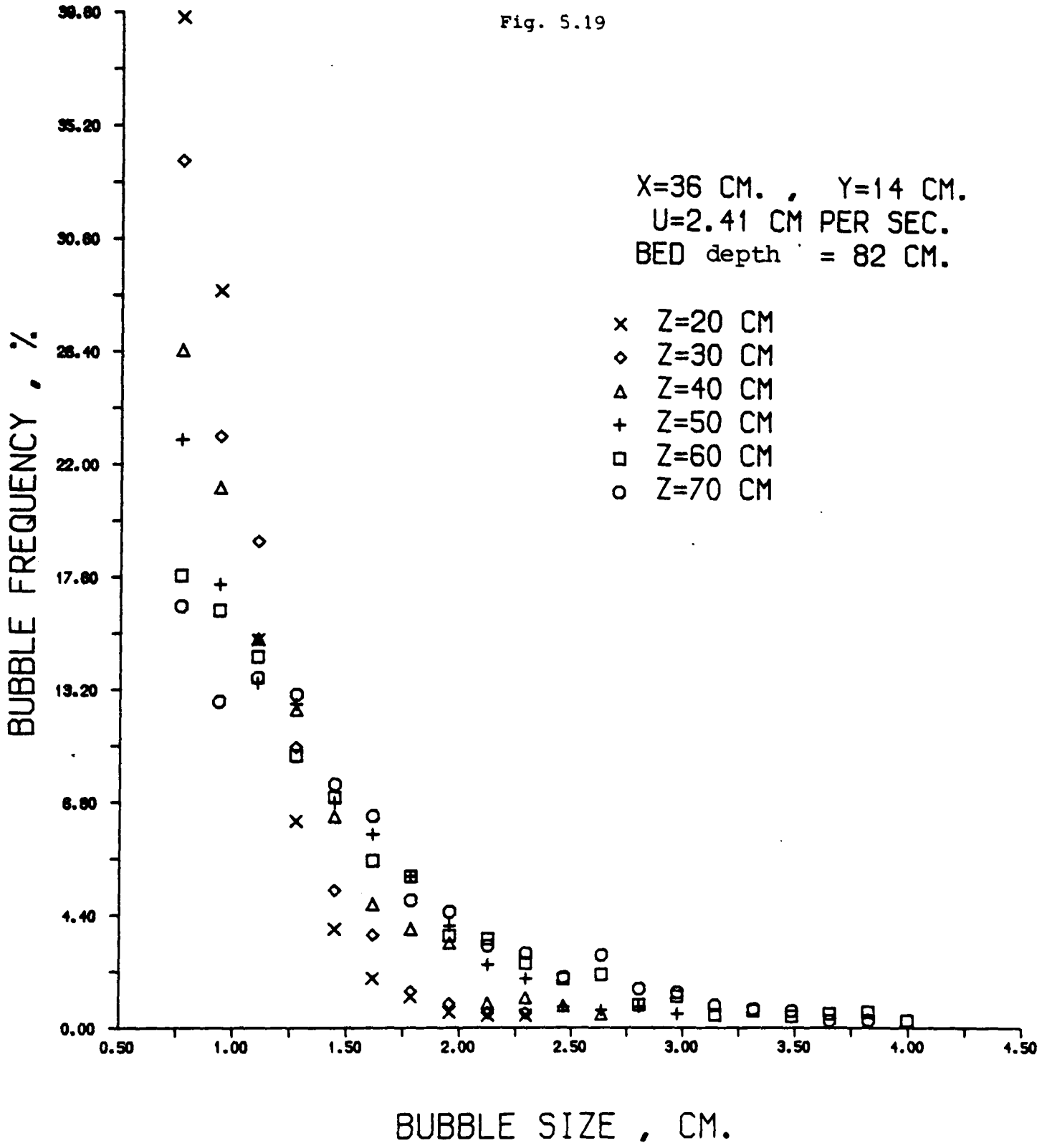
X=36 CM. , Y=14 CM.
U=2.41 CM PER SEC.
BED depth = 82 CM.
× Z=20 CM
◇ Z=30 CM
△ Z=40 CM
+ Z=50 CM
□ Z=60 CM
○ Z=70 CM
BUBBLE FREQUENCY , %
30.80
35.20
30.80
26.40
22.00
17.60
13.20
8.80
4.40
0.00
0.50
1.00
1.50
2.00
2.50
3.00
3.50
4.00
4.50
BUBBLE SIZE , CM.

Fig. 5.20

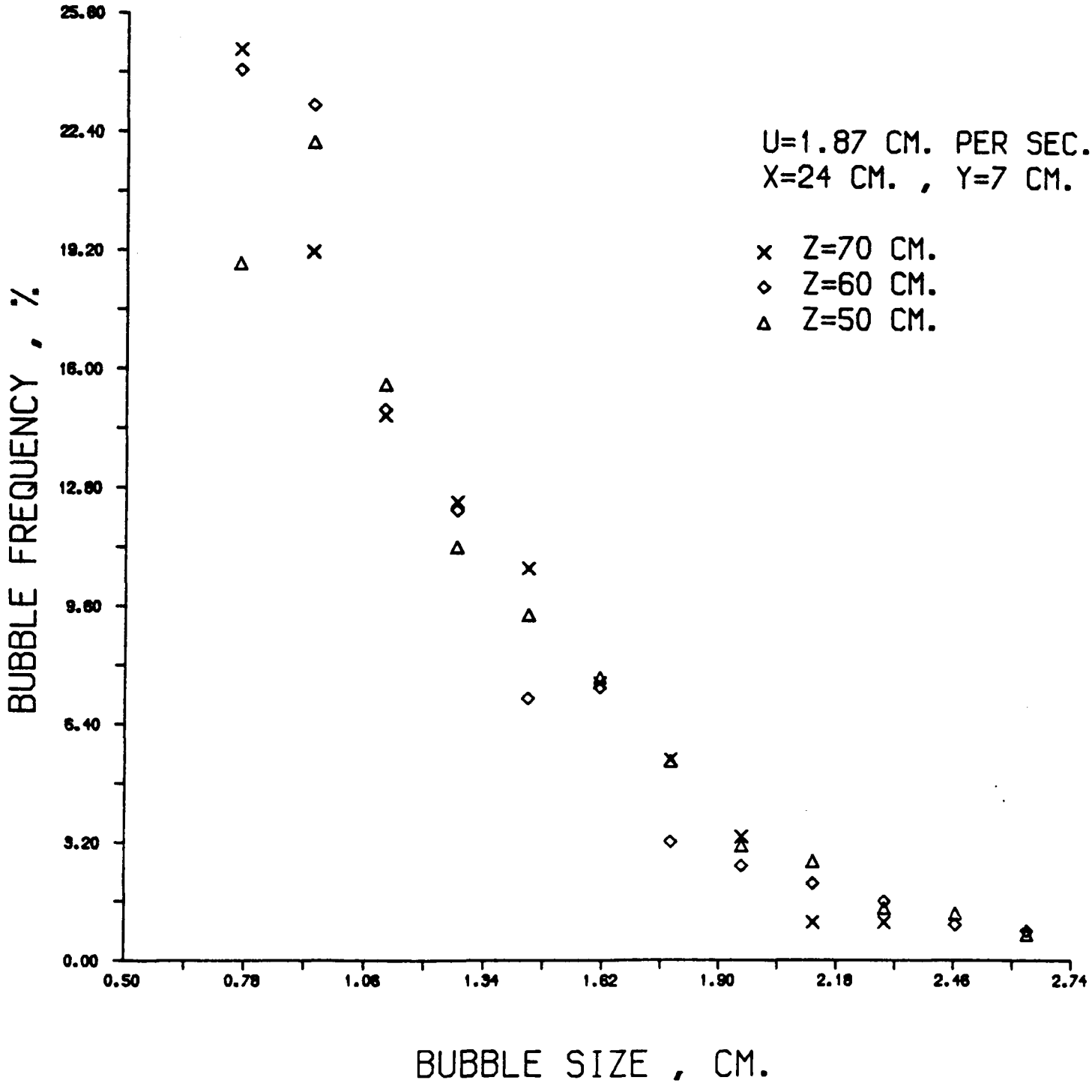
U=1.87 CM. PER SEC.
X=24 CM. , Y=7 CM.
× Z=70 CM.
◇ Z=60 CM.
△ Z=50 CM.
BUBBLE FREQUENCY , %
25.60
22.40
19.20
16.00
12.80
9.60
6.40
3.20
0.00
0.50
0.78
1.06
1.34
1.62
1.90
2.18
2.46
2.74
BUBBLE SIZE , CM.

L

Fig. 5.21

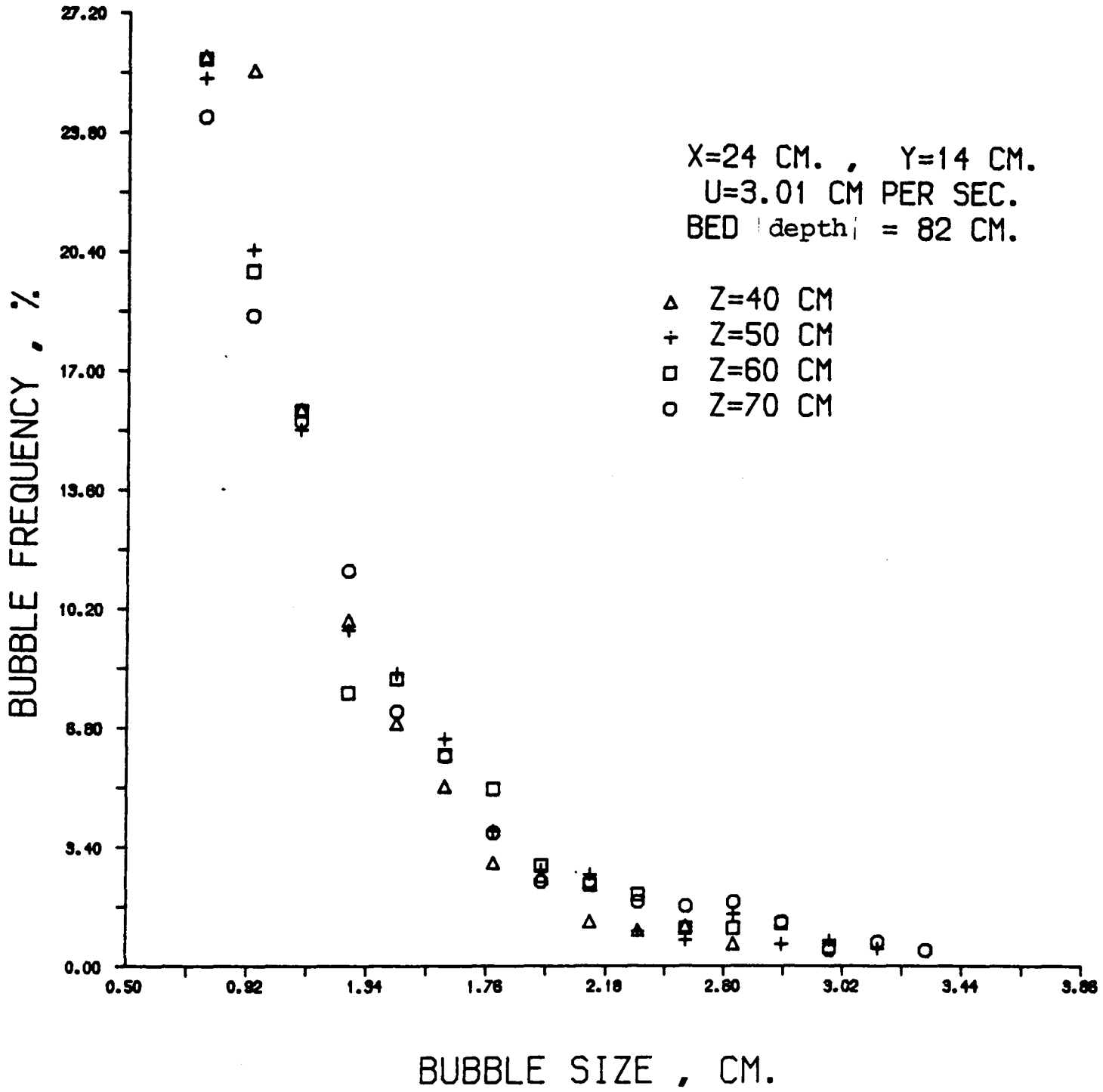
X=24 CM. , Y=14 CM.
U=3.01 CM PER SEC.
BED depth = 82 CM.
Δ Z=40 CM
+ Z=50 CM
□ Z=60 CM
o Z=70 CM
BUBBLE FREQUENCY , %
27.20
23.80
20.40
17.00
13.60
10.20
6.80
3.40
0.00
0.50
0.92
1.34
1.76
2.18
2.60
3.02
3.44
3.86
BUBBLE SIZE , CM.

In Figure (5.22), cumulative oversize curves for a superficial velocity of 2.41 cm/sec and heights of 20, 40 and 70 cm above the gas distributor are plotted. As in the distribution obtained for the porosint plate, there is a shift towards higher bubble sizes at greater heights in the bed. Again, the effect of small bubbles coalescing and forming larger bubbles, as they rise in the bed is clearly visible.

Figure (5.23) shows these cumulative oversize curves, for the same point but at a higher velocity of 3.01 cm/sec, and three elevations of 30, 50 and 70 cm above the distributor plate. A similar pattern to that of Figure (5.22) is revealed, in that the frequency is decreasing with increasing bubble size, and the curves are displaced in the direction of greater bubble size for greater elevations.

A comparison of 5.22 and 5.23 shows that the curves corresponding to greater elevations in the bed lie close together, whereas there are substantial variations of frequency with elevation at lower points in the bed. This suggests that the rate of coalescence is greater at small elevations.

Burgess and Calderbank (6), using a cylindrical bed, concluded that on the bed centreline, close to the distributor, the bubbles are almost the same size with a very small number of large bubbles. However, coalescence increases the fraction of large bubbles at the expense of small ones, thus changing the shape of the distribution markedly, Figure (5.24).

Multiorifice Distributor

X = 36 cm

Y = 7 cm

U = 2.41 cm.sec^{-1}

× Z = 20 cm

\+ Z = 40 cm

□ Z = 70 cm

Fig. 5.22

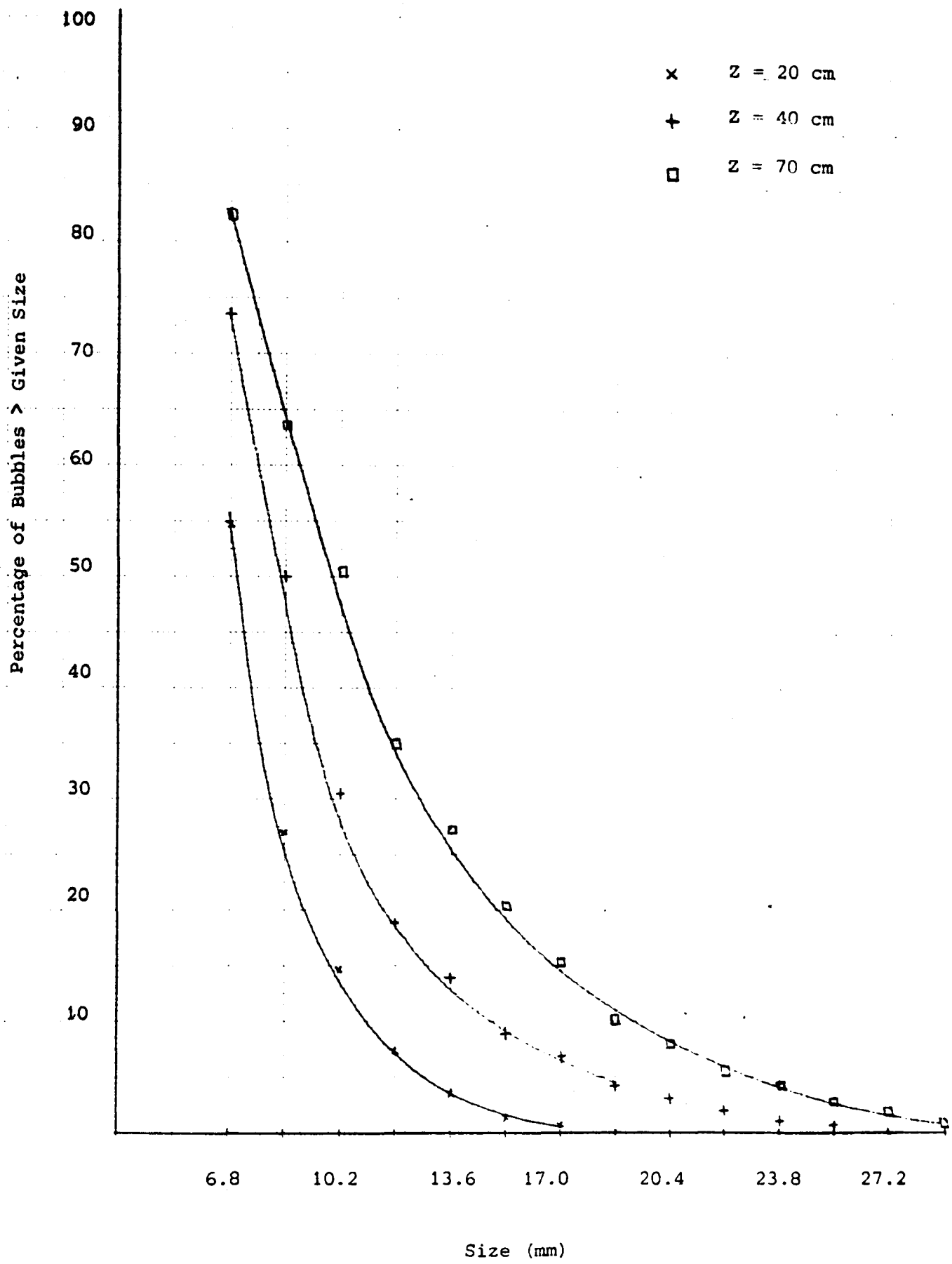

Multiorifice Distributor

X = 36 cm

Y = 7 cm

U = 3.01 cm/sec

Fig. 5.23

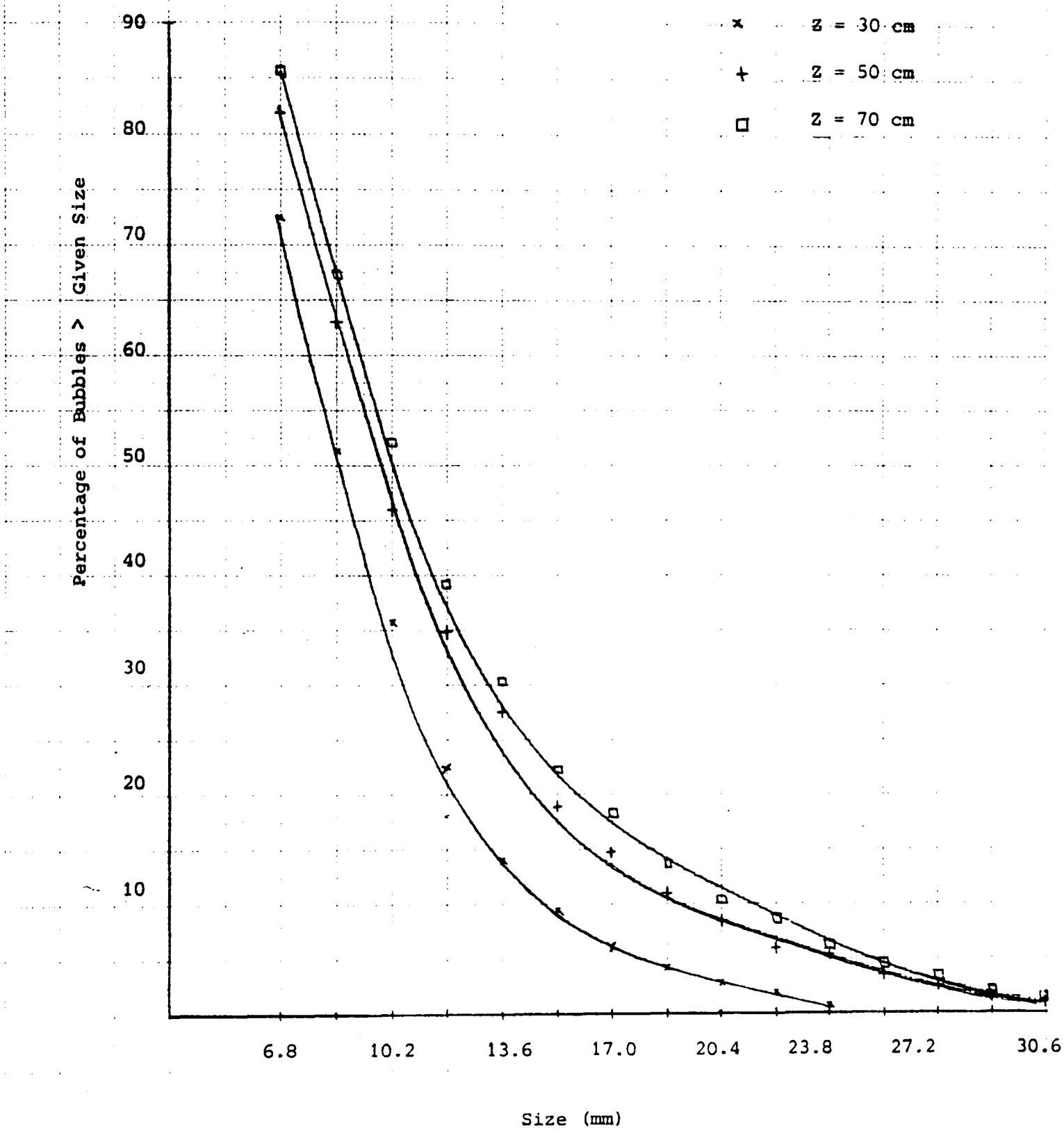

They emphasise that the system is complex, since macroscopic circulation patterns exist in the bed and these affect the bubble velocities with respect to an external observer. These patterns also affect the bubble size distributions, as it appears that the larger bubbles in the bed exist in regions of upward emulsion phase movement. They produced Figure (5.24A) which shows the variation of size distribution on the bed centreline with elevation above the gas distributor indicating that the peak bubble size increases with level in the bed. They further showed how the size distribution changes with radial position at the top of the bed, Figures (5.24B), as well as, at the bottom of the bed, Figure (5.24C). They postulated that at the top of the bed, large bubbles exist preferentially at the bed centreline, which may be recognised as the position of upward emulsion phase movement.

At the bottom of the bed, the opposite trend obtains with the bubbles near the wall being larger than those near the centre.

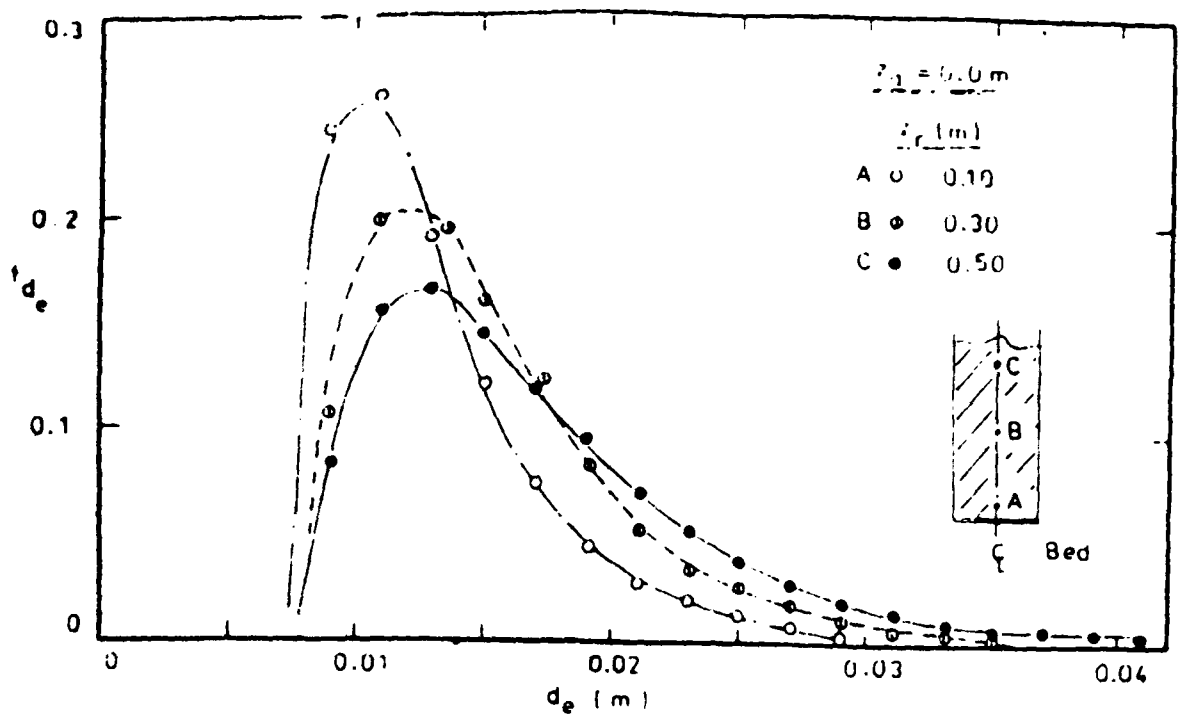

A Variation of gamma-function bubble size distributions with level in the bed on the bed centreline.

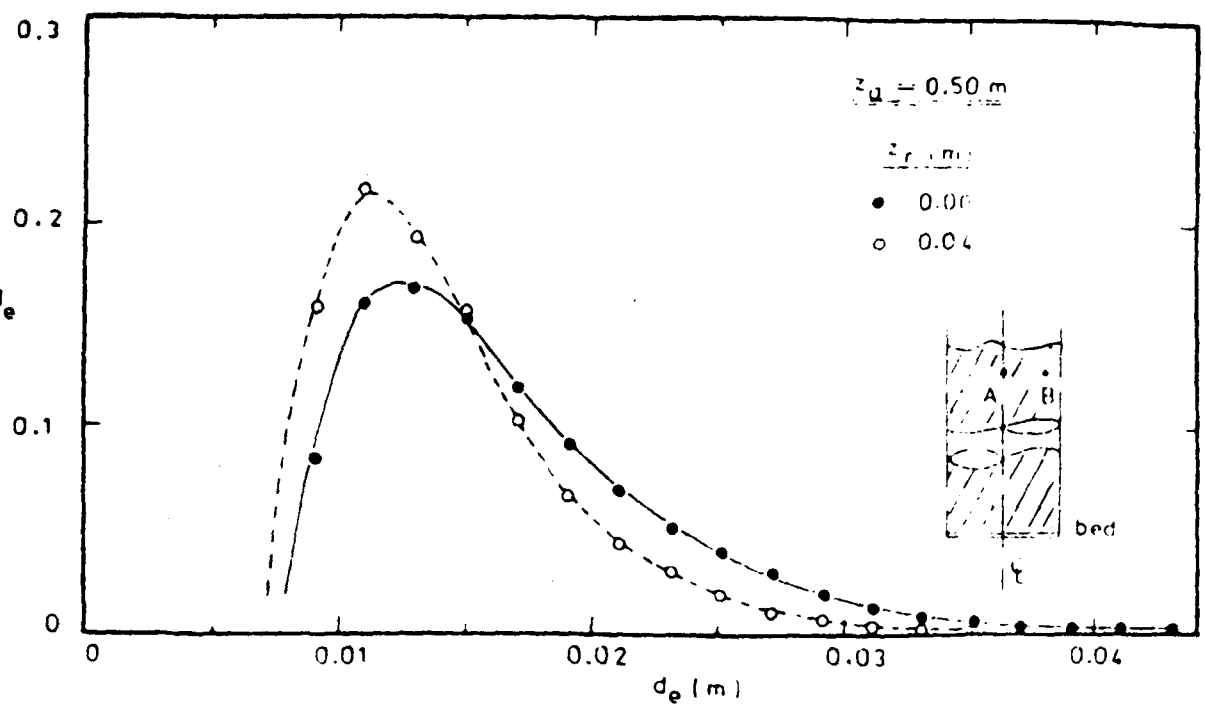

B Variation of gamma-function bubble size distributions with radial position in the bed at the top of the bed.

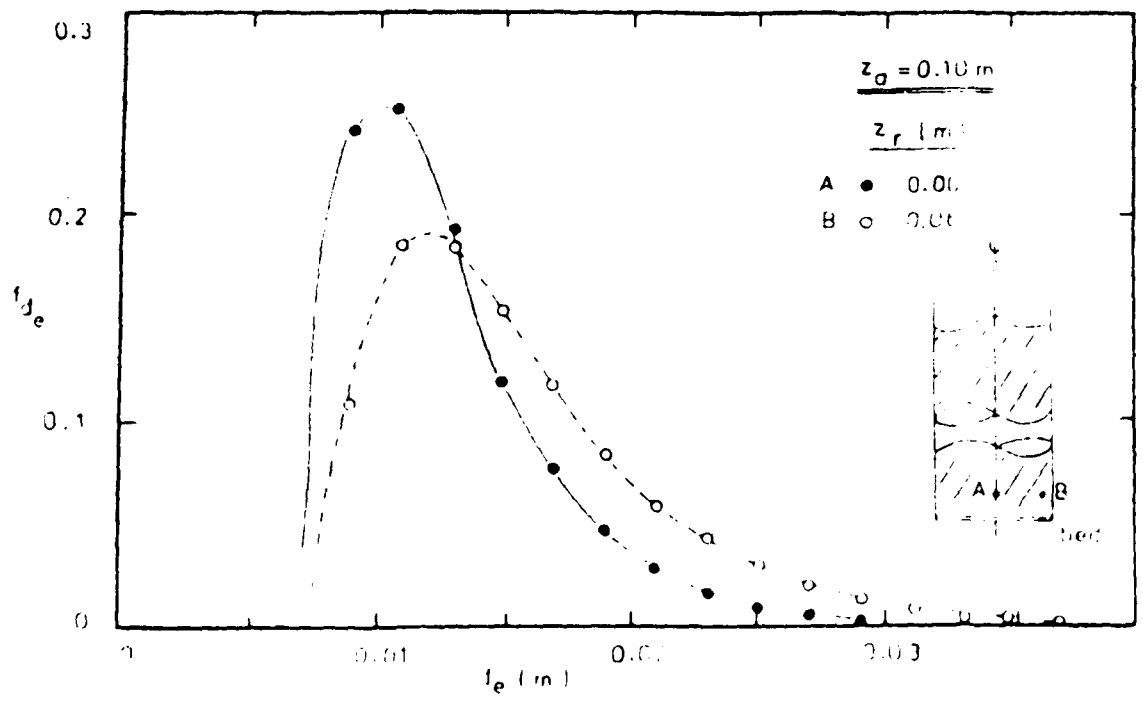

C Variation of gamma-function bubble size distributions with radial position in the bed at the bottom of the bed

Fig. 5.24

5.3.3 Effect of Bed Height on the Bubble Size Distribution

To investigate the effect of bed height on the bubble size frequency and the particle circulation patterns in the bed, two sets of experiments were carried out with the multiorifice distributor. The bubble statistics were recorded, in the first instance, when the bed was gradually filled up. In fact three different depths of 42, 52 and 82 cm were tried, in each case the probe tip being kept a few centimeters below the bed surface. The results from these experiments are compared with those obtained when the bed height was always kept at a uniform height of 82 cm.

Figure (5.25) shows the effect of increasing bed depth on the frequency-size relationship at a point 20 cm above the distributor plate and at a velocity of 2.41 $cm.sec^{-1}$. The two experiments are carried out under identical conditions except for the bed depth, which is almost doubled from 42 cm to 82 cm, above the distributor plate. The two distribution curves are markedly different, both in the lower as well as the higher size ranges. With the greater bed depth there is a much higher proportion of very small bubbles and a correspondingly much smaller proportion of large bubbles, vice versa for the lower bed depths.

The two curves intersect at a point, fairly close to the lowest sizes recorded. This pattern is repeated, again when the relationship is investigated at another point across the bed cross-sectional area, Figure (5.26). Here, the fluidising velocity and elevation of the sampling point are maintained but

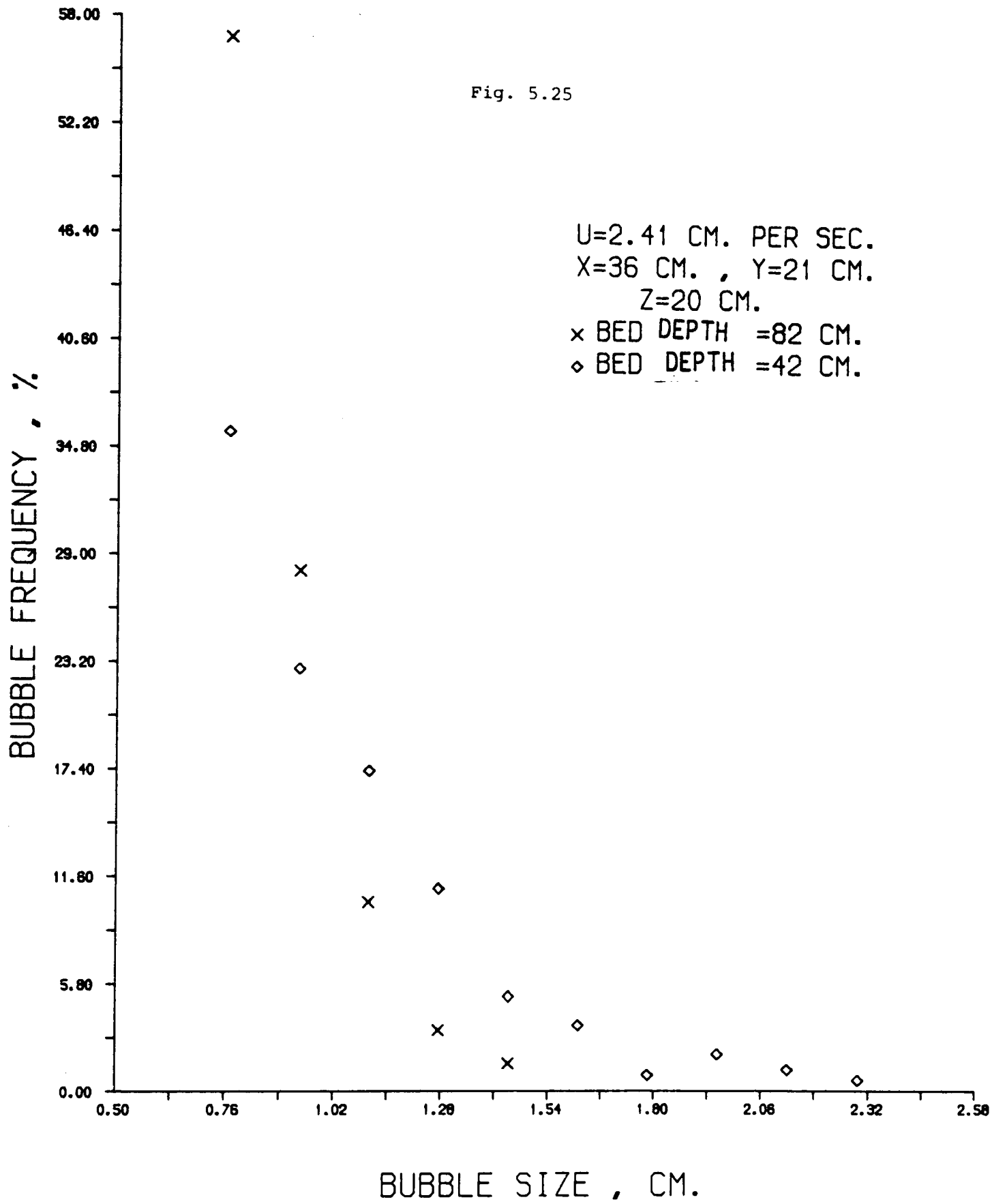
58.00
52.20
46.40
40.60
34.80
29.00
23.20
17.40
11.60
5.80
0.00
0.50
0.76
1.02
1.28
1.54
1.80
2.06
2.32
2.58
BUBBLE FREQUENCY , %
BUBBLE SIZE , CM.
U=2.41 CM. PER SEC.
X=36 CM. , Y=21 CM.
Z=20 CM.
× BED DEPTH =82 CM.
◇ BED DEPTH =42 CM.

Fig. 5.25

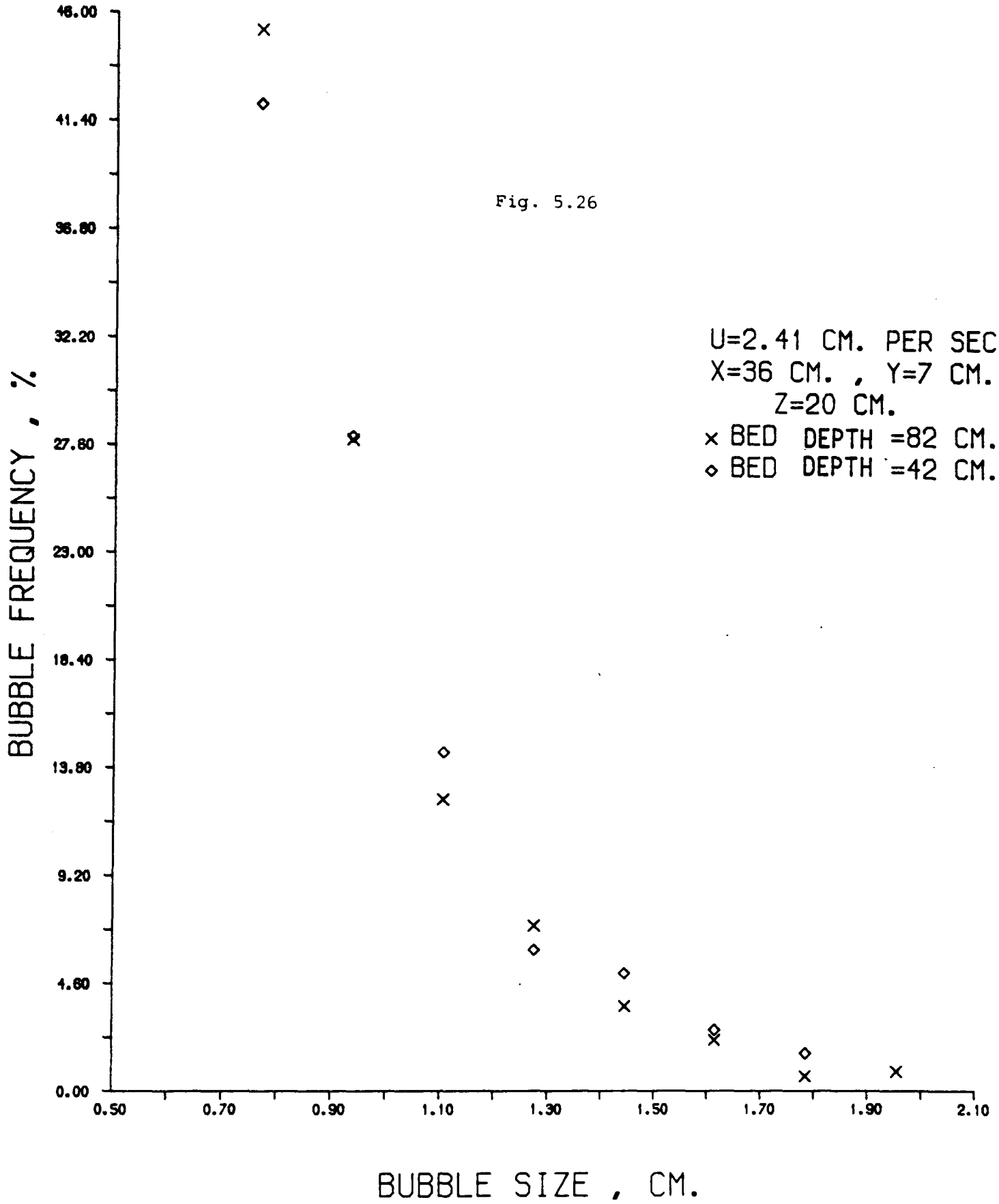
46.00
41.40
36.80
32.20
27.60
23.00
18.40
13.80
9.20
4.60
0.00
0.50
0.70
0.90
1.10
1.30
1.50
1.70
1.90
2.10
BUBBLE FREQUENCY , %
BUBBLE SIZE , CM.
U=2.41 CM. PER SEC.
X=36 CM. , Y=7 CM.
Z=20 CM.
× BED DEPTH =82 CM.
◇ BED DEPTH =42 CM.

Fig. 5.26

the point is 14 cm nearer to the front wall of the bed. A comparison of the two graphs reveals a similar pattern, but less variation at this new point. In fact, as the size increases the two curves overlap. It seems reasonable to assume that the paths which the bubbles take when they rise up the bed are different in the two cases, (i.e. with different bed depths).

Furthermore, the particle circulation patterns are markedly different when the bed depth is doubled (chapter 4). This will be discussed in more detail in chapter 6.

Figures (5.27) and (5.28) show the variation of size distribution at two higher elevations of 30 and 40 cm, while the remaining conditions are maintained.

A comparison of Figures (5.27) and (5.28) shows a marked change in that the difference between the two sets of points seems non-significant in Figure (5.27) but not in (5.28).

Figure (5.29) shows the effect of yet further increase in elevation on the same vertical axis (as in Figures 5.27 and 5.28), to Z = 50 cm above the distributor plate. The superficial fluidising velocity is also increased to 3.01 cm/sec.

The two sets of points seem to be significantly different in Figure (5.29). Both show peaks in 8 - 10 mm size-range, the higher of the two corresponding to the greater bed depth. Nevertheless the pattern of Figures (5.26 - 5.28) is repeated in that the curves cross at a fairly low bubble size, giving a greater proportion of larger bubbles with the lower bed depth. Once more, this seems to reflect the different particulate-phase circulation patterns prevailing at the increased bed depth.

Fig. 5.27

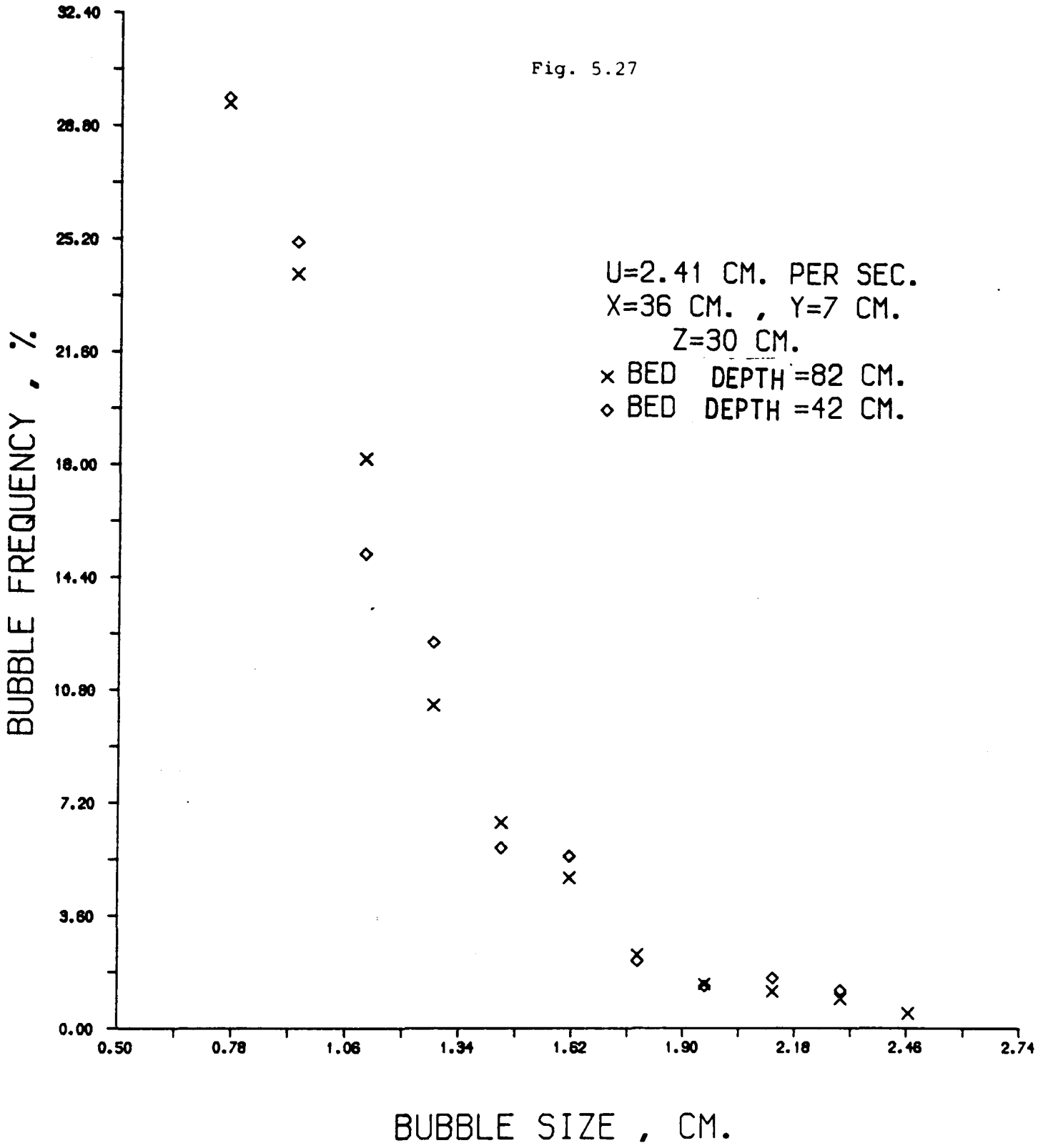
32.40
28.80
25.20
21.60
18.00
14.40
10.80
7.20
3.60
0.00
BUBBLE FREQUENCY , %
0.50
0.78
1.06
1.34
1.62
1.90
2.18
2.46
2.74
BUBBLE SIZE , CM.
U=2.41 CM. PER SEC.
X=36 CM. , Y=7 CM.
Z=30 CM.
× BED DEPTH =82 CM.
◇ BED DEPTH =42 CM.

Fig. 5.28

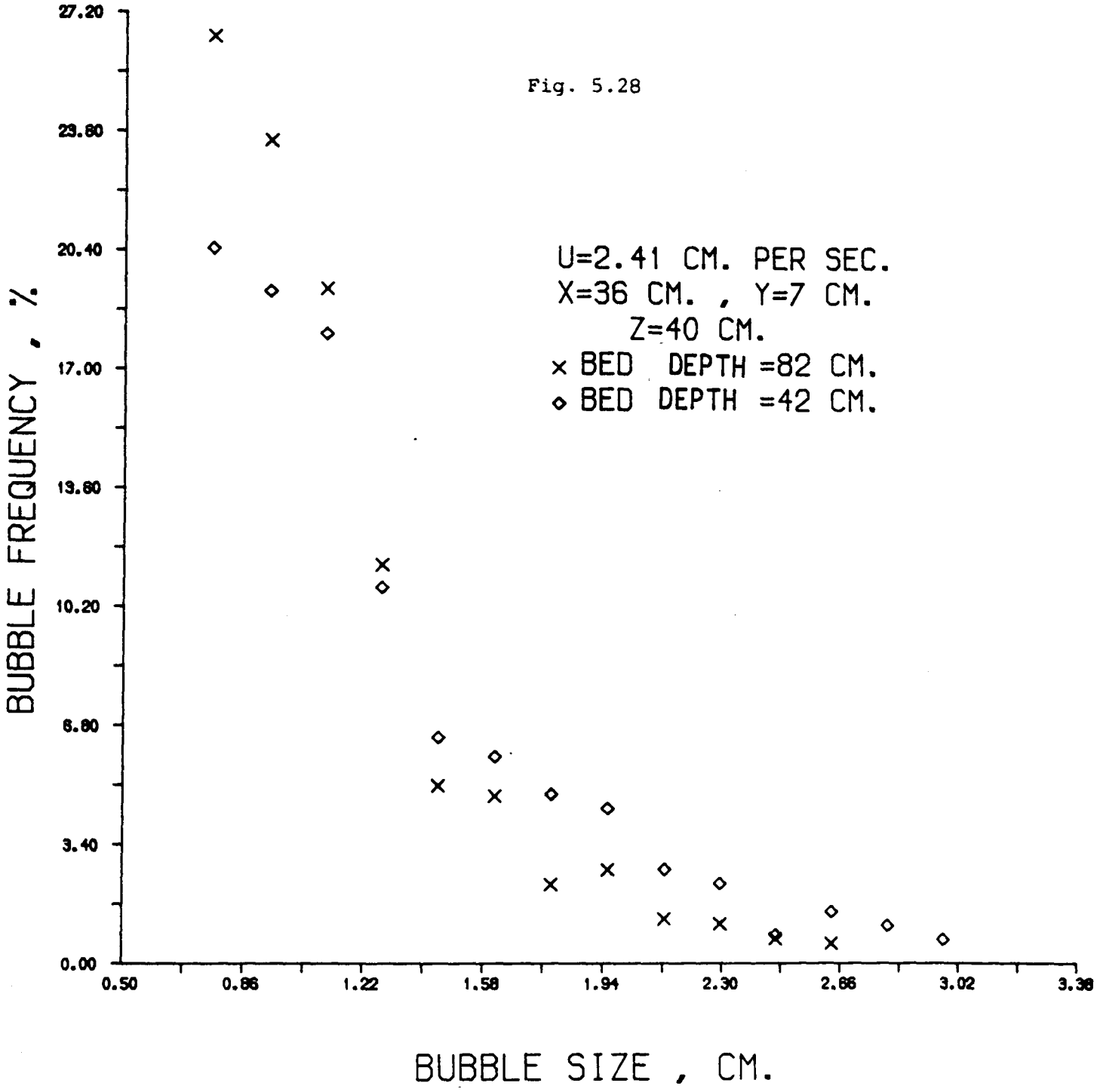
U=2.41 CM. PER SEC.
X=36 CM. , Y=7 CM.
Z=40 CM.
× BED DEPTH =82 CM.
◇ BED DEPTH =42 CM.
BUBBLE FREQUENCY , %
27.20
23.80
20.40
17.00
13.60
10.20
6.80
3.40
0.00
0.50
0.86
1.22
1.58
1.94
2.30
2.66
3.02
3.38
BUBBLE SIZE , CM.

Fig. 5.29

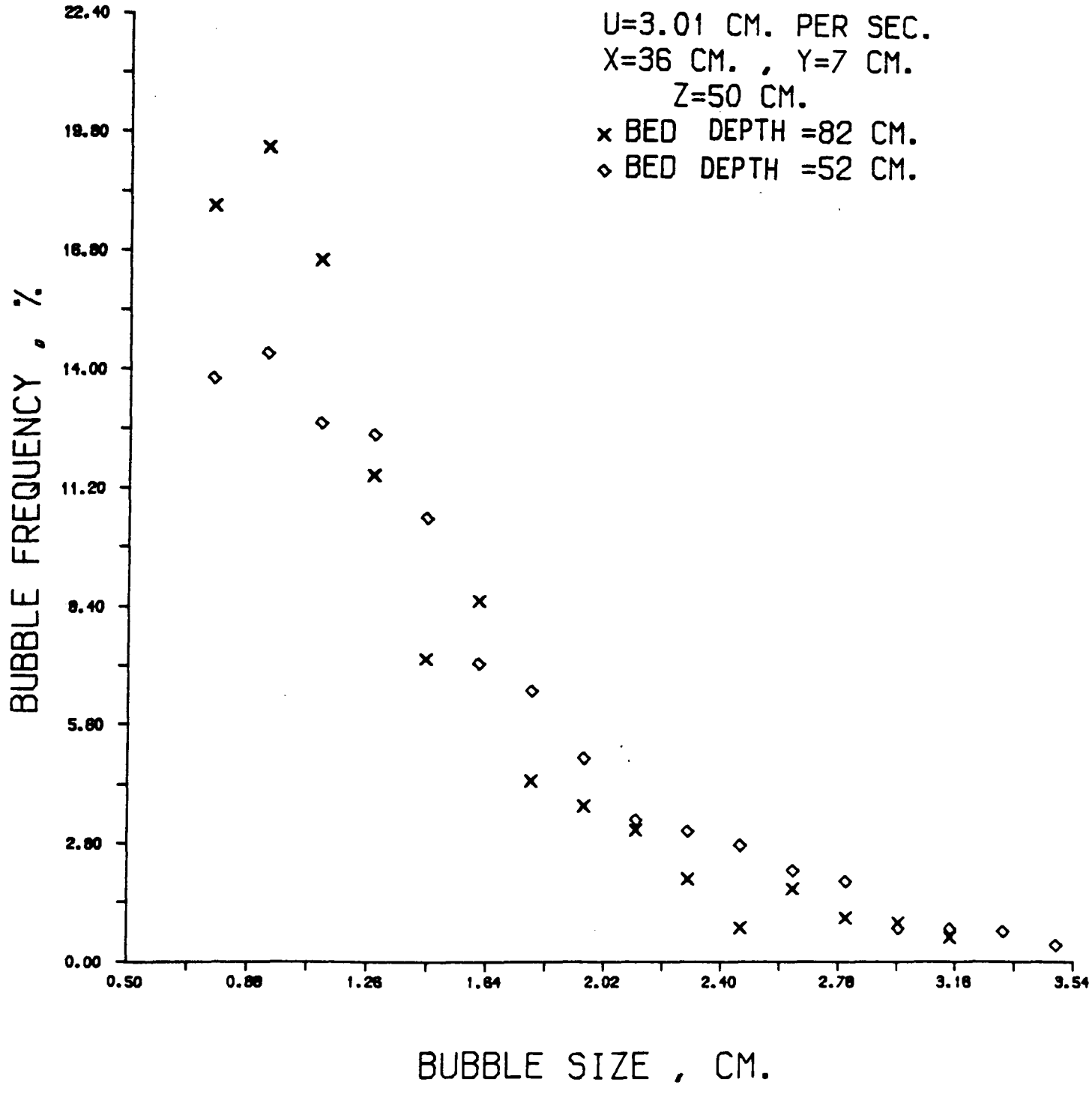
U=3.01 CM. PER SEC.
X=36 CM. , Y=7 CM.
Z=50 CM.
× BED DEPTH =82 CM.
◇ BED DEPTH =52 CM.
BUBBLE FREQUENCY , %
22.40
19.80
16.80
14.00
11.20
8.40
5.60
2.80
0.00
0.50
0.88
1.26
1.64
2.02
2.40
2.78
3.16
3.54
BUBBLE SIZE , CM.

5.4 Variation Across the Bed Cross-Section

Figure (5.30) shows the variation of bubble size distribution along the X-axis (on the longitudinal centreline), at an elevation of 20 cm above the distributor plate and a superficial velocity of 3.01 $cm.sec^{-1}$. The point with the greatest value of X = 36 cm is the farthest from the air inlet.

The data for the point nearest to the air inlet, (X = 12 cm), shows the highest frequencies for the smallest bubbles recorded. The three curves intersect at points between 8 - 10 mm size range which are very close to the smallest size measured. From the points of intersection on the curves corresponding to the X = 24 cm and X = 36 cm show higher frequencies for the same bubble sizes. Frequency decreases more sharply for the point with X = 12 cm.

This phenomenon is investigated (Figure 5.31), for two points, on the longitudinal centreline (X-axis), at a greater elevation of 40 cm above the distributor plate. The operating conditions are maintained at U = 3.01 $cm.sec^{-1}$ and the bed height = 42 cm. Bubble frequency decreases with increasing bubble size but the decrease is more gradual than when Z = 20 cm. The two curves corresponding to X = 24 cm and X = 36 cm intersect and a similar pattern to that of Figure (5.30) is revealed.

In Figure (5.32) the bed depth is increased to 82 cm and the sampling points are all located at the Z = 70 cm plane above the gas distributor. Superficial fluidising velocity is 3.01 $cm.sec^{-1}$. The three points are, again equally distanced along the X-axis.

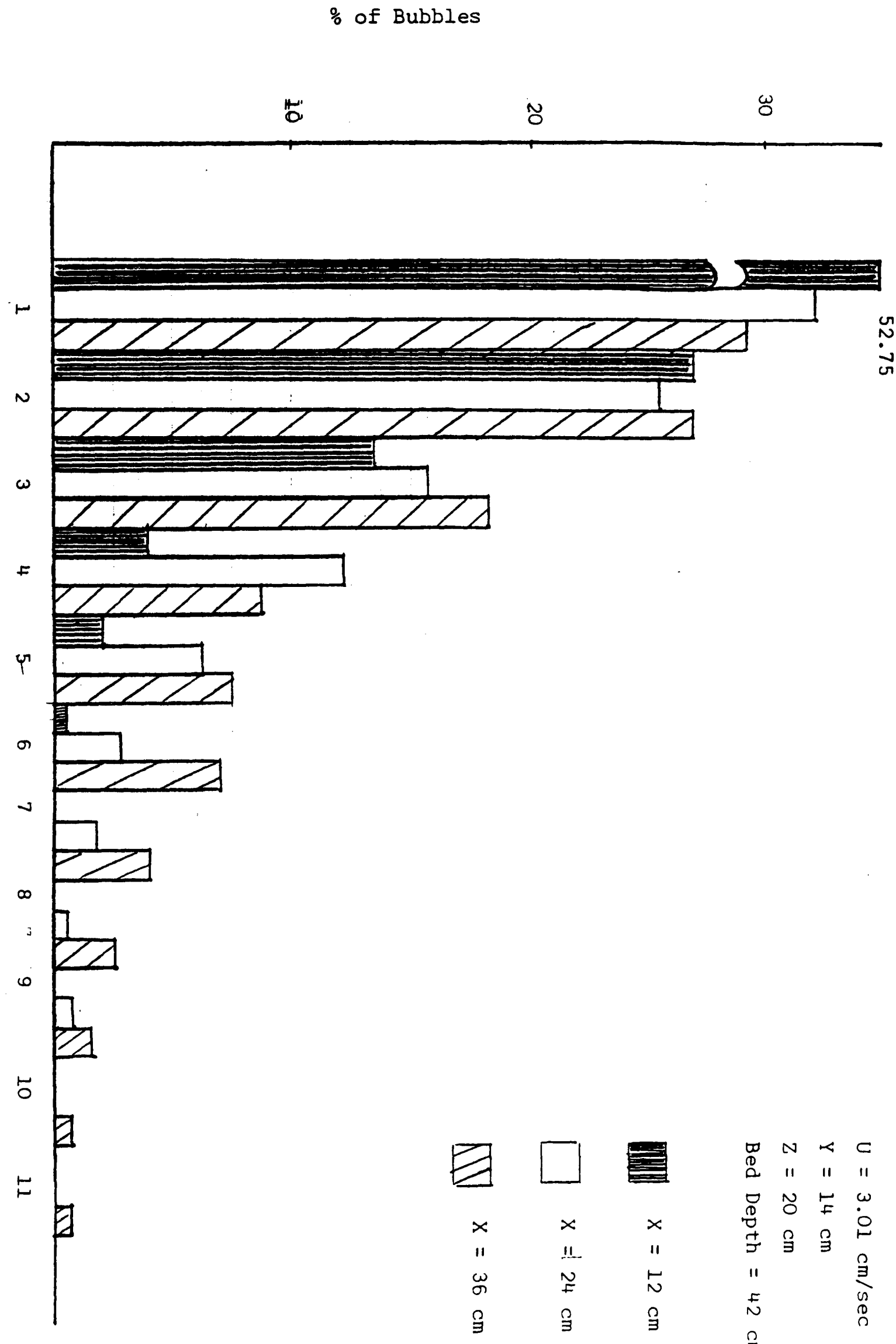
% of Bubbles
10
20
30
52.75
1
2
3
4
5
6
7
8
9
10
11
Slot Number
U = 3.01 cm/sec
Y = 14 cm
Z = 20 cm
Bed Depth = 42 cm
X = 12 cm
X = 24 cm
X = 36 cm

Fig. 5.30

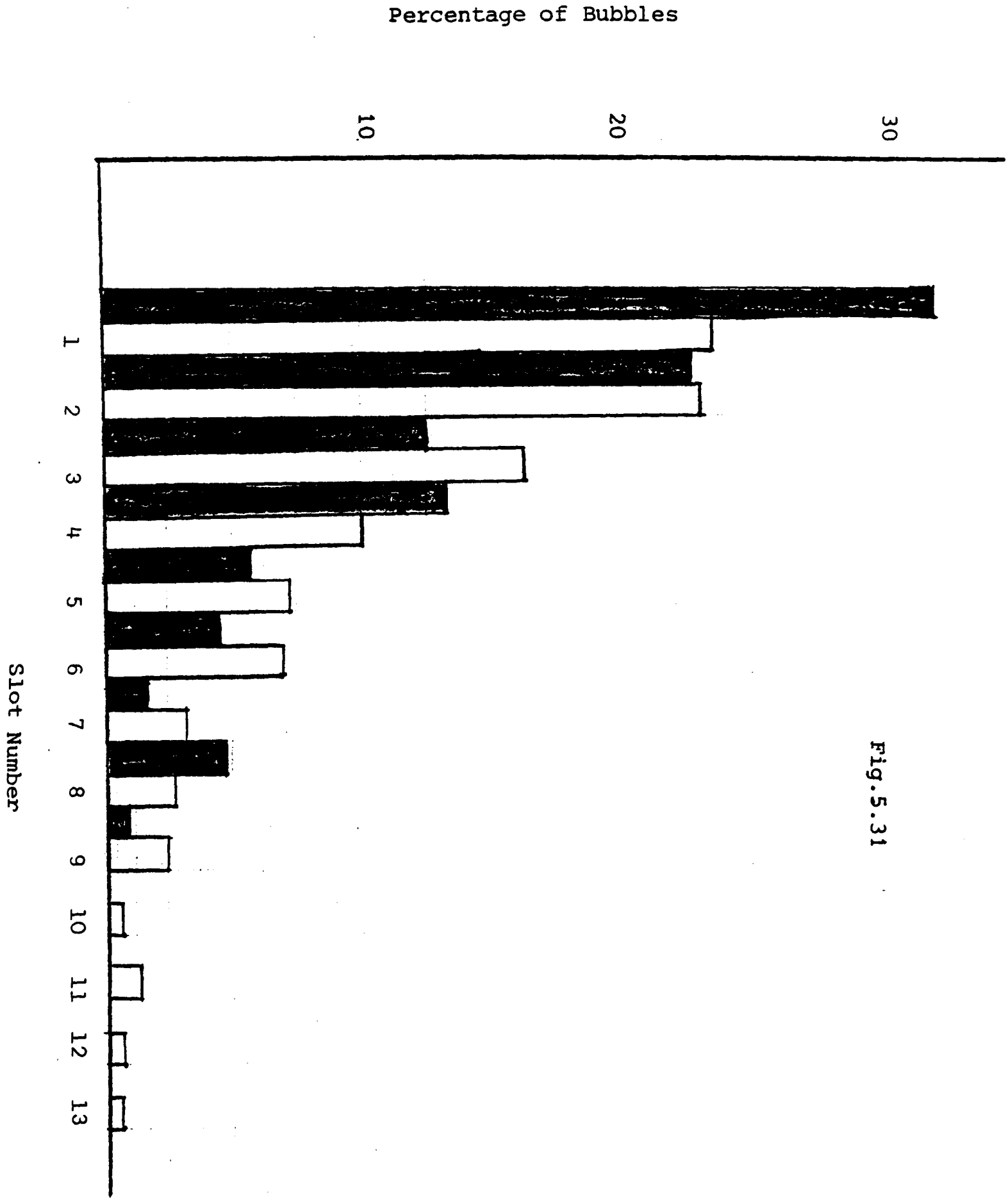
Percentage of Bubbles
10
20
30
1
2
3
4
5
6
7
8
9
10
11
12
13
Slot Number
U = 3.01 cm/sec
Z = 40 cm
Y = 14 cm
Bed Depth = 42 cm
X = 24 cm
X = 36 cm

Fig.5.31

Fig. 5.32

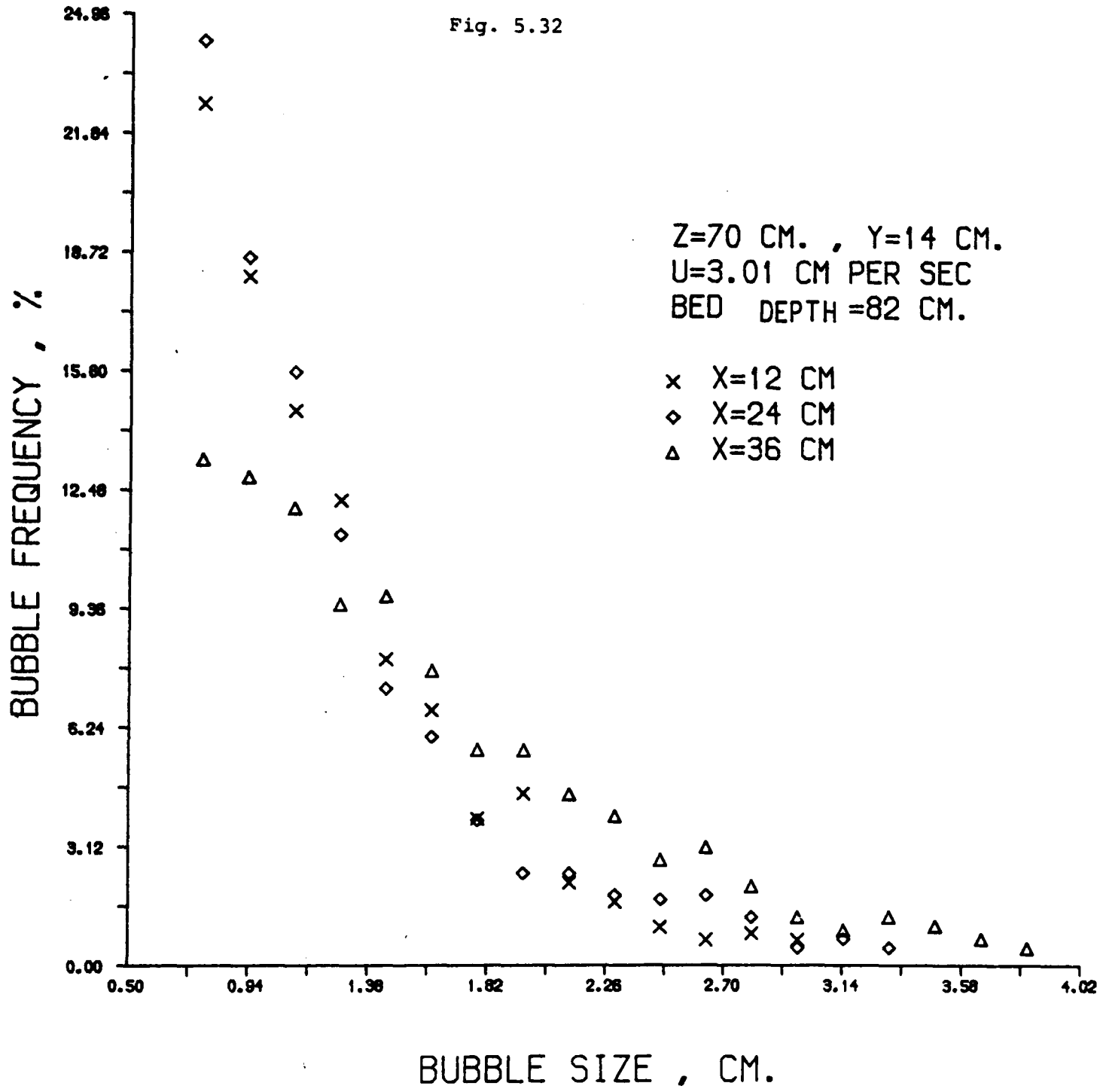
Z=70 CM. , Y=14 CM.
U=3.01 CM PER SEC
BED DEPTH =82 CM.
X=12 CM
X=24 CM
X=36 CM
BUBBLE FREQUENCY , %
24.96
21.84
18.72
15.60
12.48
9.36
6.24
3.12
0.00
0.50
0.94
1.38
1.82
2.26
2.70
3.14
3.58
4.02
BUBBLE SIZE , CM.

Comparisons of Figures 5.30, 5.31 and 5.32 reveals that the pattern of size distribution variation at the bottom of the bed is the reverse of that prevailing at the top of the bed.

This diagram (5.32), cannot be compared directly with either Figure (5.30) or (5.31), since they are for a different bed depth (42 cm). But the pattern mentioned above is clearly visible in Figure (5.32) as well. Initially greater frequencies are recorded for the point on the bed vertical centreline.

As we have seen in chapter 4, at the bottom of the bed, the bubbles located near the vessel walls are rising faster than those in the central zones (with a bed depth of 42 cm). It was concluded that, from their enhanced velocity, these bubbles seem to be in a region of upward emulsion phase movement.

Figure (5.30) seems to confirm this theory, in that the points for X = 36 cm show larger frequencies for large bubbles than those for X = 24 cm.

In Figure (5.31), (top of the bed), the picture is not so clear. After an initial interval of bubble height, in which points corresponding to X = 24 cm show much greater frequency, the two curves overlap and there does not seem to be a significant difference between the two.

Figure (5.32), on the other hand, shows that at the top of the bed, (when the depth is 82 cm), larger bubbles are near the "right hand side wall".

When the bed is filled to a maximum depth of 82 cm (Figure 5.32), the particle phase circulation patterns are quite different from those in a bed with 42 cm depth, (chapter 4).

Bubble size distribution variation along the Y-axis (Y-coordinate) is shown in Figure (5.33) for three points on the transverse centreline at an elevation of 20 cm above the distributor plate. Superficial fluidising velocity is 3.01 $cm.sec^{-1}$. The data for all three points show no significant difference in the bubble frequencies. Bubbles nearer to the front wall seem to be slightly more frequent in the lower size ranges. Frequency decreases with bubble size, almost equally for all the three points.

A very different picture is revealed when this variation is studied at a greater elevation of 40 cm, Figure (5.34). Greater number of larger bubbles exist in the central zones at this elevation, suggesting the existence of particle flow patterns with different directions when the elevation is increased to Z = 40 cm.

Fig. 5.33

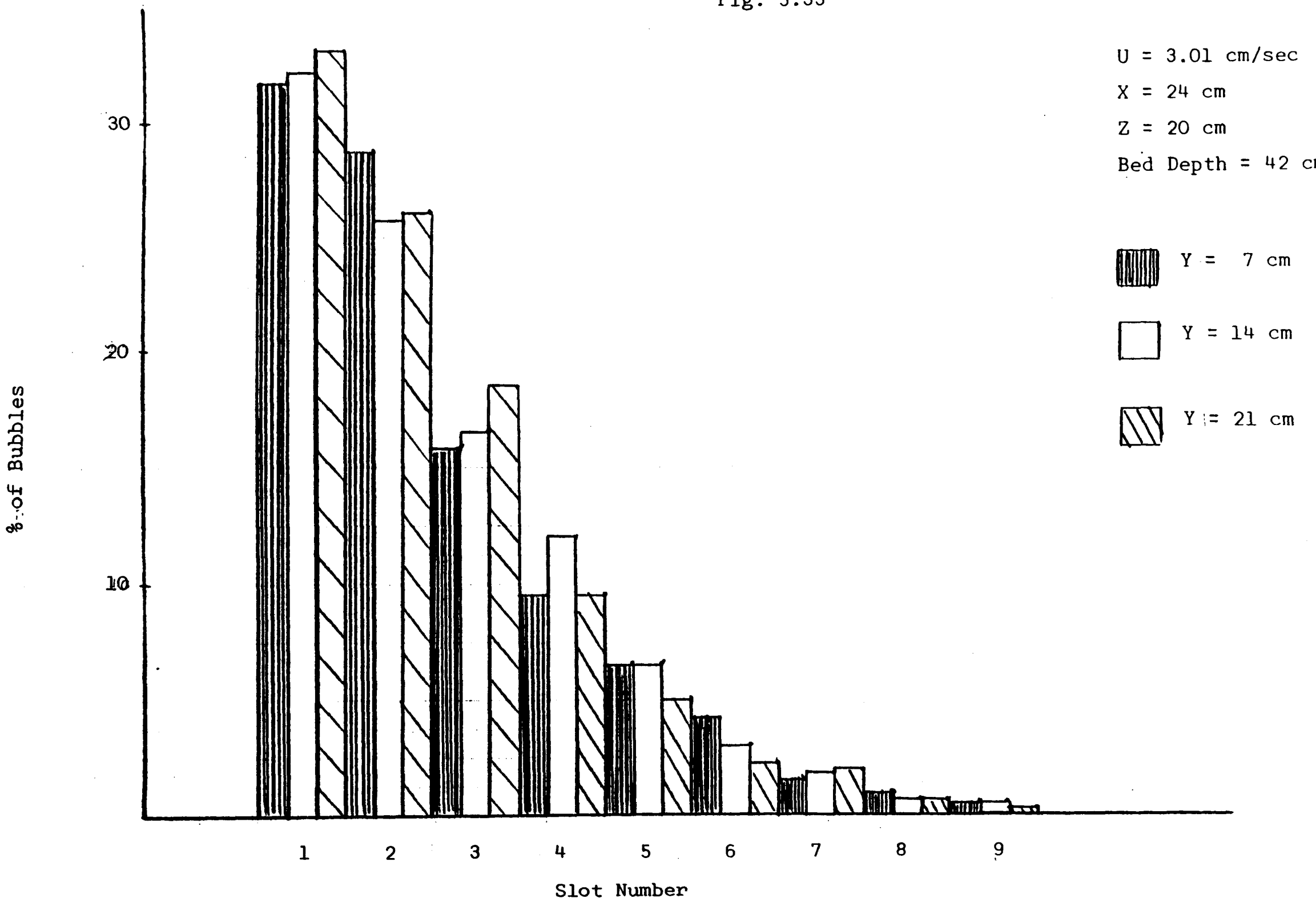
U = 3.01 cm/sec
X = 24 cm
Z = 20 cm
Bed Depth = 42 cm
Y = 7 cm
Y = 14 cm
Y = 21 cm
% of Bubbles
30
20
10
1
2
3
4
5
6
7
8
9
Slot Number

Fig. 5.34

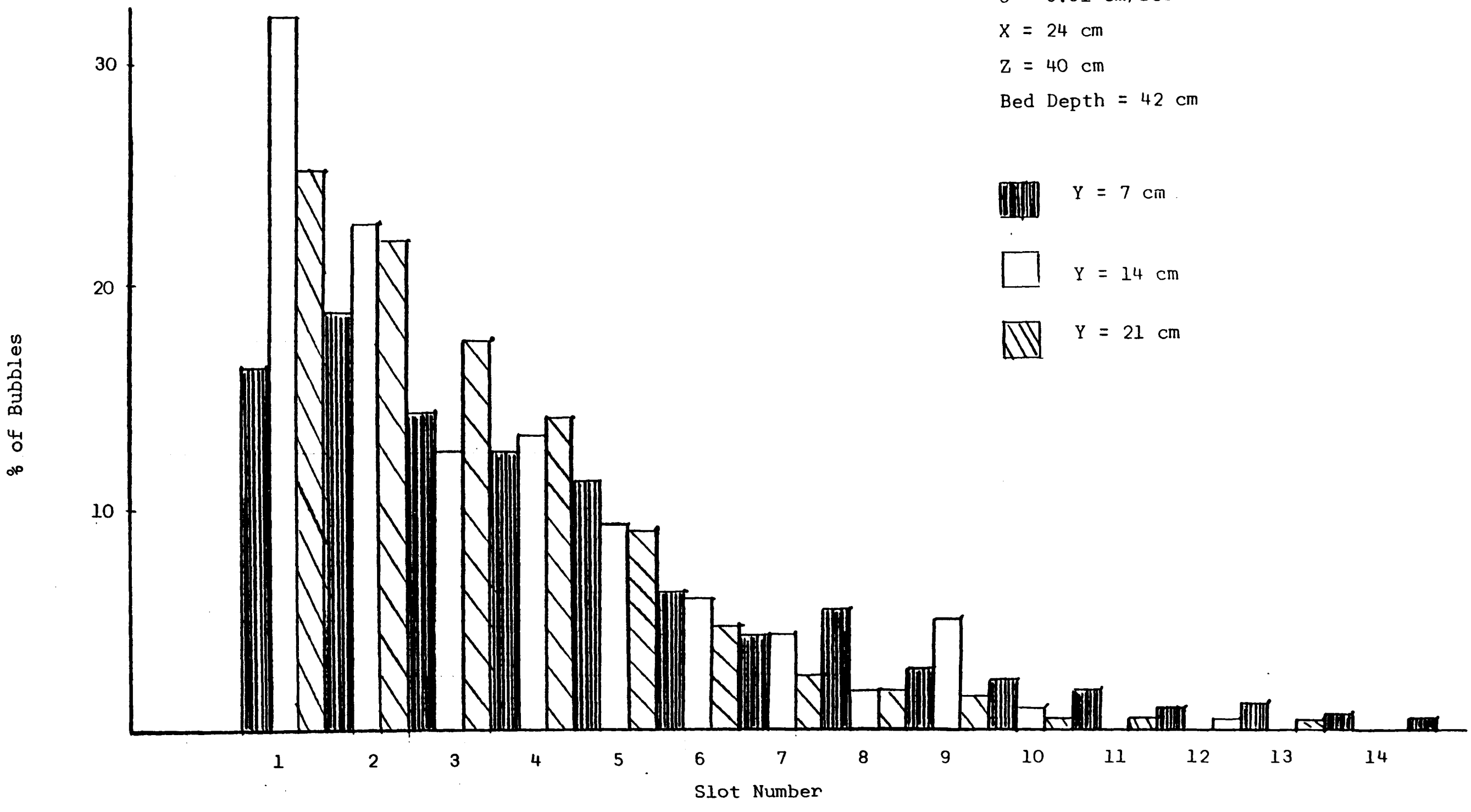
U = 3.01 cm/sec
X = 24 cm
Z = 40 cm
Bed Depth = 42 cm
Y = 7 cm
Y = 14 cm
Y = 21 cm
% of Bubbles
30
20
10
1
2
3
4
5
6
7
8
9
10
11
12
13
14
Slot Number

5.5 Conclusions

Bubble size distributions are studied with two different gas distributors employed. The effects of bed height, gas flow rate and the bed depth on the frequency-size relationship were investigated in this chapter. The following conclusions can be drawn:

1. A greater proportion of small bubbles is found in the vicinity of the distributor plate. As the elevation above the distributor increases, the proportion of larger bubbles is correspondingly increased.

   Bubble frequency decreases with increasing bubble size. At high elevations this decrease is more gradual. Conversely, at low elevations, we invariably find a very sharp drop in frequency within a relatively small size-range. Very few large bubbles are found near the distributor plate. Due to the fact that very small bubbles are excluded from the size distributions (in this work), an accurate picture of bubble size-bubble frequency dependence cannot be obtained. Nevertheless, the general pattern (of skewed distributions of bubble sizes in gas fluidised beds) is revealed. Peaks in the 8-10 mm size range are recorded, except at very high elevations above the distributor plate, where this range is increased to 10-12.5 mm.

2. Superficial fluidising velocity has a direct effect on the size-distribution of bubbles generated by both distributor plates. Greater bubble sizes are recorded with higher superficial fluidising velocities. Cumulative oversize curves invariably show that the size distribution curves are displaced in the direction of greater bubble size for the higher superficial fluidising velocities, Figures (5.3 - 5.5).

3. The effect of the particulate phase circulation patterns are investigated from two different aspects:-

   (a) Bubble size distributions are compared at various points across the bed cross-section, but under identical operating conditions. It is reported (as mentioned earlier) that, the larger bubbles in the bed exist in regions of upward emulsion phase movement.

We have found that the circulation patterns affect the bubble size distribution, in that larger bubbles exist near the "right hand side" wall of the bed, at low elevations. As the elevation is increased, there is a shift in the position of these bubbles, towards the centre of the bed. But this is not as clear as one would expect, especially along the X-axis of the bed. Since the lowest elevation tried is 20 cm above the distributor plate, it is thought that, perhaps, the process of coalescence has produced a number of large bubbles in this 20 cm rise (and correspondingly eliminated a large number of small bubbles).

(b) The second aspect of the particulate phase circulation patterns affecting the size distribution is clearly demonstrated by varying the bed depth and comparing the size distribution variation at a given point under identical conditions, except for the bed depth, Figures (5.26 - 5.29).

Since the elevation of the sampling point is the same in both sets of experiments, the marked difference in the frequency-size variation can only be attributed to the circulation patterns prevailing in the bed. Invariably, a greater proportion of larger bubbles are found with the lower bed depth.

4. A comparison of bubble size distributions, at the same point and under identical operating conditions, produced by the two gas distributors, reveals an interesting picture. Figure (5.35) shows the bubble size histograms at a point 20 cm above the two distributor plates. These are produced under identical operating conditions. The histogram corresponding to the multiorifice distributor shows a much greater proportion of small bubbles. Conversely, the porosint distributor histogram reveals a greater proportion of larger bubbles. Although the bubble size range encountered at this low height is relatively small, nevertheless the pattern is clear. This phenomenon is further discussed in chapter 8.

Fig. 5.35

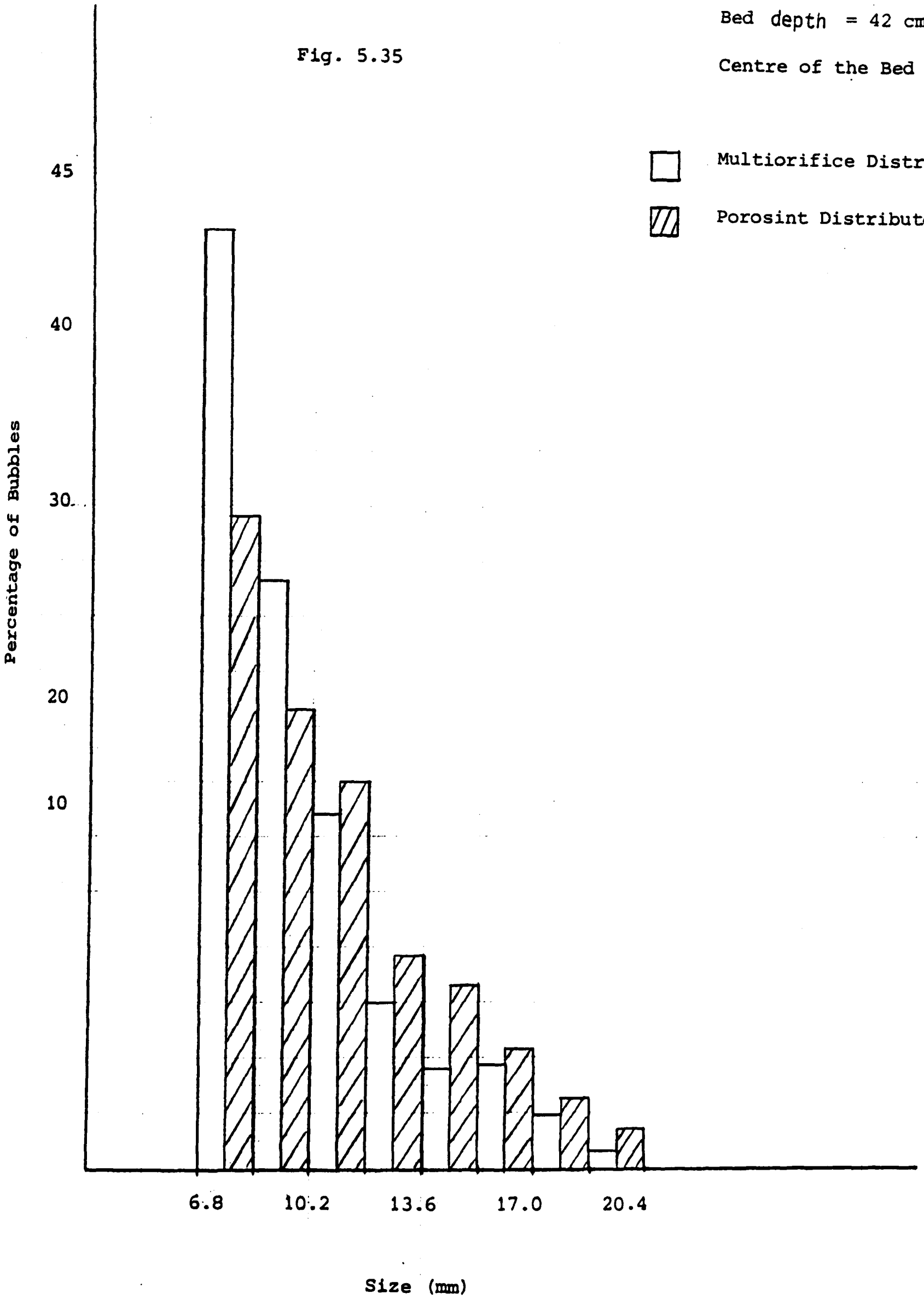
Z = 20 cm
U = 2.41 cm/sec
Bed depth = 42 cm
Centre of the Bed
Multiorifice Distributor
Porosint Distributor
45
40
30
20
10
Percentage of Bubbles
6.8
10.2
13.6
17.0
20.4
Size (mm)

Extending this comparison to greater elevations in the bed, shows that this pattern persists, but the difference between the two sets of data is less pronounced as the elevation is increased.

Figure (5.36) shows the frequency-size variation for a different point, at 60 cm above the two distributor plates. The shapes of the histograms are markedly different in the small size-ranges. The histogram corresponding to the multiorifice distributor has already peaked, the most frequent size being less than 6.8 mm. On the other hand, the data in the second case shows bubbles with the most frequent size in the 8.5 - 10 mm range.

Even at this elevation, a much greater number of small bubbles is encountered in the bed with the multiorifice distributor. For larger bubbles, the difference between the two sets of data diminishes and the histograms show almost identical frequency-size relationships. This similarity of the histograms for larger bubbles is striking but in view of the small numbers of bubbles involved, too much significance cannot be attached to the phenomenon.

Fig. 5.36

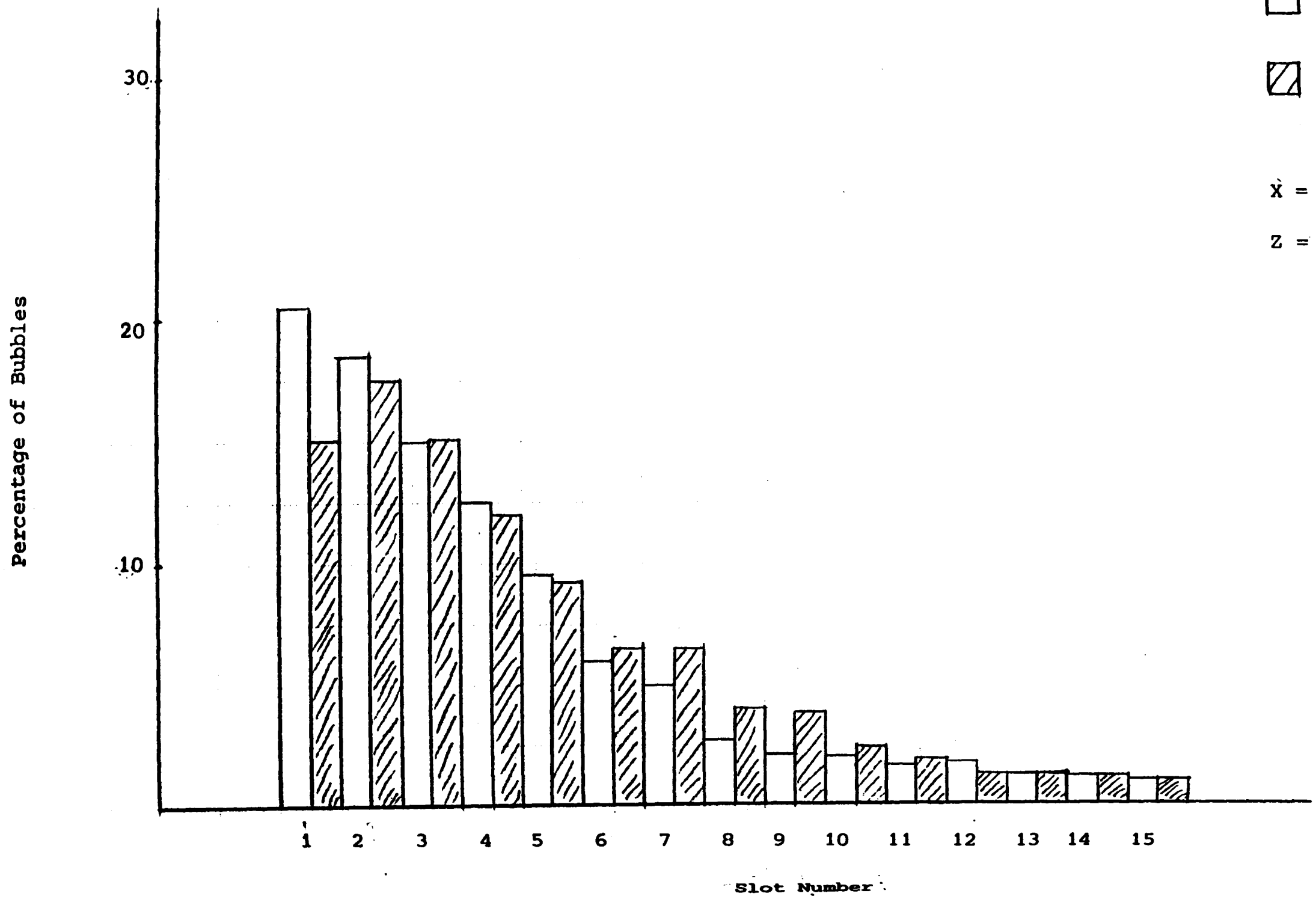

U = 2.41 cm/sec.

Bed Depth = 82 cm

Multiorifice Distrib.

Porosint Distributor

X = 36 cm, Y = 7 cm

Z = 60 cm

CHAPTER 6

Bubble Frequency and Its Spatial Distribution

6.1 Bubble Frequency and Distribution

The term "bubble frequency" has been used rather freely in the literature. Bubble properties such as number of bubbles passing a certain height per unit time, number of bubbles striking a probe per unit time and average number of bubbles present in a given volume are all sometimes referred to as bubble frequency. Although the above quantities are numerically different from each other, they are closely inter-related and show a similar variation with bed height and with gas flow rate (1). There are two 'bubble frequency' measurements used in this work, depending on the 'mode' of recording bubbles by the microprocessor system, as described in chapter (3).

In 'B' mode, only those bubbles are collected, which satisfy the constraints imposed by the software as well as the hardware. The frequency F, in 'C' mode, is a more accurate measure of the number of bubbles passing a point since there are no constraints on the detection and recording of bubbles. Only one probe is used to detect the passage of bubbles in 'C' mode.

In this chapter, both these frequencies are used as a frame of reference for comparison of the bubbling activity at various points across the bed cross-sectional area.

There are actually two constraints imposed on the bubble detection and storage in the microprocessor memory in 'B' mode. First is the constraint imposed by the software, namely $T1 < T2$, which ensures the rejection of any bubble smaller than a fixed size, ℓ, (the separation length).

Secondly, there is the constraint provided in the hardware, namely the jitter time. This is the time between the first arrival of a bubble at one of the coplanar probes and the subsequent complete immersion of all three of them. This constraint which is imposed on the trailing as well as the leading edges of the bubble is to ensure that only bubbles which are coaxial with the probe are counted. A comparison of the actual jitter with the maximum allowable jitter (entered via keyboard) is made, the result of which is that the microprocessor discards the invalid events, (jitter too great).

6.1.2 Effect of Chosen "Jitter" Time on Proportion of Bubbles Collected

Jitter time selection imposes a constraint on the fraction of bubbles collected. In other words, depending on the bubble rise velocity and the jitter time, the radius of the circle in which the axis of a bubble must lie in order to be picked up by the probe, varies. It is intended to find this radius for a typical bubble, rising with a velocity of U_b = 25 cm.sec^{-1}, Fig (6.1).

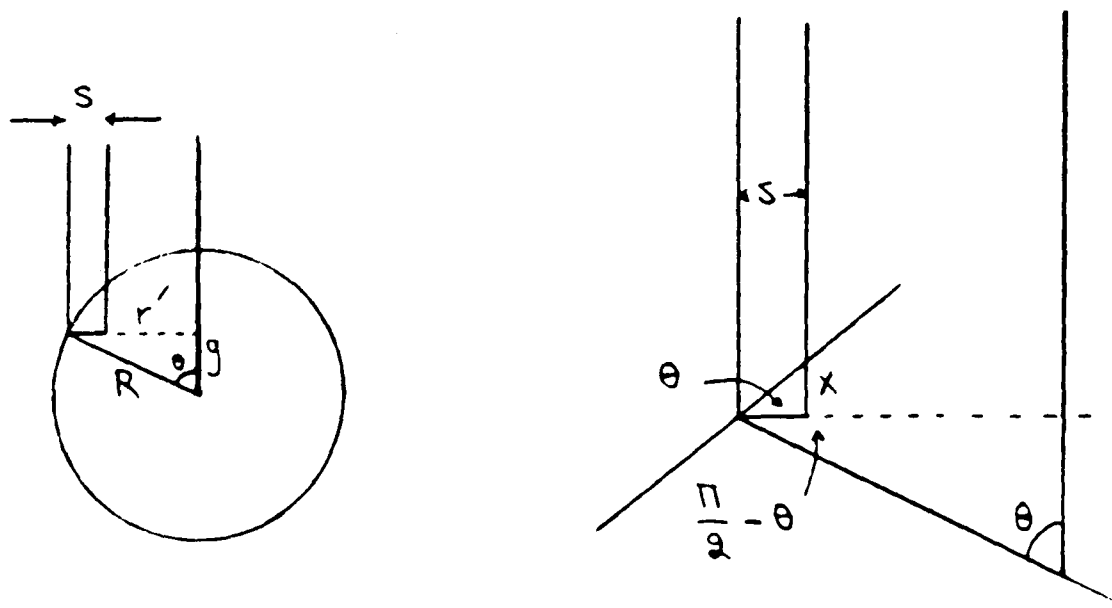

Fig. (6.1)

Jitter time j can be approximated by $j = \frac{x}{U_b}$. If r' is the radius of the circle in which the bubble must lie to be picked up by the probe.

$$r' = g.\tan\theta \qquad 6.1$$

we have also

$$x = s.\tan\theta \qquad 6.2$$

So $$j = \frac{s.\tan\theta}{U_b} \qquad 6.3$$

Now $$g = \sqrt{R^2 - r'^2} \qquad 6.4$$

Therefore $$\tan\theta = \frac{r'}{g} = \frac{r'}{\sqrt{R^2 - r'^2}} \qquad 6.5$$

So $$j = \frac{S.r'}{U_b\sqrt{R^2 - r'^2}} \qquad 6.6$$

or $$j^2 = \frac{S^2.\ r'^2}{U_b^2(R^2 - r'^2)}$$

Therefore $$r'^2\ (S^2 + U_b^2.j^2) = U_b^2.j^2.R^2$$

So $$\frac{r'}{R} = \frac{d'}{d_B} = \sqrt{\frac{j^2\ U_b^2}{S^2 + U_b^2\ j^2}}$$

The frontal view of the probe is as shown below, with the distance from the central probe to any of the coplanar ones equal to 6.5 mm.

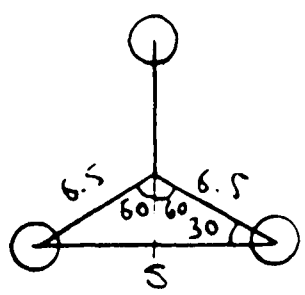

Fig. (6.2)

$S = 2 \times 6.5 \cos 30^{\circ} = 11.25$ mm

$U_b = 25$ cm.sec^{-1}

jitter j, set at 32×10^{-3} sec.

$$\text{So } \frac{d'}{d_B} = \sqrt{\frac{(32 \times 10^{-3} \times 25)^2}{(1.125)^2 + (32 \times 10^{-3} \times 25)^2}}$$

$$\text{and } \frac{d'}{d_B} = 0.58 \qquad 6.7$$

Expression 6.7 shows that any bubble whose centre-line is located within a circle, centred on the probe, of radius equal to half the bubble radius will be detected and collected.

Measurements of bubble frequency were carried out at nine symmetrically distributed points on the 12 x 7 cm grid, mentioned in Chapter 4.

A complete picture of bubble frequency variation with height above the distributor plate and gas flow rate, for the two different gas distributors used, is given in Tables (6.5) - (6.10).

6.2 Porosint Plate Distributor

Table (6.5) shows the point values of bubble frequency, F, (in 'B' mode), at the nine points mentioned earlier, when the porosint plate distributor is employed. It shows the effect of increasing superficial fluidising velocity on the bubble frequency at these nine points. At low depths in the bed($Z \leqslant 20$ cm) and low gas velocity the maximum bubble vertical size has not reached 6.8 mm so as to be detectable by the probe. An increase in height by 10 cm changes the picture very slightly. Bubble frequency is still undetectably low over much of the bed cross-sectional area until a height of 40 cm and a gas velocity of 3.01 $cm.sec^{-1}$ is reached. Here, except at the centre of the bed, some kind of uniformity of bubble frequency prevails. Even under these conditions, regions closer to the front wall seem to be more active than regions nearer the back wall of the bed.

Increasing gas flow rate increases the bubble frequency at certain positions. Here, again, the front wall seems to attract more bubbles. Uniformity seems to increase with increasing gas flow rate.

Bubble frequency seems to increase at every point sampled with an increase in elevation until $\sim Z = 50$ cm, whence it decreases with increasing height for high gas flow rates.

Z = 40 cm	0.15 <0.1 <0.1 <0.1 <0.1 0.29 <0.1 0.17 4.00	0.68 0.82 <0.1 0.71 1.69 3.02 4.23 3.68 6.10	3.50 3.85 3.02 3.20 0.73 3.02 5.17 2.39 6.49
	U = 1.87	U = 2.41	U = 3.01
Z = 30 cm	<0.1 <0.1 <0.1 <0.1 <0.1 <0.1 <0.1 <0.1 0.38	0.37 0.45 <0.1 <0.1 0.24 1.07 1.43 2.53 2.73	1.77 1.75 1.27 <0.1 0.80 4.74 1.17 1.59 2.94
	U = 1.87	U = 2.41	U = 3.01
Z = 20 cm	<0.1 <0.1 <0.1 <0.1 <0.1 <0.1 <0.1 <0.1 <0.1	0.10 <0.1 <0.1 <0.1 0.16 0.12 0.67 0.54 1.18	0.45 0.27 0.57 0.53 0.73 1.10 0.93 1.40 1.11
	U = 1.87	U = 2.41	U = 3.01

TABLE 6.5

Bubble Frequencies ('B' mode) = min^{-1}

Bed depth = 42 cm

Porosint Distributor

Z = 70 cm

<0.1	<0.1	<0.1
1.68	<0.1	8.9
1.55	11.44	26.25

U = 1.87

1.16	0.66	<0.1
4.97	0.2	2.22
29.38	3.12	28.45

U = 2.41

4.76	0.40	<0.1
19.58	0.1	2.52
36.88	1.87	38.60

U = 3.01

Z = 60 cm

<0.1	<0.1	<0.1
<0.1	<0.1	4.69
3.38	6.15	15.75

U = 1.87

<0.1	<0.1	1.12
0.52	<0.1	1.00
12.21	7.81	15.75

U = 2.41

4.1	<0.1	<0.1
2.21	<0.1	1.26
17.24	4.32	25.24

U = 3.01

Z = 50 cm

<0.1	<0.1	<0.1
<0.1	<0.1	1.62
3.15	11.61	21.83

U = 1.8

<0.1	<0.1	<0.1
<0.1	<0.1	<0.1
5.80	3.76	14.88

U = 2.41

<0.1	<0.1	<0.1
<0.1	<0.1	<0.1
7.71	2.91	16.00

U = 3.01

TABLE 6.5 continued

(Bed depth = 52 cm and 82 cm)

At low gas flow rates bubble frequency actually increases with increasing height, or remains constant.

At elevations of Z = 60 - 70 cm above the distributor, there seem to be two regions of very high bubbling activity close to the "front" wall and at either side of the transverse (shorter) centreline.

Table (6.5A) below, shows the variation of the "total number of bubbles" (per minute) passing the nine sampling points at each of the six elevations investigated. It shows a steady increase in the 'total' frequency with height above the distributor plate.

Z (cm)	20	30	40	50	60	70 cm
F_t (U = 1.87)	0	0.38	4.61	38.21	29.97	49.82
F_t (U = 2.91)	2.77	8.82	20.93	24.44	38.41	70.16
F_t (U = 3.01)	7.09	16.03	31.37	26.62	54.37	104.71

This table does not reveal a true picture of bubble frequency variation with elevation in the bed. The "total frequency", F_t, in Table (6.5A) is a fraction of the total number of bubbles passing through any cross-section of the bed, (at any height), due to the fact that a very large number of small bubbles cannot be detected and therefore are not recorded. Secondly, the number of sampling points, (nine), is not sufficient to allow an accurate count of even the large bubbles to be made at these six elevations.

Figure (6.11) shows the variation of the bubble frequency, F, with height above the distributor plate, at three gas velocities of 1.87, 2.41 and 3.01 $cm.sec^{-1}$, for a point on the transverse centreline. Figures (6.10) and (6.12) represent this relationship at two points to either side of this point.

The two Figures (6.10) and (6.12) reveal a markedly different 'F' - 'Z' relationship from that on the centreline.

For the point on the centreline, Fig. (6.11), the F - Z graphs show that frequency increases with elevation until about 60 cm and then decreases. But for the two points at either side of this point, the bubble frequency seems to increase with elevation and the higher the superficial velocity, the steeper the rise. An exception to this, is the curve for U = 1.87 $cm.sec^{-1}$ on Figure (6.12) where a maximum is reached at $\sim$60 cm, although the frequencies in this case are probably non-significant, and the magnitude of 'F' for this maximum is much smaller than the corresponding values for the central point.

Figures 6.13 and 6.14 show the frequency-elevation variation along the central x-axis, the points in Fig. 6.14 being on the vertical centreline. The graph corresponding to the low superficial fluidising velocity of 1.87 $cm.sec^{-1}$, (in Figure 6.14), shows uncharacteristically low frequencies. This could be due to the fact that bubbles are too small to be detected. Coalescence of small bubbles, forming large ones higher up in the bed, accounts for the steep rise of the frequency curve in Fig. (6.13).

Graphs corresponding to the higher gas velocities of 2.41 and 3.01 $cm.sec^{-1}$ in Fig. 6.13 show a minimum at 50 cm elevation.

Figure 6.14, (which corresponds to the bed vertical centreline), shows a maximum at 40 cm elevation for the gas velocity of 2.41 $cm.sec^{-1}$. It has to be borne in mind that when the bed depth is increased from 42 cm to 82 cm above the distributor plate, the particle phase circulation patterns which exist at the lower depth, break up and new ones (on a larger scale) appear.

Caution must be exercised in comparing the results of experiments with different bed depths.

In conclusion, the porosint distributor seems to generate small bubbles, undetectable by the probe, hence showing very low frequencies, at low elevations above the distributor. Near the walls of the bed, the upward movement of the emulsion phase seems to enhance the bubble frequency by moving the bubbles towards the sampling points at the bottom of the bed (Z = 20 cm, 30 cm), Figures (6.10 - 6.12).

In the centre of the bed, these emulsion movements seem to have an upward direction at the top of the bed. This would explain the very high frequencies encountered at an elevation of 40 cm above the distributor plate, on the bed vertical centreline, when the bed depth is 42 cm, (Fig. 6.14).

Fig. 6.10

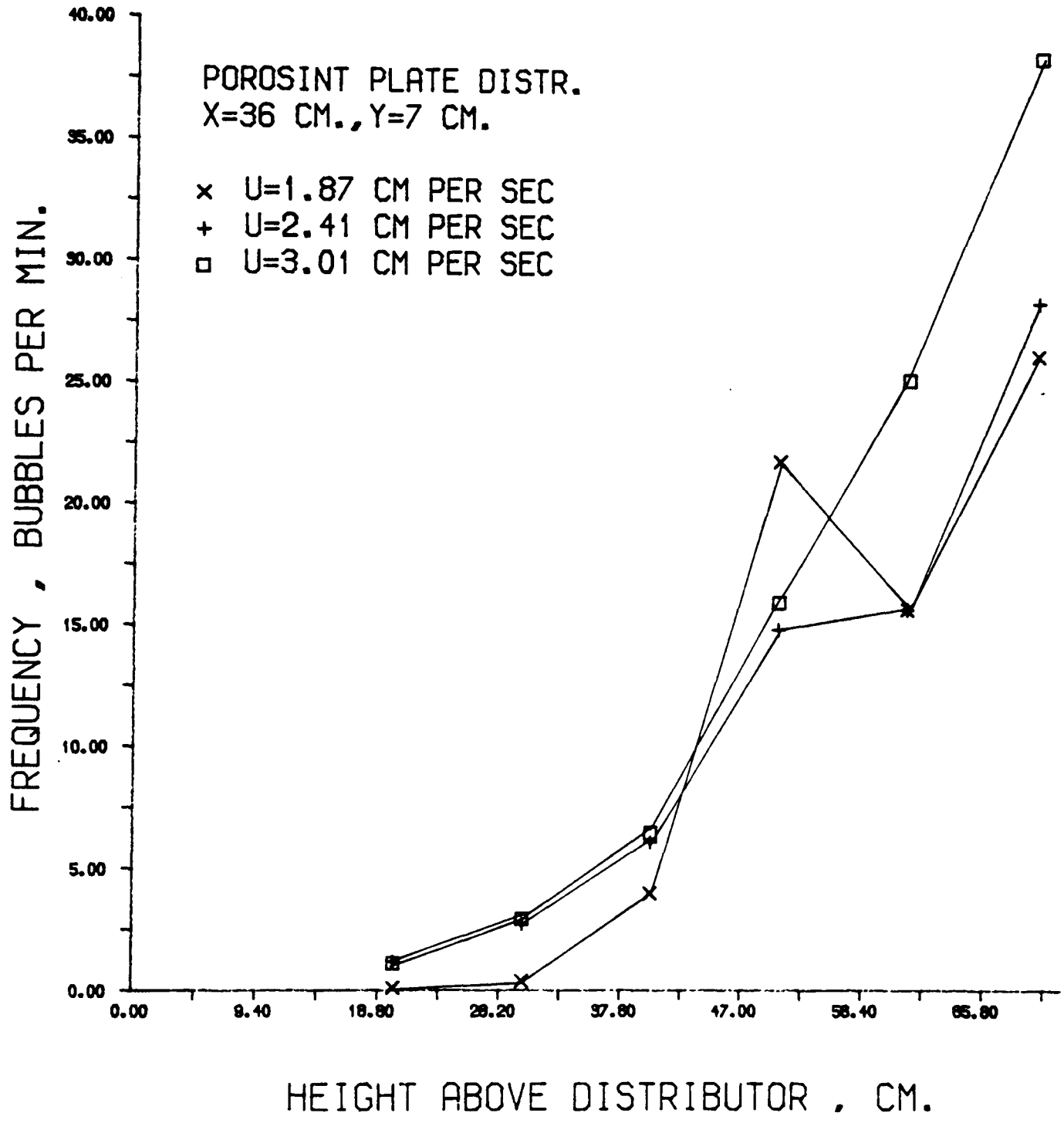
POROSINT PLATE DISTR.
X=36 CM., Y=7 CM.
× U=1.87 CM PER SEC
+ U=2.41 CM PER SEC
□ U=3.01 CM PER SEC
FREQUENCY , BUBBLES PER MIN.
40.00
35.00
30.00
25.00
20.00
15.00
10.00
5.00
0.00
0.00
9.40
18.80
28.20
37.60
47.00
56.40
65.80
HEIGHT ABOVE DISTRIBUTOR , CM.

Fig. 6.11

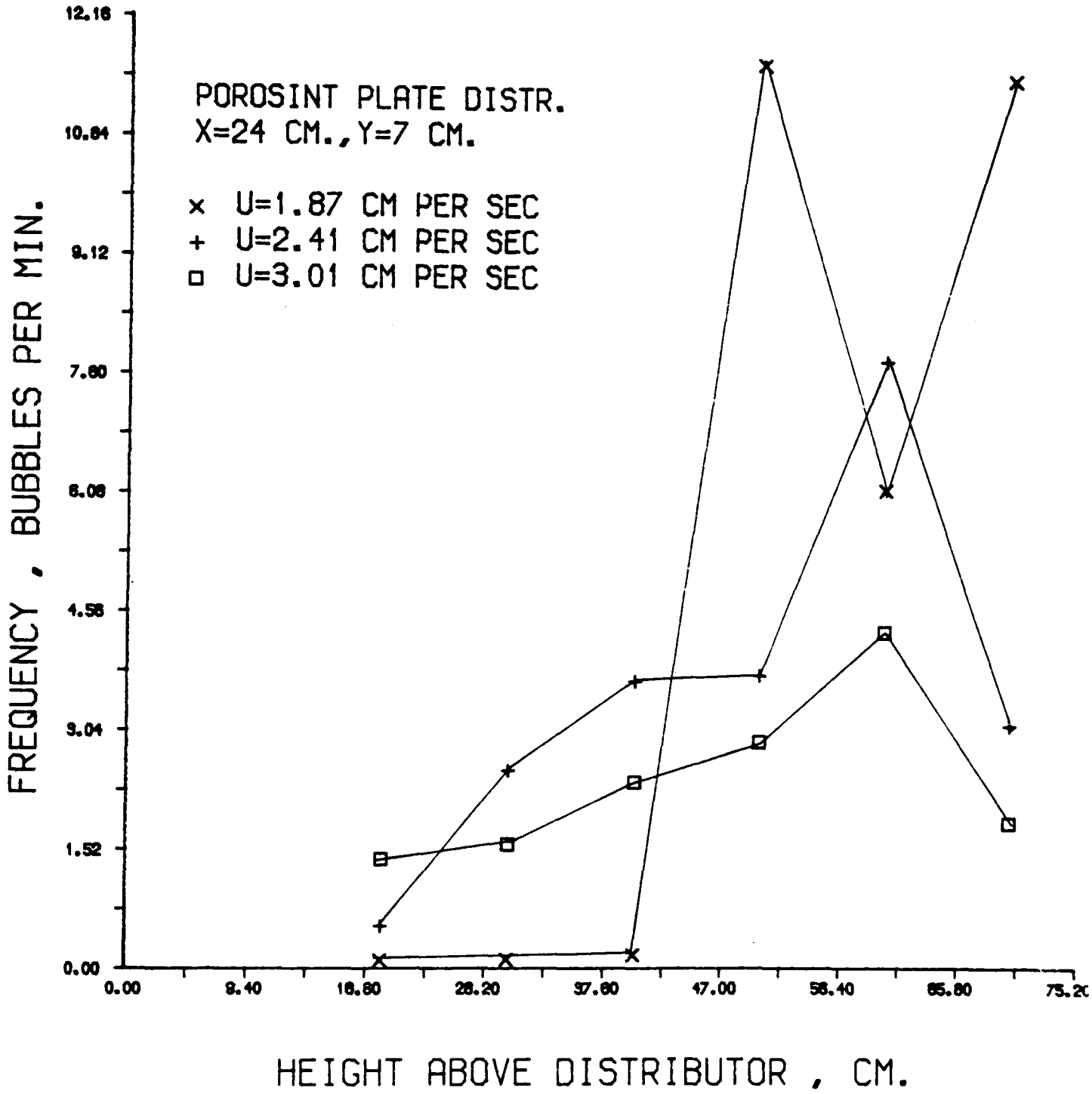
POROSINT PLATE DISTR.
X=24 CM., Y=7 CM.
× U=1.87 CM PER SEC
+ U=2.41 CM PER SEC
□ U=3.01 CM PER SEC
FREQUENCY , BUBBLES PER MIN.
12.16
10.64
9.12
7.60
6.08
4.56
3.04
1.52
0.00
0.00
9.40
18.80
28.20
37.60
47.00
56.40
65.80
75.20
HEIGHT ABOVE DISTRIBUTOR , CM.

Fig. 6.12

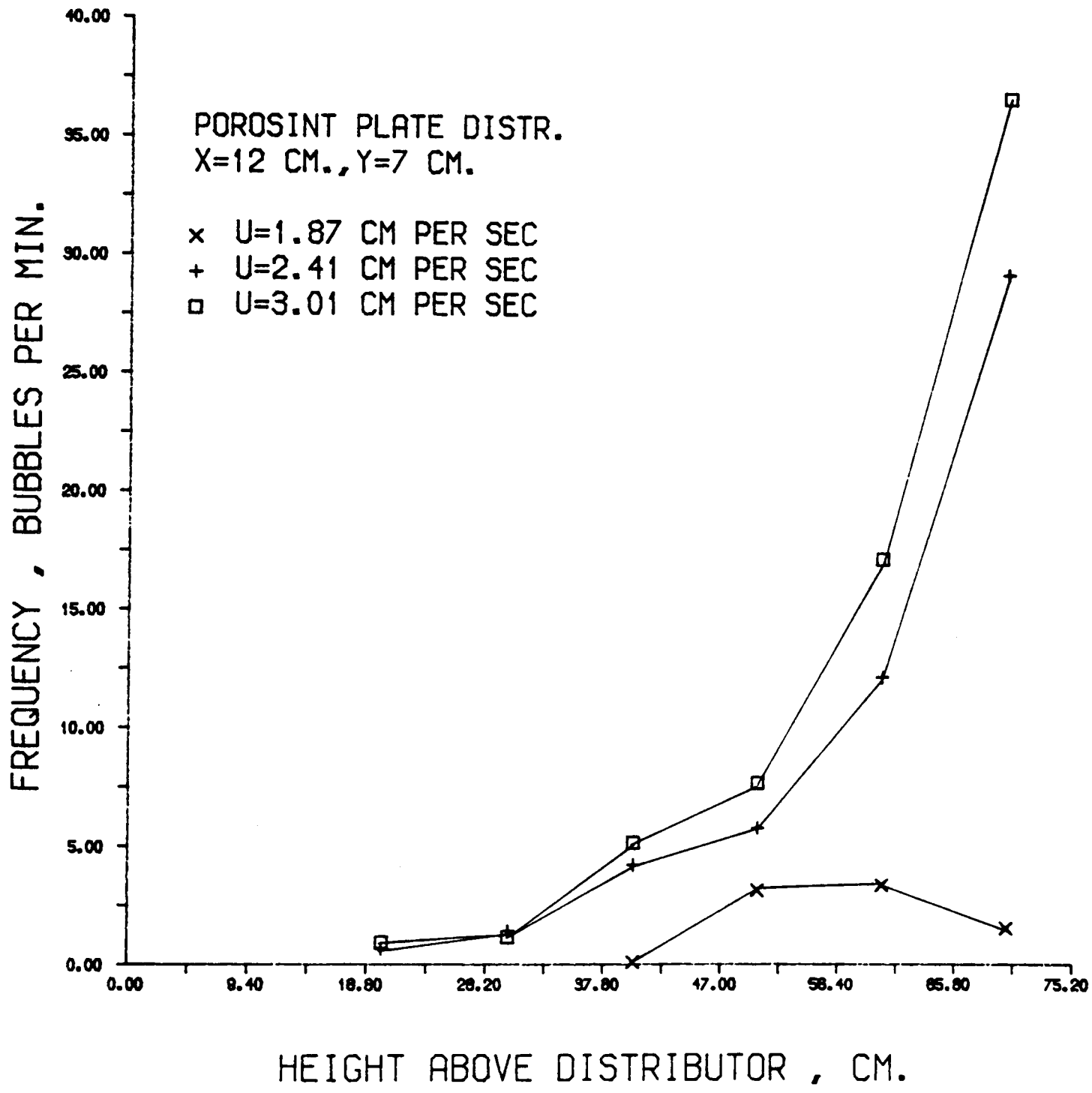
POROSINT PLATE DISTR.
X=12 CM., Y=7 CM.
× U=1.87 CM PER SEC
+ U=2.41 CM PER SEC
□ U=3.01 CM PER SEC
FREQUENCY , BUBBLES PER MIN.
40.00
35.00
30.00
25.00
20.00
15.00
10.00
5.00
0.00
0.00
9.40
18.80
28.20
37.60
47.00
56.40
65.80
75.20
HEIGHT ABOVE DISTRIBUTOR , CM.

Fig. 6.13

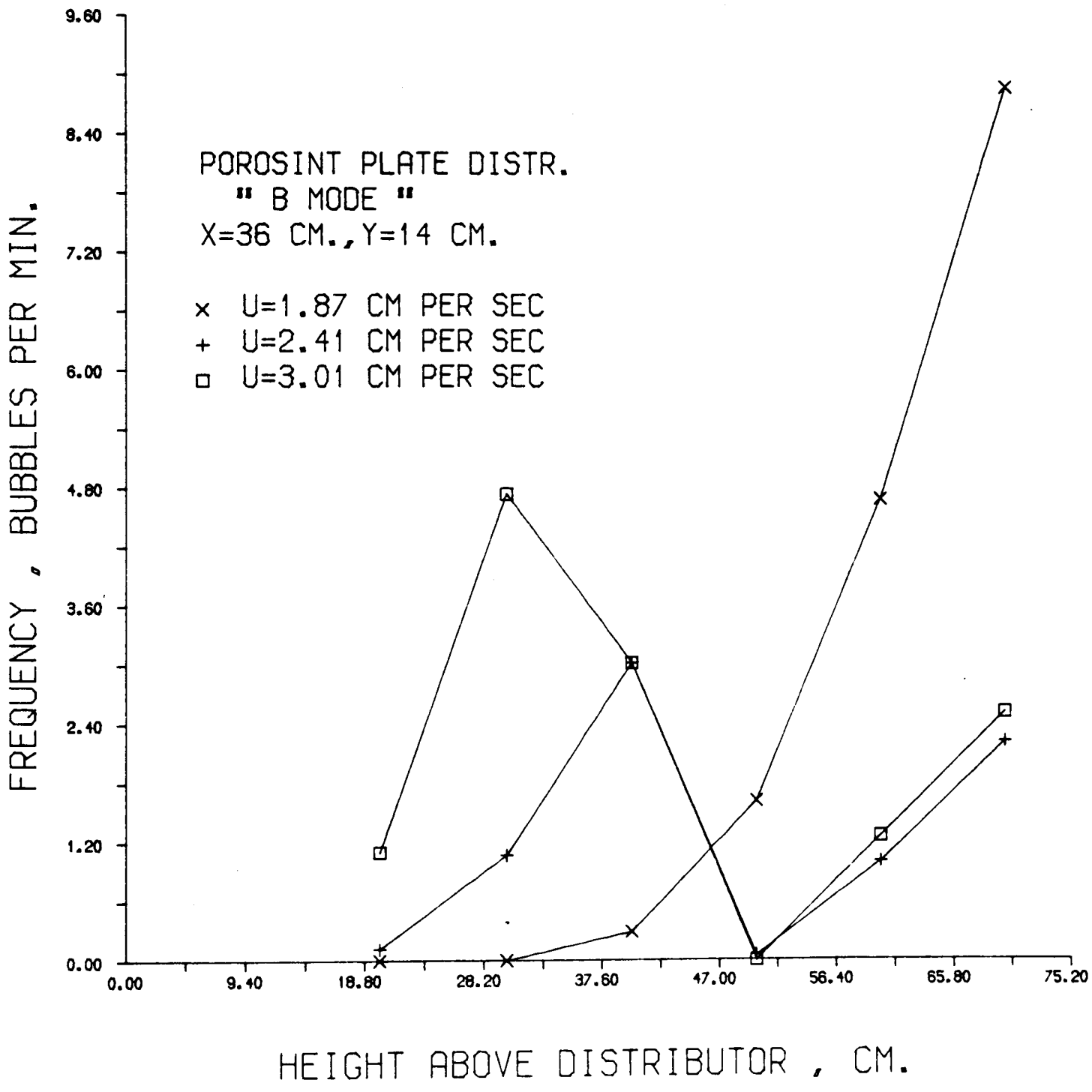
POROSINT PLATE DISTR.
" B MODE "
X=36 CM., Y=14 CM.
× U=1.87 CM PER SEC
+ U=2.41 CM PER SEC
□ U=3.01 CM PER SEC
FREQUENCY , BUBBLES PER MIN.
9.60
8.40
7.20
6.00
4.80
3.60
2.40
1.20
0.00
0.00
9.40
18.80
28.20
37.60
47.00
56.40
65.80
75.20
HEIGHT ABOVE DISTRIBUTOR , CM.

Fig. 6.14

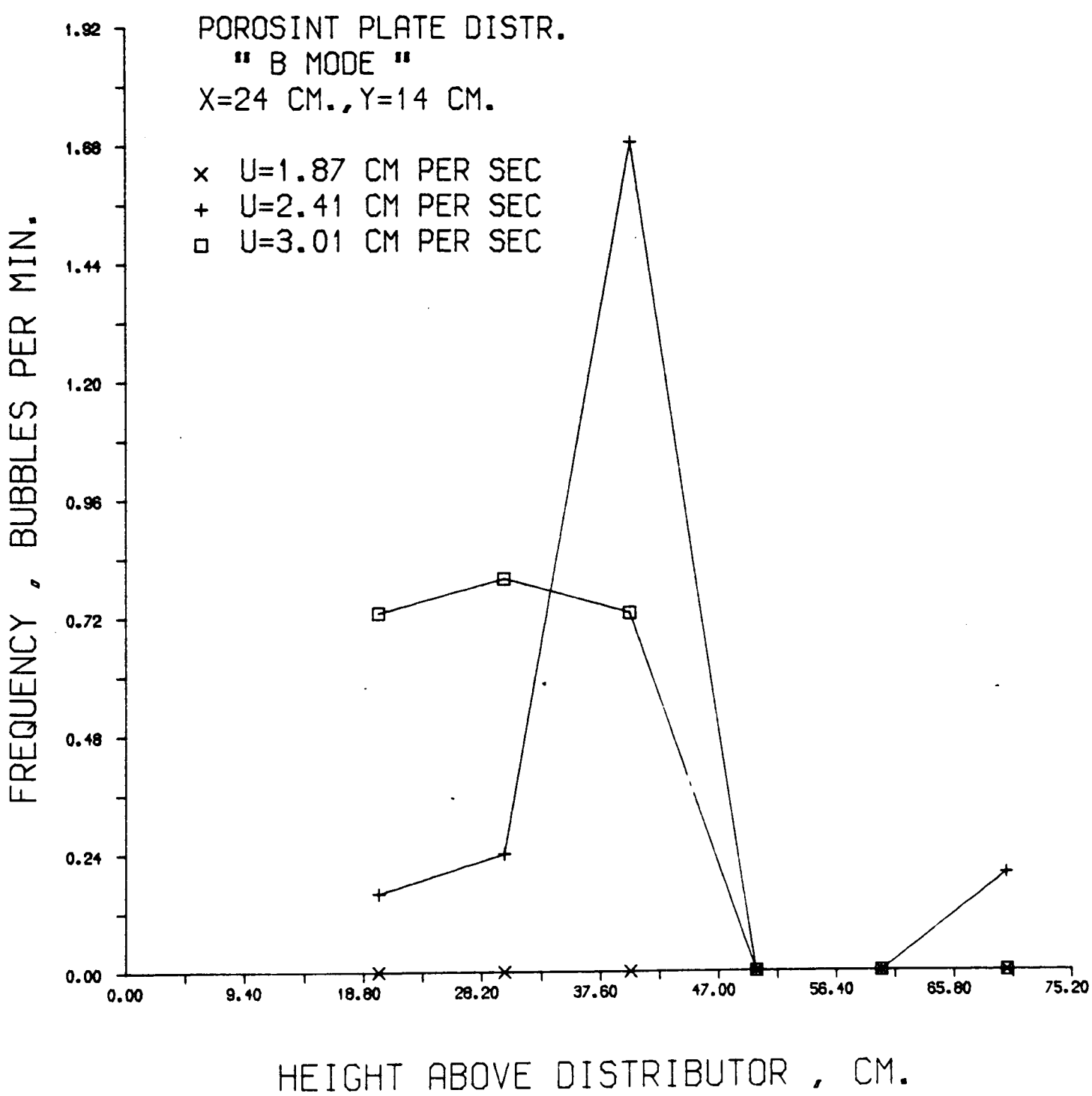
POROSINT PLATE DISTR.
" B MODE "
X=24 CM., Y=14 CM.
× U=1.87 CM PER SEC
+ U=2.41 CM PER SEC
□ U=3.01 CM PER SEC
FREQUENCY , BUBBLES PER MIN.
1.92
1.68
1.44
1.20
0.96
0.72
0.48
0.24
0.00
0.00
9.40
18.80
28.20
37.60
47.00
56.40
65.80
75.20
HEIGHT ABOVE DISTRIBUTOR , CM.

6.3 Multiorifice Distributor

Bubbles Frequencies were measured in 'B' mode, when the multi-orifice distributor was employed, in two separate sets of experiments. One was a duplication of the experiments carried out with the porosint distributor, in that the bed was gradually filled up and the probe tip was always kept a few centimetres below the bed surface.

The second set of experiments was done when the bed was initially filled to maximum depth and all the frequency measurements were made with a uniform bed depth of 82 cm.

Tables 6.6 and 6.7 show the frequency distributions across the bed cross-sectional area, at various elevations and gas velocities.

Z = 40 cm	<0.1	0.76	11.29
	0.55	<0.1	6.36
	47.26	16.28	15.55

U = 1.87

	0.47	9.38	12.68
	0.96	0.70	2.47
	28.93	19.65	25.10

U = 2.41

	7.89	15.59	19.74
	2.56	1.38	9.35
	30.32	25.79	32.20

U = 3.01

Z = 30 cm	<0.1	0.97	7.67
	<0.1	7.74	14.74
	26.18	20.80	8.49

U = 1.87

	<0.1	14.22	14.70
	4.28	10.97	3.62
	23.79	20.35	9.86

U = 2.41

	2.48	27.42	23.29
	5.84	8.63	1.89
	27.50	25.03	7.43

U = 3.01

Z = 20 cm	<0.1	0.69	8.46
	<0.1	3.00	12.05
	7.17	14.60	1.67

U = 1.87

	<0.1	12.40	15.46
	1.73	7.72	5.00
	6.93	16.67	4.10

U = 2.41

	4.69	18.14	24.23
	5.26	6.99	3.52
	9.31	11.50	2.44

U = 3.01

TABLE 6.6

Multiorifice Distributor

Bubble Frequencies in 'B' Mode = min^{-1}

Bed depth = 42 cm

Z = 70 cm

<0.1	0.38	0.75
<0.1	5.15	23.00
3.76	1.33	6.50

U = 1.87

<0.1	0.33	0.60
0.70	5.79	40.74
3.43	1.15	6.61

U = 2.41

0.17	0.47	0.92
2.46	3.87	46.47
4.14	1.80	7.59

U = 3.01

Z = 60 cm

<0.1	0.60	1.57
<0.1	2.25	19.59
1.89	2.65	6.81

U = 1.87

<0.1	0.93	0.95
0.10	4.28	34.5
1.55	0.97	9.19

U = 2.41

<0.1	0.57	1.12
0.77	2.96	39.16
2.37	1.32	10.38

U = 3.01

Z = 50 cm

<0.1	1.93	5.61
1.52	8.28	1.65
34.10	9.09	13.41

U = 1.87

1.40	10.12	11.71
1.85	8.54	3.77
23.58	17.28	31.44

U = 2.41

5.74	9.66	12.70
6.71	10.59	8.46
28.29	13.56	27.98

U = 3.01

TABLE 6.6 continued

(Bed depth = 52 cm and 82 cm)

Z = 40 cm	<0.1	<0.1	0.82
	<0.1	3.07	7.32
	<0.1	6.30	10.37

U = 1.87

	<0.1	<0.1	5.56
	<0.1	3.88	14.51
	4.85	13.00	8.86

U = 2.41

	<0.1	<0.1	2.97
	<0.1	2.52	17.85
	5.65	10.88	11.80

U = 3.01

Z = 30 cm	<0.1	<0.1	1.70
	<0.1	0.27	6.09
	<0.1	1.40	3.08

U = 1.87

	<0.1	<0.1	4.79
	<0.1	2.39	9.08
	0.80	2.10	11.78

U = 2.41

	<0.1	<0.1	7.54
	0.33	3.35	10.83
	4.60	2.57	14.09

U = 3.01

Z = 20 cm	<0.1	<0.1	<0.1
	<0.1	<0.1	5.67
	<0.1	<0.1	5.95

U = 1.87

	<0.1	<0.1	3.30
	<0.1	<0.1	7.52
	0.40	0.97	4.41

U = 2.41

	<0.1	<0.1	<0.1
	<0.1	<0.1	5.78
	1.29	3.20	3.27

U = 3.01

TABLE 6.7

Bubble Frequencies in 'B' Mode = min^{-1}

Multiorifice Distributor

Bed depth = 82 cm

Z = 70 cm

<0.1	0.38	0.75
<0.1	5.15	23.00
3.76	1.33	6.50

U = 1.87

<0.1	0.33	0.60
0.70	5.79	40.74
3.43	1.15	6.61

U = 2.41

0.17	0.47	0.92
2.46	3.87	46.47
4.14	1.80	7.59

U = 3.01

Z = 60 cm

<0.1	0.60	1.57
<0.1	2.25	19.59
1.89	2.65	6.81

U = 1.87

<0.1	0.93	0.95
0.10	4.28	34.5
1.55	0.97	9.19

U = 2.41

<0.1	0.57	1.12
0.77	2.96	39.16
2.37	1.32	10.38

U = 3.01

Z = 50 cm

< 0.1	<0.1	0.95
< 0.1	0.95	8.62
<0.1	4.23	8.46

U = 1.87

<0.1	<0.1	0.75
<0.1	4.66	24.83
6.47	2.19	8.59

U = 2.41

<0.1	<0.1	1.63
0.13	2.72	36.20
11.08	1.21	10.22

U = 3.01

TABLE 6.7 continued

Yue and Kolaczkowski (127) proposed a method for the design of a multiorifice distributor for a gas fluidised bed. They suggested that the number of active orifices could be obtained from the following equation:

$$\frac{N_1}{N} = \frac{\left(\frac{U}{U_{mf}} - 1\right)}{\left[1 + (2a_o^2\, N^2/\rho_f\, U_{mf}^2\, A^2)\,\rho_s\, g h_s (1 - \frac{2}{\pi})(1 - e_{mf})\right]^{\frac{1}{2}} - 1}$$

where:

U = total superficial gas velocity

U_{mf} = superficial gas velocity at minimum fluidisation

a_o = area of orifice

A = total area of fluidised bed

h_s = height of spout or jet

ρ_f = density of fluidising fluid

e_{mf} = bed voidage at minimum fluidisation

N_1 = number of active orifices

N = total number of orifices.

Using this equation, the ratio $\frac{N_1}{N}$ gives a value of 0.132 which suggests that only 9 of the 66 orifices are active, when the superficial fluidising velocity is 1.87 $cm.sec^{-1}$.

The multiorifice distributor produced much uniform bubble frequency distributions in the bed. Even at very low depths, the number of bubbles with vertical size exceeding the set value of 6.8 cm, is greater than that generated by the porosint plate distributor.

Although in (5.5) it was stated that the porosint plate distributor produced a higher proportion of larger bubbles, this referred to a higher proportion of a much lower number of bubbles sampled. The multiorifice distributor consistently produces a much greater number of bubbles in the size-range detectable by the probe.

Bubble frequency is higher closer to the "front" wall of the bed. It increases with elevation until 40 - 50 cm above the distributor plate whence it decreases. There are very few zones of inactivity even at the lowest elevations investigated.

At low elevations an increase in gas velocity results in an increase in the bubble frequency. At higher elevations of 60 - 70 cm the reverse obtains and the bubble frequency decreases or remains constant with increasing gas velocity.

This phenomenon presumably shows the dependence of frequency F, on the location of the sampling point vis-a-vis the particle circulation patterns. If the sampling point were on the downward flow of the emulsion phase movement, increasing the gas flow rate would result in a decrease in the frequency measured, since the downward circulation would be enhanced. On the other hand, sampling points located on the upward movement of the emulsion phase would show an increase in the measured frequency with an increase in gas flow rate. In short, increasing the gas flow rate only makes the prevailing circulation pattern more pronounced, rather than change it.

Another feature of this distributor is the fact that the bubble frequency is less uniformly distributed at very low and very high elevations in the bed. At heights of 60 - 70 cm above the gas distributor, bubbling activity is concentrated more or less at one particular zone, which persists at low, as well as high gas velocities. This could be due to the coalescence of small bubbles as they rise in the bed, forming larger bubbles, at some particular zones. The surrounding areas of bed will be depleted of bubbles.

Figures (6.15) - (6.23) show the frequency-elevation variation for the nine points across the bed cross-section and at three superficial fluidising velocities. Figures (6.15, 6.16 and 6.17) show the 'F' - 'Z' relationship at a plane (Y = 7 cm) near the front wall. This distance is increased to 14 cm in Figures (6.18, 6.19 and 6.20) and to 21 cm in Figures (6.21, 6.22 and 6.23).

All three graphs in Figures (6.15 - 6.17) reveal a similar pattern. Frequency increases with height, reaches a maximum at 30 - 50 cm elevation range and then decreases. Increasing the X-coordinate from 12 cm to 36 cm seems to have the effect of shifting this maximum frequency towards slightly higher elevations. As mentioned in chapter (4), at low elevations, the particle circulation patterns are moving upwards near the walls. When the bed depth is greater than 40 cm the upward movement of these circulation patterns shifts towards more central zones at $\sim$40 cm above the distributor plate. As the direction of the emulsion phase movement is reversed, the bubble frequency begins to drop, and decreases as

the elevation is increased. This seems to indicate that the upward movement of the emulsion phase enhances the bubble frequency.

As mentioned before, increasing bed depth gradually will not permit a true picture to be obtained of what goes on in the bed. Nevertheless, these graphs can be used for comparison of frequency-elevation variation across the bed at these nine points, as well as for the comparison of the two different methods of filling the bed.

Figures (6.18, 6.19 and 6.20) show the F - Z variation across the longer centreline, the point in Figure (6.19) being on the bed vertical centreline. Almost all these graphs show a minimum at 40 cm elevation, and peaks at 30 and 50 cm, respectively, above the distributor plate.

One exception is the Figure (6.20) where the frequency increases steadily with elevation after the 40 cm mark and shows very high frequencies at $\sim$ 70 cm elevation. These experimental points, (in Figure 6.20), are on the vertical axis with x = 36 and y = 14 coordinates. They presumably lie on the upward moving circulation flow patterns.

The pattern in Figure 6.19 suggests that on the vertical centreline, at 40 cm elevation, the bubbles are swept away, sideways by these circulation patterns.

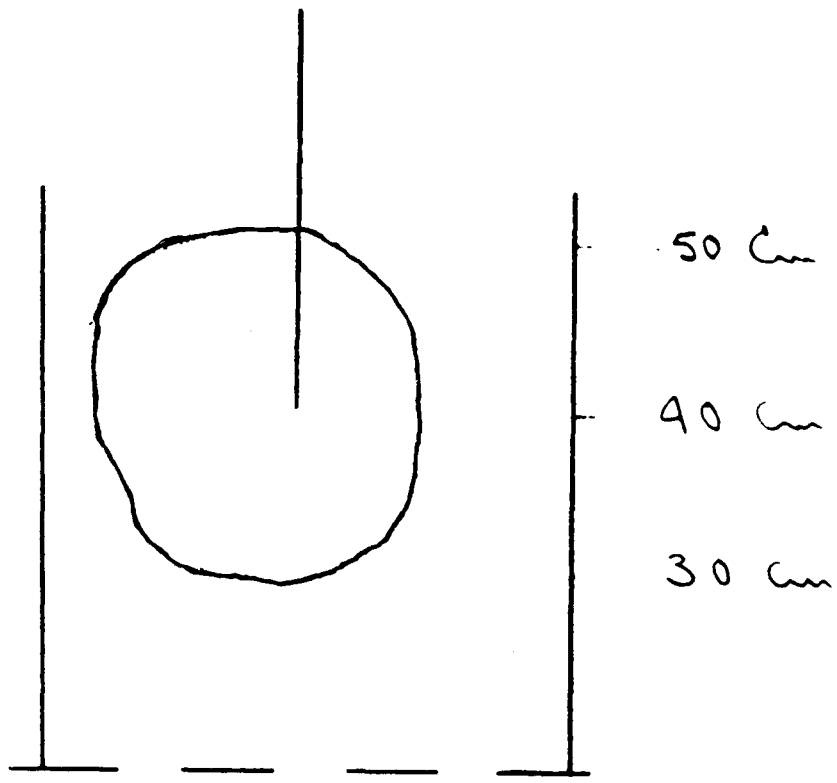

Finally the 'F' - 'Z' variation along the X-coordinate near the "back" wall of the bed, is studied in Figures (6.21), (6.22) and (6.23). They all reveal a similar trend, but the figures corresponding to the points nearest the air inlet, Figures (6.21) and (6.22) do not show any appreciable change in the frequencies at U = 1.87 cm.sec^{-1}. In fact the frequencies are all too small to be compared with data at another point. This indicates that at greater heights above the distributor, the points near the "back" wall of the bed coincide with the downward movement of the circulation patterns. These patterns move upwards until elevations around 40 cm above the distributor plate are reached. Then they change direction, which would explain why all the graphs show frequency decreasing with increasing elevation after the 40 cm mark. Unfortunately, the bed has not been filled up gradually enough to find out, accurately, where this radical change in circulation patterns occurs.

Burgess and Calderbank (6) suggest that this change of direction occurs at about one vessel diameter (in a cylindrical bed), above the gas distributor. In a bed of rectangular cross-section (such as used in this work) one would expect to find this distance to

be the "equivalent" of one vessel diameter. The "equivalent diameter" defined as four times the hydraulic radius, ($= 4 \times r_H = 4 \times \frac{\text{cross sectional area}}{\text{wetted perimeter}} = 37.5$ cm), seems to be a good approximation, in these experiments.

When the bed is filled to a depth of 42 cm, it was found that the change of direction (of flow) occurred, invariably at $\sim$40 cm above the distributor plate.

Fig. 6.15

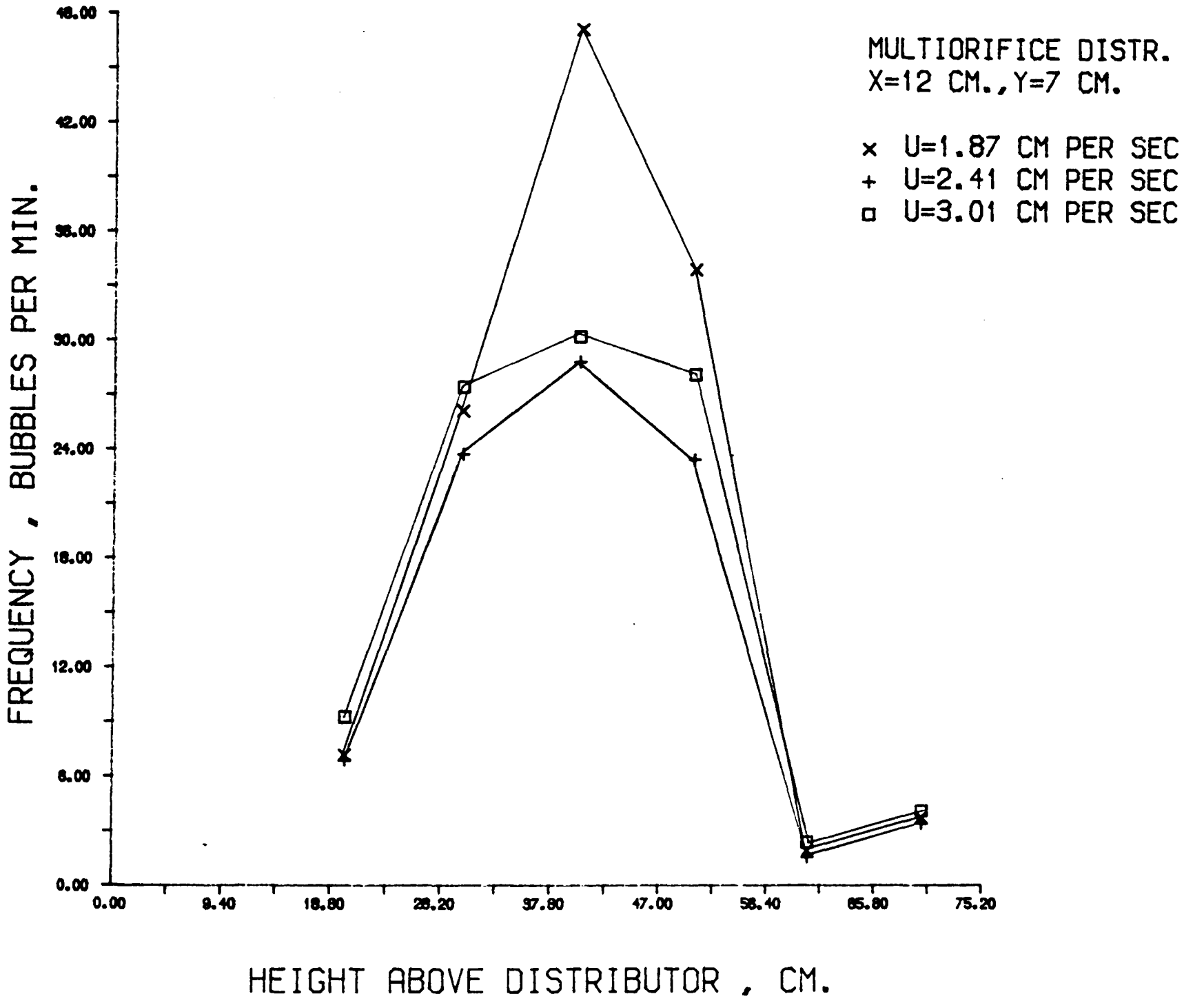
MULTIORIFICE DISTR.
X=12 CM., Y=7 CM.
× U=1.87 CM PER SEC
+ U=2.41 CM PER SEC
□ U=3.01 CM PER SEC
FREQUENCY , BUBBLES PER MIN.
48.00
42.00
36.00
30.00
24.00
18.00
12.00
6.00
0.00
0.00
9.40
18.80
28.20
37.80
47.00
56.40
65.80
75.20
HEIGHT ABOVE DISTRIBUTOR , CM.

Fig. 6.16

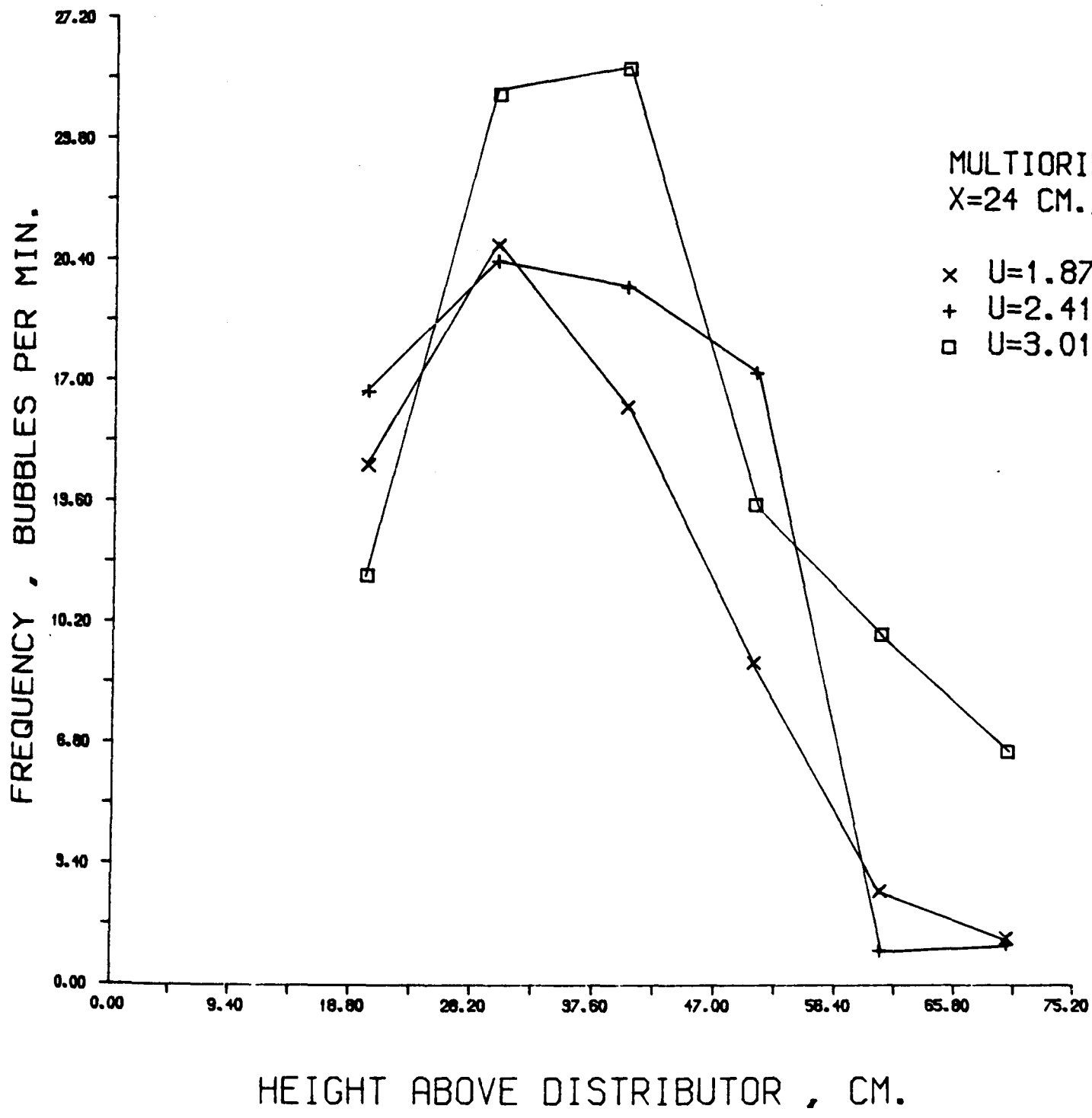
MULTIORIFICE DISTR.
X=24 CM.,Y=7 CM.
× U=1.87 CM PER SEC
+ U=2.41 CM PER SEC
□ U=3.01 CM PER SEC
FREQUENCY , BUBBLES PER MIN.
27.20
23.80
20.40
17.00
13.60
10.20
6.80
3.40
0.00
0.00
9.40
18.80
28.20
37.60
47.00
56.40
65.80
75.20
HEIGHT ABOVE DISTRIBUTOR , CM.

Fig. 6.17

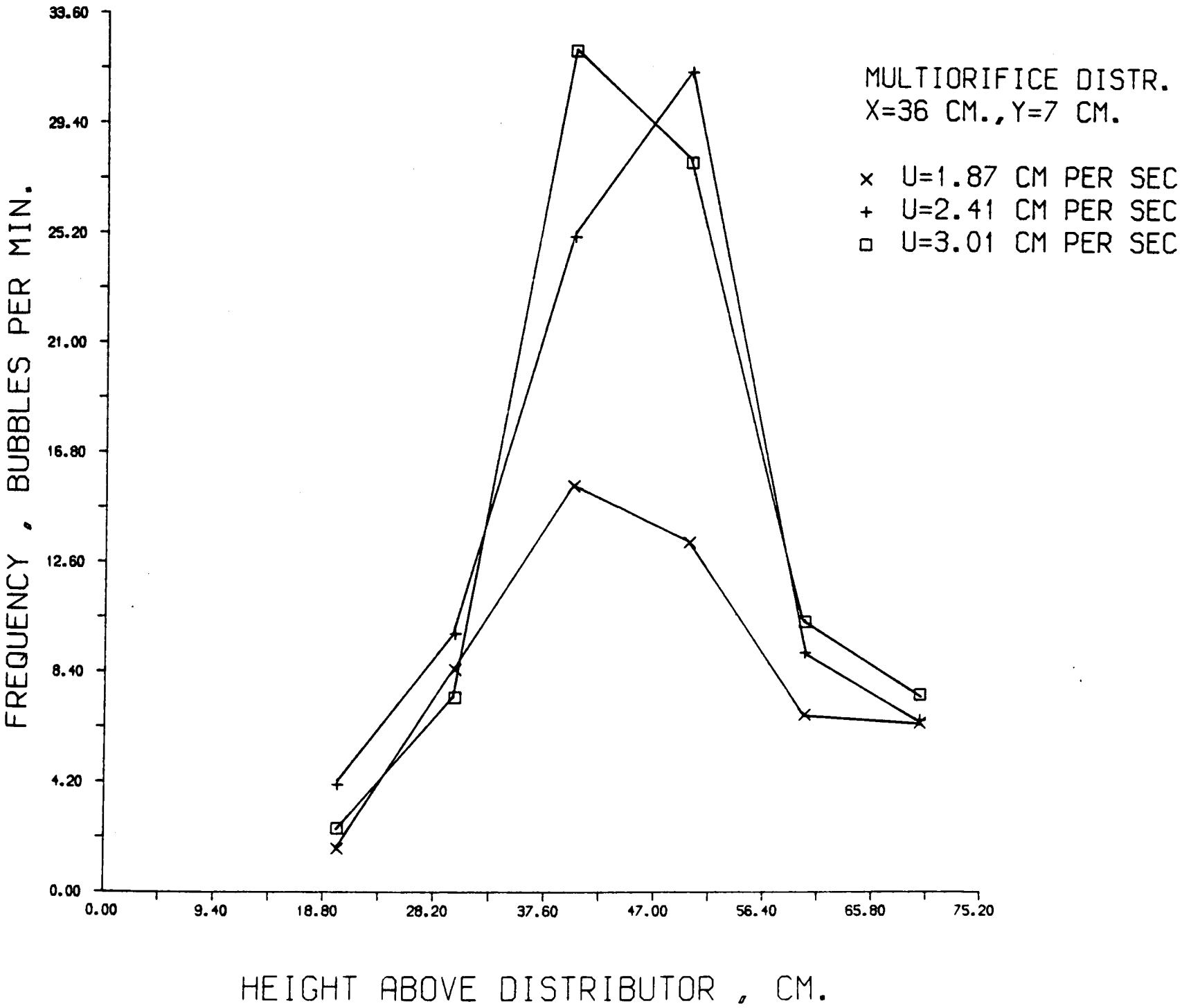
MULTIORIFICE DISTR.
X=36 CM., Y=7 CM.
× U=1.87 CM PER SEC
+ U=2.41 CM PER SEC
□ U=3.01 CM PER SEC
FREQUENCY , BUBBLES PER MIN.
33.60
29.40
25.20
21.00
16.80
12.60
8.40
4.20
0.00
0.00
9.40
18.80
28.20
37.60
47.00
56.40
65.80
75.20
HEIGHT ABOVE DISTRIBUTOR , CM.

Fig. 6.18

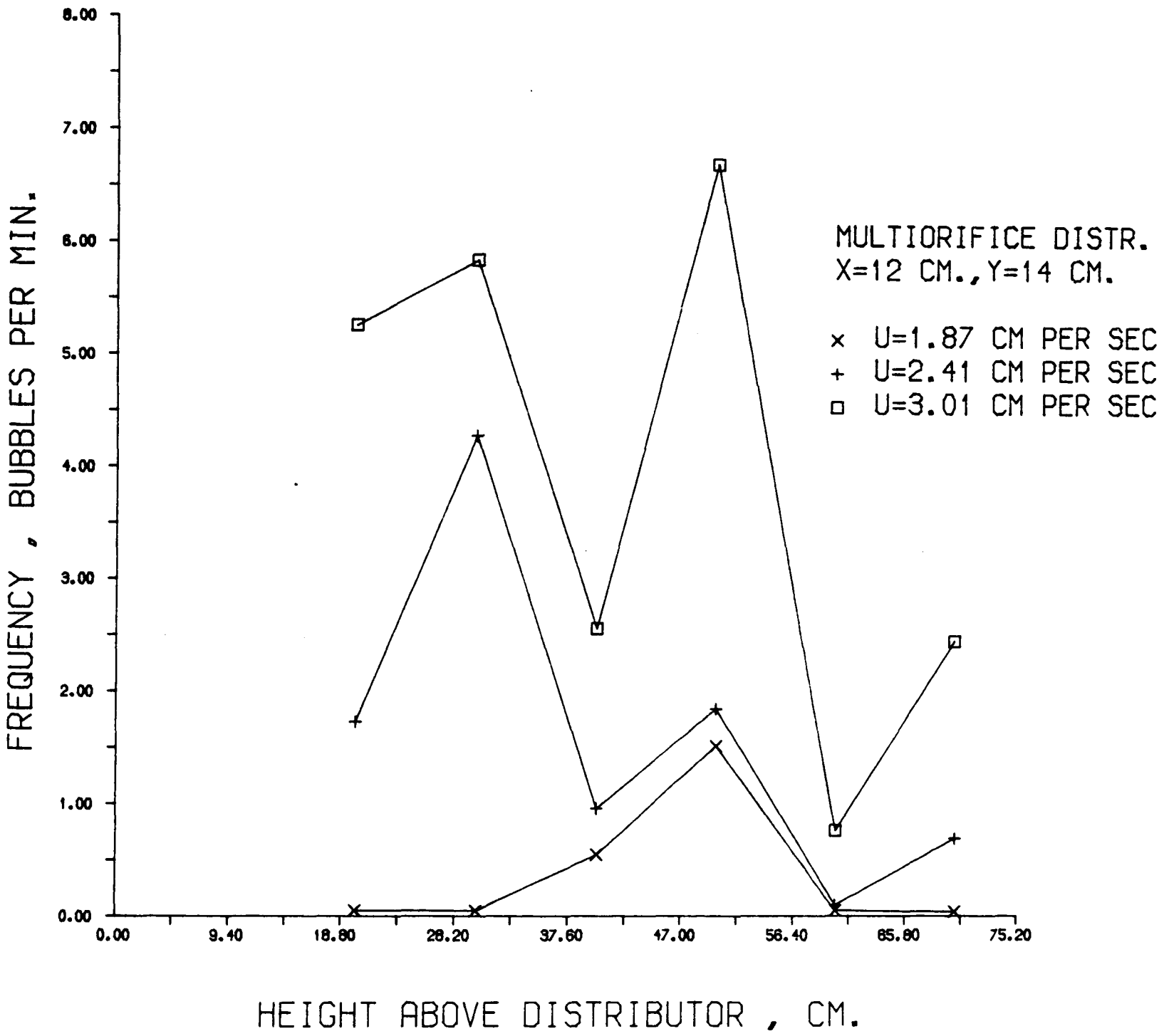
FREQUENCY , BUBBLES PER MIN.
8.00
7.00
6.00
5.00
4.00
3.00
2.00
1.00
0.00
0.00
9.40
18.80
28.20
37.60
47.00
56.40
65.80
75.20
HEIGHT ABOVE DISTRIBUTOR , CM.
MULTIORIFICE DISTR.
X=12 CM., Y=14 CM.
× U=1.87 CM PER SEC
+ U=2.41 CM PER SEC
□ U=3.01 CM PER SEC

Fig. 6.19

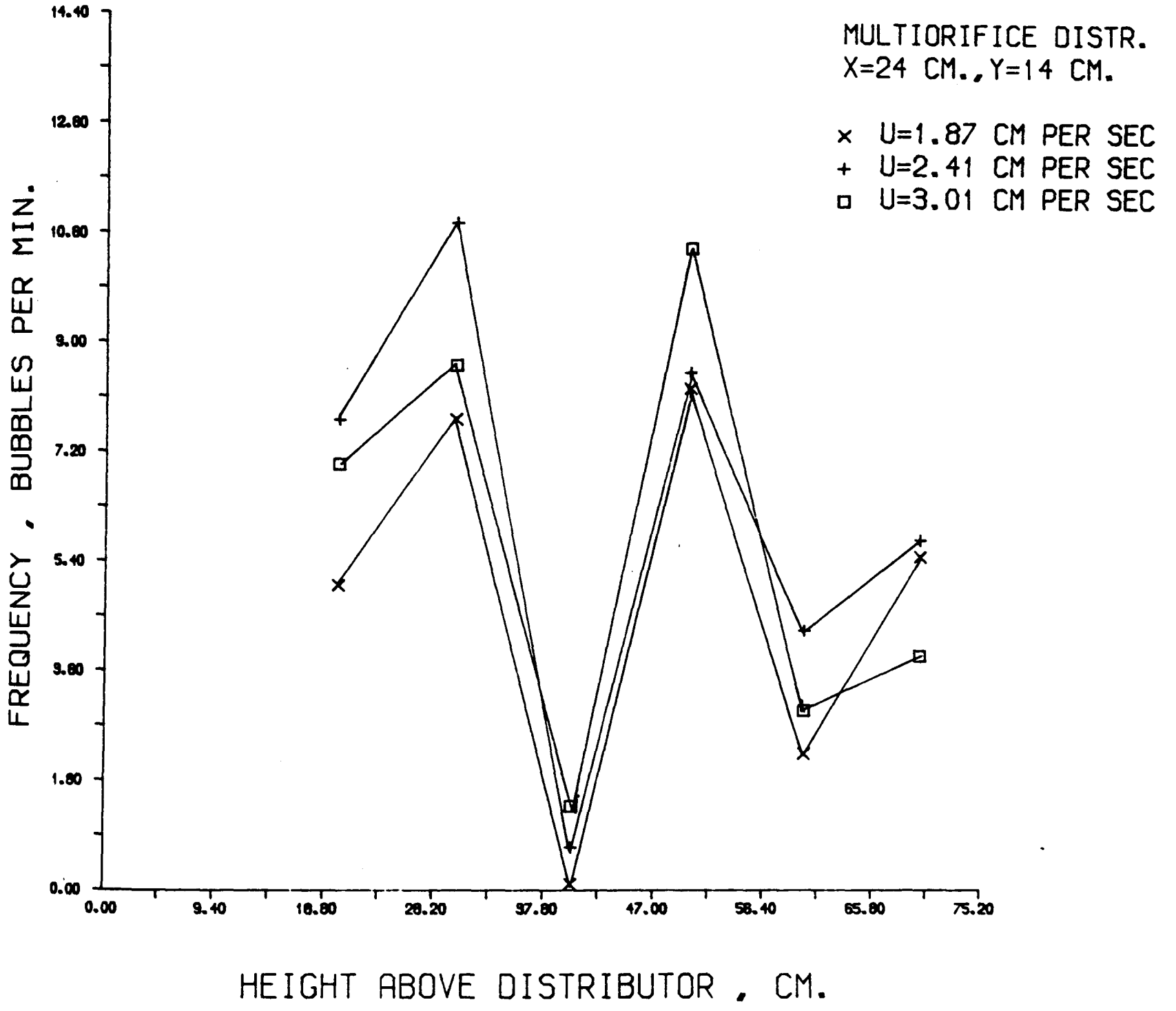
MULTIORIFICE DISTR.
X=24 CM., Y=14 CM.
× U=1.87 CM PER SEC
+ U=2.41 CM PER SEC
□ U=3.01 CM PER SEC
FREQUENCY , BUBBLES PER MIN.
14.40
12.60
10.80
9.00
7.20
5.40
3.60
1.80
0.00
0.00
9.40
18.80
28.20
37.60
47.00
56.40
65.80
75.20
HEIGHT ABOVE DISTRIBUTOR , CM.

Fig. 6.20

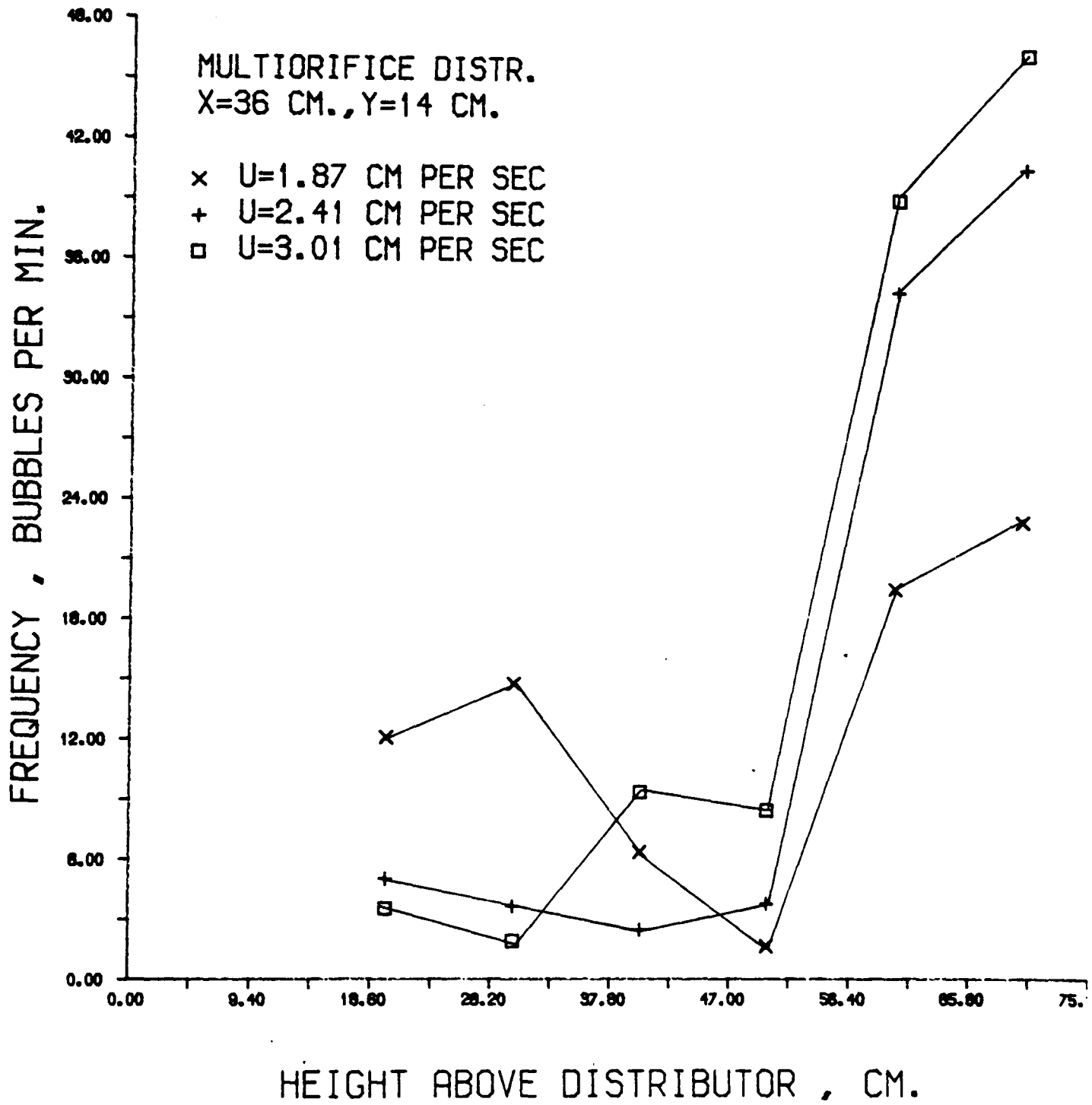
MULTIORIFICE DISTR.
X=36 CM., Y=14 CM.
× U=1.87 CM PER SEC
+ U=2.41 CM PER SEC
□ U=3.01 CM PER SEC
FREQUENCY , BUBBLES PER MIN.
48.00
42.00
36.00
30.00
24.00
18.00
12.00
6.00
0.00
0.00
9.40
18.80
28.20
37.60
47.00
56.40
65.80
75.
HEIGHT ABOVE DISTRIBUTOR , CM.

Fig. 6.21

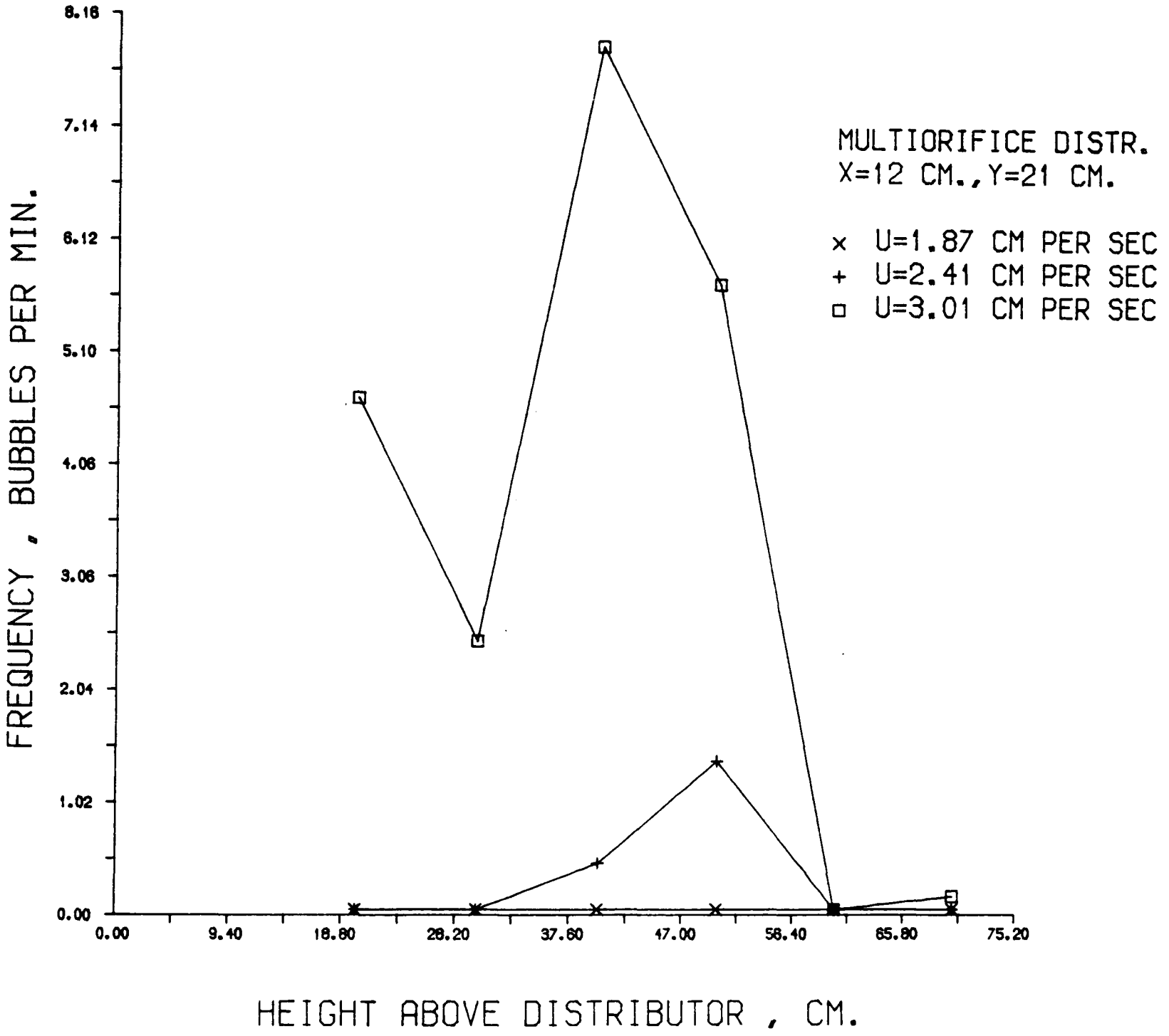
MULTIORIFICE DISTR.
X=12 CM., Y=21 CM.
× U=1.87 CM PER SEC
+ U=2.41 CM PER SEC
□ U=3.01 CM PER SEC
FREQUENCY , BUBBLES PER MIN.
8.16
7.14
6.12
5.10
4.06
3.06
2.04
1.02
0.00
0.00
9.40
18.80
28.20
37.60
47.00
56.40
65.80
75.20
HEIGHT ABOVE DISTRIBUTOR , CM.

Fig. 6.22

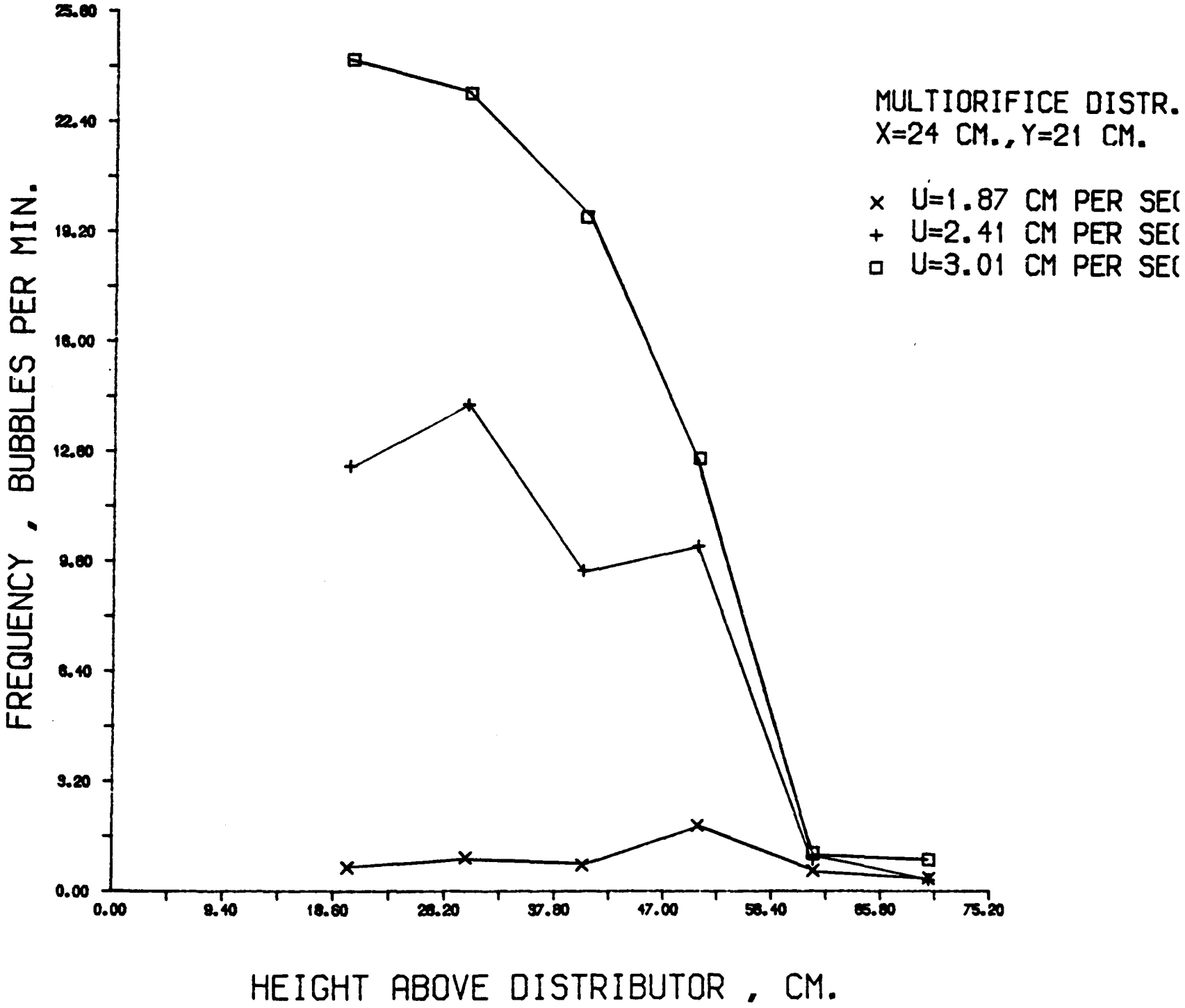
MULTIORIFICE DISTR.
X=24 CM., Y=21 CM.
x U=1.87 CM PER SEC
+ U=2.41 CM PER SEC
□ U=3.01 CM PER SEC
FREQUENCY , BUBBLES PER MIN.
25.60
22.40
19.20
16.00
12.80
9.60
6.40
3.20
0.00
0.00
9.40
18.80
28.20
37.80
47.00
56.40
65.80
75.20
HEIGHT ABOVE DISTRIBUTOR , CM.

Fig. 6.23

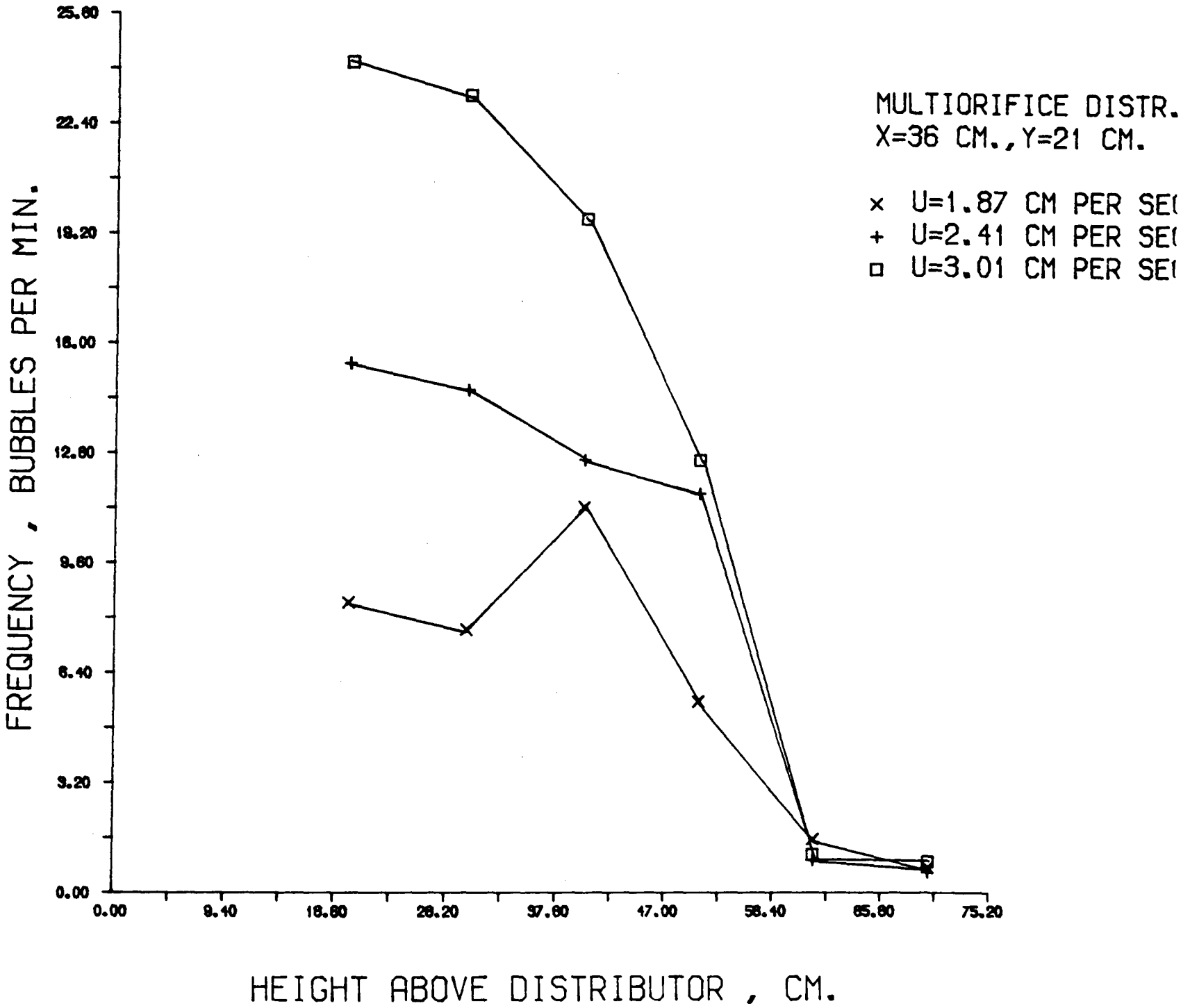
MULTIORIFICE DISTR.
X=36 CM., Y=21 CM.
× U=1.87 CM PER SE(
+ U=2.41 CM PER SE(
□ U=3.01 CM PER SE(
FREQUENCY , BUBBLES PER MIN.
25.60
22.40
19.20
16.00
12.80
9.60
6.40
3.20
0.00
0.00
9.40
18.80
28.20
37.60
47.00
56.40
65.80
75.20
HEIGHT ABOVE DISTRIBUTOR , CM.

6.4 Frequency-Elevation Variation across the Bed with Uniform Depth of 82 cm

In these experiments the bed was filled to a maximum depth of 82 cm and all the frequency measurements were made under these conditions.

Table (6.7) shows the frequency distribution across the bed cross-section, (at the nine points mentioned earlier), at elevations of 20, 30, 40 and 50 cm and three gas velocities of 1.87, 2.41 and 3.01 $cm.sec^{-1}$.

The frequency measurements at 60 and 70 cm elevations are the same in both sets of experiments.

The picture revealed by this table is markedly different from Table (6.7), presumably because:

1. the bubbles are taking different paths when they rise in the bed.
2. the particle flow patterns are quite different in the two cases.

The frequency distribution is much less uniform and the bubbling activity is concentrated in two or three zones on the bed cross-sectional area from much lower elevations, (e.g. 40 - 50 cm compared to 60 - 70 cm in Table (6.8)). The "front" wall is favoured by the bubbles from the very lowest elevations measured. Increases of superficial fluidising velocity change the picture very slightly.

Figures 6.24 - 6.29 show the F - Z variation across the bed cross-section.

Figures 6.24, 6.25 and 6.26 show the frequency-elevation relationship at three sets of points close to the "front wall" of the bed. The pattern in all three graphs is similar and all three show a maximum at around 40 cm elevation. The point of maximum frequency has shifted towards a higher elevation of 50 cm above the distributor at the points nearest to the point of air inlet. At this point, Figure (6.24), and a low gas velocity of 1.87 $cm.sec^{-1}$, the frequencies are too low to measure at very low elevations. The curve corresponding to this superficial velocity (1.87 $cm.sec^{-1}$) does not show any change until an elevation of 50 cm, below which the frequencies are nearly zero.

This is, presumably due to the large number of inactive orifices associated with this low gas velocity.

There are two factors affecting the frequency distribution across this cross-section. First is the effect of the circulation patterns on the bubble frequency, which enhances the frequency when the bubbles lie on the upward movement of these flow patterns. The graphs reveal that near the "front wall", the frequency increases with elevation up to heights of 30 - 50 cm range, coinciding with the fact that the circulation patterns have an upward direction in the 0 - 40 cm elevation range.

The second effect, which is a minor one, concerns the location of the sampling point with respect to the point of air inlet. This influence manifests itself in the magnitude of the elevation where the maximum frequency is recorded (30 cm in Figure 6.26, 40 cm in Figure 6.25 and 50 cm in Figure 6.24).

Figure (6.29) shows the variation of bubble frequency with elevation above the distributor plate, for points on the vertical axis with X = 36 cm and Y = 21 cm coordinates.

These points are near the "back" wall of the bed. Three gas velocities : 1.87, 2.41 and 3.01 $cm.sec^{-1}$ are used. This graph, again, reveals that the data corresponding to the low velocity of 1.87 $cm.sec^{-1}$ do not show any appreciable change with elevation and very low frequencies are recorded for this superficial fluidising velocity.

This recurring phenomenon points to the fact that some of the orifices are inactive at this low gas flow rate.

Figure 6.28 shows the F - Z variation for points on the longitudinal centreline, nearer the "right hand side" wall of the bed. Very high frequencies are recorded, specially at high elevations above the gas distributor. Frequency is increasing steadily with elevation, the highest rise corresponding to the highest of the three superficial velocities (i.e. 3.01 $cm.sec^{-1}$). This is an indication that these points coincide with upward-moving circulation patterns.

It must be remembered that the bed depth is 82 cm in these experiments and the highest elevation investigated is 70 cm above the distributor plate. It seems reasonable to assume that the circulation patterns near this wall (right hand side wall) are moving upwards up to 70 cm elevation.

In Figure 6.27, the F - Z relationship is shown for points on the bed vertical centreline. Except for a few rogue points, the trend of the curves is steadily upwards. The data show more scatter for the low superficial fluidising velocity of 1.87 cm. sec^{-1}. This feature appears on most of the graphs in this section. The experimental points for U = 1.87 cm.sec^{-1} reveal a more irregular pattern of the frequency - elevation relationship. This could be due to the fact that, at this low gas rate, the bed is not as uniformly fluidised, since some of the perforations are not active.

A comparison of the graphs for the two sets of experiments carried out with the multiorifice distributor reveals a number of similarities, (Figures (6.15 - 6.17) - Figures (6.24 - 6.26)). The points near the "back wall" of the bed show frequency decreasing with increasing elevation. On the other hand, the points near the front wall all show the frequency increasing until a point is reached where, presumably, the flow patterns reverse direction, whence the frequency decreases with increasing elevation.

The same argument can be made for the points on the bed vertical centreline.

Fig. 6.24

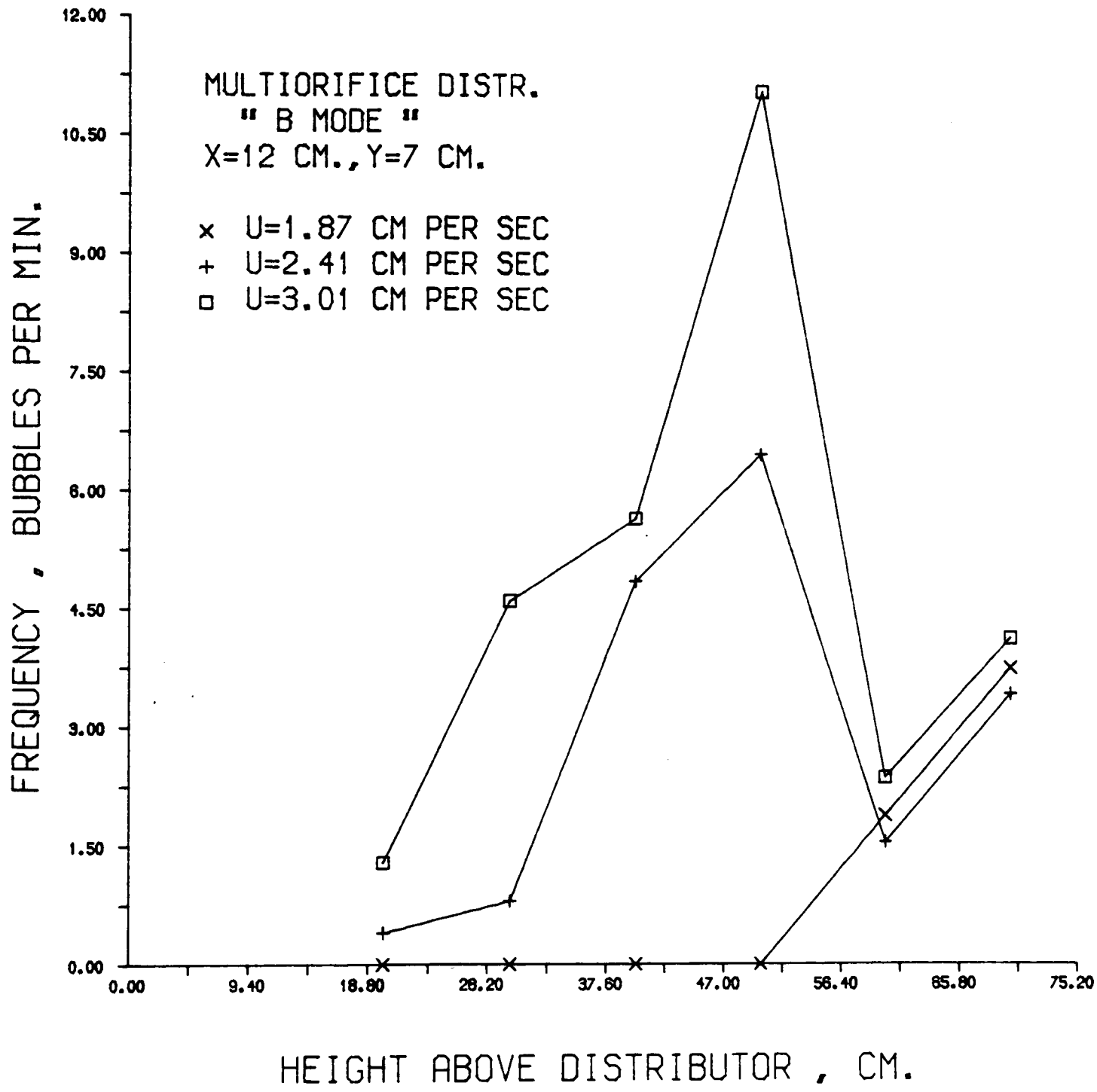
MULTIORIFICE DISTR.
" B MODE "
X=12 CM., Y=7 CM.
× U=1.87 CM PER SEC
+ U=2.41 CM PER SEC
□ U=3.01 CM PER SEC
FREQUENCY , BUBBLES PER MIN.
12.00
10.50
9.00
7.50
6.00
4.50
3.00
1.50
0.00
0.00
9.40
18.80
28.20
37.60
47.00
56.40
65.80
75.20
HEIGHT ABOVE DISTRIBUTOR , CM.

Fig. 6.25

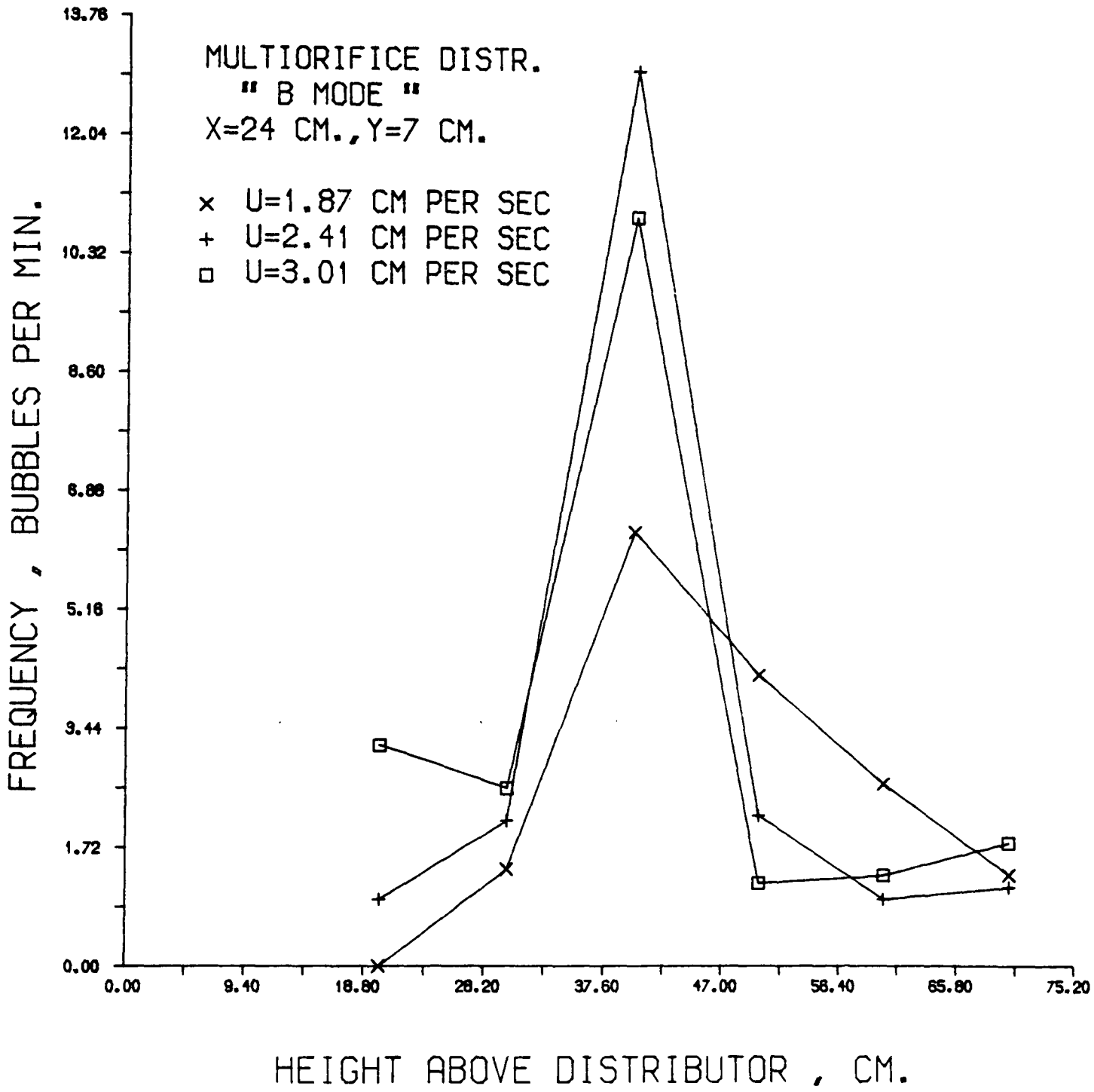
MULTIORIFICE DISTR.
" B MODE "
X=24 CM., Y=7 CM.
× U=1.87 CM PER SEC
+ U=2.41 CM PER SEC
□ U=3.01 CM PER SEC
FREQUENCY , BUBBLES PER MIN.
13.76
12.04
10.32
8.60
6.88
5.16
3.44
1.72
0.00
0.00
9.40
18.80
28.20
37.60
47.00
56.40
65.80
75.20
HEIGHT ABOVE DISTRIBUTOR , CM.

Fig. 6.26

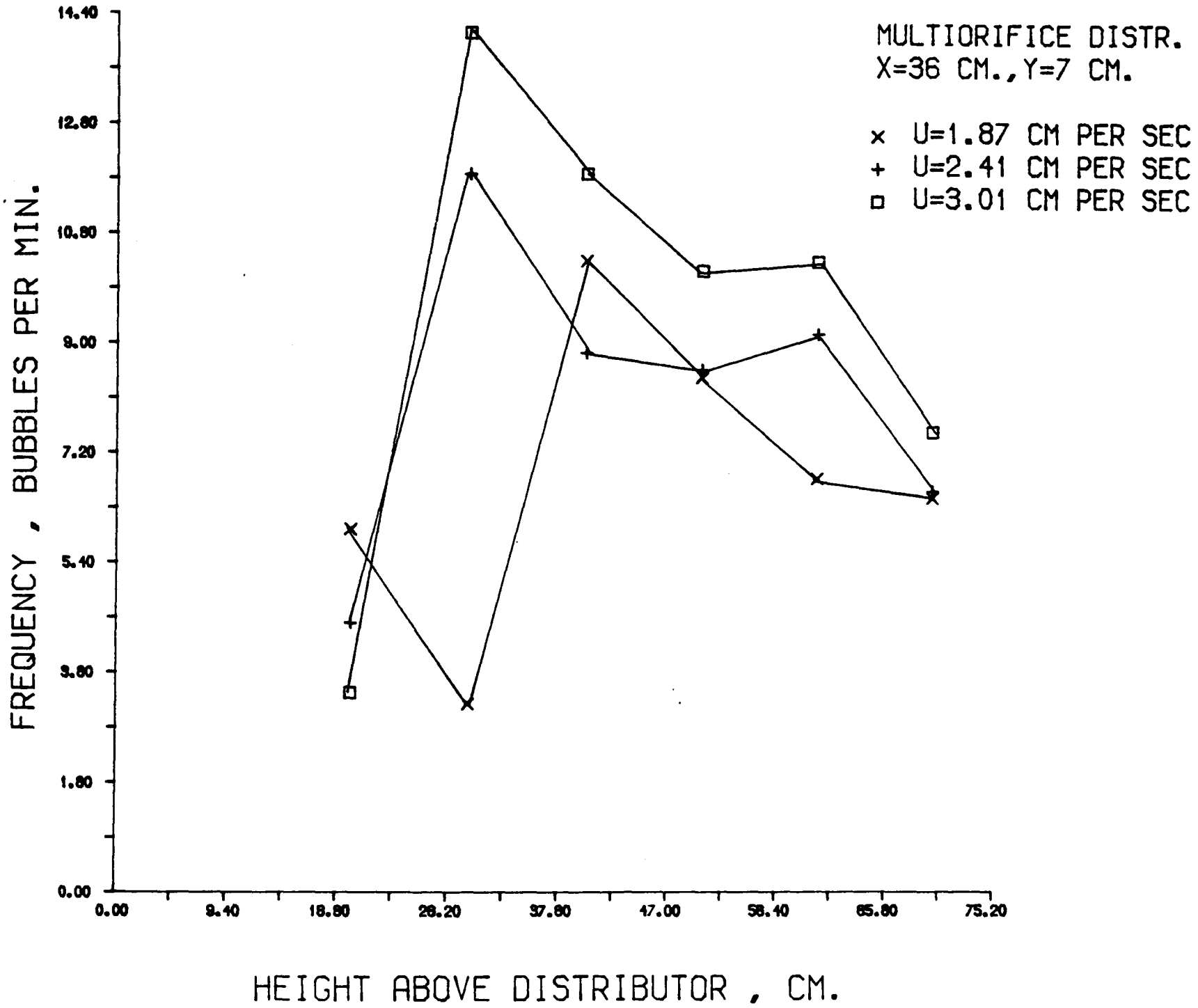
MULTIORIFICE DISTR.
X=36 CM., Y=7 CM.
× U=1.87 CM PER SEC
+ U=2.41 CM PER SEC
□ U=3.01 CM PER SEC
FREQUENCY , BUBBLES PER MIN.
14.40
12.60
10.80
9.00
7.20
5.40
3.60
1.80
0.00
0.00
9.40
18.80
28.20
37.60
47.00
56.40
65.80
75.20
HEIGHT ABOVE DISTRIBUTOR , CM.

Fig. 6.27

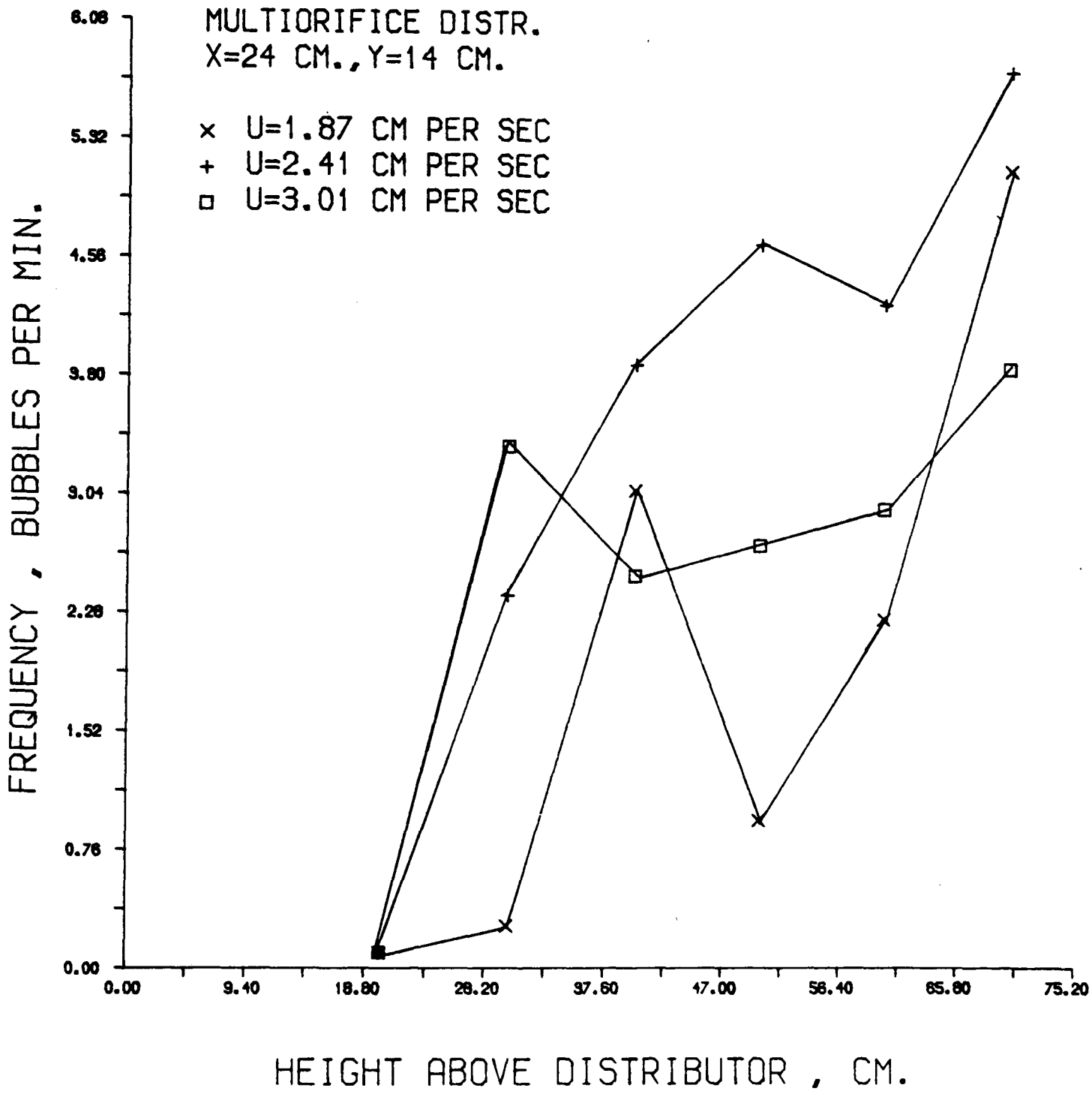
MULTIORIFICE DISTR.
X=24 CM., Y=14 CM.
× U=1.87 CM PER SEC
+ U=2.41 CM PER SEC
□ U=3.01 CM PER SEC
FREQUENCY , BUBBLES PER MIN.
6.08
5.32
4.56
3.80
3.04
2.28
1.52
0.76
0.00
0.00
9.40
18.80
28.20
37.60
47.00
56.40
65.80
75.20
HEIGHT ABOVE DISTRIBUTOR , CM.

Fig. 6.28

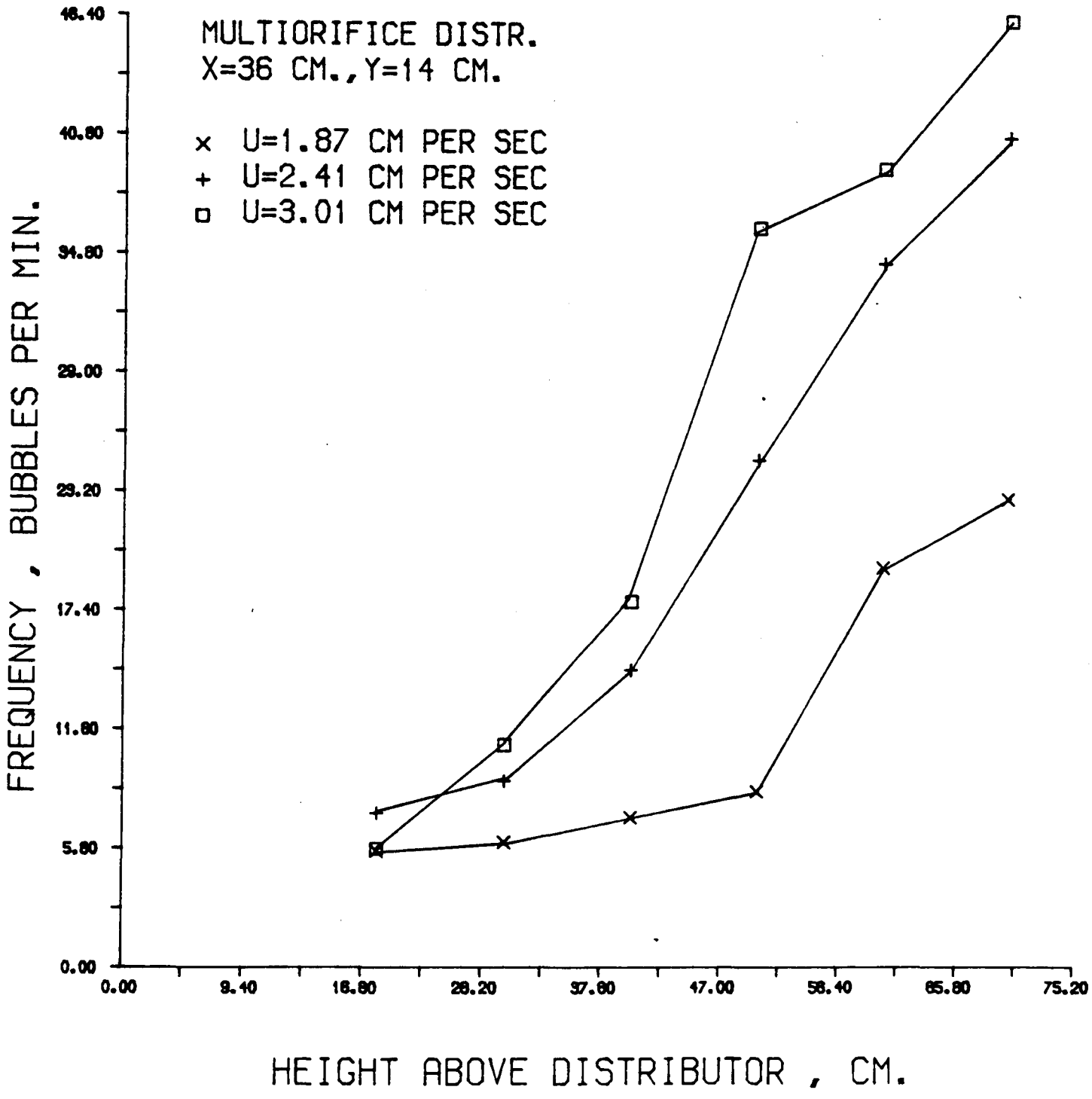
MULTIORIFICE DISTR.
X=36 CM., Y=14 CM.
x U=1.87 CM PER SEC
+ U=2.41 CM PER SEC
□ U=3.01 CM PER SEC
FREQUENCY , BUBBLES PER MIN.
46.40
40.60
34.80
29.00
23.20
17.40
11.60
5.80
0.00
0.00
9.40
18.80
28.20
37.60
47.00
56.40
65.80
75.20
HEIGHT ABOVE DISTRIBUTOR , CM.

Fig. 6.29

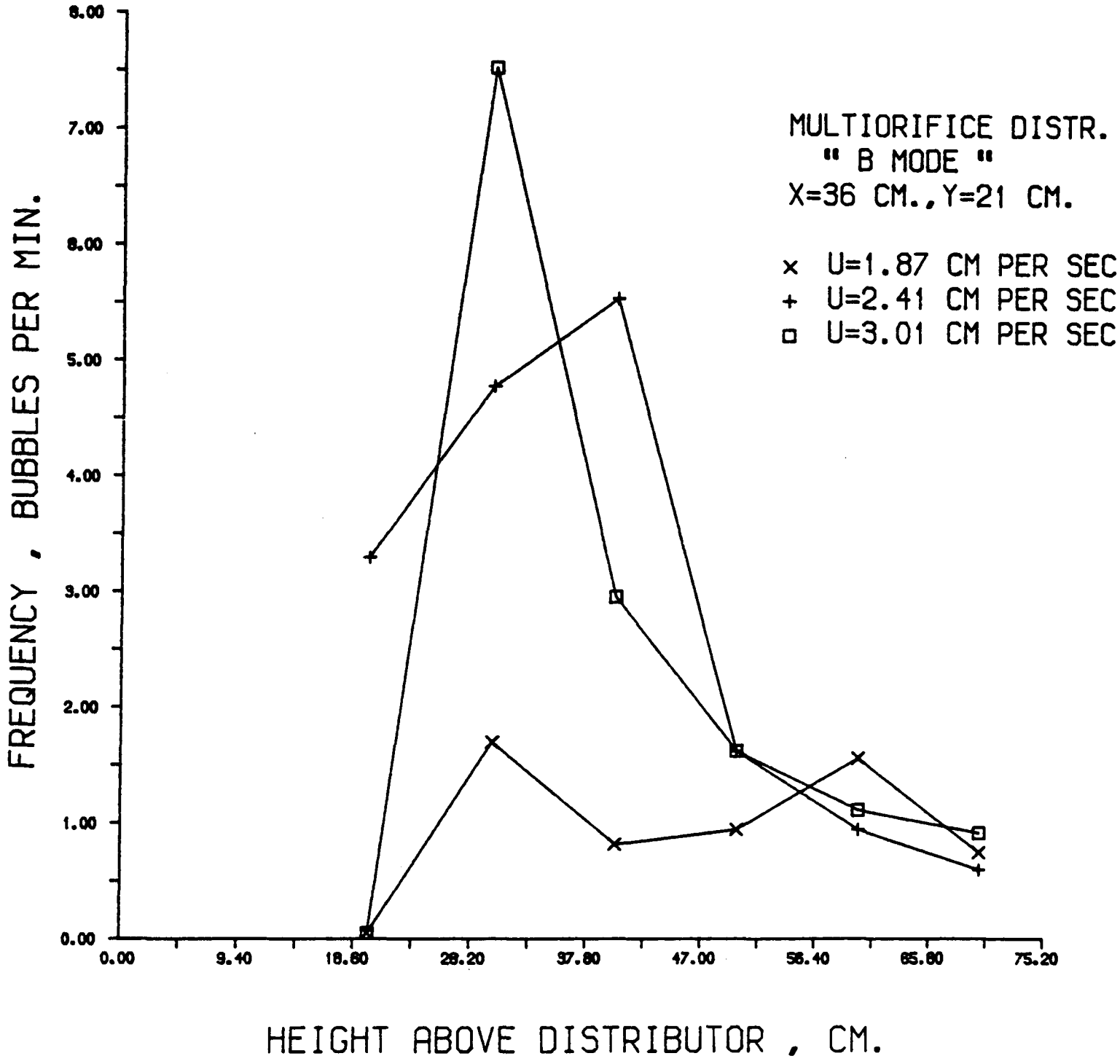
FREQUENCY , BUBBLES PER MIN.
8.00
7.00
6.00
5.00
4.00
3.00
2.00
1.00
0.00
0.00
9.40
18.80
28.20
37.60
47.00
56.40
65.80
75.20
HEIGHT ABOVE DISTRIBUTOR , CM.
MULTIORIFICE DISTR.
" B MODE "
X=36 CM., Y=21 CM.
× U=1.87 CM PER SEC
+ U=2.41 CM PER SEC
□ U=3.01 CM PER SEC

6.5 Frequencies Measured in 'C' Mode

In Table (6.8) are tabulated the bubble frequencies across the bed cross-section at six different elevations and three superficial fluidising velocities. The data shows much higher point values for frequencies in almost all the 162 experiments than tables (6.6 and 6.7).

This is of course, due to the fact that there are no constraints imposed on the bubble-sizes recorded in this mode.

Although the frequency distribution is much more uniform than in table (6.7) nevertheless the familiar trend of the "front" and "right hand side walls" attracting more bubbles persists.

It is interesting to note that at some points in the bed, the frequencies measured are as low as recorded in 'B' mode. This suggests that the reason for very low bubbling activity shown at these points is not only due to the constraints imposed on bubble selection and collection . Physical conditions, such as the prevailing circulation patterns and/or inactive perforations, could also cause these irregularities in the spatial frequency distributions in a gas fluidised bed.

The pattern of the frequency distributions (in mode 'C') follows that in 'B' mode at most of the elevations investigated. At very high elevations above the distributor plate, the 'B' mode distributions are more irregular, those of 'C' mode on the other hand, more uniform across the bed cross-section.

Z = 40 cm	<0.1	<0.1	6.87
	<0.1	5.60	40.38
	82.60	35.83	44.29

U = 1.87

	<0.1	<0.1	50.00
	54.00	38.08	50.67
	102.70	35.89	75.50

U = 2.41

	6.20	10.75	50.10
	71.70	63.58	79.44
	99.20	48.14	89.25

U = 3.01

Z = 30 cm	<0.1	1.03	66.67
	<0.1	13.80	54.86
	94.17	2.08	64.40

U = 1.87

	<0.1	43.67	54.60
	0.50	26.83	52.33
	103.80	4.40	91.70

U = 2.41

	32.50	64.00	82.31
	25.80	61.00	54.60
	128.40	3.00	99.67

U = 3.01

Z = 20 cm	<0.1	28.60	41.88
	<0.1	0.5	40.22
	92.8	1.00	36.50

U = 1.87

	<0.1	56.60	31.70
	1.0	1.43	34.89
	59.80	1.70	71.36

U = 2.41

	35.94	43.60	40.70
	8.60	1.50	56.25
	78.80	6.59	122.50

U = 3.01

TABLE 6.8

Bubble Frequencies in 'C' Mode = min^{-1}

Multiorifice Distributor

Bed Depth = 82 cm

Z = 70 cm	0.20	3.80	15.00
	9.20	12.90	71.40
	29.80	20.57	47.22

U = 1.87

8.20	17.67	49.20
55.00	34.29	113.80
62.08	32.75	71.60

U = 2.41

36.20	35.71	69.82
84.50	53.30	117.00
52.70	43.30	80.20

U = 3.01

Z = 60 cm	<0.1	0.20	1.86
	0.20	16.86	48.43
	12.00	21.40	42.00

U = 1.87

0.30	3.40	27.14
57.70	21.00	87.50
62.00	24.40	63.13

U = 2.41

13.18	18.63	58.50
95.50	49.00	105.33
42.40	36.10	66.42

U = 3.01

Z = 50 cm	<0.1	0.15	1.00
	0.10	13.50	62.67
	20.60	35.13	31.14

U = 1.87

0.10	0.40	7.55
68.90	27.40	89.75
82.36	37.70	36.63

U = 2.41

6.00	9.20	33.13
99.00	64.07	117.00
66.90	41.80	62.11

U = 3.01

TABLE 6.8 continued

Table (6.8A) below, shows the sum of the point frequencies, at the nine sampling points, at the six elevations investigated. The frequencies in this table, are the bubble frequencies, measured in 'C' mode.

Z(cm) / Ft min^{-1}	20	30	40	50	60	70 cm
Ft(U = 1.87)	241	297	216	169	143	210
Ft(U = 2.41)	258	378	407	351	347	445
Ft(U = 3.01)	394	551	518	499	485	573

Table (6.8A) shows a steady decline in the 'total frequency' with elevation, except for the first and last points. This pattern of steady decline (except for the Z = 20 cm and Z = 70 cm elevations), also prevails in the 'total frequency' - elevation tables when the 'B' mode frequencies are used. This, presumably, is an indication of how the coalescence of small bubbles is influencing the bubble count with the multiorifice distributor.

In Figures (6.30) - (6.38) the frequency - elevation variation is plotted with the frequencies measured in 'C' mode.

Figures (6.30, 6.31 and 6.32) show the F - Z relationship at points near the front wall of the bed. All three graphs show frequency increasing with elevation, reaching a maximum at 30 - 40 cm elevation range and then decreasing to a minimum at heights of 50 - 60 cm above the distributor plate.

At the vertical centre-plane (Y = 14 cm) the picture is markedly different. Figure (6.35), representing the points near the "right hand side wall" of the bed, shows frequency increasing steadily with increasing elevation. The highest frequencies are encountered at these points in both 'B' and 'C' modes.

When the bed is filled to a depth of 82 cm, there seem to be large circulation patterns in the bed moving upwards near the "right hand side wall", which would explain the prevailing pattern in Figure 6.35.

Figures 6.30 and 6.33 represent points near the "left hand side wall", which show the frequency increasing with elevation up to a point, ($\sim$ 40 cm above the distributor) and then decreasing with an increase in elevation.

Figure 6.36 shows the F - Z relationship at points near the "top left hand corner". No appreciable frequencies are recorded for 1.87 and 2.41 $cm.sec^{-1}$ gas velocities. For U = 3.01 $cm.sec^{-1}$, the graph shows a minimum at $\sim$ 40 cm elevation.

Figure 6.37 reveals a similar pattern. This figure corresponds to the points on the X = 24 cm and the Y = 21 cm planes. Here, all three curves show minima at 30 - 50 cm range. Frequencies of relatively higher magnitudes (than in Figure 6.36) are measured for two of the superficial fluidising velocities.

In Figure (6.38), this representation is extended to points in the "top right hand corner" of the bed. A similar pattern to those in Figures (6.36) and (6.37) prevails.

It must be mentioned here that all the three graphs (6.36 - 6.38), representing points near the "back wall" of the bed, show exactly the opposite trend to the points near the "front wall".

This, presumably, indicates the existence of particle phase circulation patterns with opposing directions, close to the "front" and the "back" walls of the bed.

Finally, Figures (6.33 - 6.35) represent the points on the longer centre-plane, at Y = 14 cm. They all show frequency increasing with elevation. The data for points on the bed vertical centreline reveal very small frequencies for U = 1.87 $cm.sec^{-1}$.

Points nearest the position of gas inlet do not show measurable frequencies at a low gas velocity of 1.87 $cm.sec^{-1}$, Figure (6.33).

Fig. 6.30

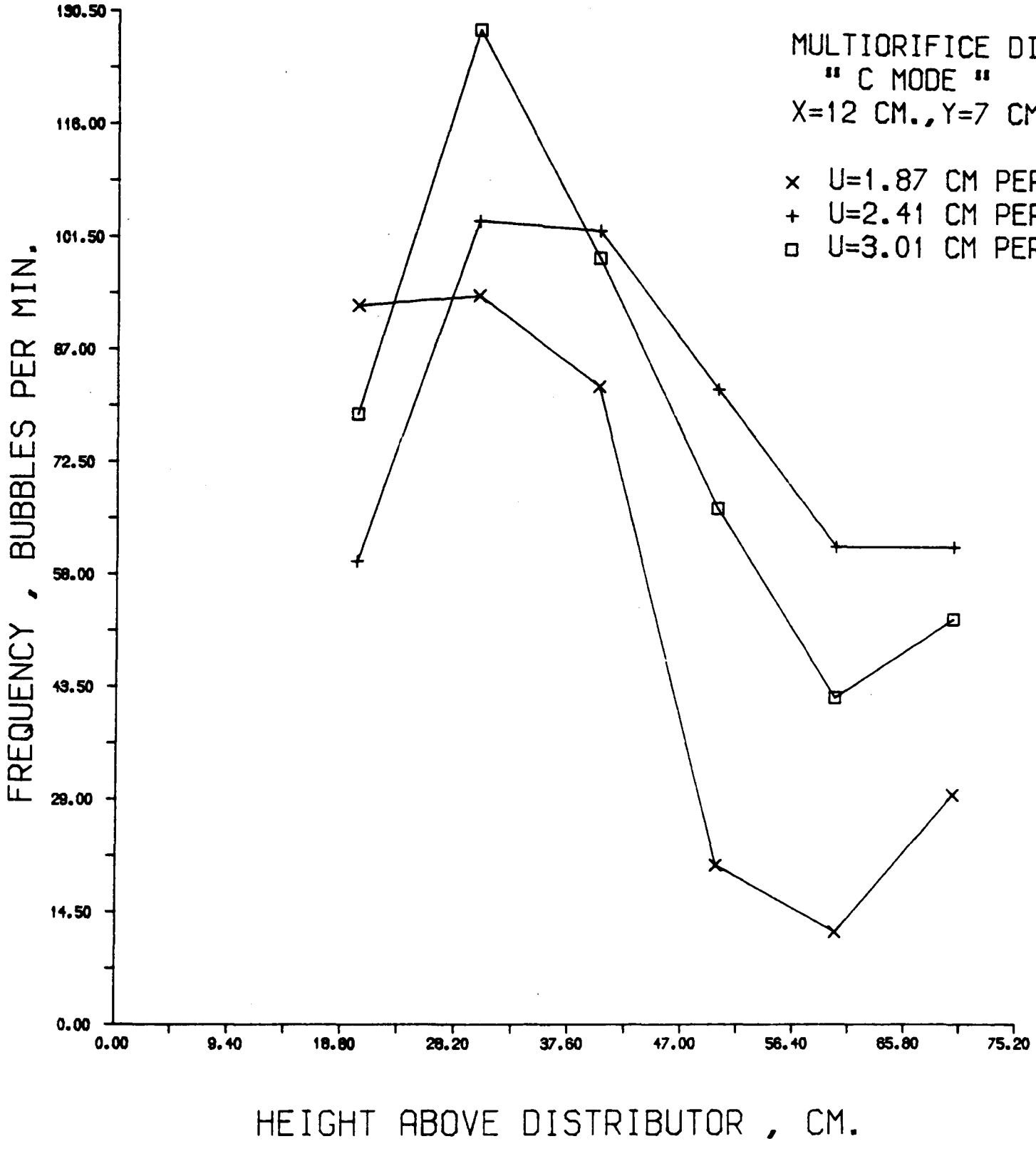
MULTIORIFICE DISTR.
" C MODE "
X=12 CM., Y=7 CM.
× U=1.87 CM PER SEC
+ U=2.41 CM PER SEC
□ U=3.01 CM PER SEC
FREQUENCY , BUBBLES PER MIN.
130.50
116.00
101.50
87.00
72.50
58.00
43.50
29.00
14.50
0.00
0.00
9.40
18.80
28.20
37.60
47.00
56.40
65.80
75.20
HEIGHT ABOVE DISTRIBUTOR , CM.

Fig. 6.31

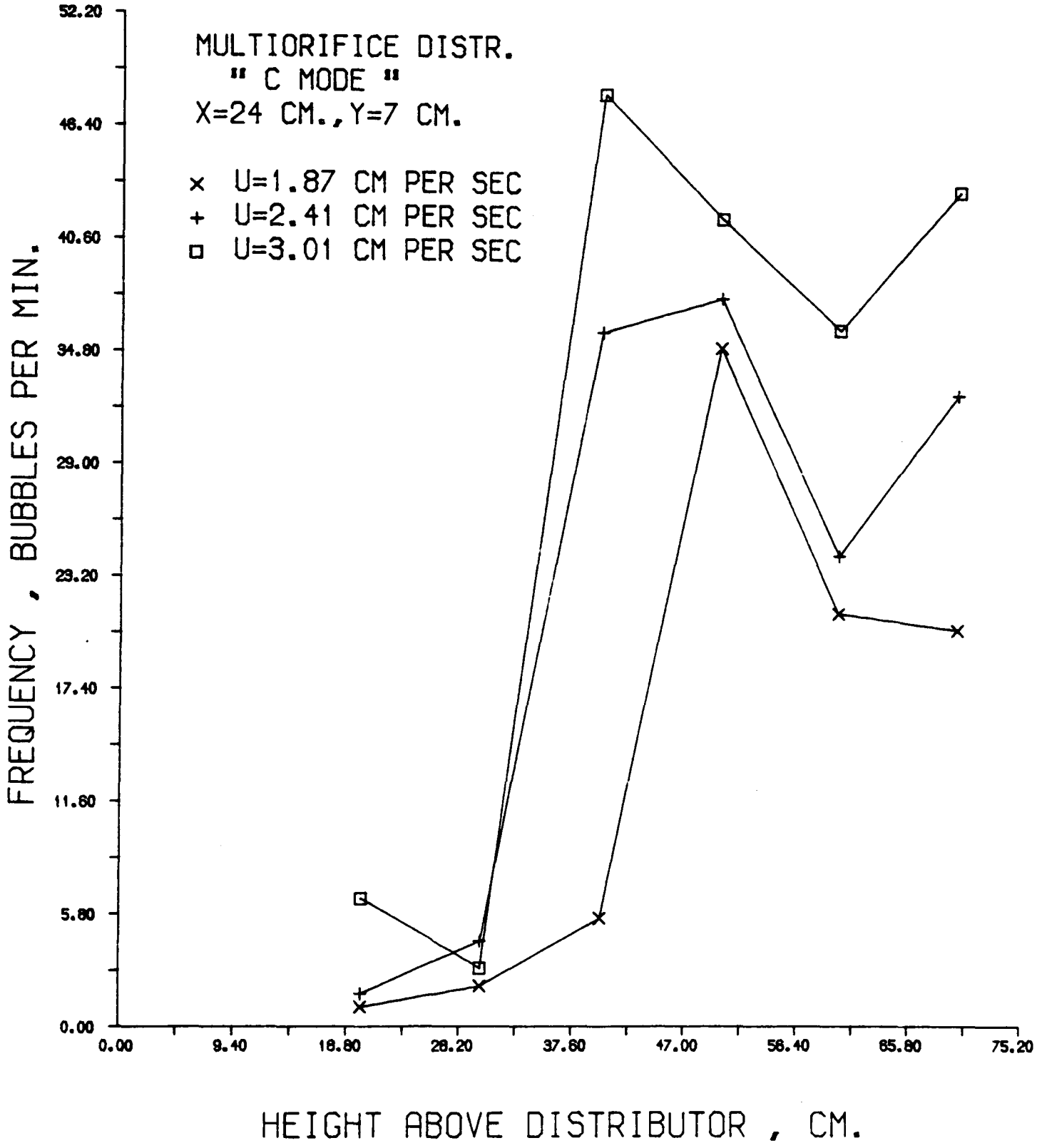
MULTIORIFICE DISTR.
" C MODE "
X=24 CM., Y=7 CM.
× U=1.87 CM PER SEC
+ U=2.41 CM PER SEC
□ U=3.01 CM PER SEC
FREQUENCY , BUBBLES PER MIN.
52.20
46.40
40.60
34.80
29.00
23.20
17.40
11.60
5.80
0.00
0.00
9.40
18.80
28.20
37.60
47.00
56.40
65.80
75.20
HEIGHT ABOVE DISTRIBUTOR , CM.

Fig. 6.32

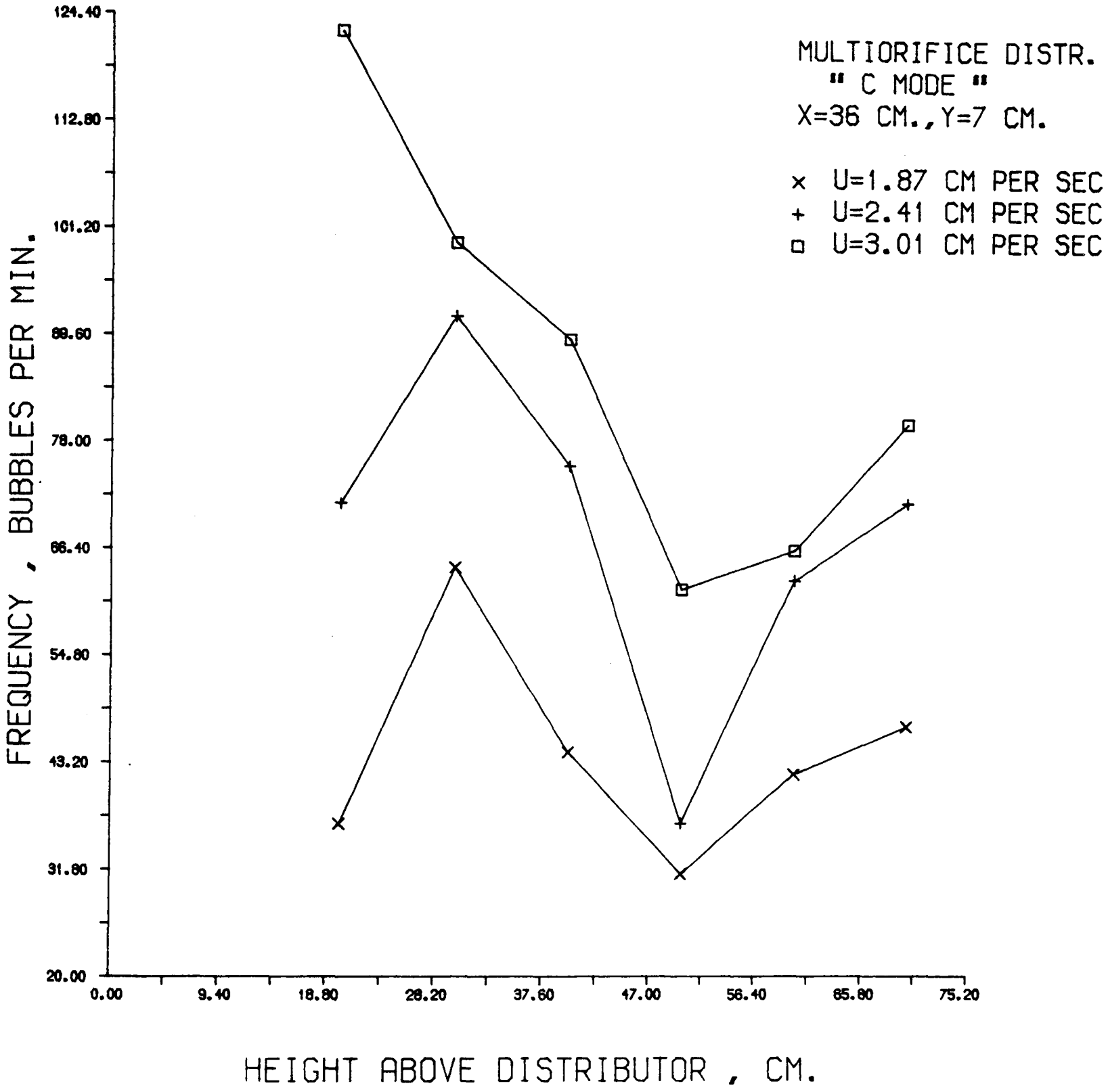
MULTIORIFICE DISTR.
" C MODE "
X=36 CM., Y=7 CM.
× U=1.87 CM PER SEC
+ U=2.41 CM PER SEC
□ U=3.01 CM PER SEC
FREQUENCY , BUBBLES PER MIN.
124.40
112.80
101.20
89.60
78.00
66.40
54.80
43.20
31.60
20.00
0.00
9.40
18.80
28.20
37.60
47.00
56.40
65.80
75.20
HEIGHT ABOVE DISTRIBUTOR , CM.

Fig. 6.33

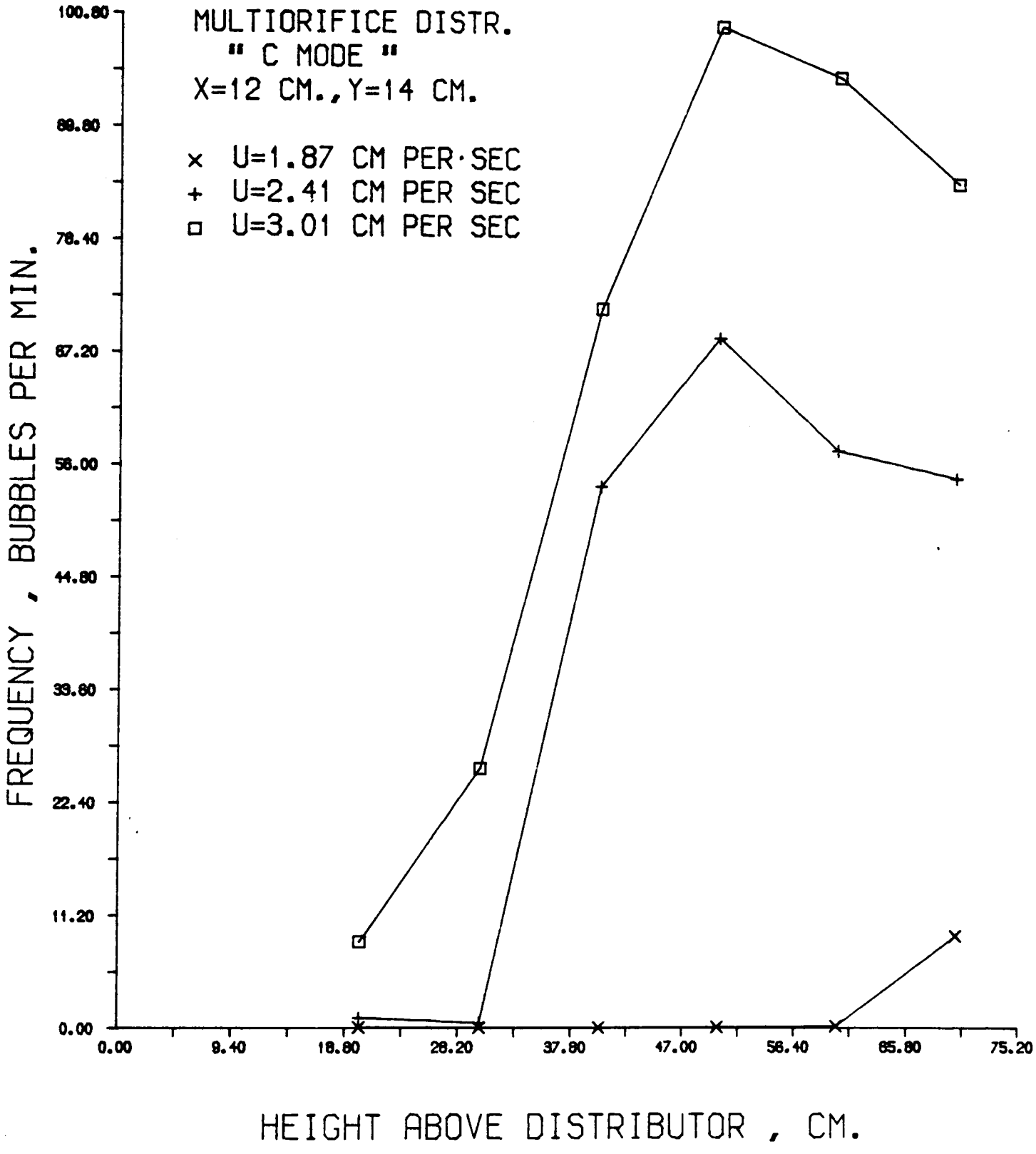
MULTIORIFICE DISTR.
" C MODE "
X=12 CM., Y=14 CM.
× U=1.87 CM PER·SEC
+ U=2.41 CM PER SEC
□ U=3.01 CM PER SEC
FREQUENCY , BUBBLES PER MIN.
100.80
89.60
78.40
67.20
56.00
44.80
33.60
22.40
11.20
0.00
0.00
9.40
18.80
28.20
37.80
47.00
56.40
65.80
75.20
HEIGHT ABOVE DISTRIBUTOR , CM.

Fig. 6.34

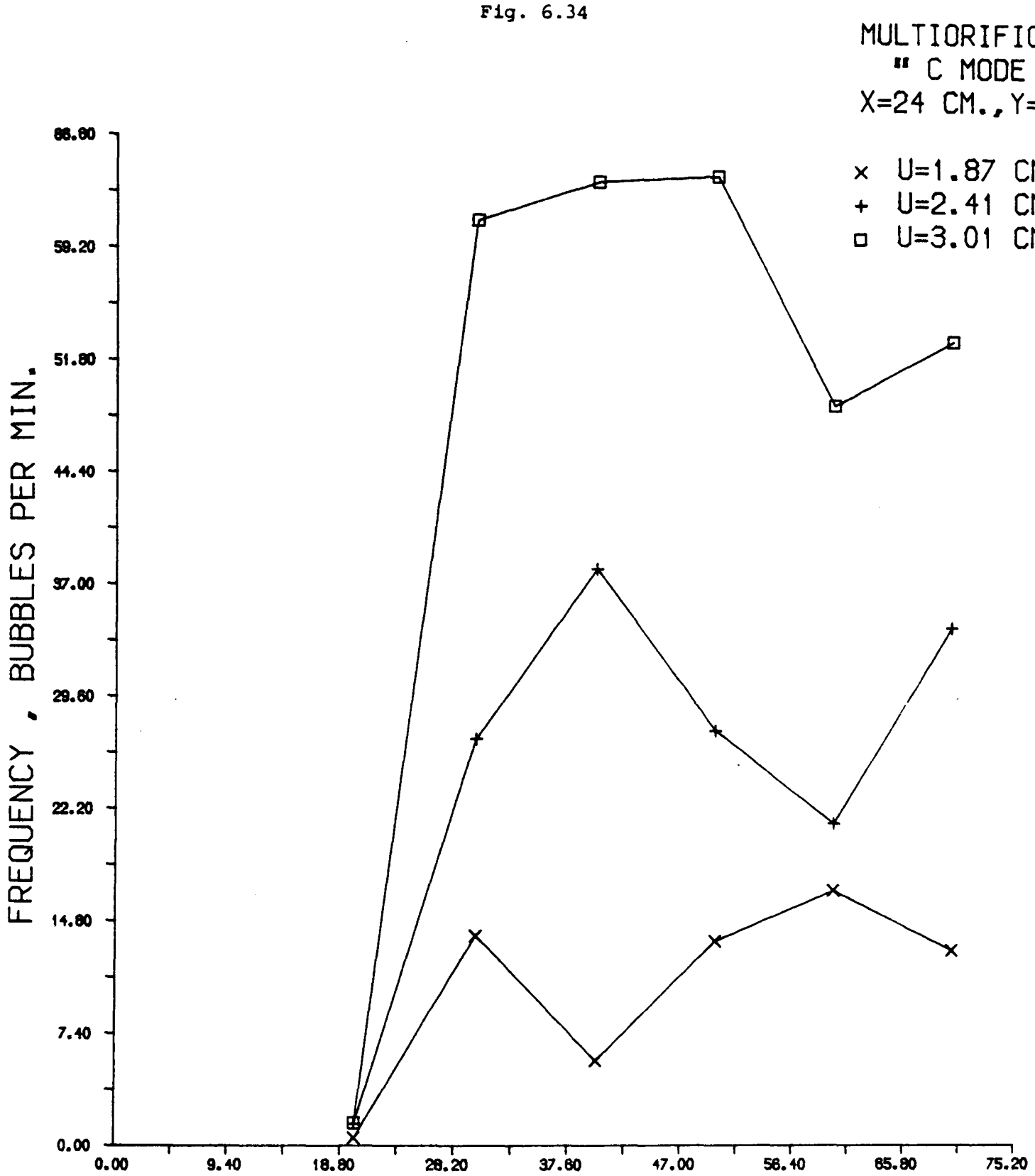
MULTIORIFICE DISTR.
" C MODE "
X=24 CM., Y=14 CM.
× U=1.87 CM PER SEC
+ U=2.41 CM PER SEC
□ U=3.01 CM PER SEC
FREQUENCY , BUBBLES PER MIN.
88.80
59.20
51.80
44.40
37.00
29.60
22.20
14.80
7.40
0.00
0.00
9.40
18.80
28.20
37.60
47.00
56.40
65.80
75.20
HEIGHT ABOVE DISTRIBUTOR , CM.

Fig. 6.35

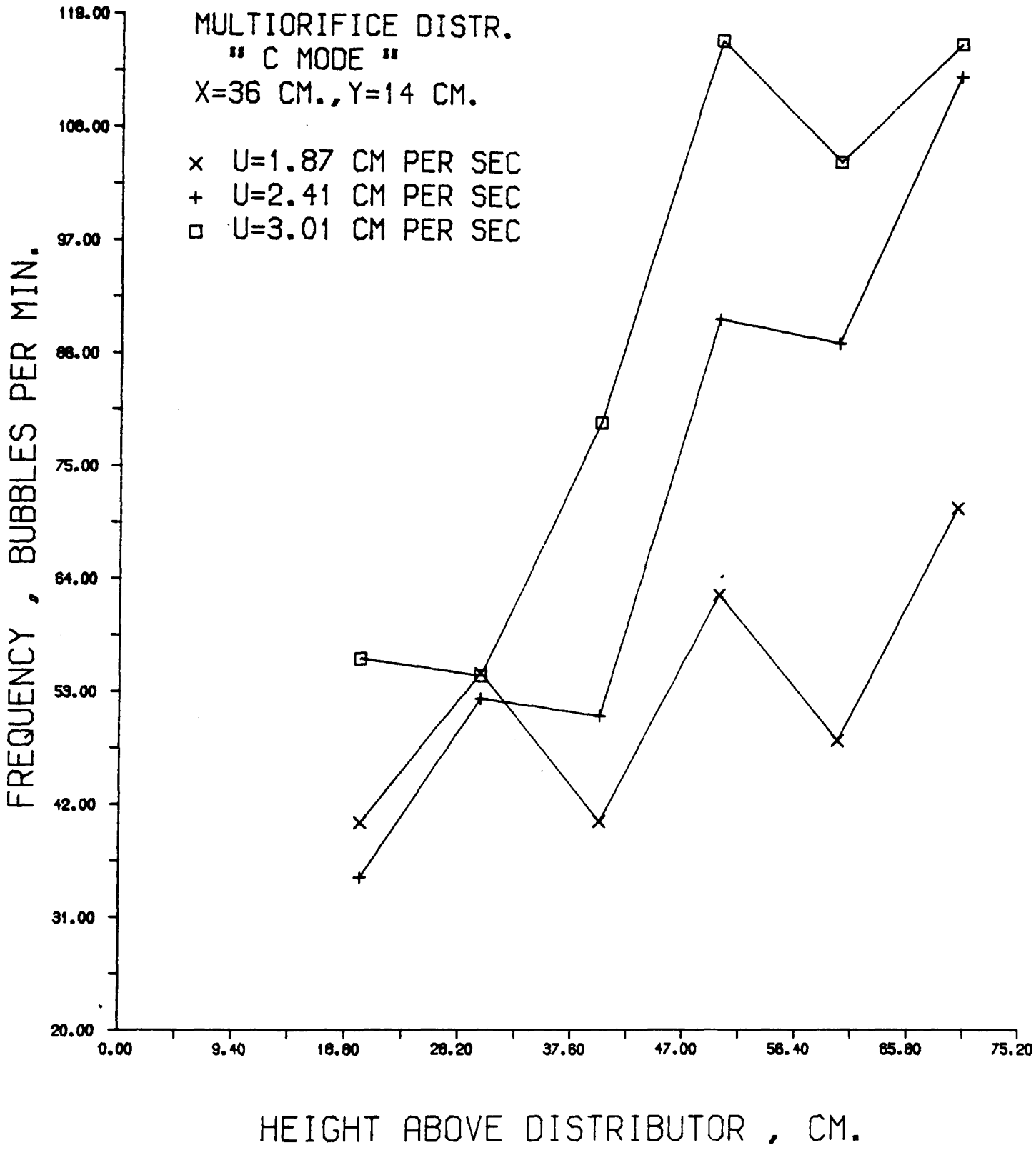
MULTIORIFICE DISTR.
" C MODE "
X=36 CM., Y=14 CM.
× U=1.87 CM PER SEC
+ U=2.41 CM PER SEC
□ U=3.01 CM PER SEC
FREQUENCY , BUBBLES PER MIN.
119.00
108.00
97.00
86.00
75.00
64.00
53.00
42.00
31.00
20.00
0.00
9.40
18.80
28.20
37.60
47.00
56.40
65.80
75.20
HEIGHT ABOVE DISTRIBUTOR , CM.

Fig. 6.36

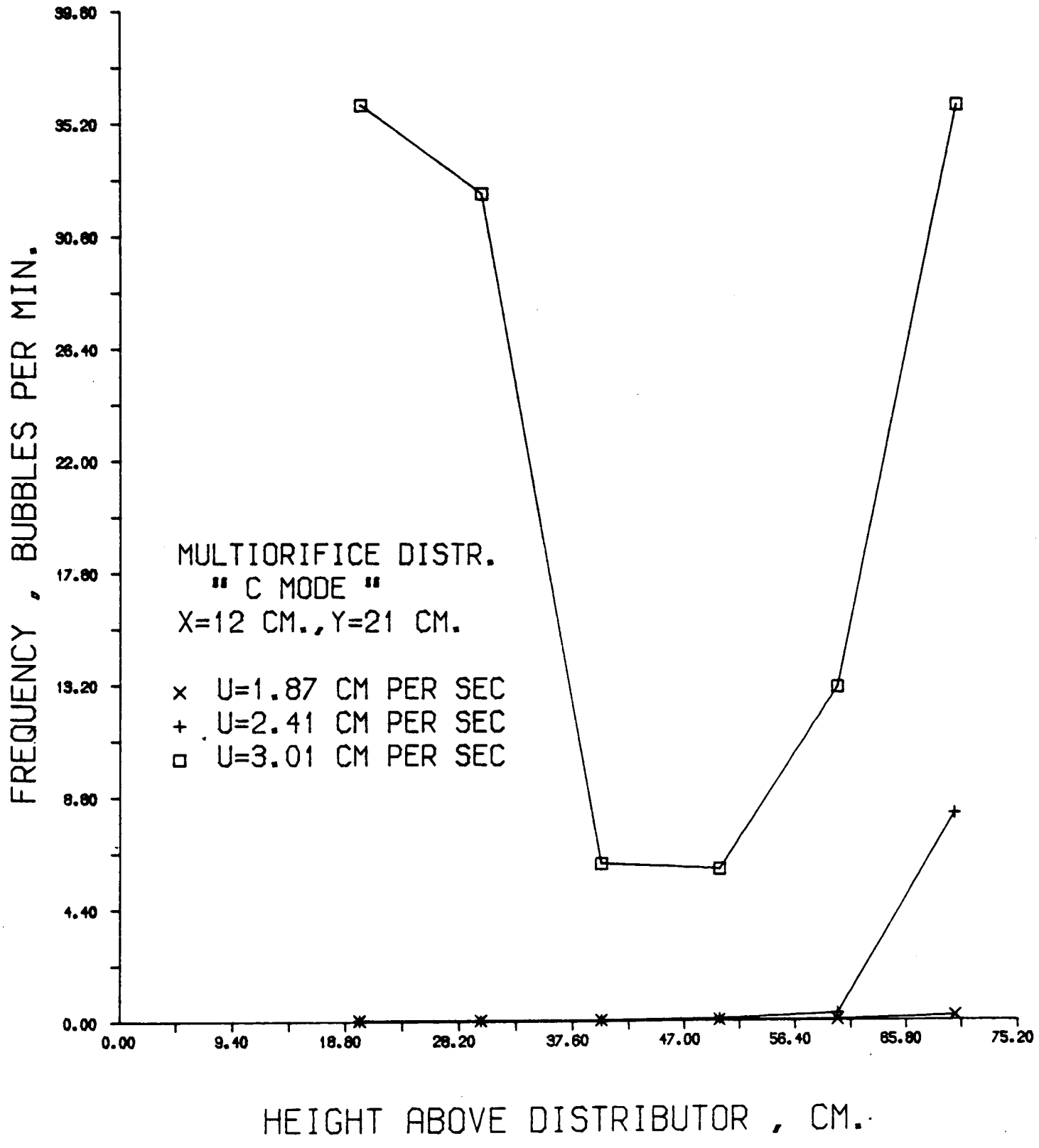
FREQUENCY , BUBBLES PER MIN.
39.60
35.20
30.80
26.40
22.00
17.60
13.20
8.80
4.40
0.00
0.00
9.40
18.80
28.20
37.60
47.00
56.40
65.80
75.20
MULTIORIFICE DISTR.
" C MODE "
X=12 CM.,Y=21 CM.
× U=1.87 CM PER SEC
+ U=2.41 CM PER SEC
□ U=3.01 CM PER SEC
HEIGHT ABOVE DISTRIBUTOR , CM.

Fig. 6.37

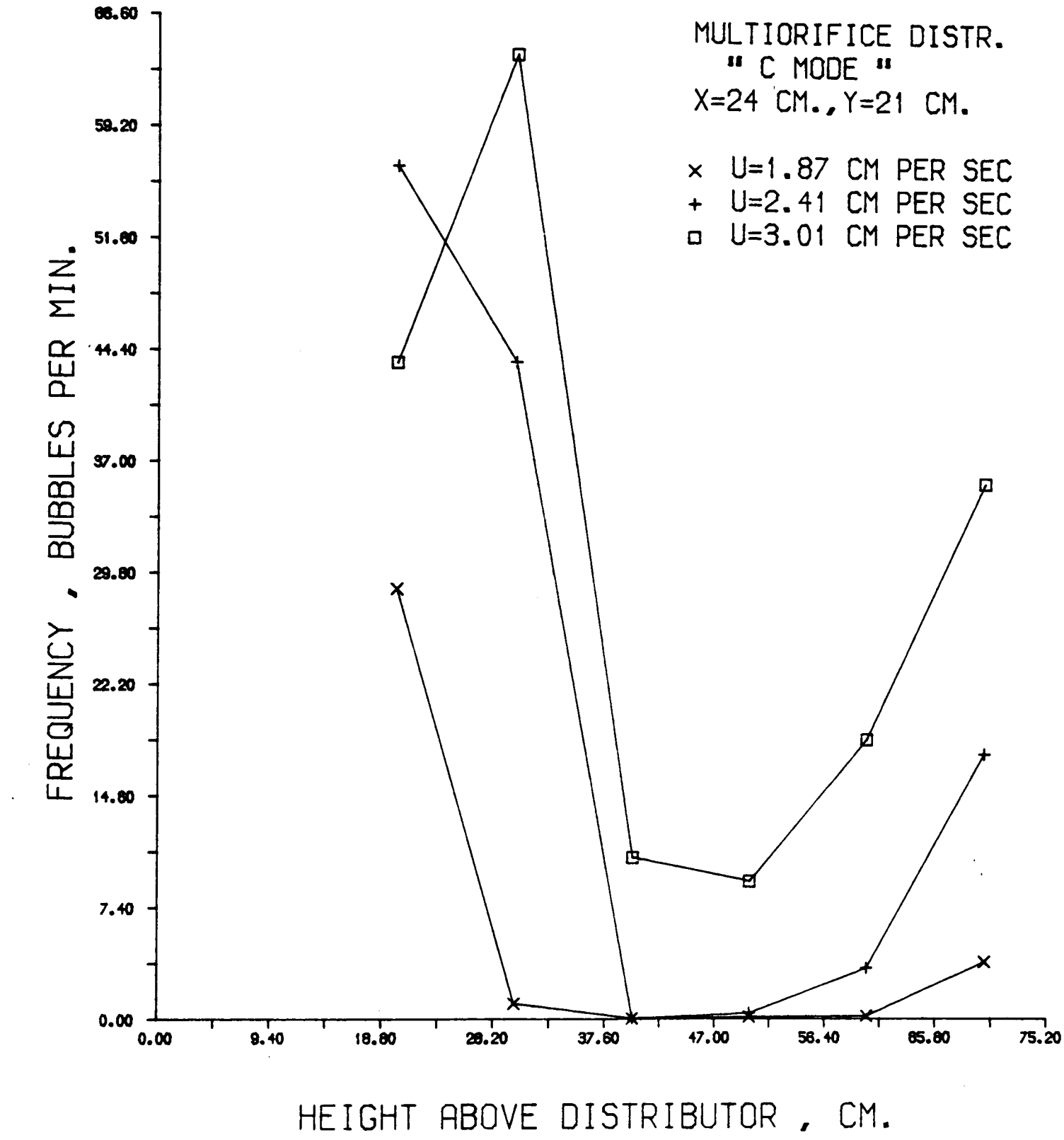
MULTIORIFICE DISTR.
" C MODE "
X=24 CM., Y=21 CM.
× U=1.87 CM PER SEC
+ U=2.41 CM PER SEC
□ U=3.01 CM PER SEC
FREQUENCY , BUBBLES PER MIN.
66.60
59.20
51.80
44.40
37.00
29.60
22.20
14.80
7.40
0.00
0.00
9.40
18.80
28.20
37.60
47.00
56.40
65.80
75.20
HEIGHT ABOVE DISTRIBUTOR , CM.

Fig. 6.38

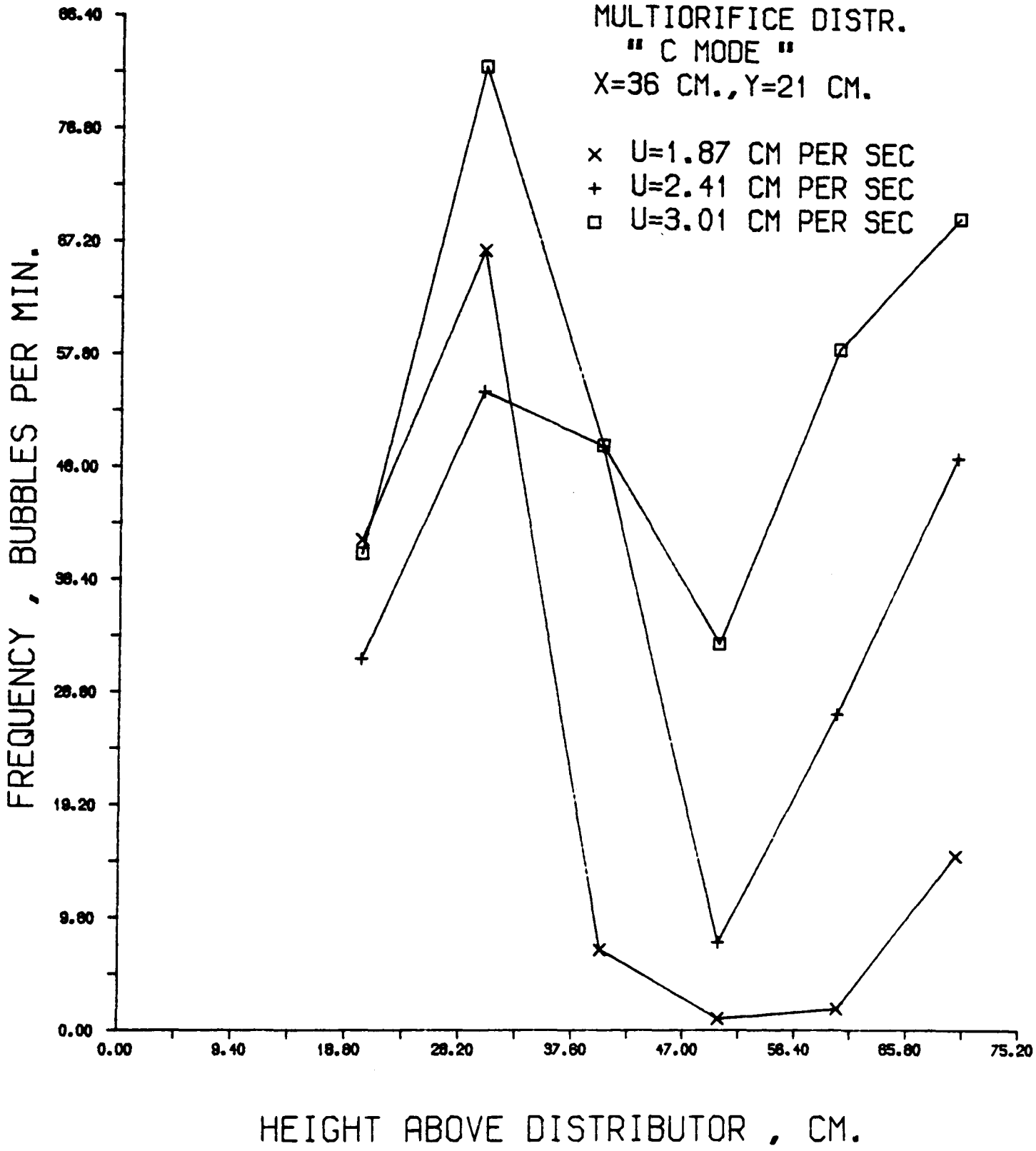
MULTIORIFICE DISTR.
" C MODE "
X=36 CM., Y=21 CM.
× U=1.87 CM PER SEC
+ U=2.41 CM PER SEC
□ U=3.01 CM PER SEC
FREQUENCY , BUBBLES PER MIN.
0.00
9.60
19.20
28.80
38.40
48.00
57.60
67.20
76.80
86.40
0.00
9.40
18.80
28.20
37.60
47.00
56.40
65.80
75.20
HEIGHT ABOVE DISTRIBUTOR , CM.

6.6 Conclusions

Allahwala (1), using a computer model, based on the following assumptions, predicted the bubble frequency variation with height above the distributor plate, as shown in Figure 6.39, below.

He assumed that:

(a) All bubbles were spherical in shape, and the rise velocity of a bubble was not influenced by a leading bubble, except during coalescence.

(b) There was no leakage of gas from bubbles as they were formed at the orifice. Frequency of bubble formation at an orifice remained constant at 20 bubbles per second.

(c) The only assumption made as the criterion of coalescence was that a leading bubble would influence the velocity of a trailing bubble when their nose to nose separation was less than, or equal to, twice the diameter of the leading bubble.

Based on the above-mentioned assumptions, he reported that his model predicted a fairly uniform frequency distribution at low heights in the bed. At intermediate heights, however, the model predicted a zone of high frequency near the bed walls with a relatively low frequency at the wall. Moreover, the model predicts that the zone of high frequency moves towards the bed axis with further increases in height.

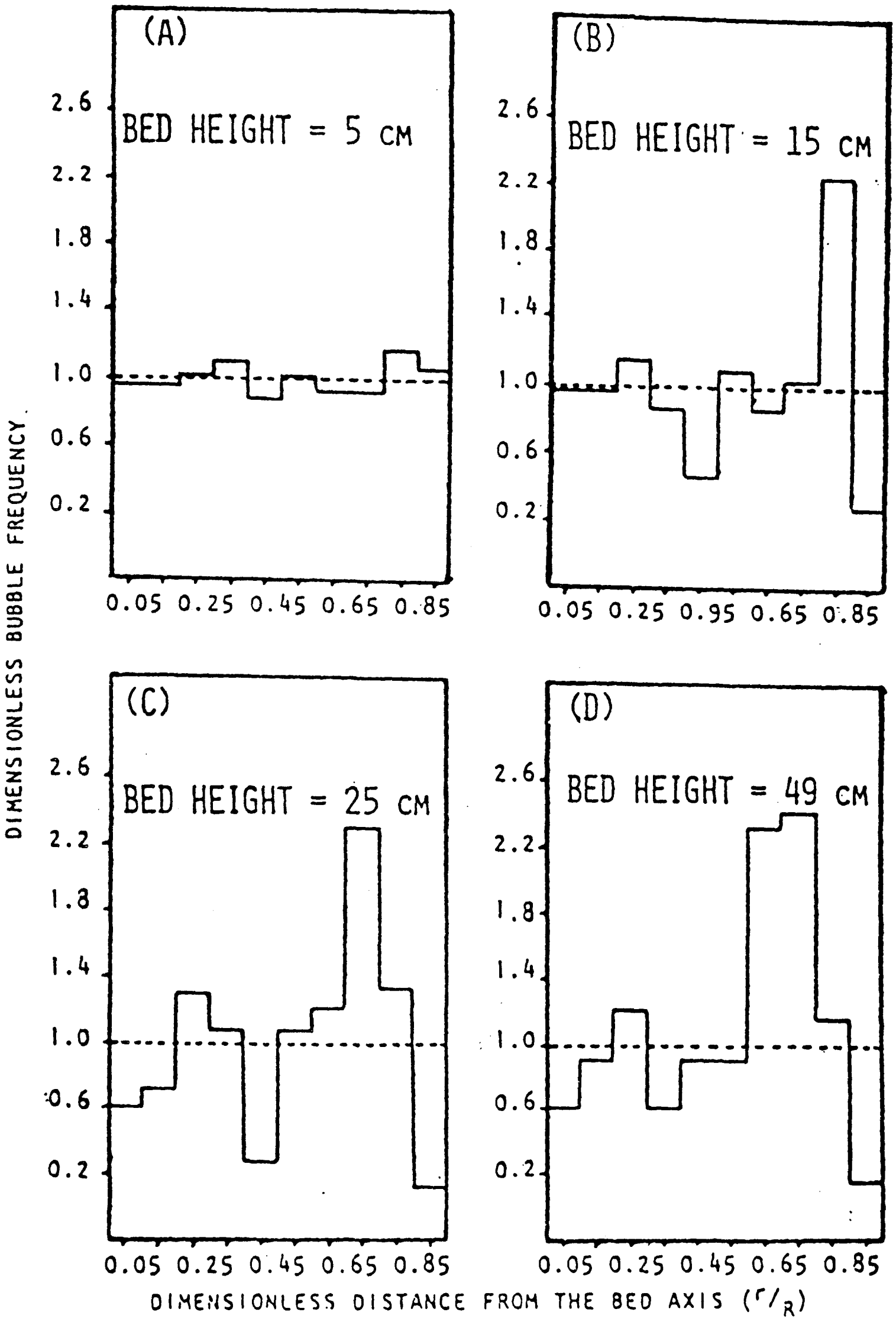

Predicted frequency distributions at different heights in the bed as a function of position when the orifices are in a line and bubble diameter is small compared to the vessel dimensions. Bed height = 55 cm, bed width = 45 cm G_b = 250.0 $cm^3\ sec^{-1}\ W^{-1}$.

FIG. 6.39

Although the data in this chapter show a bewildering complexity of variation with the experimental parameters, nevertheless, some general patterns have emerged which can be summarised as follows:

1. Particle circulation patterns in the bed affect the bubble frequency distribution across the bed cross-sectional area. They enhance the bubble frequency when the probe position (i.e. the sampling points) happens to coincide with the upward movement of these patterns. This is clearly demonstrated when the frequency distributions near the "front" and "back" walls of the bed are compared (Figures (6.31 - 6.33) to Figures (6.36 - 6.38)).

   Furthermore, at certain positions we encounter a trend of frequency increasing with height up to ∿40 cm above the distributor plate, whence it decreases. This reversal probably coincide with a change of direction of the particle phase circulation patterns in the bed. These circulation patterns have an upward direction near the vessel wall, at low elevations, moving towards the central zones as the elevation above the distributor is increased. There is some evidence that higher bubble frequencies are recorded near the vessel walls, close to the distributor plate. Conversely, points of high bubbling activity (and high bubble frequencies) are located in central zones at higher elevations.

In Figure 6.40 below, these circulation patterns are shown for a bed with a depth of 42 cm.

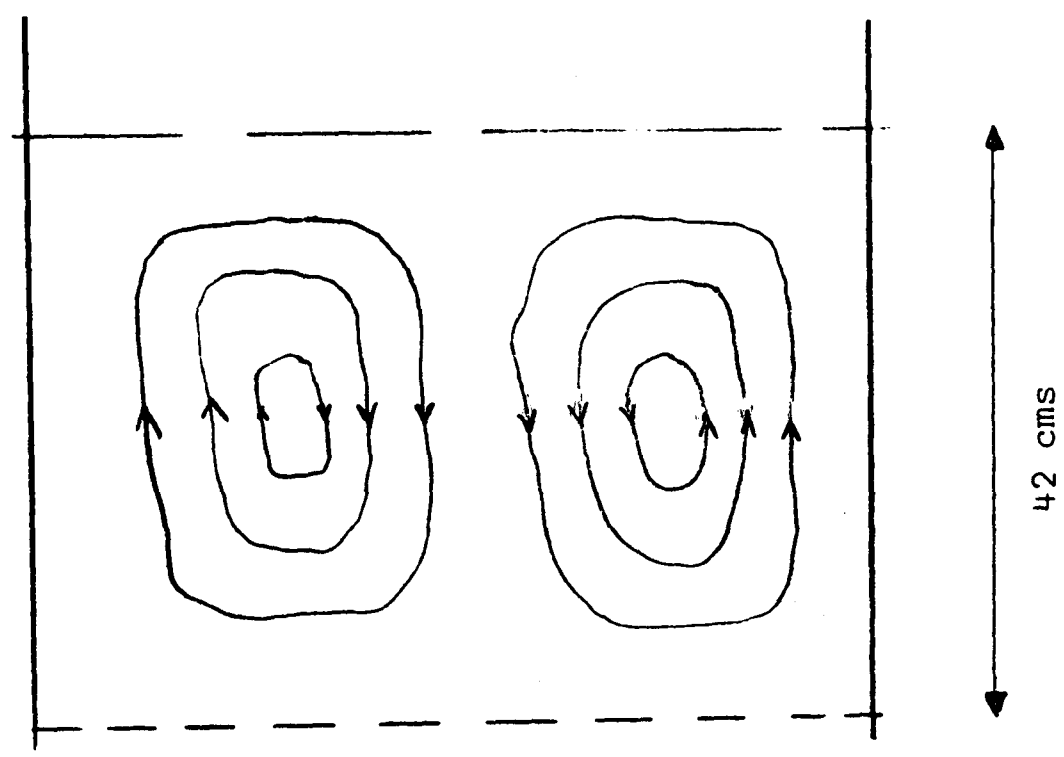

Fig. (6.40)

The binodal shape of the centreline frequency-elevation curve for the multiorifice distributor could be explained by Fig. 6.40. The readings for Z = 20, 30 and 40 cm were taken with a bed depth of 42 cm and the flow situation would be the same in each case. The particle circulation patterns could cause the bubbles to be carried away from the probe position.

2. At some positions in the bed, there are no bubbles to be found, suggesting that the circulation patterns carry the bubbles away from these positions. It also could be due to inactive orifices (when the multiorifice distributor is employed), especially at low superficial fluidising velocities. The evidence for the latter is the existence of very low bubble frequencies measured with U = 1.87 $cm.sec^{-1}$, at certain points across the bed cross-section. This phenomenon

persists at all the six elevations investigated at some of these points, Figs. (6.33,6.36). When the superficial fluidising velocity is increased, this picture changes and reasonable frequencies are recorded at these points. With a further increase in gas flow rate, the bubble frequencies increase appreciably, indicating an increase in the number of active perforations. This argument is reinforced by the fact that the experimental data, obtained under identical operating conditions, but using the porosint distributor, does not show such an irregular pattern with $U = 1.87\ cm.sec^{-1}$. Most of the frequency-elevation graphs for the porosint plate distributor follow a similar pattern for all three superficial fluidising velocities used.

3. The truncation of the bubble size distribution by the probe must have an effect on the spatial frequency distributions measured at various elevations above the distributor plate. Consider the frequency-size variation for two different elevations in the bed. Invariably, we find that the two curves intersect at a point marginally to the right of the cut-off point, shown below:

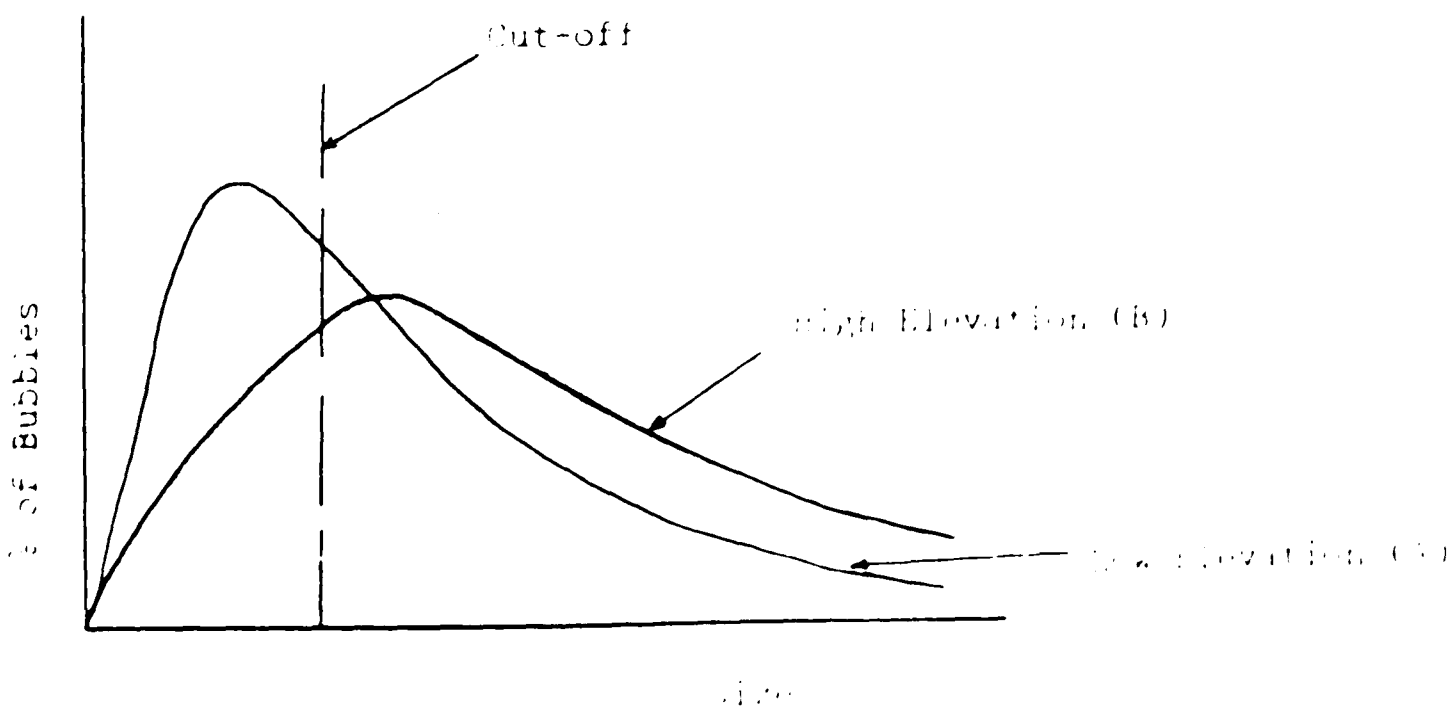

The area under curve A is greater than that under curve B, indicating more bubbles, but the part of the area to the right of the cut off is less, indicating apparently less bubbles to the monitor.

The porosint distributor generates large numbers of small bubbles. As these rise and coalesce the number of bubbles in the range of measurement actually increases, giving the observed behaviour. The multiorifice distributor, which generates a smaller proportion of larger bubbles, first show an increase as more bubbles move into the measured range, followed by a decrease as the total number declines further by coalescence.

4. Finally, the reduced frequency due to coalescence as elevation in the bed increases must be one of the reasons why at high elevations (i.e. 60 - 70 cm) above the distributor plate, the least uniform frequency distributions are encountered.

   Very high bubbling activity concentrated at a few points, together with very low bubble frequencies in the neighbouring regions, reflect the effect of coalescence on the spatial frequency distributions in the bed.

CHAPTER 7

Effect of an Immersed Tube-Bank in the Bed

7.1 Experiments with Tube-Bank in the Bed

Bubble frequencies and rise velocities were measured, with the tube-bank immersed in the bed, at the nine symmetrically distributed points, mentioned earlier, but at only three elevations of 50, 60 and 70 cm above the distributor plate. The bed height was always 82 cm and three superficial fluidising velocities (1.87, 2.41 and 3.01 $cm.sec^{-1}$) were investigated.

These experiments were carried out with both gas distributors. All the bubble frequencies measured are in 'B' mode.

7.1.1 Rise Velocity-Size Relationship

Variation with Superficial Fluidising Velocity

Figure (7.1) shows the rise velocity-size variation for three gas velocities of 1.87, 2.41 and 3.01 $cm.sec^{-1}$ when the porosint plate is employed. The data is collected at a point with X = 24 cm, Y = 7 cm and Z = 50 cm coordinates. Clearly, the bubbles exhibit considerable scatter, especially at high gas flow rates.

Bubble rise velocities are greater for the lower gas velocity of 1.87 $cm.sec^{-1}$ in the lower size-ranges, but gradually the pattern changes and at higher gas flow rates, greater rise velocities are measured for larger bubbles.

Fig. 7.1

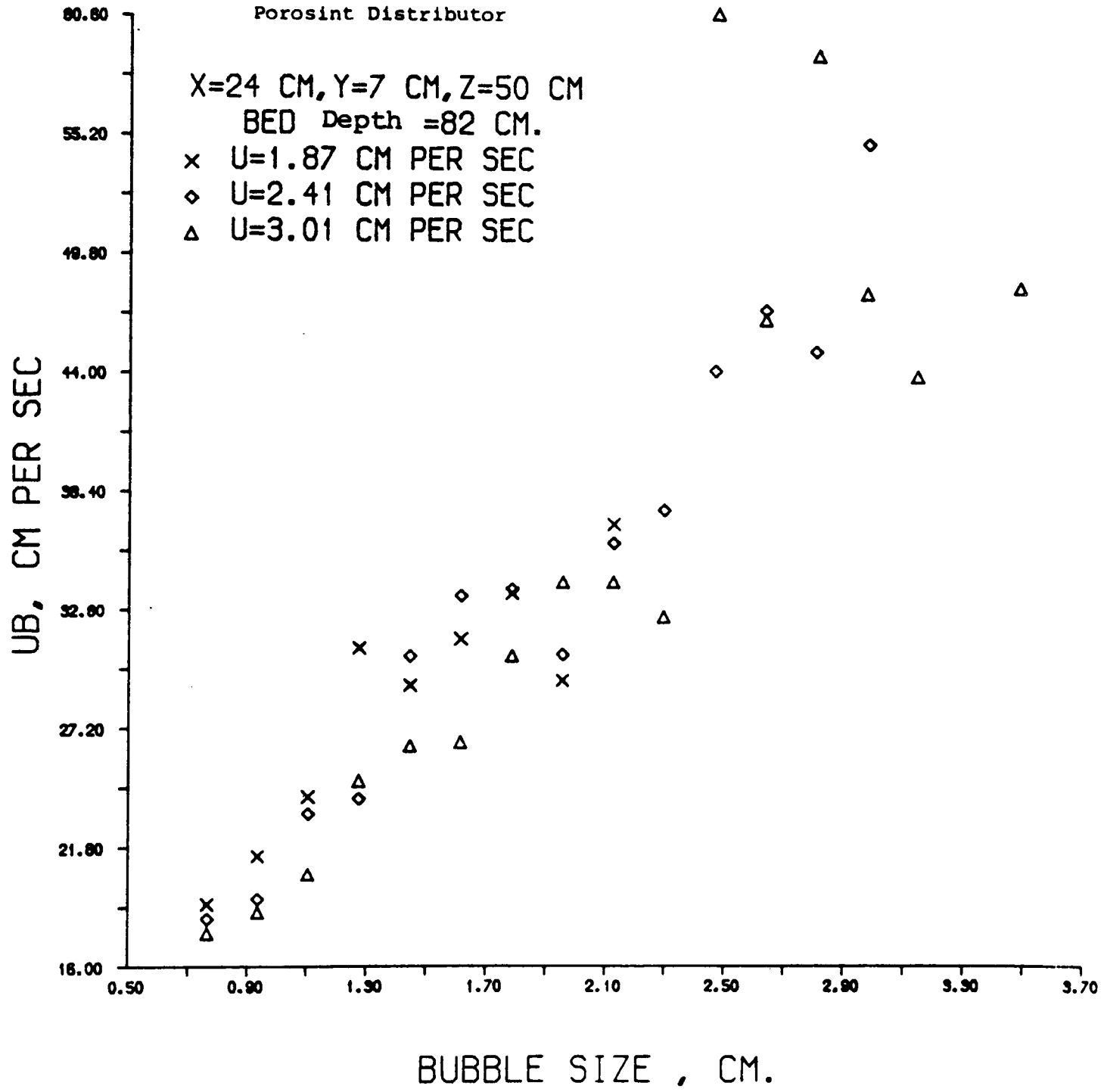
Porosint Distributor
X=24 CM, Y=7 CM, Z=50 CM
BED Depth =82 CM.
× U=1.87 CM PER SEC
◇ U=2.41 CM PER SEC
△ U=3.01 CM PER SEC
CM PER SEC
UB,
60.80
55.20
49.60
44.00
38.40
32.80
27.20
21.60
16.00
0.50
0.90
1.30
1.70
2.10
2.50
2.90
3.30
3.70
BUBBLE SIZE , CM.

Figure (7.2) shows the same variation for the same point and under identical conditions except for the type of distributor plate. In this case the multiorifice distributor is employed. The bed depth is 82 cm in Figures (7.1) and (7.2).

Figure (7.2) shows that for a given bubble size the rise velocities are ordered U = 1.87 > U = 2.41 > U = 3.01 $cm.sec^{-1}$.

Another feature of this graph (Figure 7.2) is the small scatter compared to Figure (7.1) produced by the porosint plate distributor. It is interesting to remember that this point (X = 24 cm, Y = 7 cm, Z = 50 cm), seemed to coincide with the upward movement of the particle phase circulation patterns in the experiments carried out without the solid obstacles . When the bed was filled to a maximum depth of 82 cm (which is the case here, too) the large circulation patterns were shown to be moving upwards near the "front wall" of the bed at a corresponding point. But here we witness a phenomenon (namely, the higher the superficial gas velocity the lower the rise velocity for each interval of bubble height) which is associated with points on the downward flow of the emulsion phase. This could be due to the fact that 50 cm above the distributor plate is actually 20 cm above the top array of the tubes immersed in the bed. In this respect, the tube-bank seems itself to be acting as a kind of distributor or redistributor. Therefore, a very different particle phase flow pattern seems to exist with the tube-bank present.

It is interesting to observe that again the magnitude of the rise velocities recorded, for each interval of bubble height, is greater when the porosint plate is used as the gas distributor.

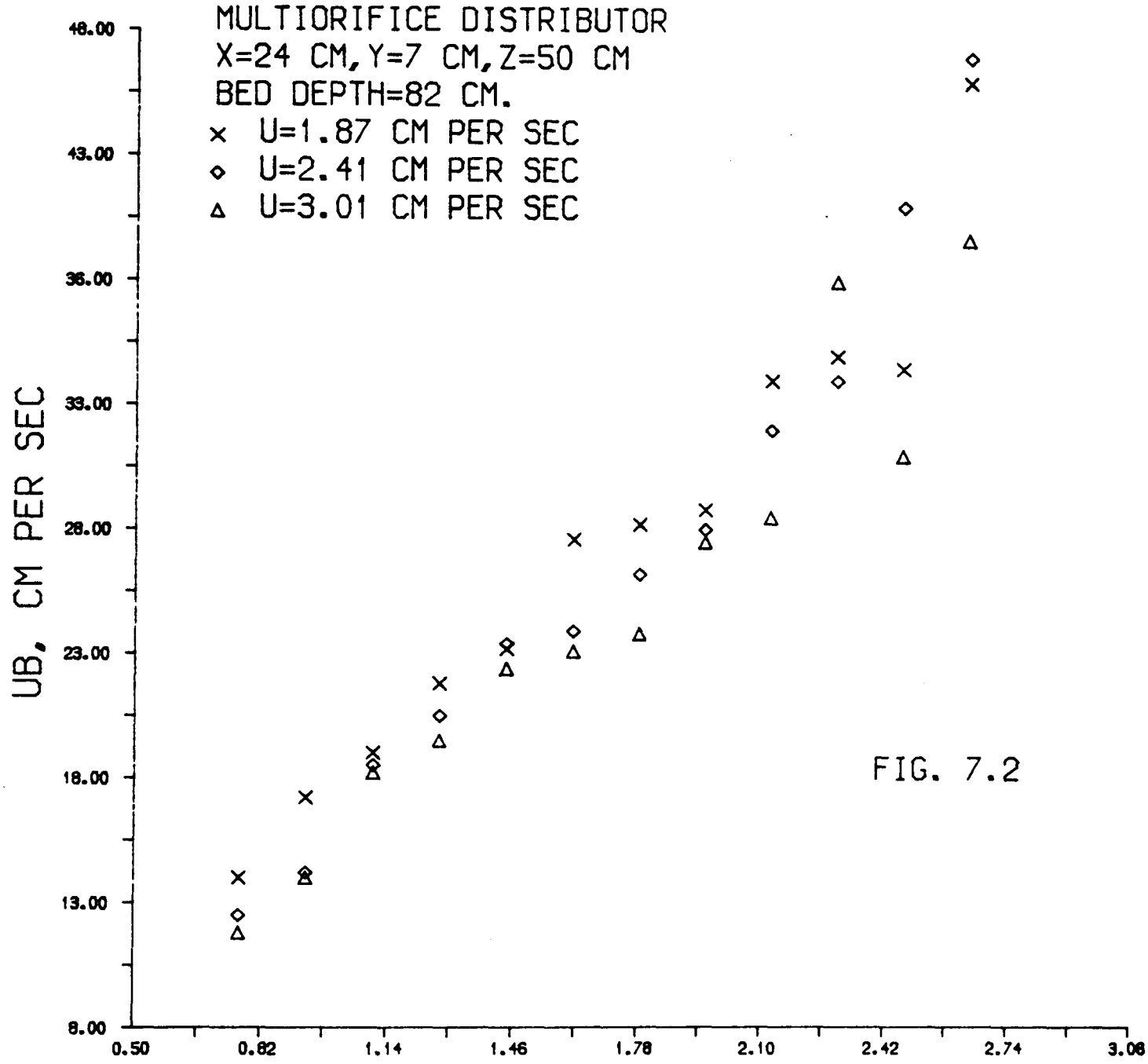
MULTIORIFICE DISTRIBUTOR
X=24 CM, Y=7 CM, Z=50 CM
BED DEPTH=82 CM.
× U=1.87 CM PER SEC
◇ U=2.41 CM PER SEC
△ U=3.01 CM PER SEC
UB, CM PER SEC
48.00
43.00
38.00
33.00
28.00
23.00
18.00
13.00
8.00
0.50
0.82
1.14
1.46
1.78
2.10
2.42
2.74
3.06
BUBBLE SIZE , CM.

FIG. 7.2

L

Figure (7.3) shows this variation at 70 cm above the distributor plate but on the same vertical axis and for the same operating conditions as in Figure (7.2). The same pattern of rise velocity variation with bubble size prevails in Figure (7.3), in that, for each interval of bubble height, greater rise velocities have been recorded for lower superficial fluidising velocities. In fact the difference in the magnitude of the rise velocity U_b, found between the two sets of data (for U = 1.87 and U = 2.41), in Figure (7.3) is more pronounced than the corresponding values in Figure (7.2).

7.1.2 Variation with Height

Figure (7.4) shows the variation of the bubble rise velocities with the measured size, at three different elevations above the porosint distributor plate. The points are on the vertical with X = 24 cm and Y = 7 cm coordinates, and the superficial fluidising velocity is fixed at U = 3.01 $cm.sec^{-1}$. There does not seem to be a significant difference in the magnitude of the bubble rise velocities corresponding to the three elevations, in lower size-ranges.

Bubbles, again exhibit considerable scatter in the greater size-ranges ($\geqslant 5 \times \ell$).

In Figure (7.5), this variation is shown for the bubbles generated by the multiorifice distributor. Three points at the same elevations of 50, 60 and 70 cm above the distributor and on the same vertical

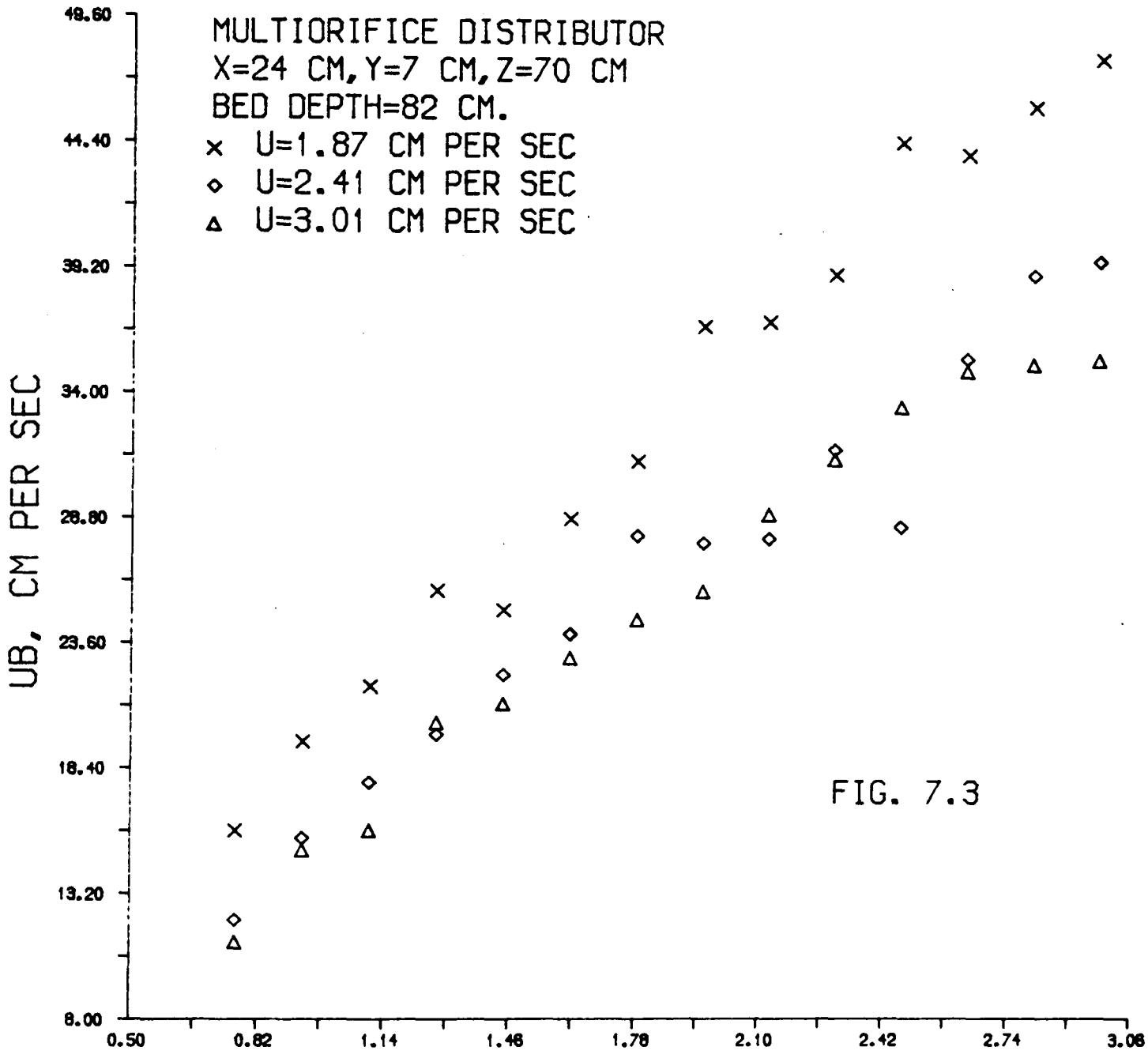
MULTIORIFICE DISTRIBUTOR
X=24 CM, Y=7 CM, Z=70 CM
BED DEPTH=82 CM.
× U=1.87 CM PER SEC
◇ U=2.41 CM PER SEC
△ U=3.01 CM PER SEC
UB, CM PER SEC
49.60
44.40
39.20
34.00
28.80
23.60
18.40
13.20
8.00
0.50
0.82
1.14
1.46
1.78
2.10
2.42
2.74
3.06
BUBBLE SIZE , CM.

FIG. 7.3

Fig. 7.4

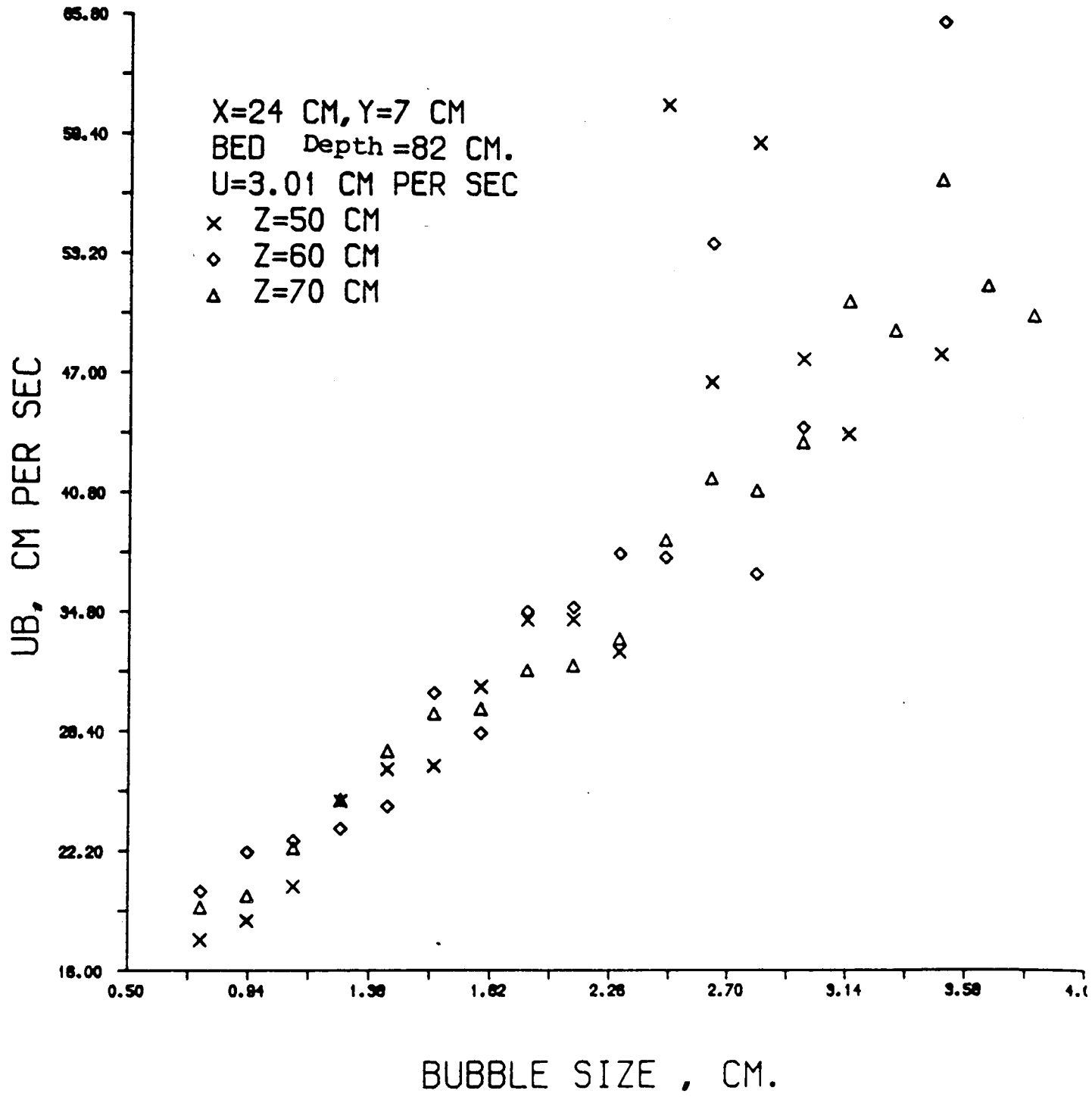
X=24 CM, Y=7 CM
BED Depth =82 CM.
U=3.01 CM PER SEC
× Z=50 CM
◇ Z=60 CM
△ Z=70 CM
UB, CM PER SEC
65.80
59.40
53.20
47.00
40.80
34.60
28.40
22.20
16.00
0.50
0.84
1.38
1.82
2.26
2.70
3.14
3.58
BUBBLE SIZE , CM.

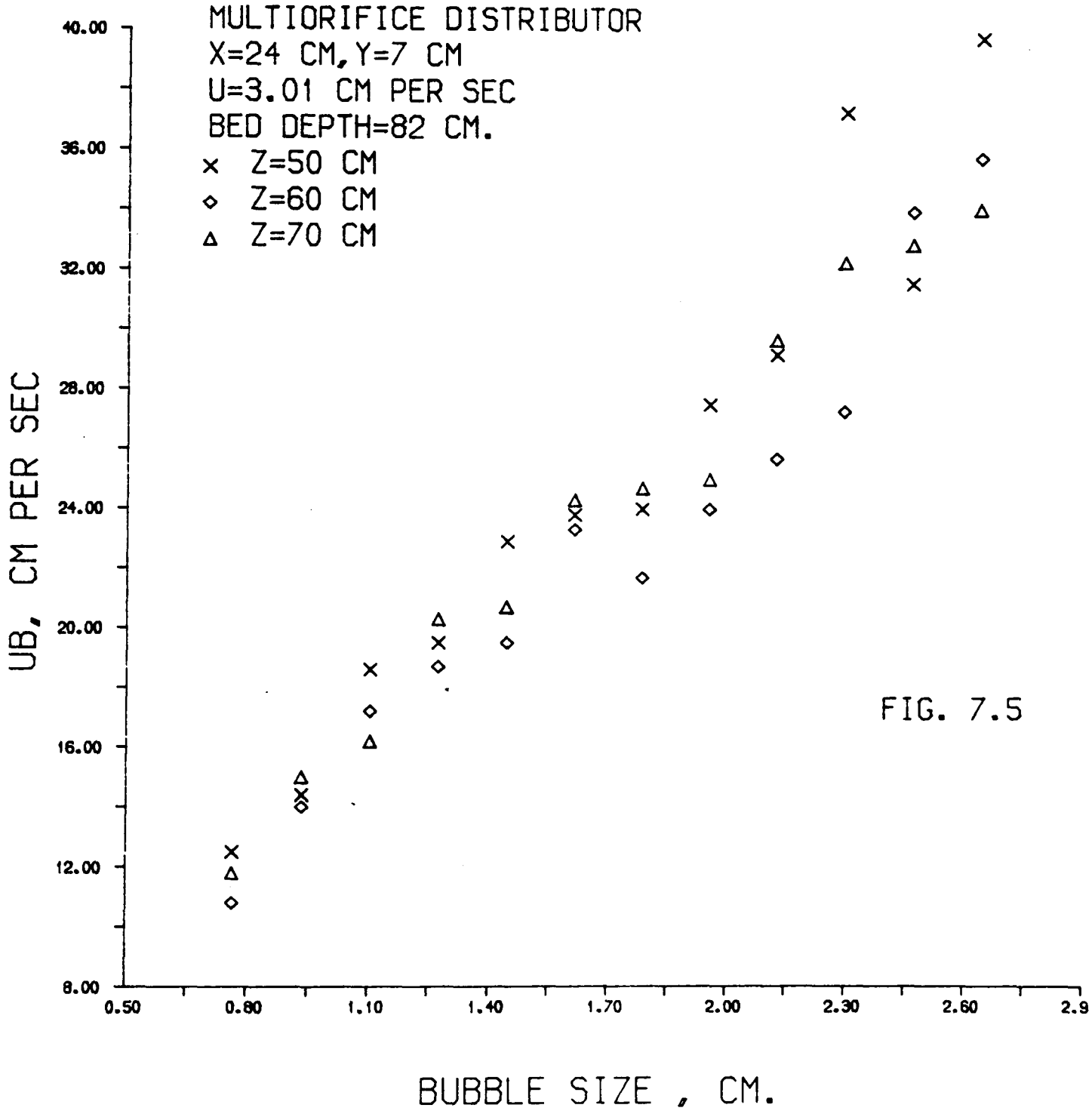
MULTIORIFICE DISTRIBUTOR
X=24 CM, Y=7 CM
U=3.01 CM PER SEC
BED DEPTH=82 CM.
× Z=50 CM
◇ Z=60 CM
△ Z=70 CM
UB, CM PER SEC
40.00
36.00
32.00
28.00
24.00
20.00
16.00
12.00
8.00
0.50
0.80
1.10
1.40
1.70
2.00
2.30
2.60
2.9
BUBBLE SIZE , CM.

FIG. 7.5

axis are selected. The same superficial fluidising velocity, ($U = 3.01$ cm.sec^{-1}) and the same bed depth of 82 cm are maintained. Again, the experimental points show very little scatter and there does not seem to be a significant difference between the three sets of data.

Bubble rise velocity does not change significantly in 20 cm (from $Z = 50$ cm to $Z = 70$ cm) with the tube-bank in the bed. Again, rise velocities measured with the porosint distributor employed are greater than the corresponding values with the multiorifice distributor present.

7.1.3 Variation Across the Bed Cross-Section

Table (7.1) shows the rise velocity-size relationship for bubbles generated by the porosint distributor at three points along the central X-axis. All three points are on the $Z = 50$ cm plane, the bed depth is 82 cm and the superficial fluidising velocity is fixed at 3.01 cm.sec^{-1}. The data for the three points show very small differences in the magnitude of the rise velocities. The bubbles near the "right hand side" wall seem to be rising slightly faster than those near the "left side wall" of the bed.

Size (cm)	U_B(X = 12 cm)	U_B(X = 24 cm)	U_B(X = 36 cm)
0.765	17.962	18.768	19.454
0.935	20.482	20.350	21.128
1.105	21.648	21.998	22.444
1.275	24.212	24.459	25.560
1.445	24.854	23.387	26.795
1.615	27.911	28.643	27.891
1.785	30.970	29.647	31.451
1.955	33.143	34.752	39.683
2.125	35.318	31.522	39.683
2.295	41.002	38.043	42.764
2.465	43.633	37.823	39.293
2.635	36.758	41.358	45.582
2.805	52.696	42.862	46.290
2.975	-	40.889	-
3.145	56.197	39.610	45.718
3.315	-	42.657	65.611
3.485	-	50.772	61.866
3.655	-	44.024	-
3.825	-	-	66.700

TABLE (7.1)

Z = 50 cm

U = 3.01 cm.sec^{-1}

Y = 14 cm

Porosint Distributor

In Table (7.2), the same variation is shown for three points on a higher plane, Z = 70 cm above the distributor plate. The porosint distributor is employed and all the operating conditions are identical to those in Table (7.1). No significant change is revealed. It seems that the circulation patterns prevalent in the bed without the solid obstacles disappear, or the effect of these on the bubble rise velocity is much reduced, when the tube-bank is immersed in the bed .

Size (cm)	U_B(X = 12 cm)	(U_B at X = 24)	U_B(X = 36 cm)
0.765	23.760	21.187	23.917
0.935	22.825	21.973	23.526
1.105	25.450	21.854	24.830
1.275	27.886	29.002	26.717
1.445	28.238	28.062	30.752
1.615	31.363	30.496	31.216
1.785	34.349	30.145	33.301
1.955	37.354	34.654	37.969
2.125	40.538	35.279	35.657
2.295	44.874	51.519	41.236
2.465	42.989	36.358	41.080
2.635	48.257	52.584	40.015
2.805	46.978	48.409	47.969
2.975	54.488	50.411	52.896
3.145	50.674	60.909	57.603
3.315	-	48.458	50.455
3.485	61.915	67.794	62.920
3.655	-	-	60.596
3.825	-	-	61.006
3.995	63.331	-	-

TABLE (7.2)

Z = 70 cm

U = 3.01 cm.sec^{-1}

Y = 14 cm

Porosint Distributor

Table (7.3) shows the rise velocity-size variation for the same three points as in Table (7.2) (and under identical operating conditions), except that the multiorifice distributor plate is employed.

The only change is a marked difference in the rise velocities of bubble measured near the "right hand side wall"* of the bed. These are significantly greater than corresponding values at the other two points. It must be noted that these are all significantly less than the corresponding rise velocities of bubbles generated by the porosint distributor.

To extend this comparison between the distributors , Table (7.4), which is directly comparable to Table (7.1), is tabulated below. All the operating conditions are identical in these tables except that two different distributors are employed.

A comparison of Tables (7.1) and (7.4) shows much smaller velocities measured when the multiorifice distributor is used. Otherwise, a similar pattern is revealed in that the experimental points are very close, and no significant difference is found, in the rise velocities for corresponding intervals of bubble height.

* i.e. at higher values of x.

Size (cm)	U_B(X = 12 cm)	U_B(X = 24 cm)	U_B(X = 36 cm)
0.765	13.951	13.032	18.526
0.935	17.911	17.083	21.136
1.105	19.300	19.761	21.439
1.275	25.057	21.329	26.168
1.445	23.472	24.014	31.421
1.615	26.956	25.084	32.295
1.785	27.606	26.573	36.424
1.955	39.586	28.846	35.377
2.125	37.252	27.198	36.895
2.295	32.471	29.781	38.052
2.465	35.076	37.596	41.143
2.635	40.889	46.695	44.249
2.805	34.595	37.889	45.059
2.975	46.768	44.014	45.157
3.145	56.104	42.979	47.315
3.315		49.410	46.094
3.485		50.132	43.868
3.655		55.420	46.622
3.825		66.534	61.719
3.995			52.481
4.165			57.862
4.335			64.844
4.505			68.062
4.675			88.077

TABLE (7.3)

Z = 70 cm

U = 3.01 $cm.sec^{-1}$

Y = 14 cm

Multiorifice Distributor

Size (cm)	U_B(X = 12 cm)	U_B(X = 24 cm)	U_B(X = 36 cm
0.765	14.676	13.334	12.757
0.935	17.930	14.419	14.908
1.105	19.332	17.884	19.034
1.275	22.703	21.048	21.517
1.445	24.756	22.686	21.893
1.615	26.150	26.036	28.765
1.785	30.601	25.687	26.756
1.955	28.060	27.015	28.743
2.125	34.024	34.297	32.925
2.295	29.639	30.513	30.250
2.465	33.448	48.721	31.846
2.635	38.257	34.998	35.525
2.805	-	34.791	42.364
2.975	40.420	-	43.126
3.145	-	40.171	-
3.315	-	42.320	-

TABLE (7.4)

Z = 50 cm

U = 3.01 $cm.sec^{-1}$

Y = 14 cm

Multiorifice Distributor

Table (7.5) shows the rise velocities of bubbles at three points along the shorter centre-plane, all three on the Z = 50 cm plane. The superficial fluidising velocity is fixed at 3.01 cm/sec and the bed depth is 82 cm. In this table, the rise velocities of bubbles generated by the porosint distributor are tabulated against the bubble size. The bubble rise velocity recorded for each interval of bubble height is greater at 21 cm (near the "back" wall of the bed), than at the other two points. The data shows the smallest rise velocities measured near the "front" wall of the bed.

It was suggested, (Figure 7.1), that the particle phase circulation patterns moved downward near the "front" wall of the bed. This is reinforced by observing the data in Table (7.5).

In Table (7.6) the rise velocities of bubble of various "sizes" are tabulated, for three points, again on the "shorter" centre-plane, but all three at a higher elevation of 70 cm above the porosint distributor plate. All the operating conditions are the same as for Table (7.5). Again, rise velocities of greater magnitude than at the other two points are measured at Y = 21 cm but the differences in the three sets of data are not so pronounced as in Table 7.5 . For larger bubbles the difference is not significant at all. Nevertheless, it is an indication of the still prevalent pattern of the particle phase circulation patterns moving upwards near the "back wall" of the bed and downwards near the "front wall".

Size (cm)	U_B(Y = 7 cm)	U_B(Y = 14 cm)	U_B(Y = 21 cm)
0.765	17.571	18.768	21.299
0.935	18.565	20.350	22.186
1.105	20.352	21.998	23.873
1.275	24.773	24.459	24.788
1.445	26.412	23.387	31.561
1.615	26.568	28.643	30.308
1.785	30.667	29.647	29.395
1.955	34.173	34.752	33.187
2.125	34.195	31.522	34.429
2.295	32.532	38.043	38.692
2.465	61.021	37.823	41.514
2.635	46.612	41.358	41.421
2.805	59.102	42.862	67.203
2.975	47.837	40.889	60.049
3.145	43.946	39.610	-
3.315	-	42.657	-
3.485	48.135	50.772	-
3.655	-	44.024	-

TABLE (7.5)

Z = 50 cm

U = 3.01 cm/sec.

X = 24 cm

Porosint Distributor

Size (cm)	U_B(Y = 7 cm)	U_B(Y = 14 cm)	U_B(Y = 21 cm
0.765	19.295	21.187	20.543
0.935	19.888	21.973	22.430
1.105	22.357	21.854	24.329
1.275	24.852	29.002	25.467
1.445	27.361	28.062	26.658
1.615	29.288	30.496	28.365
1.785	29.537	30.145	37.681
1.955	31.561	34.654	36.202
2.125	31.819	35.279	44.556
2.295	33.221	51.519	46.739
2.465	38.389	36.358	41.309
2.635	41.617	52.584	38.126
2.805	40.997	48.409	44.659
2.975	43.521	50.411	42.789
3.145	50.875	60.909	55.567
3.315	49.366	48.458	57.754
3.485	57.256	67.794	71.817
3.655	51.749	-	53.150
3.825	50.196	-	-
3.995	-	-	-

TABLE (7.6)

Z = 70 cm

U = 3.01 $cm.sec^{-1}$

X = 24 cm

Porosint Distributor

Tables (7.7) and (7.8) show the same U_B - "Size" variation for bubbles generated by the multiorifice distributor. Table (7.7) shows the data corresponding to the same three points and operating conditions as in Table (7.5). There does not seem to be a significant difference in the three sets of data (corresponding to the three points), but, nevertheless, the bubbles located on the bed vertical axis (the centre point), seem to be rising slightly faster. Even this slight difference diminishes as the bubble size increases.

Table (7.8) shows the data for only two points on the transverse (shorter) centre-plane. Insufficient data could be collected at the Y = 21 cm point. Here, rise velocities significantly greater in magnitude have been measured at the central point. Even for larger bubbles the difference between the two sets of data does not diminish. Together with the evidence of a low bubbling activity near the "back" wall of the bed and the fact that the bubbles are rising faster on the bed vertical axis, this is a clear indication of a change of flow patterns from those produced by the porosint plate distributor.

This observation corroborates the conclusion drawn in Section 7.1.1, (Figures 7.2 and 7.3).

Size (cm)	U_B(Y = 7 cm)	U_B(Y = 14 cm)	U_B(Y = 21 cm)
0.765	12.260	13.334	12.686
0.935	14.572	14.419	15.611
1.105	18.594	17.884	16.631
1.275	18.997	21.048	18.577
1.445	22.571	22.686	20.223
1.615	23.167	26.036	24.151
1.785	23.709	25.687	22.603
1.955	27.713	27.015	25.904
2.125	28.572	34.297	25.867
2.295	37.535	30.513	30.472
2.465	30.565	48.721	27.608
2.635	39.639	34.998	36.819
2.805	-	34.791	-
2.975	-	-	38.150
3.145	-	-	
3.315	59.307	42.320	
3.485	53.775	-	

TABLE (7.7)

Z = 50 cm

U = 3.01 $cm.sec^{-1}$

X = 24 cm

Multiorifice Distributor

Size (cm)	U_B (Y = 7 cm)	U_B (Y = 14 cm)
0.765	11.956	13.032
0.935	15.203	17.083
1.105	15.991	19.761
1.275	20.525	21.329
1.445	20.853	24.014
1.615	23.431	25.084
1.785	24.605	26.573
1.955	25.049	28.846
2.125	29.285	27.198
2.295	31.544	29.781
2.465	33.526	37.596
2.635	34.622	46.695
2.805	35.538	37.889
2.975	32.142	44.014
3.145		42.979
3.315		49.410
3.485		50.132
3.655		55.420
3.825		66.534

TABLE (7.8)

Z = 70 cm

U = 3.01 cm.sec^{-1}

X = 24 cm

Multiorifice Distributor

7.1.4 Comparison of the Rise Velocities With and Without the Tube-Bank

A comparison of the rise velocities measured at elevations of 50, 60 and 70 cm above the distributor plates, with and without the presence of a solid obstacle is given in Tables (7.9) and (7.10) below:

	Z = 50 cm		Z = 60 cm		Z = 70 cm	
Size (cm)	U_B cm/sec (with)	U_B (Without)	U_B (with)	U_B (Without)	U_B (With)	U_B (Without)
0.765	21.753	26.395	21.273	27.125	21.480	29.290
0.935	23.238	27.642	23.218	28.897	26.390	33.077
1.105	23.787	34.134	24.544	29.940	27.449	31.941
1.275	25.071	34.417	27.676	33.760	29.481	31.973
1.445	29.256	35.228	28.992	31.905	30.914	32.896
1.615	28.267	41.387	33.526	38.843	31.202	37.217
1.785	32.930	42.066	31.585	45.132	37.354	39.878
1.955	33.172	44.752	39.537	41.778	38.072	42.027
2.125	37.894	54.961	39.361	48.111	42.037	46.265
2.295	39.322	56.094	39.000	45.694	45.337	49.219
2.465	35.298	47.974	42.960	59.312	54.507	60.235
2.635	41.939	59.800	46.700	47.745	52.608	63.453
2.805	46.143	53.448	48.399	61.939	52.999	52.120
2.975	44.195	63.624	47.242	61.749	53.677	54.463
3.145	48.528	66.797	51.797	69.034	46.192	68.995
3.315					51.905	64.087
3.485					52.960	67.745

TABLE (7.9)

U = 3.01 cm/sec.

X = 36 cm

Y = 7 cm

Porosint Distributor

Multiorifice Distributor

	Z = 50 cm		Z = 60 cm		Z = 70 cm	
Bubble Size (cm)	U_B With	U_B Without	U_B With	U_B Without	U_B With	U_B Without
0.765	14.275	20.665	14.120	20.840	15.010	21.907
0.935	16.179	22.947	17.558	22.769	17.300	20.518
1.105	22.764	24.488	20.613	25.335	18.628	22.459
1.275	21.568	25.276	22.476	25.667	24.195	25.330
1.445	26.273	25.645	24.061	29.022	27.615	27.923
1.615	31.849	31.456	24.625	31.497	26.270	30.872
1.785	27.549	31.124	25.377	29.900	26.673	34.568
1.955	34.156	30.118	29.336	40.274	34.073	37.442
2.125	32.620	33.968	32.989	37.857	31.653	36.470
2.295	33.003	38.057	30.955	33.594	36.019	36.973
2.465	38.511	60.079	44.087	37.125	35.596	44.561
2.635	34.979	52.813	32.720	39.019	31.641	41.148
2.805	43.541	52.706	38.419	43.511	36.951	43.819
2.975	36.246	49.483	50.157	46.524	44.170	54.424
3.145	41.651	57.330	43.624	43.624	35.413	58.018
3.315			47.159	50.684	47.178	50.674

TABLE (7.10)

$U = 3.01$ cm.sec^{-1}

X = 36 cm

Y = 7 cm

Table (7.9) shows the rise velocities of bubbles, generated by the porosint distributor, tabulated against the bubble size, for two sets of experiments, (with and without the tube-bank immersed in the bed). Three points are selected at elevations of Z = 50, 60 and 70 cm above the distributor plate. All the other operating conditions are identical.

Bubble rise velocities, for each interval of bubble height, measured at these elevations are significantly greater when the bed is free of any solid obstacles. It must be remembered that the point of measurement when Z = 50 cm and the tube-bank is present, is only $\sim$20 cm above the top array.

Table (7.10), referring to the multiorifice distributor, shows a similar trend for the three elevations compared. In Table (7.10), the three sets of data corresponding to the bed free of the solid obstacles show greater rise velocities for each interval of bubble height. This, presumably reflects the effect of the particle phase circulation patterns in these two cases.

It is clear that these circulation patterns are very different, which manifests itself in the different bubble rise velocities recorded at the same points with and without the tube-bank in the bed.

Table (7.11) shows the rise velocities at three points 50, 60 and 70 cm above the distributor plate, but on the bed vertical axis. The superficial gas velocity and the bed depth are the same as in Table 7.10. Again, we find much greater bubble rise velocities are recorded in a bed without a solid obstacle. Here, the differences are not as pronounced as in Table (7.10). In fact, at an elevation of 70 cm (in Table 7.11), the differences in the magnitude of the rise velocities are almost non-existent for large bubbles.

This could be due to the relative positions of these points (in these two tables), with respect to the particle circulation patterns prevalent at this elevation in the bed.

Multiorifice Distributor

	Z = 50 cm		Z = 60 cm		Z = 70 cm	
Bubble Size (cm)	With	Without	With	Without	With	Without
0.765	13.334	15.356	12.977	14.484	13.032	17.374
0.935	14.419	19.293	16.670	18.211	17.083	17.787
1.105	17.884	21.165	17.957	19.495	19.761	21.856
1.275	21.048	23.333	19.041	23.521	21.329	24.310
1.445	22.686	29.241	21.793	26.539	24.014	26.397
1.615	26.036	29.417	24.024	26.707	25.084	26.941
1.785	25.687	33.670	24.712	31.959	26.573	33.243
1.955	27.015	32.315	28.003	29.598	28.846	34.673
2.125	34.297	37.850	29.632	37.479	27.198	34.144
2.295	30.513	36.265	33.160	30.396	29.781	34.839
2.465	48.721	39.971	34.976	44.258	37.596	37.266
2.635	34.998	45.543	35.916	39.073	46.695	40.928
2.805	34.791	47.686	38.785	46.382	37.889	38.550
2.975	40.171	55.254	41.348	42.061	44.014	44.376
3.145	42.320	61.739	50.914	-	42.979	53.057

TABLE (7.11)

$U = 3.01\ cm.sec^{-1}$

X = 24 cm

Y = 14 cm

7.2 Bubble Size Distribution

7.2.1 Variation with Superficial Fluidising Velocity

Figure (7.6) shows the variation of bubble size distribution with superficial fluidising velocity at a point on the shorter (transverse) centre-plane at a fixed elevation of 70 cm above the distributor plate.

Frequency decreases very sharply with increasing bubble size at the low velocity of 1.87 $cm.sec^{-1}$, indicating a greater proportion of bubbles in the lower size-ranges.

Figure (7.7) shows the same variation at another point across the bed cross-section, (X = 24 cm, Y = 21 cm). A very similar pattern is revealed. Both graphs show peaks at 8 - 10 mm size-range for the high superficial velocity (U = 3.01 $cm.sec^{-1}$) only. Both graphs represent data generated by the porosint plate distributor.

Figure (7.8) shows the frequency-size distribution at a fixed height of 50 cm above the distributor plate and for the same three gas velocities.

A similar pattern of frequency decreasing with increasing size (as in Figure (7.6) , is revealed. Again, the decrease is steeper for the lowest gas velocity of 1.87 $cm.sec^{-1}$, indicating the greater number of bubbles in the small size-ranges, corresponding to this gas velocity. Figure (7.8) also represents data of bubbles generated by the porosint plate distributor.

Fig 7.6

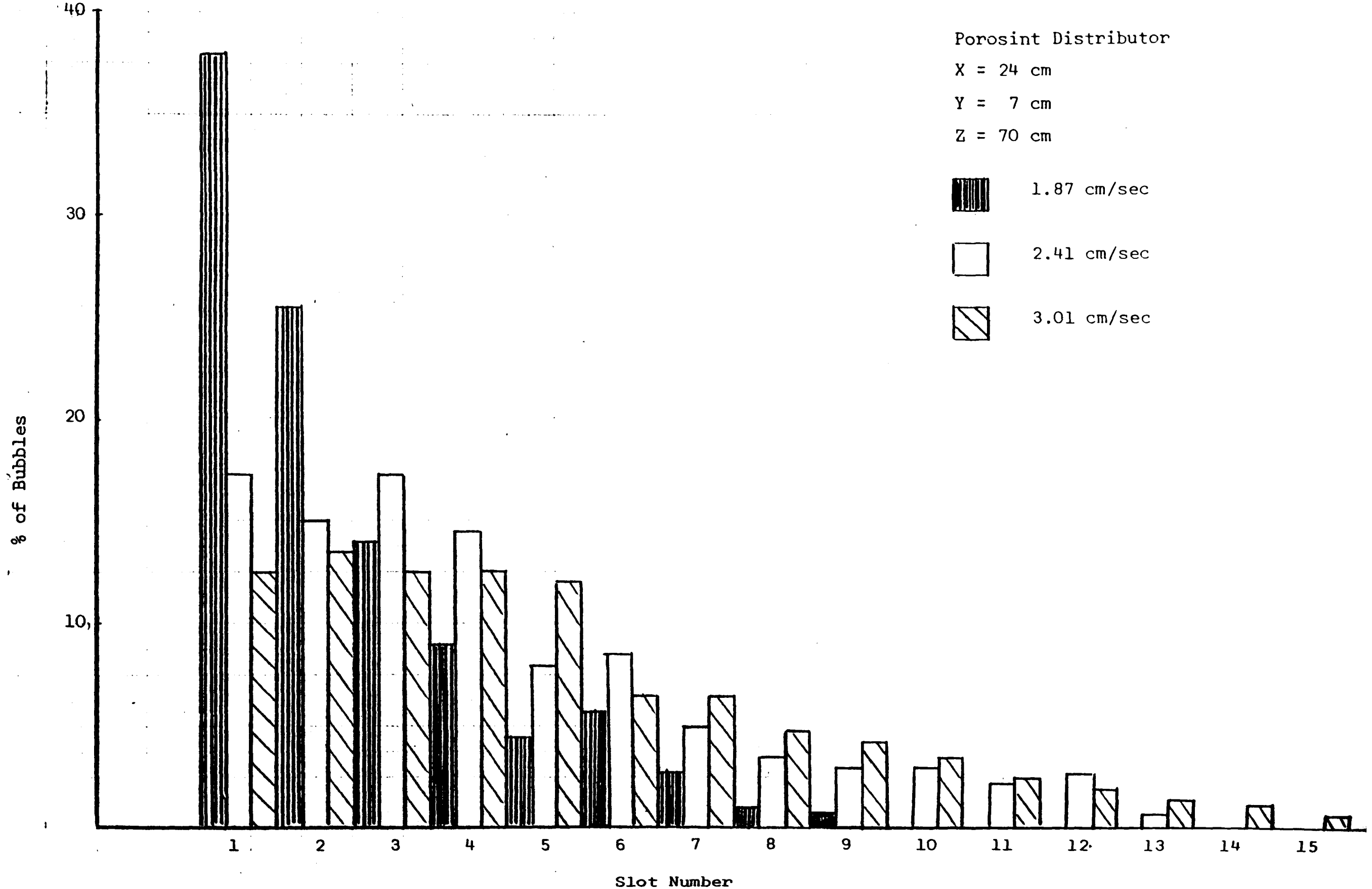
Porosint Distributor
X = 24 cm
Y = 7 cm
Z = 70 cm
1.87 cm/sec
2.41 cm/sec
3.01 cm/sec
% of Bubbles
40
30
20
10
1
2
3
4
5
6
7
8
9
10
11
12
13
14
15
Slot Number

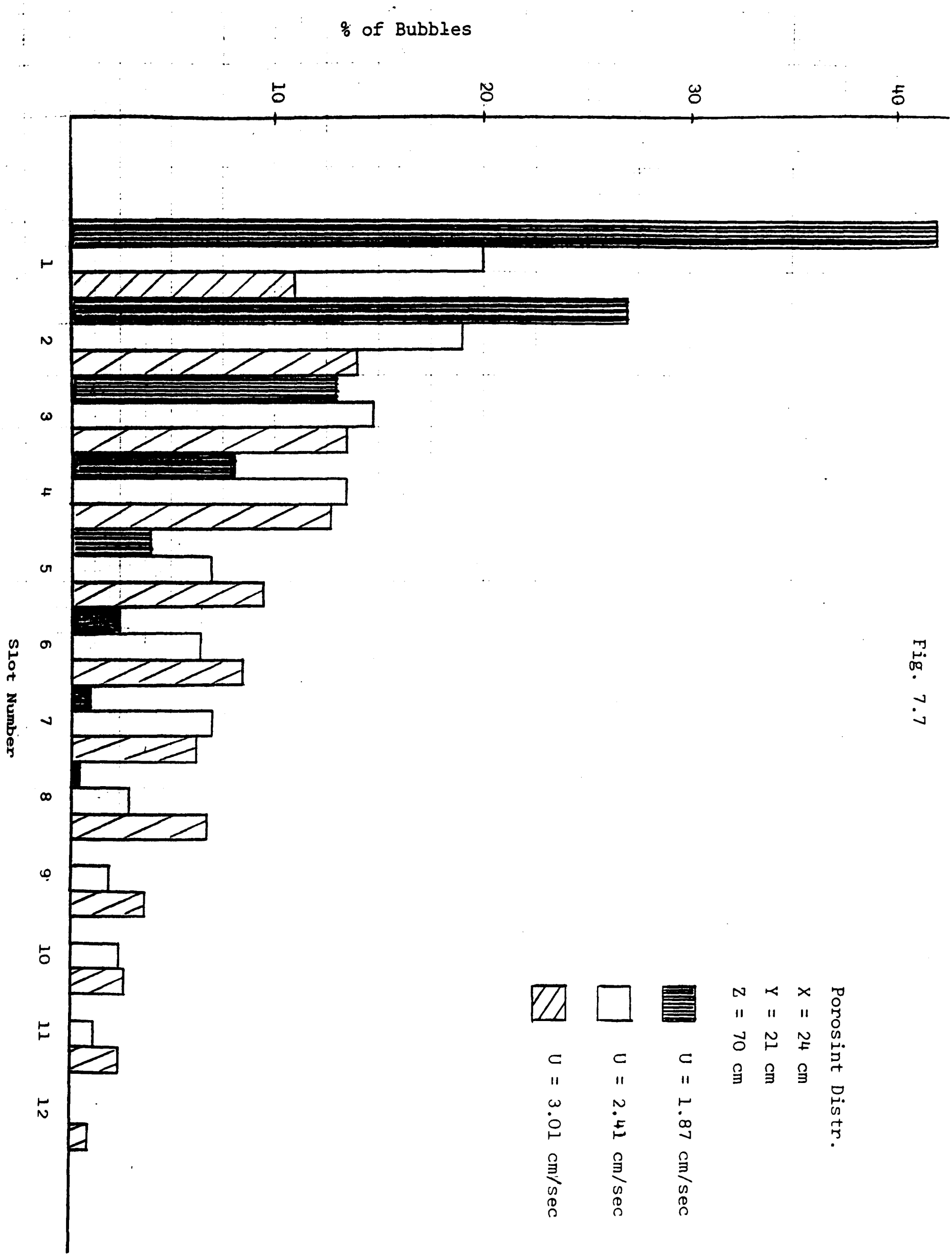
% of Bubbles
10
20
30
40
1
2
3
4
5
6
7
8
9
10
11
12
Slot Number
Porosint Distr.
X = 24 cm
Y = 21 cm
Z = 70 cm
U = 1.87 cm/sec
U = 2.41 cm/sec
U = 3.01 cm/sec

Fig. 7.7

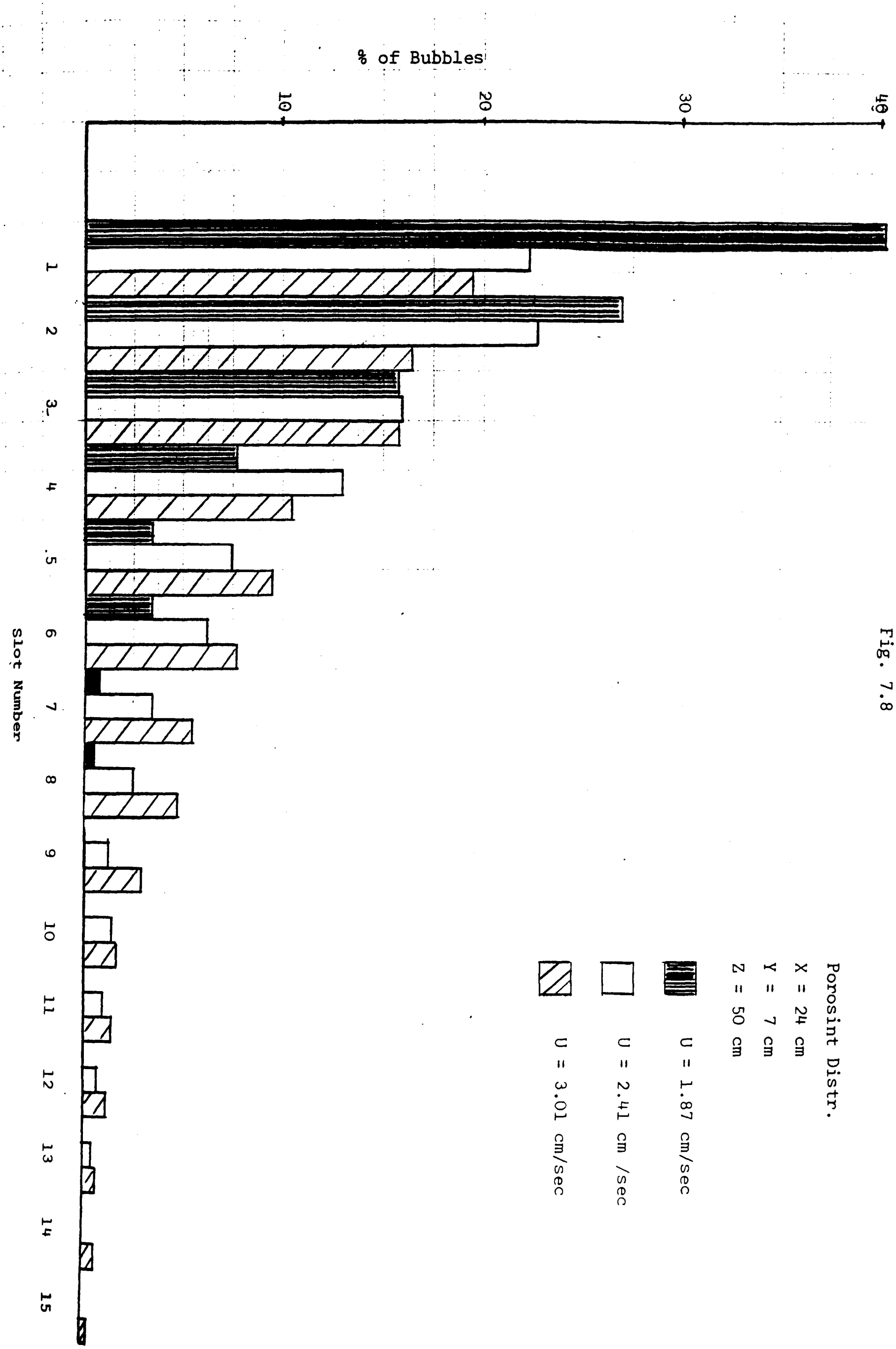
% of Bubbles
10
20
30
40
1
2
3
4
5
6
7
8
9
10
11
12
13
14
15
Slot Number
Porosint Distr.
X = 24 cm
Y = 7 cm
Z = 50 cm
U = 1.87 cm/sec
U = 2.41 cm /sec
U = 3.01 cm/sec

Fig. 7.8

Figure (7.9) shows the variation of bubble size distribution with size for three superficial fluidising velocities, when the multiorifice distributor is employed. None of the histograms shows a peak in the size-range investigated. A comparison of this graph with Figure (7.6), (produced by the porosint distributor but under identical operating conditions), reveals a change in the most frequent size. In Figure (7.6), the histogram corresponding to U = 3.01 cm/sec shows a peak in the 8.5 - 10 mm size-range.

A comparison of the frequencies corresponding to the first interval of bubble height, in these two graphs, shows a much larger frequency ($\sim$22%) for U = 3.01 $cm.sec^{-1}$, when the multiorifice distributor is employed, (compared to $\sim$12% for the porosint distributor).

For larger bubbles, both distributors show a similar trend (of frequency decreasing gradually with increasing bubble size) but the bubble frequency, for each interval of bubble height, is greater for bubbles generated by the porosint plate distributor.

This would seem to indicate the fact that larger bubbles are encountered by the probe in the bed with the porosint plate distributor present.

Fig. 7.9

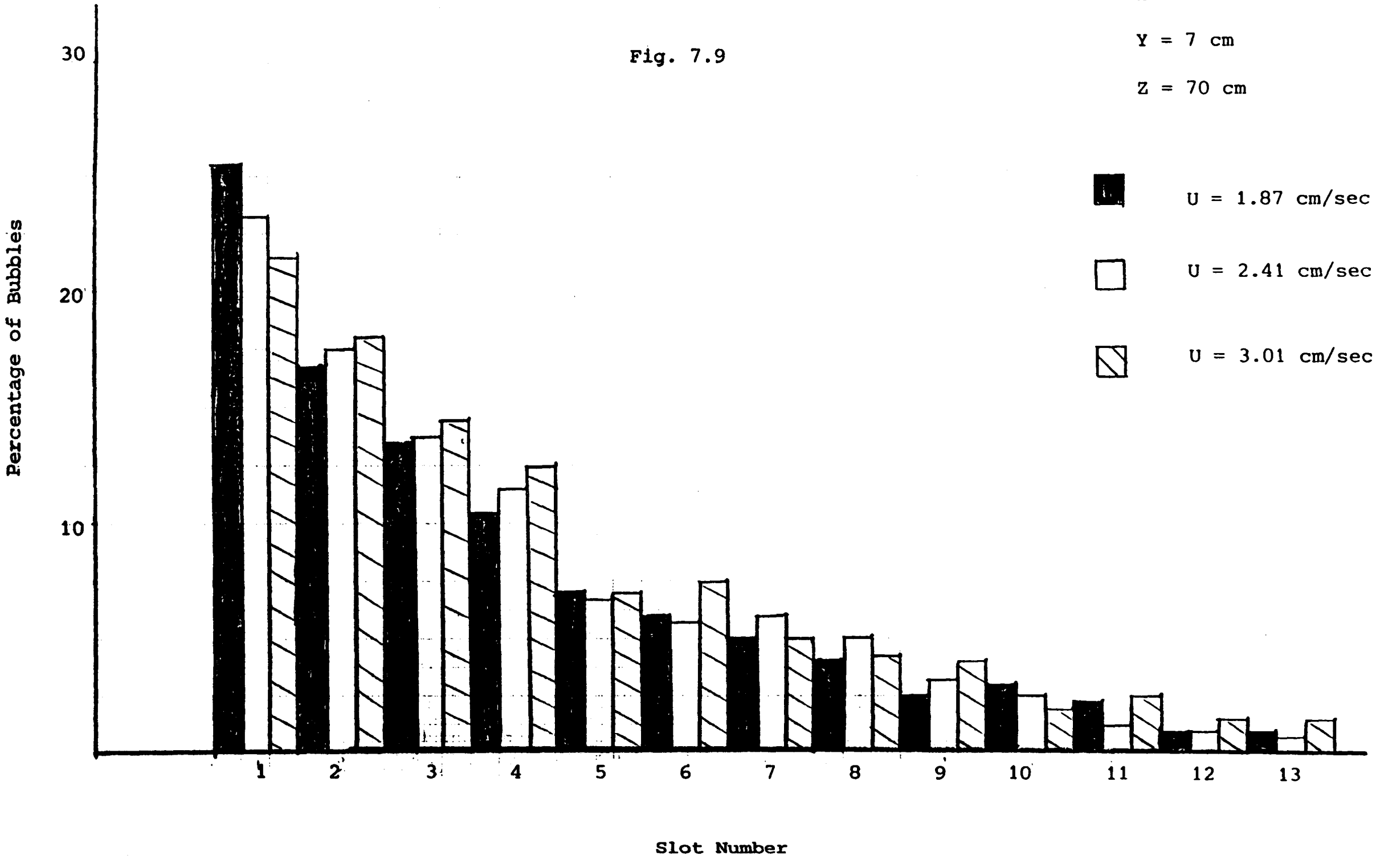
Multiorifice Distributor
X = 24 cm
Y = 7 cm
Z = 70 cm
U = 1.87 cm/sec
U = 2.41 cm/sec
U = 3.01 cm/sec
Percentage of Bubbles
30
20
10
1
2
3
4
5
6
7
8
9
10
11
12
13
Slot Number

7.2.2 Variation with Height above Distributor Plate

Figure (7.9a) shows the variation of the bubble size distribution with height above the distributor plate at three elevations of 50, 60 and 70 cm and at a fixed superficial fluidising velocity of 3.01 $cm.sec^{-1}$.

At this position, elevation does not seem much to affect the size distribution but the histograms corresponding to the higher elevations of 60 and 70 cm show peaks. The histogram for the Z = 50 cm elevation has already peaked.

Figure (7.10) shows the variation of frequency with size at the same superficial fluidising velocity of 3.01 $cm.sec^{-1}$ for three different points, on a plane 14 cm nearer to the "back wall" of the bed. This graph shows a very similar pattern of frequency decreasing with increasing bubble size to that of Figure (7.9a) In Figure (7.10), all three histograms show peaks at the same size-range, (8 - 10 mm).

Figures (7.11) and (7.12) show the frequency-size histograms at a lower gas velocity of 2.41 $cm.sec^{-1}$. The points in these two graphs are located on two planes 12 cm apart, along the X-axis (both at Y = 7 cm).

None of the histograms in Figure (7.12) show peaks in the size-ranges investigated, indicating the fact that the most frequent size is reduced with a decrease in gas flow rate.

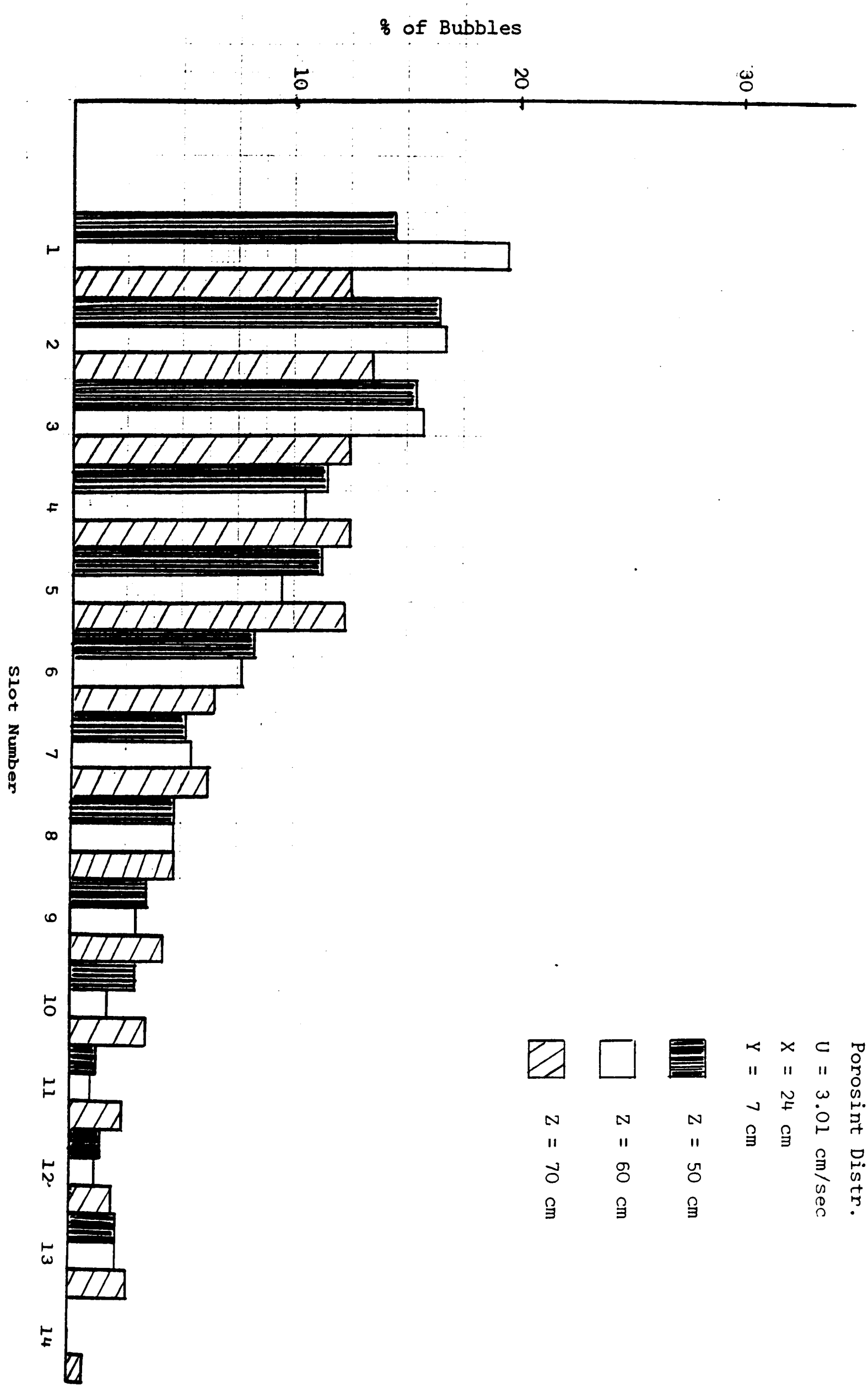
% of Bubbles
10
20
30
1
2
3
4
5
6
7
8
9
10
11
12
13
14
Slot Number
Porosint Distr.
U = 3.01 cm/sec
X = 24 cm
Y = 7 cm
Z = 50 cm
Z = 60 cm
Z = 70 cm

Fig. 7.9a

Fig. 7.10

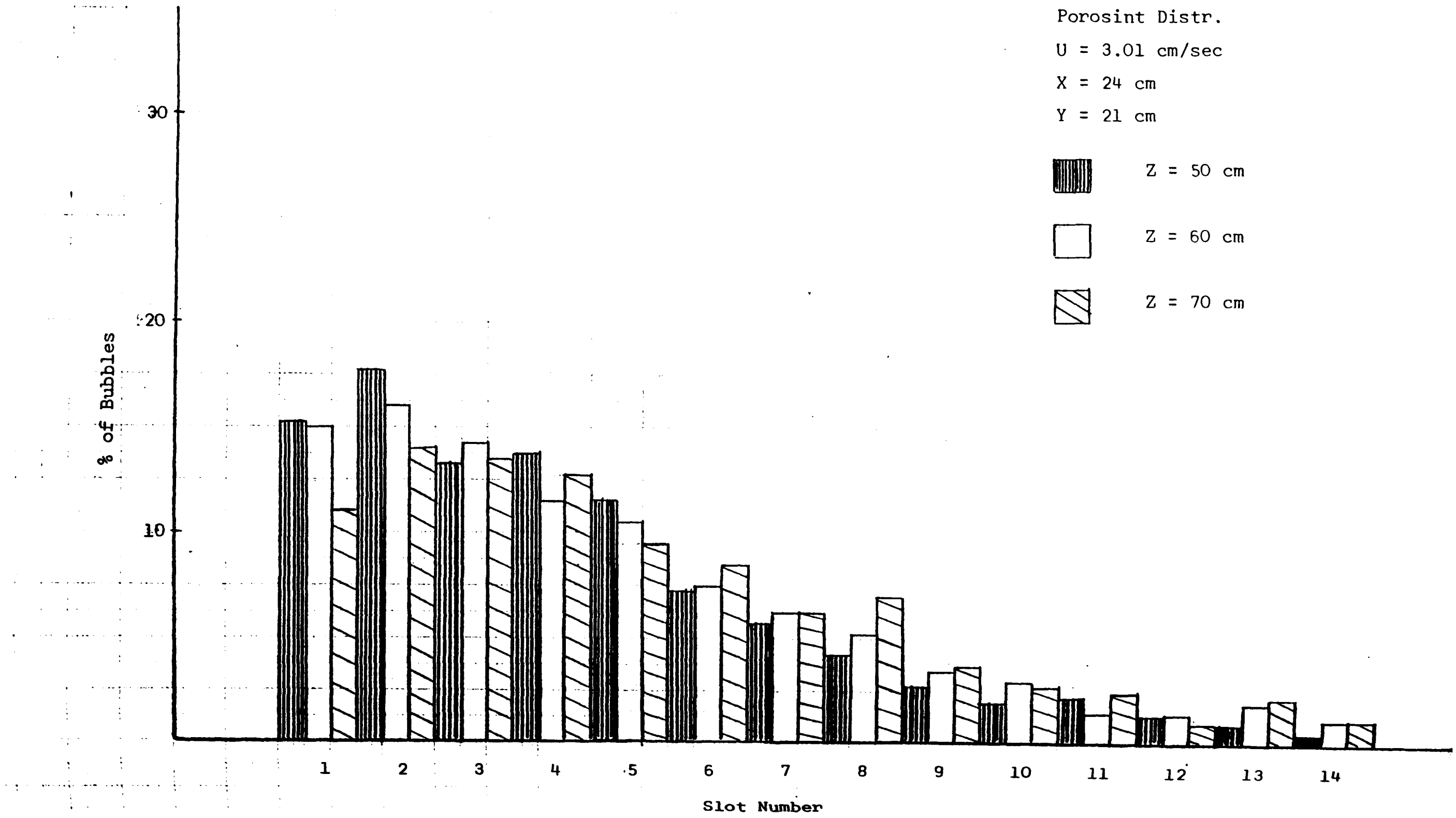
Porosint Distr.
U = 3.01 cm/sec
X = 24 cm
Y = 21 cm
Z = 50 cm
Z = 60 cm
Z = 70 cm
% of Bubbles
30
20
10
1
2
3
4
5
6
7
8
9
10
11
12
13
14
Slot Number

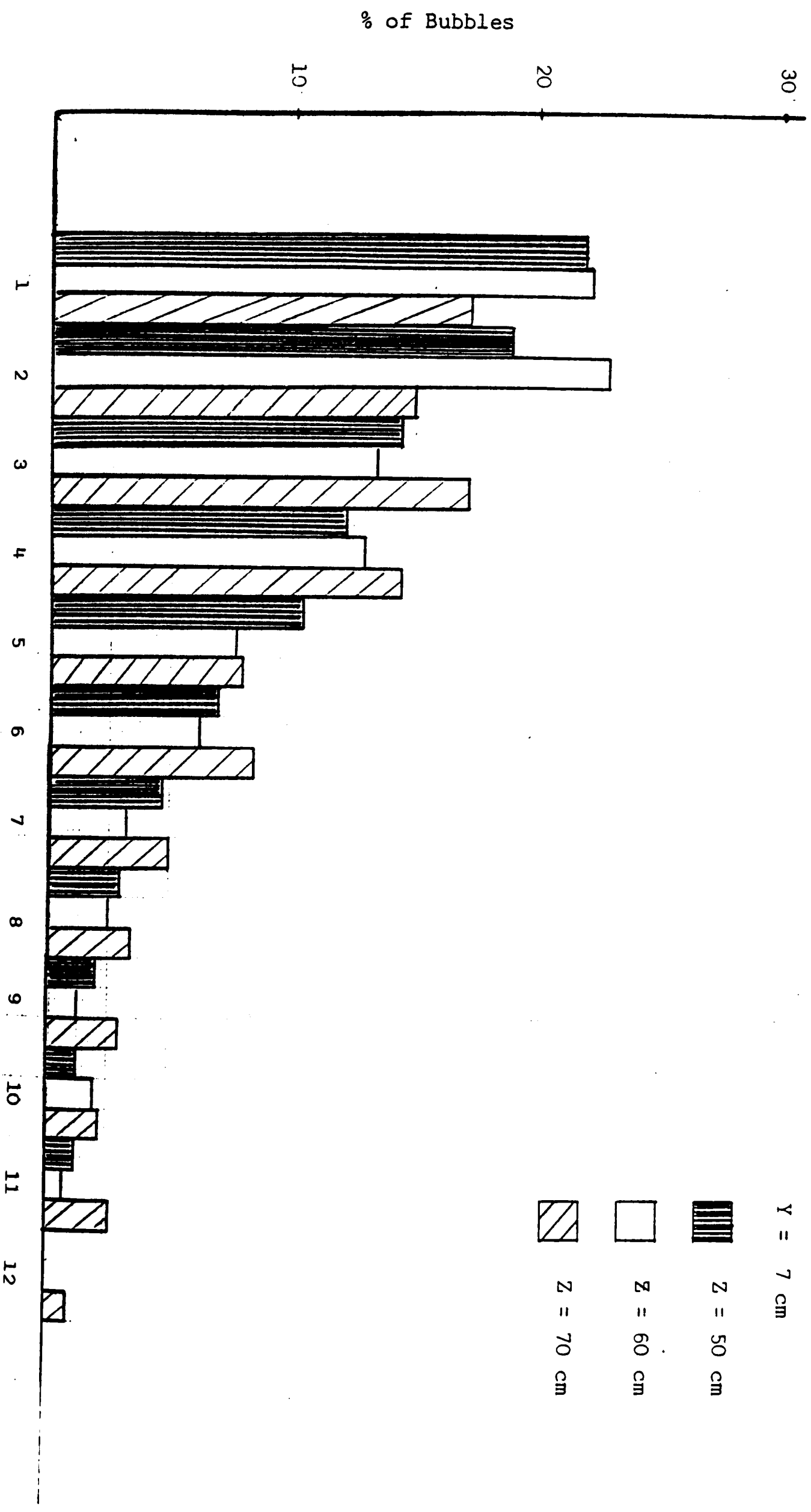
% of Bubbles
10
20
30
1
2
3
4
5
6
7
8
9
10
11
12
Slot Number
Porosint Distr.
U = 2.41 cm/sec
X = 24 cm
Y = 7 cm
Z = 50 cm
Z = 60 cm
Z = 70 cm

Fig. 7.11

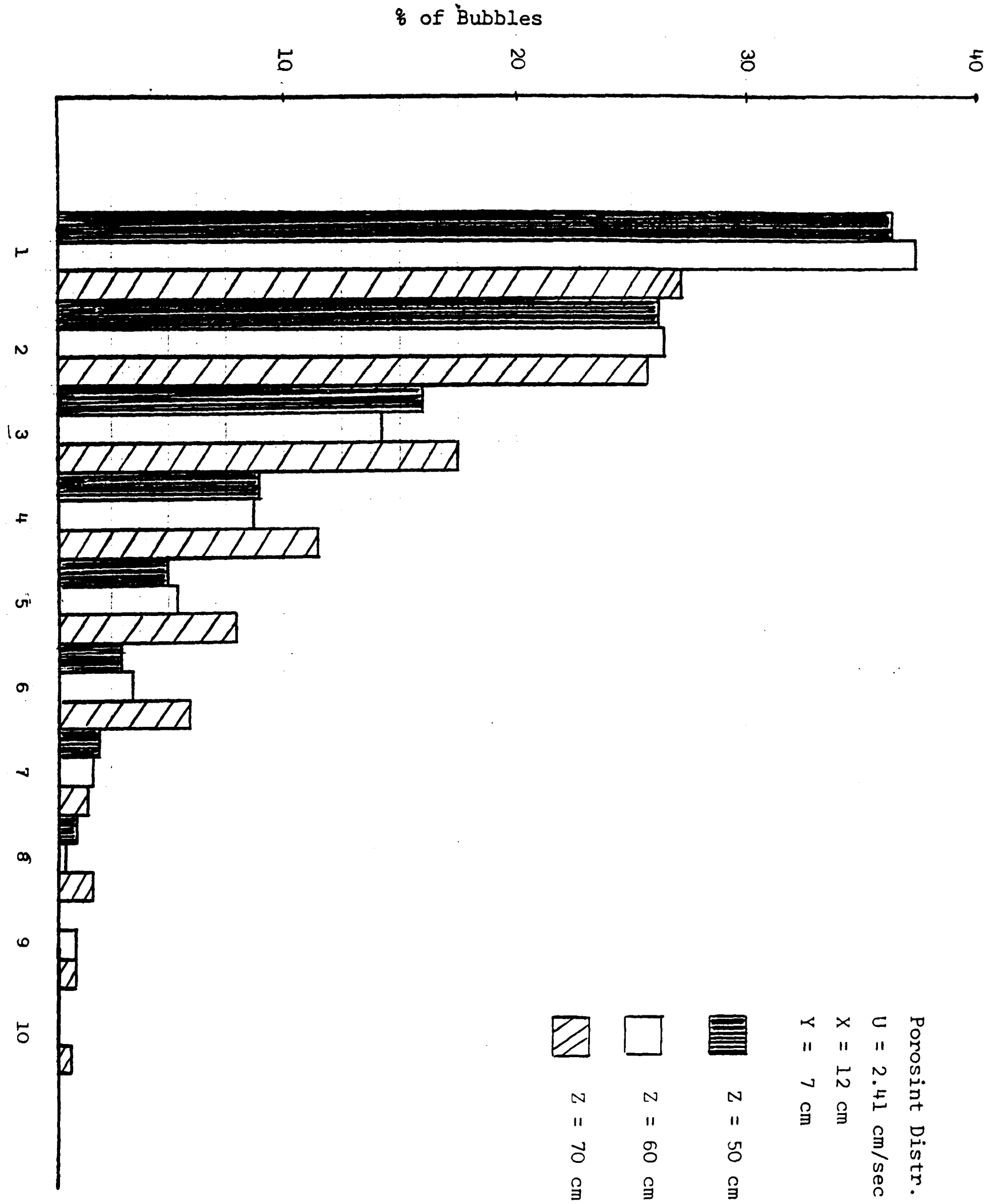
% of Bubbles
10
20
30
40
1
2
3
4
5
6
7
8
9
10
Slot Number
Porosint Distr.
U = 2.41 cm/sec
X = 12 cm
Y = 7 cm
Z = 50 cm
Z = 60 cm
Z = 70 cm

Fig. 7.12

All these graphs (7.7 - 7.12) represent data of bubbles generated by the porosint plate distributor. Figure (7.13) shows the size distribution variation with height for bubbles generated by the multiorifice distributor.

The operating conditions are the same as in Figure (7.11). In fact these two graphs can be directly compared to reveal the difference, if any, in the bubble sizes, encountered by the probe at 50, 60 and 70 cm above the two distributor plates.

Histograms in Figure (7.13), do not show a peak for any one of the three elevations. The frequency is decreasing steadily with increasing size in both, but the histograms corresponding to two of the elevations (60 and 70 cm) show peaks in the 8 - 10.5 mm range when the porosint distributor is employed.

A comparison of these two graphs (Figures 7.11 and 7.13) indicates a greater proportion of smaller bubbles encountered by the probe when the multiorifice distributor is employed. Conversely, in the greater size-ranges, higher bubble frequencies are recorded with the porosint plate distributor. This is in agreement with what was observed in Section 7.2.1 (Figures 7.6 and 7.9).

Fig. 7.13

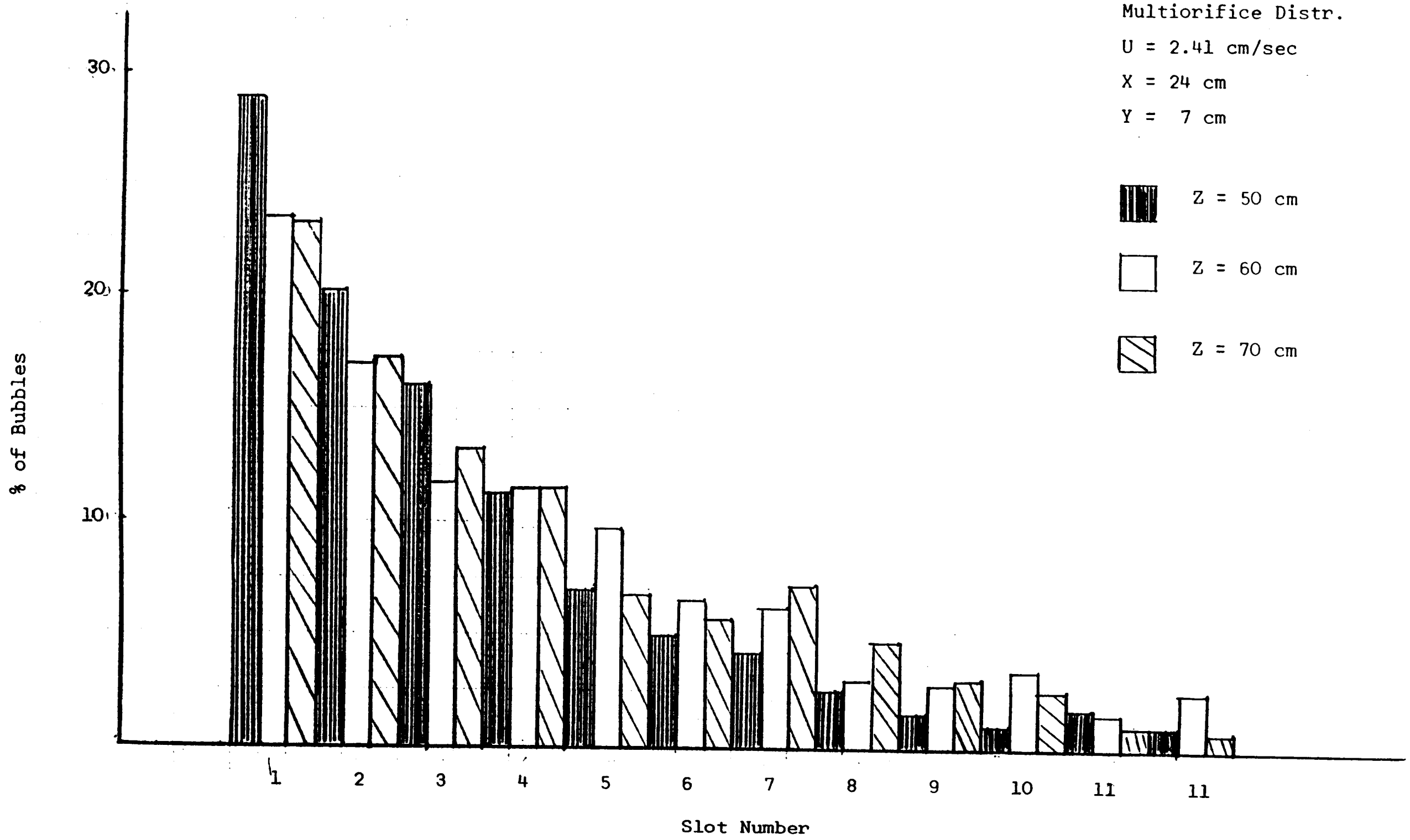
Multiorifice Distr.
U = 2.41 cm/sec
X = 24 cm
Y = 7 cm
Z = 50 cm
Z = 60 cm
Z = 70 cm
% of Bubbles
30
20
10
1
2
3
4
5
6
7
8
9
10
11
11
Slot Number

7.2.3 Variation across the Bed Cross-Sectional Area

Figure (7.14) shows the bubble frequency (percentage of bubbles in each slot) plotted against the slot width for three points with Y = 7 cm, 14 cm and 21 cm. All three points are on the X = 24 cm and Z = 50 cm planes. The superficial fluidising velocity is fixed at U = 3.01 $cm.sec^{-1}$. The values of frequencies are close and do not show a significant difference in the three sets of data. Bubble frequencies show peaks in the 8 - 10 mm size range but the histogram corresponding to Y = 7 cm has already peaked.

In Figure (7.15), the bubble frequency is plotted against the slot width, for three points on the Z = 70 cm plane. The rest of the operating conditions are the same as in Figure (7.14).

Here, all three histograms show peaks at 8 - 10 mm size-range. Bubble frequency, for small bubbles, is less for each interval of bubble height than in Figure (7.14). Again all three sets of data are close which indicates a very uniform distribution of bubbling activity across this axis, compared to a bed without the tube-bank.

Figures (7.16) and (7.17) show the frequency-variation for bubbles generated by the multiorifice distributor. Figure (7.16) shows this variation for three points on the Z = 50 cm plane whereas Figure (7.17) corresponds to three points on the Z = 70 cm plane. Otherwise, the superficial fluidising velocity, bed height and the X and Y coordinates are the same in these four Figures (7.14 - 7.17).


Percentage of Bubbles
10
20
30
1
2
3
4
5
6
7
8
9
10
11
12
13
14
15
Slot Number
Porosint Distributor
U = 3.01 cm/sec.
X = 24 cm
Z = 50 cm
Y = 7 cm
Y = 14 cm
Y = 21 cm

Fig. 7.14

Fig. 7.15

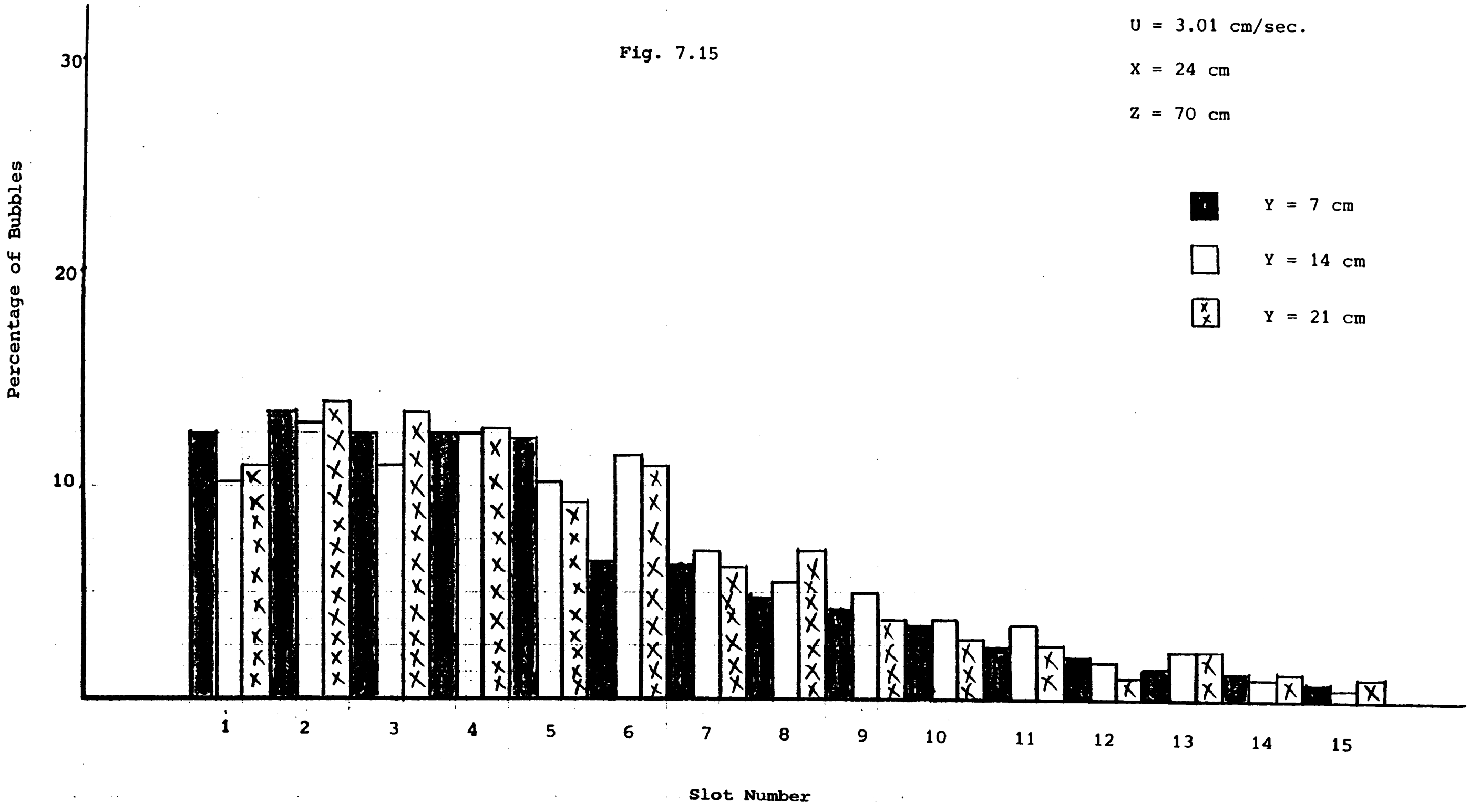
Porosint Distributor
U = 3.01 cm/sec.
X = 24 cm
Z = 70 cm
Y = 7 cm
Y = 14 cm
Y = 21 cm
Percentage of Bubbles
30
20
10
1
2
3
4
5
6
7
8
9
10
11
12
13
14
15
Slot Number

Fig. 7.16

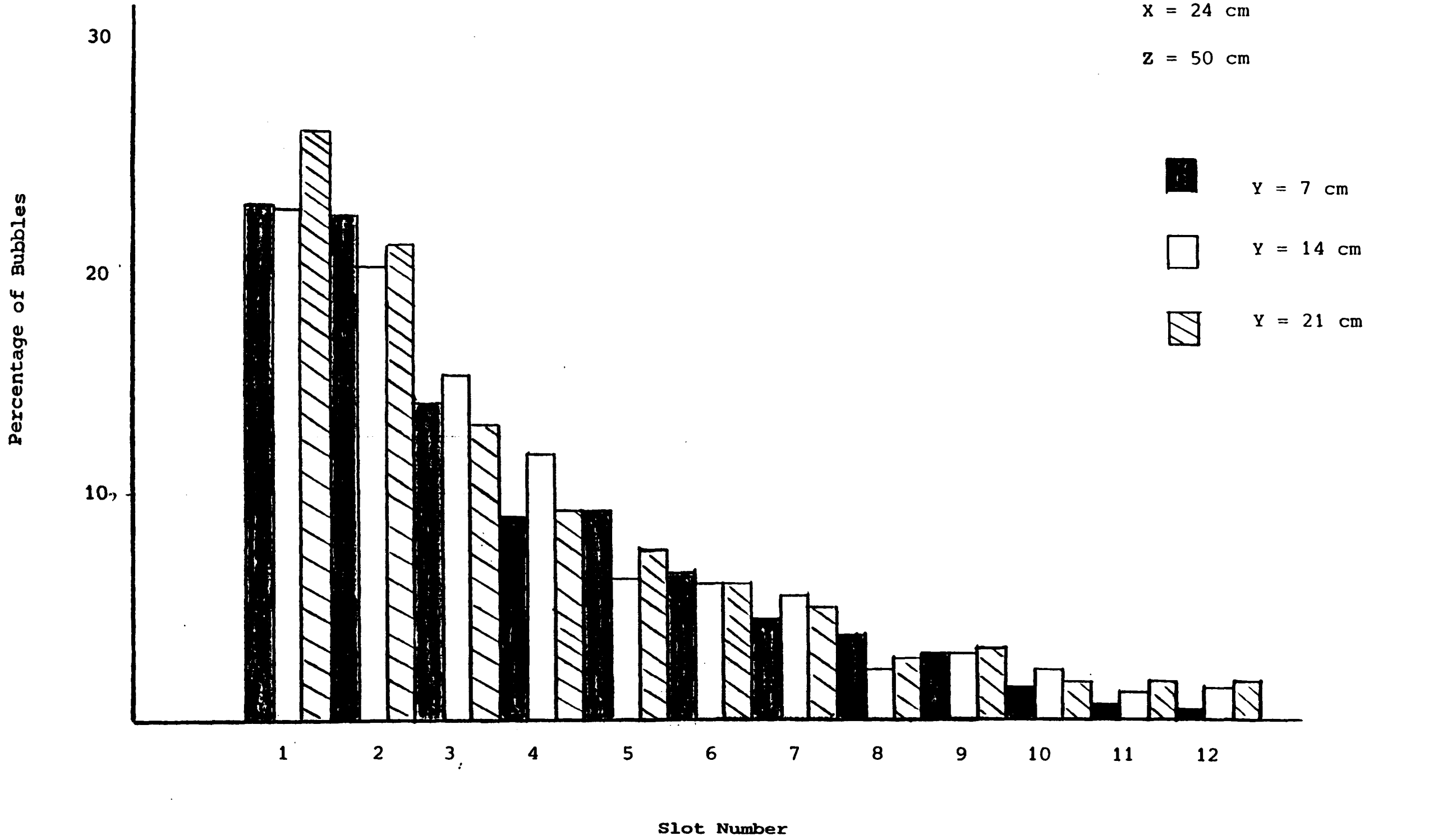
Multiorifice Distributor
U = 3.01 cm/sec.
X = 24 cm
Z = 50 cm
Y = 7 cm
Y = 14 cm
Y = 21 cm
Percentage of Bubbles
30
20
10
1
2
3
4
5
6
7
8
9
10
11
12
Slot Number

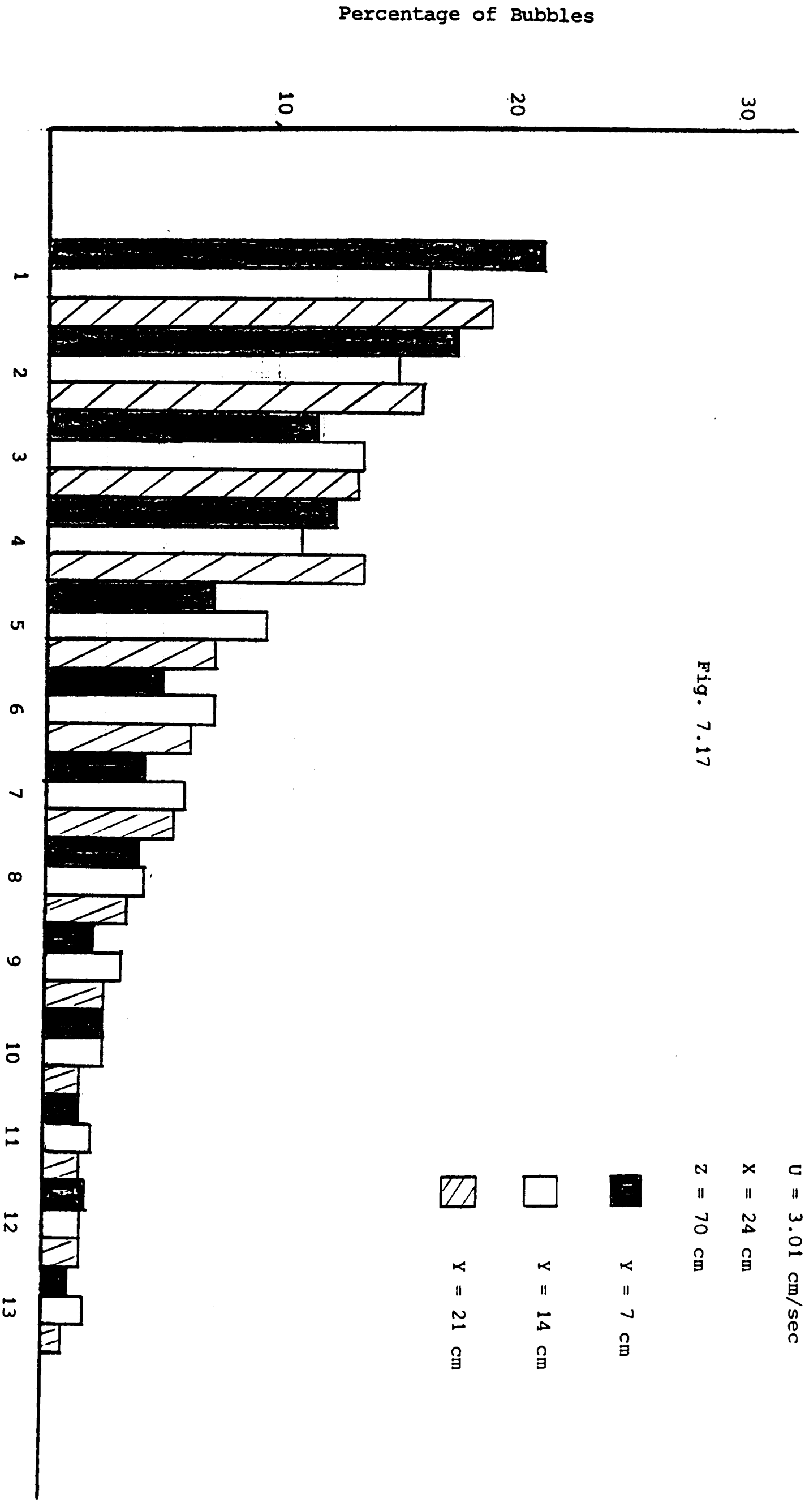
Percentage of Bubbles
10
20
30
1
2
3
4
5
6
7
8
9
10
11
12
13
Slot Number
Multiorifice Distributor
U = 3.01 cm/sec
X = 24 cm
Z = 70 cm
Y = 7 cm
Y = 14 cm
Y = 21 cm

Fig. 7.17

A comparison of these two Figures (7.16 and 7.17) reveals a similar pattern of bubble frequency decreasing (from a maximum), steadily and none of the histograms shows a peak in the size-range investigated. Much higher bubble frequencies are recorded, for small bubbles, with the multiorifice distributor (compare Figures 7.14, 7.16 and 7.15 to 7.17). For large bubbles, there does not seem to be a significant difference in the bubble frequencies, for corresponding intervals of bubble height, with the two distributors.

All this indicates, again, a greater proportion of smaller bubbles existing (at the points where the probe tip is located), when the multiorifice distributor is used.

Figures (7.18) and (7.19) show the frequency-size distribution along the X coordinates, when the porosint plate is employed. Figure (7.18) represents data at three points on the Z = 50 cm plane while (7.19) corresponds to three points on a plane 20 cm higher (i.e. Z = 70 cm above the distributor plate). In both, the superficial fluidising velocity is fixed at 3.01 $cm.sec^{-1}$ and Y = 14 cm. All the histograms show a peak in the 8.5 - 10 mm size-range.

Frequencies corresponding to the Z = 50 cm elevation are greater than those for Z = 70 cm for the first four intervals of bubble height (i.e. for small bubbles). This indicates a greater proportion of small bubbles encountered at the lower elevation of 50 cm. One would expect to find this to be the case, since

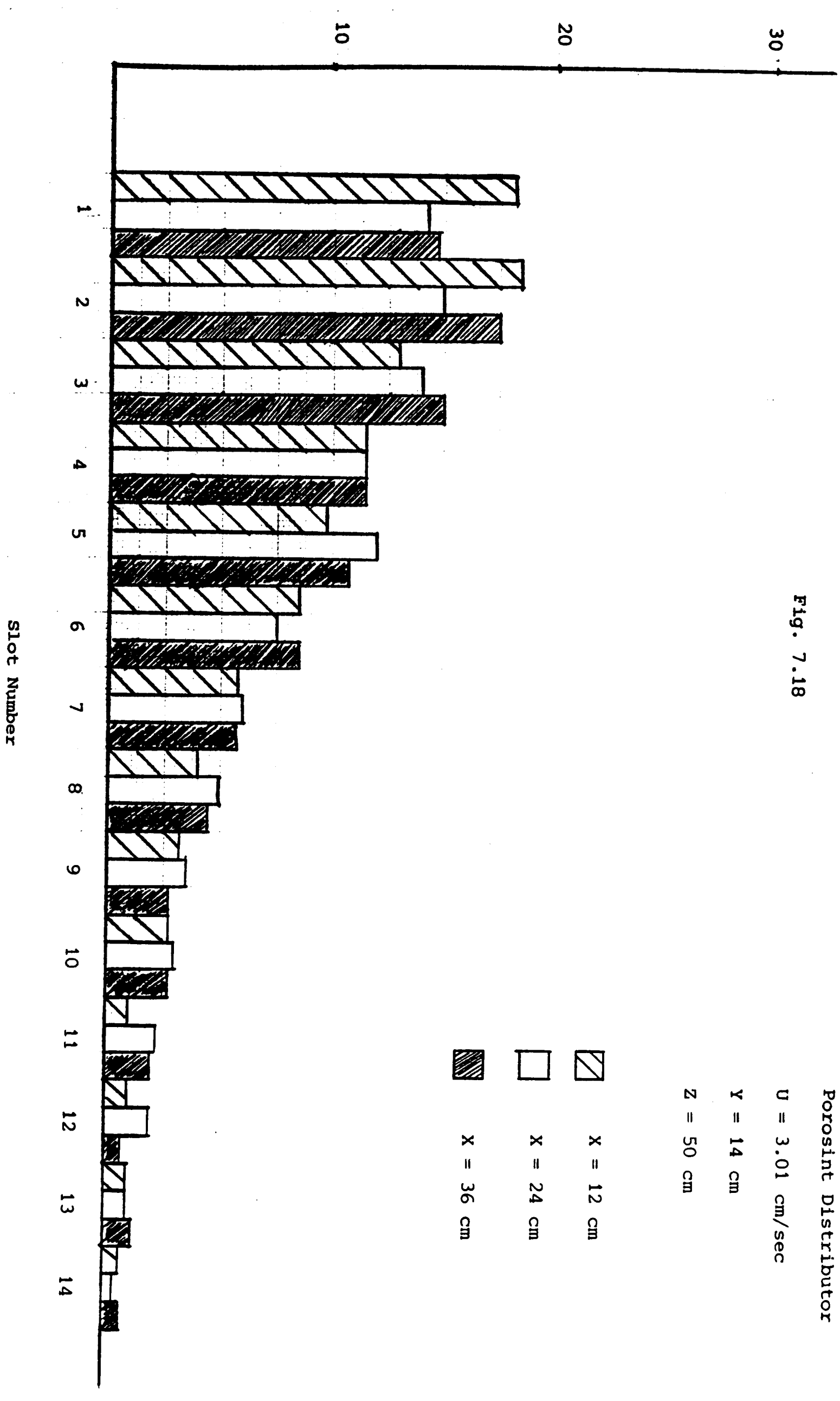
Percentage of Bubbles
10
20
30
1
2
3
4
5
6
7
8
9
10
11
12
13
14
Slot Number
Porosint Distributor
U = 3.01 cm/sec
Y = 14 cm
Z = 50 cm
X = 12 cm
X = 24 cm
X = 36 cm

Fig. 7.18

Fig. 7.19

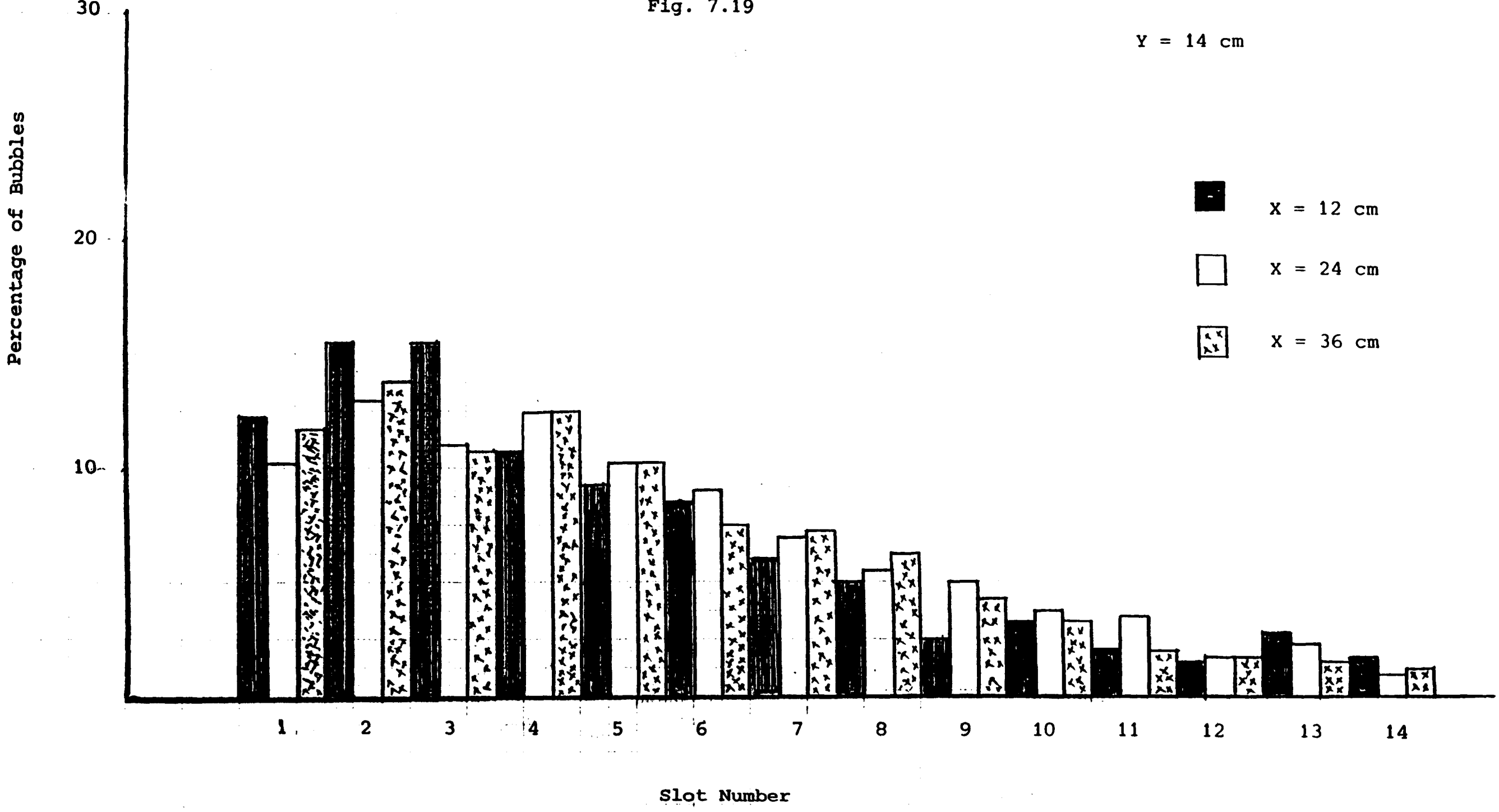
Porosint Distributor
U = 3.01 cm/sec.
Z = 70 cm
Y = 14 cm
X = 12 cm
X = 24 cm
X = 36 cm
Percentage of Bubbles
30
20
10
1
2
3
4
5
6
7
8
9
10
11
12
13
14
Slot Number

a proportion of these small bubbles would coalesce in the 20 cm rise to form larger bubbles, encountered at Z = 70 cm.

After this initial size-range (of 6.8 - 13.6 mm) the frequencies, for each of the three sets of data, are very close and do not show a significant difference along the X-axis. In other words the bubble size distribution does not vary much along the X coordinates for large bubbles.

Finally, in Figures (7.20) and (7.21) the size distribution variation is tabulated along the X coordinates for bubble generated by the multiorifice distributor. Figure (7.20) can be directly compared to Figure (7.18) and Figures (7.19) and (7.21) are obtained under identical operating conditions. Again, both these Figures, (7.20) and (7.21), show much greater frequencies for small bubbles than Figures (7.18) and (7.19). The only exception is the data obtained at the point with coordinates X = 36 cm, Y = 14 cm, Z = 70 cm. In fact, this is the only histogram to show a peak in the size ranges investigated.

It is interesting that a very significant difference exists between the bubble size distribution at this point, compared to the other two (i.e. X = 12 and X = 24 cm).

However, it follows a definite trend shown in the figures for X = 12 and X = 24. If the frequencies for the first two bubble size slots are compared in these two cases, the drop is very much greater for X = 12 than for X = 24 cm. Under the circumstances, the small rise for X = 36 cm fits in with this variation.

Fig. 7.20

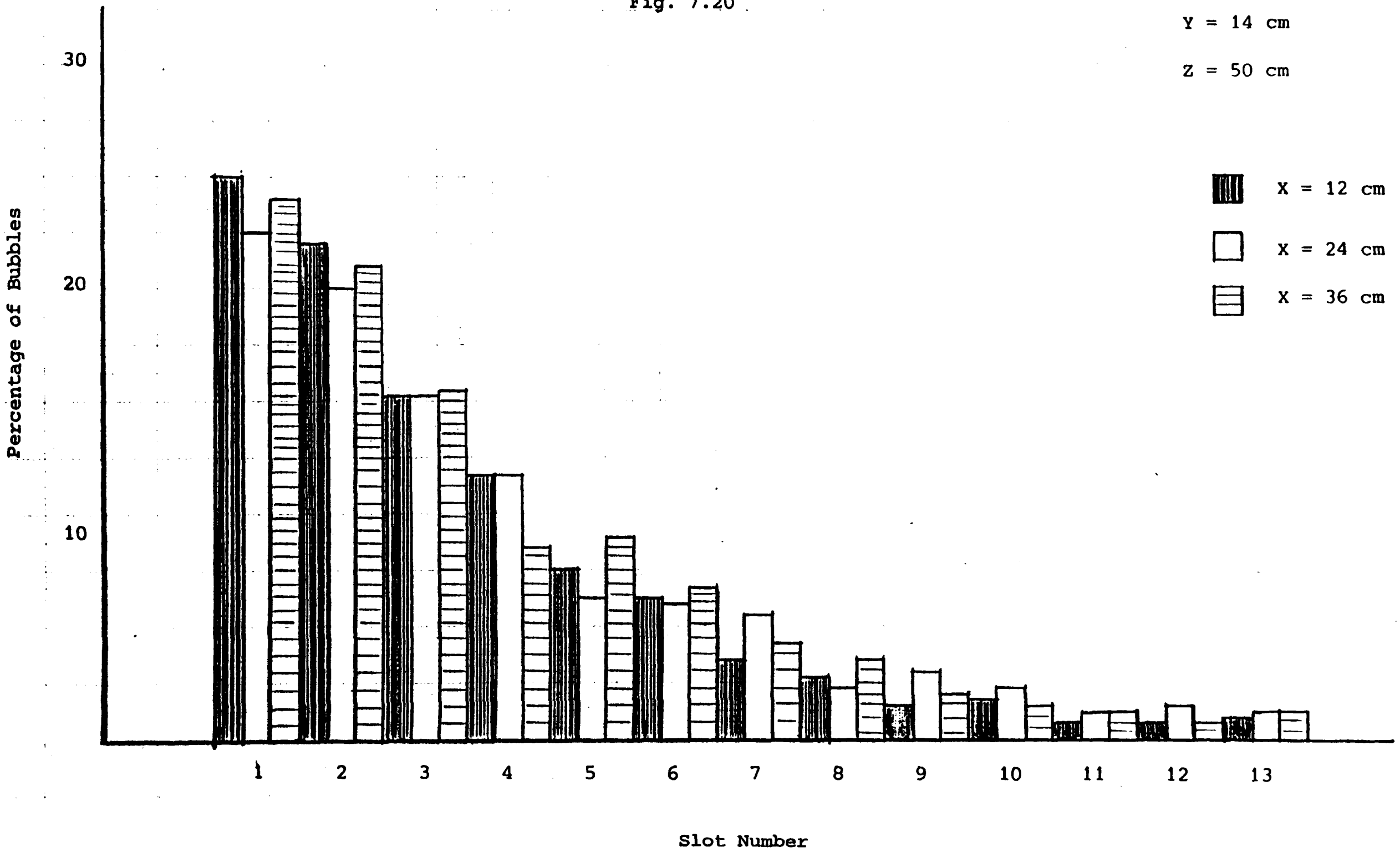
Multiorifice Distributor
U = 3.01 cm/sec.
Y = 14 cm
Z = 50 cm
X = 12 cm
X = 24 cm
X = 36 cm
Percentage of Bubbles
30
20
10
1
2
3
4
5
6
7
8
9
10
11
12
13
Slot Number

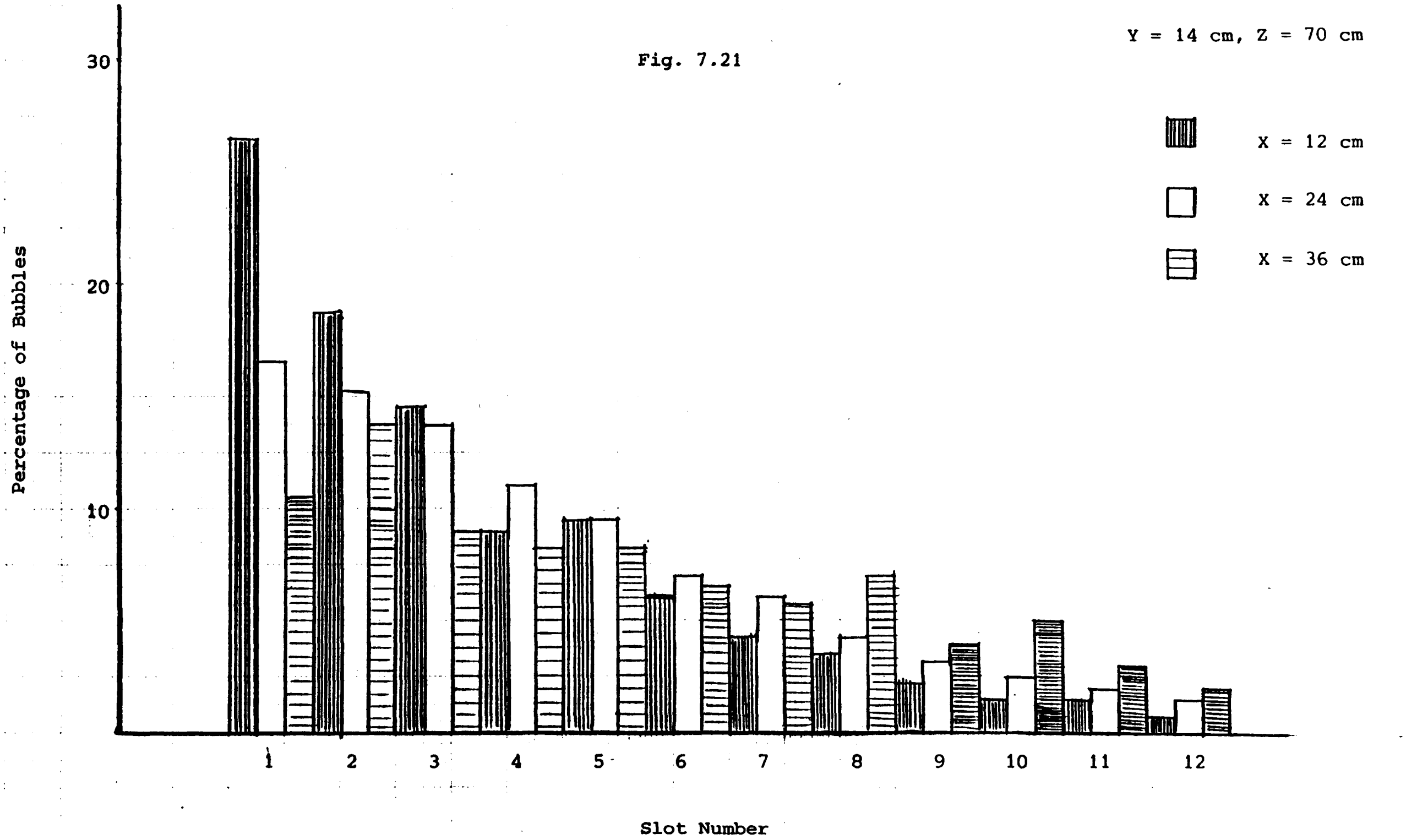
Multiorifice Distributor
U = 3.01 cm/sec
Y = 14 cm, Z = 70 cm
X = 12 cm
X = 24 cm
X = 36 cm
Percentage of Bubbles
30
20
10
1
2
3
4
5
6
7
8
9
10
11
12
Slot Number

Fig. 7.21

7.2.4 Comparison of the Frequency-Size Distributions With and Without Tube-Bank

Figure (7.22) shows the size distribution variation of bubbles encountered by the probe in the bed, with and without the tube-bank present, at a point 50 cm above the porosint distributor plate on the bed vertical centreline.

The histogram corresponding to the latter case (without the tube-bank), shows a peak in the 8 - 10 mm size range. Otherwise the two histograms follow a very similar and very close pattern of bubble frequency decreasing steadily with an increase in slot number. It seems as though the bubbles are sliding off the tubes or splitting when they hit the tubes but reforming immediately above the top array, so that no significant difference in the size distribution is revealed.

This conclusion is reinforced when this comparison is extended to another plane, 20 cm higher (i.e. 70 cm above the distributor plate), Figure (7.23). Again the two histograms reveal a similar pattern of frequency increasing to a maximum (peak value = 12 - 13%) and then decreasing steadily with increasing size. Furthermore, frequencies recorded, for each interval of bubble height, in the two cases are very close, sometimes identical.

Fig. 7.22

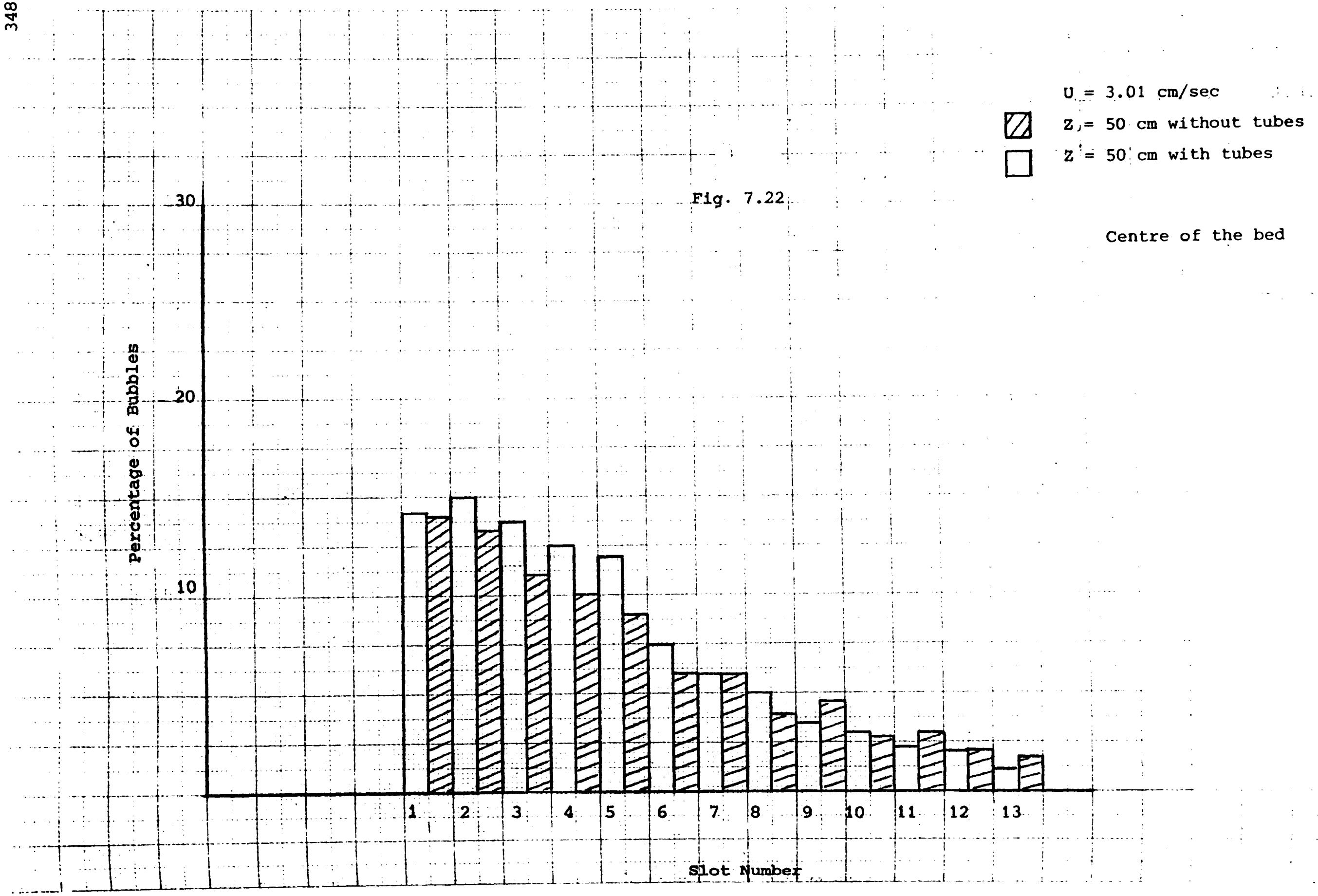
U = 3.01 cm/sec
Z = 50 cm without tubes
Z = 50 cm with tubes
Centre of the bed
30
20
10
Percentage of Bubbles
1
2
3
4
5
6
7
8
9
10
11
12
13
Slot Number

$U = 3.01\ cm.sec^{-1}$

With Tube Bank Z = 70 □

Without Tube Bank Z = 70 ▨

Centre of the Bed

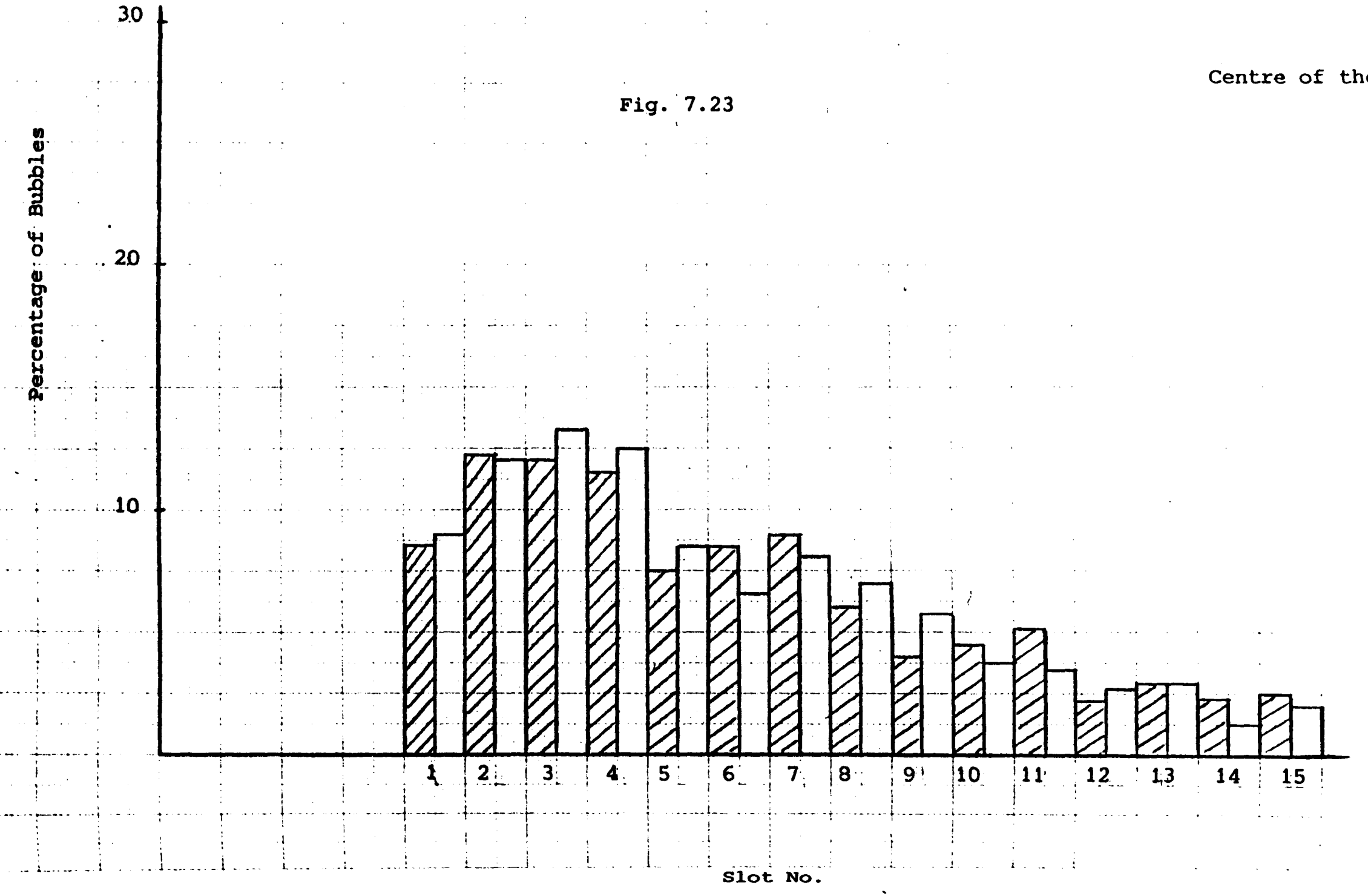

Fig. 7.23

In Figure (7.24) two bubble size distribution histograms are compared:

1. when the sampling point is 30 cm above the distributor plate but without the tube-bank.
2. to the case where the tube bank is present, but the point of measurement is 70 cm above the distributor on the bed vertical axis.

The two histograms show very different patterns of frequency-size distribution variation. The one corresponding to the point with Z = 70 cm shows a gradual increase, a peak and a steady decline. The histogram corresponding to the point with Z = 30 cm has already peaked, the most frequent size being less than 6.8 mm.

The purpose of making this comparison was to test the hypothesis that a tube-bundle acts as a redistributor for the fluidising gas. Were this the case, similar size distributions would be expected at equal heights above the distributor and the tube-bundle. As can be seen from Figure (7.24), no such similarity exists. It must therefore be concluded that the tube-bundle acts as a redistributor only to the limited extent of improving the uniformity of bubbling activity in the bed.

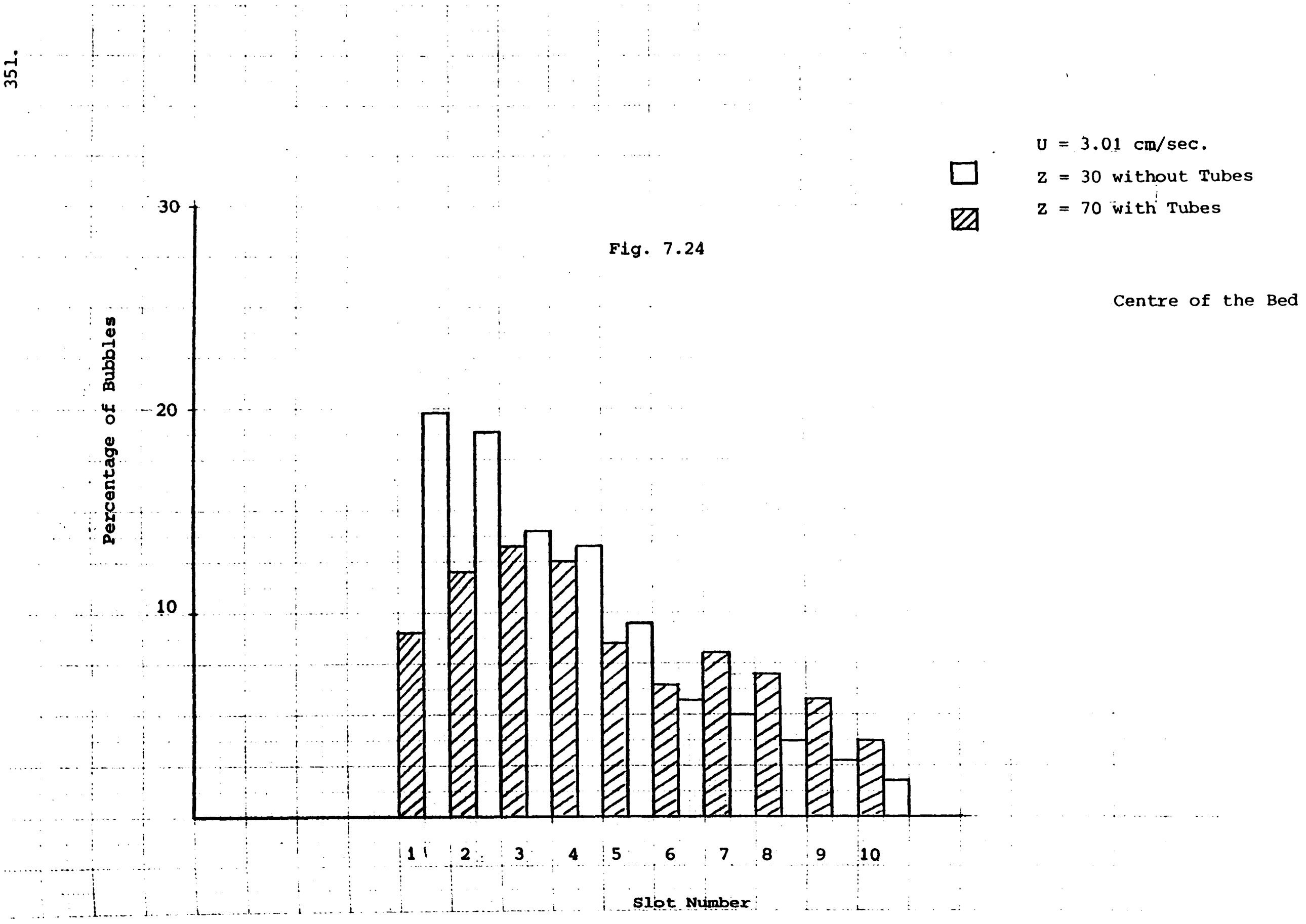
U = 3.01 cm/sec.
Z = 30 without Tubes
Z = 70 with Tubes
Centre of the Bed
Percentage of Bubbles
30
20
10
1
2
3
4
5
6
7
8
9
10
Slot Number

Fig. 7.24

7.3 Bubble Frequency Distributions

7.3.1 Porosint Plate Distributor

Table (7.9) shows the point values of the bubble frequencies recorded at the nine points, for three elevations (50, 60 and 70 cm) and three superficial fluidising velocities (1.87, 2.41 and 3.01 $cm.sec^{-1}$), with the porosint distributor employed. This table shows that the bubble frequency is very uniformly distributed, especially at high gas flow rate. At a low gas velocity of 1.87 $cm.sec^{-1}$, the distribution is less uniform, bubbles being concentrated at the centre, and at a few points near the "front wall" of the bed.

Bubble frequency increases with the superficial gas velocity and the highest frequencies are recorded with U = 3.01 $cm.sec^{-1}$. Uniformity (of frequency distribution), across the bed cross-sectional area, increases with increasing superficial fluidising velocity.

Elevation above the distributor plate seems to affect the bubble frequency and its distribution only very slightly. A comparison of the data corresponding to Z = 50 cm with those at Z = 60 cm and Z = 70 cm reveals a shift in the bubble concentration (and bubbling activity) towards the back wall of the bed.

It seems that the presence of the tube-bank helps to redistribute the bubbles across the bed cross-sectional area.

Porosint Plate Distributor

With Tube-Bank

1.18	0.56	1.34	10.44	4.40	5.63	14.22	4.46	11.14
11.76	17.02	15.18	20.00	17.12	18.88	15.25	20.97	17.60
1.49	10.83	7.00	9.27	22.90	15.91	12.57	9.06	11.04

Z = 70 cm Z = 70 cm Z = 70 cm

U = 1.87 cm.sec^{-1} U = 2.41 U = 3.01

0.37	0.32	0.29	10.45	5.43	2.38	13.77	25.67	9.03
11.99	9.25	15.18	17.02	5.22	22.88	19.40	9.20	18.14
1.78	11.00	10.36	7.03	24.43	13.23	7.00	16.02	13.73

Z = 60 cm Z = 60 cm Z = 60 cm

U = 1.87 U = 2.41 U = 3.01

0.05	0.0	0.07	0.65	0.44	0.49	10.05	12.83	4.46
20.10	6.99	10.70	20.37	10.84	18.47	21.28	18.04	15.98
0.37	13.26	9.28	9.34	23.09	7.85	14.17	11.04	15.35

Z = 50 cm Z = 50 cm Z = 50 cm

U = 1.87 U = 2.41 U = 3.01

TABLE (7.9)

Bubble Frequencies (in 'B' Mode) = min^{-1}

7.3.2 Multiorifice Distributor

Table (7.10) shows the frequency distribution across the bed cross-section when the multiorifice distributor is employed. Again, a more uniform distribution is obtained with the tube-bank present. Uniformity (defined by the prevalence of point frequencies of the same order of magnitude at the nine symmetrically distributed points) increases with increasing superficial fluidising velocity. In this case (with the multiorifice distributor), this could be attributed to a greater number of active orifices, when the gas velocity is increased. Increasing elevation above the distributor plate changes the picture very slightly.

7.3.3 Comparison of Frequency Distributions With and Without the Tube-Bank

A comparison of tables (6.5 and 6.6) to (7.9 and 7.10) shows that the presence of the tube-bank in the bed has the effect of increasing the uniformity of frequency distribution across the bed cross-sectional area. This could be due to the fact that the tube-bank helps redistribute the bubbles across the bed cross-section, (i.e. shifting the bubbles sideways, randomly, without affecting their size distribution).

Multiorifice Distributor - With Tube-Bank

<0.1	1.57	1.75
1.45	7.99	11.35
15.23	7.70	4.70

Z = 70 cm

1.11	2.22	2.38
5.58	9.75	12.22
10.88	6.08	5.50

Z = 70 cm

3.96	3.51	7.32
7.45	13.04	21.21
8.60	3.90	4.43

Z = 70 cm

<0.1	1.15	3.10
3.07	8.07	7.19
6.47	11.19	6.28

Z = 60 cm

0.37	5.14	9.10
6.80	10.60	12.23
8.92	8.96	6.87

Z = 60 cm

3.31	4.93	5.15
9.06	11.70	20.15
9.71	7.07	8.77

Z = 60 cm

<0.1	<0.1	0.80
0.32	1.75	8.39
16.18	13.93	11.46

Z = 50 cm

U = 1.87 cm/sec

<0.1	6.67	6.73
5.22	5.13	11.80
20.76	15.43	12.30

Z = 50 cm

U = 2.41 cm/sec

0.43	10.24	8.19
7.29	4.68	17.55
19.15	11.44	12.68

Z = 50 cm

U = 3.01 cm/sec

TABLE 7.10

Bubble Frequencies (in 'B' Mode) = min^{-1}

7.5 Conclusions

Introducing an array of solid obstacles (in the form of a tube-bank) into a gas-fluidised bed seems to have the following effects:

1. The direction and the scale of the particulate phase circulation patterns are changed. They are reduced in scale to a great extent and the direction of flow is sometimes the opposite to that prevalent when the solid obstacle is not present.
2. Bubble frequency distribution across the bed cross-sectional area is much more uniform when a tube-bank is immersed in the bed. The tube-bank seems to help redistribute the bubbles across the bed cross-section. Very few "dead" zones are found in the bed.
3. Bubble size distributions are not greatly affected by the presence of a solid obstacle in the bed. In these experiments, immersing a staggered tube array seems not to disrupt bubble size variation along the vertical direction in the bed. The bubbles seem to slide off the tubes. When they hit the tubes frontally and are consequently split, they seem to reform immediately above the tubes, so as not to affect the size distribution greatly.

4. The multiorifice distributor produced a greater proportion of small bubbles (i.e. encountered by the probe), at the elevations of 50, 60 and 70 cm above the distributor plate. When the tube-bank was submerged in the bed, this phenomenon prevailed again and the presence of the tube-bank did not affect the differences in the bubble size distributions already existing due to the different mechanism of bubble generation by the two gas distributors.

The tube-bundle used in these experiments was not very densely packed (pitch: diameter ratio = 3.5). It is possible that denser arrays might substantially alter bubble size-distributions, but any conclusions here must await further experimentation.

CHAPTER 8

Conclusions

and Recommendations

One of the characteristics of gas fluidised-beds is the formation of gas bubbles. Since the bubbles contain but little of the solids it is possible for much of the gas entering a fluid bed chemical reactor to by-pass the solids, thus decreasing the overall reaction efficiency as compared to a fixed bed reactor operating with the same space velocity and mass of catalyst. Most chemical reactor models thus, require knowledge of the bubble size in gas fluidised reactors. It is also important to know whether or not the bubbles may grow big enough to cause slugging both for reactor modelling and when considering carry-over of particles into the space above the bed and beyond. The relevance of the bubble parameters in designing a gas fluidised bed reactor will be dealt with in more detail later in this chapter.

The compound fibre-optic probe technique has proved a useful tool in measuring bubble sizes and rise velocities in a gas fluidised bed. Its results are in good agreement with those generated by other techniques, such as X-ray photography (92) and use of electroresistivity probes (6).

A number of conclusions can be drawn from these results which are in good agreement with most of the reported literature. These can be summarised as follows:

1. Bubbles become flatter in shape as they rise higher in the bed. Furthermore, the larger bubbles are flatter in shape irrespective of height in the bed.
2. Extremely skewed distribution curves obtained suggest that there is a high proportion of very small bubbles (size < 1.0 cm) with the most frequent size in the range of 8-12 mm. The most skewed distribution curves are encountered near the distributor plate, especially at low superficial fluidising velocities.

3. Invariably, it was found that the bubble-size histograms corresponding to the multiorifice distributor showed a much greater proportion of small bubbles than did the histograms yielded by the porosint distributor. On purely physical grounds, it seems unlikely that the microscopic pores in the sintered metal distributor in fact give rise to larger bubbles than the gross perforations in the multiorifice distributor. It is much more likely that the former distributor produces a cloud of tiny bubbles which are undetectable by the probe; and that after a rise of 20 cm (and at high superficial fluidising velocities) enough repeated coalescences have occured to produce a few detectable bubbles. At higher elevations in the bed, more and more bubbles appear in the measureable size range, indicating an apparent increase in bubble count with elevation (Table 6.5 A). In the case of the multiorifice distributor, many more of the bubbles produced are immediately in the measureable range. This gives a relatively large bubble count at 20 cm elevation. In this case, however, continued coalescence reduces the number of measureable bubbles, giving a real decrease in bubble count as elevation increases (Table 6.8 A). The true picture is thus, almost certainly,one of monotonic decline in bubble count with elevation in both cases. It is only the inability of the probe to detect very small bubbles which obscures this variation in the case of porosint plate distributor.
4. The possible incidence of inactive orifices could be another reason for unusually low bubble counts at some points on the bed cross-section, when the multiorifice distributor is employed.
5. The introduction of a solid obstacle (such as a tube-bank), in a gas fluidised bed, has the effect of spatially redistributing the bubbles without greatly affecting their size distribution.

These findings are directly relevant in designing a fluidised bed reactor. This relevance can be summarised as follows:

1. Bubble size is used as a basic design parameter by almost all workers (61, 91). (A knowledge of the residence-time distribution of gas in a fluidised-bed catalytic reactor does not give sufficient information to predict the degree of conversion since there is an unequal distribution of catalyst between the bubble and dense phases). Most fluidised bed reactor models assume uniform bubble sizes, which is clearly unrealistic. This work gives an indication of the distribution of bubble sizes in a particular freely-bubbling bed and hence some insight into the validity of these models and possibility of modifying and extending them accordingly.
2. Knowledge of the spatial distribution of bubbles in gas fluidised beds is important is view of the general need for, and assumption of, uniformity of reactor beds. This work gives measurement of the extent of non-uniformity of bubbling over the cross-section of the particular bed used in these experiments and reveals how it varies with bed depth, superficial fluidising velocity and bed internals in this particular case.
3. Serious by-passing can occur at very high values of U/U_{mf} with shallow beds or with large bubble sizes (Orcutt et al.). By-passing may occur in fluidised-bed reactors due to the preferred use of bubble caps, perforations or tuyeres, etc. where bubbles may begin to rise along preferred paths or tracks to produce a situation akin to channelling. The mechanism of bubble generation by two different gas distributors is studied and some insight is gained into the paths bubbles take when they rise up in the bed.

4. Entrainment of particles from the bed is another important factor which is affected by the bubbles, because:

   (a) bubbles eject particles into the freeboard; and

   (b) subsequent carry-over of particles depends on velocity distribution and turbulence levels in the freeboard, both of which seem to depend on bubbling (129). Levy & Lockwood (129) showed that in shallow beds, (i.e. bed depth < equivalent bed diameter), the peaks in the freeboard velocity profile are detected near the vessel walls. This agrees with the results obtained in this work, which show bubbles rising faster near the vessel walls in shallow beds.

Recommendations for further work

The truncation of the bubble size distributions by the probe (in 'B' mode) prevents construction of accurate size distribution histograms. In principle, improvement of the coverage of small bubble sizes could be achieved by reduction of the vertical distance between the leading and coplanar probes. However, any substantial reduction in this dimension below the present 6.8 mm would require a corresponding reduction of the existing lateral 6.5 mm spacing of the coplanar probes; for otherwise all bubbles would be rejected on jitter time considerations. The smallest possible horizontal spacing would be achieved by simply gluing the probes together. With the existing probes this would permit a vertical separation of $\sim$ 3 mm and the detection and measurement of bubbles down to this size. Unfortunately, however, the probe would then present a substantial, compact, obstruction to the flow and it is doubtful whether measurements made with it would truly represent bubble behaviour in the bed as a whole.

AIthough there accordingly exists a lower limit on the size of bubbles

that can be observed with this kind of probe, further work should be conducted to investigate the effect of particle size, gas-flow, and distributor design, as well as bed geometry and dimensions, to allow the present results to be generalised.

All the results in this work were obtained by experimenting with particles of one size (and density) only. It would be of interest to extend this work to include solid particles of varying sizes (up to 1.5 mm), such as are used in industry.

Observations made with the particular tube-bank arrangement mentioned in Chapter 3 should be generalised by use of different spacings and configurations of tubes. Vertical as well as horizontal tube-banks should be introduced into the bed and data on bubble behaviour, collected for these two tube-bank orientations, should be collated with existing heat transfer data for them.

Finally much emphasis has been placed here on the supposed effect of the gross circulation patterns in a gas fluidised bed (5), on the bubble rise velocity and size and frequency distributions. This influence has been inferred from discrepancies in the magnitude of rise velocities measured (± 20%) across the bed cross-sectional area but under identical operating conditions. Similar deductions have been made by earlier workers, both in fluidised beds (6) and in gas-liquid bubble columns (55). In the latter case, the existence of circulation patterns can also be verified visually; but in the case of three-dimensional fluidised beds only indirect evidence for this phenomenon has so far been available. It is clearly highly desirable to acquire independent evidence of the existence of such circulation patterns, which have not been observed

directly in the present work.

Possible techniques for demonstrating the existence of such circulation patterns are:

1. By observing lateral movement of rising bubbles caused by the horizontal component of such circulation patterns. This could be detected by the use of two probes (either compound probes of the types described here or single probes operating in 'C' mode or its equivalent) mounted fairly close together and in echelon. If the horizontal line formed by the two probes coincided with the direction of particle circulation then comparison of signals should reveal a strong correlation between the arrival of a bubble at the leading probe and a bubble encounter shortly afterwards of the trailing, and laterally displaced probe.

   If the two probes were not available, an alternative might be to mount the single probe just below the surface of the bed and to correlate the signals received from the probe with photographic records of the craters caused by bubble eruption at the bed surface. This technique would of course detect only circulation patterns just below the bed surface, but could be used to investigate the variation of the latter with bed depth. One fundamental problem with this technique is that circulation patterns only exist in freely bubbling beds at some considerable superficial velocity above the minimum fluidising velocity. It is thus difficult to ensure that the bubbles detected at different times are in fact identical.

2. Solid 'tracer' particles either of radioactive material or in the form of radio capsules, can be introduced in the bed and their paths traced using detectors or radio receivers outside the bed. This would in principle be a reliable method to employ, since it is independent of the bubbles in the bed; but practical difficulties in its application in a three-dimensional bed would be considerable.

APPENDIX A

If we take a bubble with a spherical indent of radius R and height 2 δ above the sphere base:

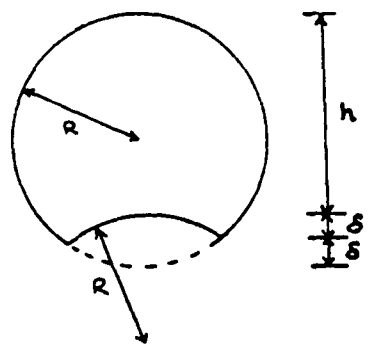

Volume of spherical cap of radius of curvature R and height δ.

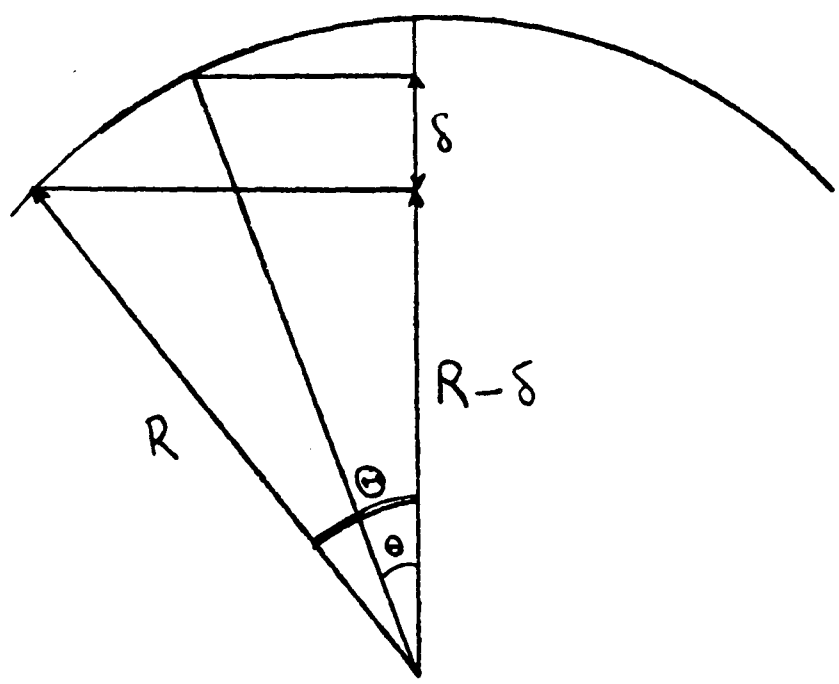

$$dv = -\int_{\theta=0}^{\theta} \pi R^2 \, \mathrm{Sin}^2\theta \; d\,(R \, \mathrm{Cos}\, \theta)$$

$$dv = -\pi \int_{\theta=0}^{\theta} R^3 \, (1 - \mathrm{Cos}^2\theta) \; d\,(\mathrm{Cos}\, \theta)$$

$$V = -\pi R^3 \left[\mathrm{Cos}\ \theta - 1 - \frac{\mathrm{Cos}^3\theta}{3} + \frac{1}{3} \right]$$

$$\text{Since} \quad \mathrm{Cos}\ \theta = \frac{R-\delta}{R} = 1 - \left(\frac{\delta}{R}\right)$$

$$V = -\pi R^3 \left[\frac{R-\delta}{R} - 1 - \frac{R^3 - 3R^2\delta + 3R\delta^2 - \delta^3}{3R^3} + \frac{1}{3} \right]$$

$$V = -\pi \left[-\delta^2 R + \frac{1}{3}\delta^3 \right]$$

$$V = \pi \delta^2 \left[R - \frac{\delta}{3} \right]$$

V_w is twice this or

$$V_w = 2\pi\delta^2 \left(R - \frac{\delta}{3}\right)$$

$$\text{so} \quad \frac{V_w}{V_s} = \frac{2\pi\delta^2 \left(R - \frac{\delta}{3}\right)}{\frac{4\pi}{3} R^3}$$

$$= \frac{3}{2} \left(\frac{\delta}{R}\right)^2 \left(1 - \frac{1}{3}\left(\frac{\delta}{R}\right)\right)$$

$$\text{therefore} \quad \frac{V_B}{V_S} = \frac{\frac{4\pi}{3} R^3 - 2\pi\delta^2 \left(R - \frac{\delta}{3}\right)}{\frac{4}{3}\pi R^3}$$

$$\text{so} \quad \frac{V_B}{V_S} = 1 - \frac{3}{2} \left(\frac{\delta}{R}\right)^2 \left(1 - \frac{1}{3}\left(\frac{\delta}{R}\right)\right)$$

APPENDIX B

Analysis of the Variance of the Data of Table 4.1

U cm/sec	Number of Observations	$S_{x_i x_i}$	$S_{x_i y_i}$	Residual Degrees of Freedom	Regression Sum of Squares
1.36	7	0.10412	0.07941	5	0.06056
1.87	11	0.27352	0.17547	9	0.11257
2.41	13	0.38233	0.25388	11	0.16858
		0.75997	0.50876	25	0.34171

Estimate of common $\beta = S_{x_i y_i} / S_{x_i x_i} = 0.66945$

Regression sum of squares for fitting common β is

$(\Sigma S_{x_i y_i})^2 \; / \; \Sigma S_{x_i x_i} = 0.34059$

Regression sum of squares for fitting separate β_i is

$\Sigma(S_{x_i y_i}{}^2 / S_{x_i x_i}) = 0.34171$

Change in sum of squares by fitting separate β_i is

$0.34171 - 0.34059 = 0.00112$

Residual m.s. when fitting separate β_i and α_i is

$\frac{1}{25} \Sigma$(residual sum of squares) $= \frac{0.07613}{25} = 0.003045$

F - statistic for parallelism $= \frac{0.22760}{2 \times 0.003045} = 0.184$

which, on (2.23) degrees of freedom, is not significant.

The regression lines are therefore parallel

Regression sum of squares for fitting common α and β is 0.11411.

Reduction in sum of squares from fitting common α and β is therefore

$0.34171 - 0.11411 = 0.22760$

F - statistic for identity $= \frac{0.22760}{2 \times 0.003045} = 18.69$

which, on (4,25) degrees of freedom, is significant at the 0.1% level. There is thus no evidence that the regression lines are identical.

APPENDIX C

Analysis of the Variance of the Data at Z = 70 cm above the Distributor Plate

U cm/sec	Number of Observations	$S_{x_i x_i}$	$S_{x_i y_i}$	D.F.	Reg. S.S.
1.36	13	0.38233	0.26984	11	0.19045
1.87	13	0.38233	0.25857	11	0.17487
2.41	12	0.32616	0.18350	10	0.10324
		1.09082	0.71191	32	0.46856

Estimate of common β is = 0.65264

Regression s.s. for fitting common β is = 0.46462

Regression s.s. for fitting separate β_i is = 0.46856

Extra s.s. from fitting common β = 0.00394

Residual m.s. when fitting separate β and α = 0.0296 / 32 = 0.000925

F statistic for parallelism is:

$$\frac{0.00394}{2 \times 0.000925} = 2.13 \text{ on } 2,32 \text{ degrees of freedom}$$

Not significant; there is no evidence that the regression lines are not parallel.

Identity Test:

Regression s.s. for fitting common α and β = 0.16458

Reduction in s.s. from fitting common α and β

= 0.46856 - 0.16458 = 0.30398

F statistic for identity $= \frac{0.30398/4}{0.000\,925}$

= 82.16 on 4 and 32 degrees of freedom.

Highly significant; i.e. there is evidence that the lines are not identical.

APPENDIX D

Analysis of the Variance of the Data of Table 4.2

Z (cm)	$S_{x_i x_i}$	$S_{x_i y_i}$	Residual Degrees of Freedom	Regression s.s.
20	0.13978	0.098386	6	0.06925
30	0.27352	0.204208	9	0.15246
40	0.27352	0.176845	9	0.11439
50	0.27352	0.233649	9	0.19959
70	0.38233	0.258569	11	0.17487
	1.34267	0.971657	44	0.71051

Parallelism:

Estimate of common slope assuming different intercepts

$= \beta = 0.72368.$

Regression sum of squares for fitting common β is = 0.703164.

Regression sum of squares for fitting separate β is = 0.71051

Extra sum of squares from fitting common slope = 0.00735.

Residual m.s. when fitting separate β_i and α_i = 0.07593 / 44

= 0.0017257

F statistic for parallelism $= \dfrac{0.00735}{4 \times 0.0017257} = 1.065$

on 4,44 degrees of freedom.

Not Significant; There is no evidence that the regression lines are not parallel.

Identity Test:

Regression s.s. with common slope and different intercepts

= 0.70316

Regression s.s. with common slope and intercept = 0.81665.

Extra s.s. due to fitting common intercept = 0.11349

F statistic for identity, (assuming parallelism)

$$F = \frac{0.11349}{4 \times 0.001726} = 16.438$$

Very highly significant; There is evidence that the regression lines are not identical.

APPENDIX E

Analysis of the Variance of the Data in Table 4.6

U(cm/sec)	$S_{x_i x_i}$	$S_{x_i y_i}$	Residual D.F.	No of Observations	Regression s.s.
1.87	0.10412	0.114842	5	7	0.126668
2.41	0.26401	0.207747	8	10	0.163474
3.01	0.38233	0.297372	11	13	0.231293
3.61	0.38233	0.350222	11	13	0.320810
	1.13279	0.970183	35	43	0.842245

Estimate of common slope $= \sum_1^4 S_{x_i y_i} / \sum_1^4 S_{x_i x_i}$

$= 0.856454$

Parallelism:

Regression s.s. for fitting common β is = 0.830918

Regression s.s. for fitting separate β_i is = 0.842245

Reduction in s.s. from fitting common β_i is

$= 0.842245 - 0.830918 = 0.011327$

Residual m.s. when fitting separate β_i and α_i

$$\sum_{i=1}^{4} \text{residual s.s.}/35 = \frac{0.05110}{35} = 0.00146$$

F statistic for parallelism is $= \frac{0.011327}{4 \times 0.00146} = 1.9395$

on 4,35 degrees of freedom.

Not significant at 1% level;

No evidence that the regression lines are not parallel.

Identity not Assuming Parallelism

Regression s.s. for fitting common α and β = 0.08761

Reduction in s.s. from fitting common α and β

$$= 0.842245 - 0.087610 = 0.754635$$

F statistic for identity $= \dfrac{0.754635 / 5}{0.001460} = 103.37$

on 5,35 degrees of freedom.

Very highly significant; There is evidence that the lines are not identical.

APPENDIX F

Analysis of the Variance of the Data of Table 4.7

Z(cm)	$S_{x_i x_i}$	$S_{x_i y_i}$	Residual D.F.	No of Observations	Regression s.s.
20	0.22472	0.220466	8	10	0.216293
30	0.27352	0.244751	9	11	0.219008
40	0.38233	0.336798	11	13	0.296688
50	0.51402	0.340507	12	14	0.225565
60	1.09812	0.822415	20	22	0.615931
70	0.72072	0.502075	16	18	0.349760
	3.21343	2.46701	76	88	1.92325

Parallelism:

Estimate of common slope $= \frac{2.46701}{3.21343} = 0.767719$

Regression s.s. for fitting common β is = 1.89397

Regression s.s. for fitting separate β_i is = 1.92325

Reduction in s.s. from fitting common β_i is

$$1.92325 - 1.89397 = 0.02928$$

Residual m.s. when fitting separate β_i and α_i

$$\sum_{1}^{6} \text{residual s.s.} / 76 = \frac{0.221610}{76} = 0.00291592$$

F statistic for parallelism is $= \dfrac{0.02928}{5 \times 0.0029159}$

F statistic = 2.0083 on 5,76 degrees of freedom.

Not significant at 1% level.

No evidence that the regression lines are not parallel.

Identity not Assuming Parallelism

Regression s.s. for fitting common α and β = 0.35352

Residual s.s. from fitting common α and β

$$= 1.92325 - 0.35352 = 1.56973$$

F statistic for identity $= \dfrac{1.56973}{7 \times 0.0029159} = 76.9$

Very highly significant; There is evidence that the lines are not identical.

NOMENCLATURE

a_o	Cross-sectional area of an orifice in a gas distributor.
A, A_T	Cross-sectional area of a fluidised bed.
A_o	"Catchment area" defined in equation (2.35).
b	Constant in equation (2.9).
C	Constant in equation (4.3).
C_D	Coefficient of discharge of orifice.
d_v	Diameter of sphere with a volume equal to the local average bubble volume, in equation (2.36).
d_o	Diameter of an orifice.
$\bar{d}_p$	Average diameter of particles.
d_p	Diameter of a particle.
d_b, D, D_b	Diameter of a bubble.
d_e, D_e	Diameter of sphere with the same volume as the bubble.
D_{bo}	Diameter of primary bubbles; Diameter of bubbles formed at the orifice (or diameter of bubbles formed at the distributor).
$\bar{D}_b$	Average bubble height at a given bed height.
D_{er}	Diameter of an eruption caused by a bubble when it breaks at the bed surface.
D_{bc}	Diameter of a combined bubble.
F	Bubble frequency.
f_b	Local number of bubbles striking the probe per unit time.
F_b	Number of bubbles passing a certain height in the bed.
F_t	Total bubble frequency (at nine points on the bed cross-section).

f_b'	Bubble frequency: average number of bubbles in a given volume.
F_{bo}	Frequency of bubble formation at a nozzle.
F_c	Coalescence frequency: the number of coalescences taking place in a certain bed volume at a given height.
F_c	Bubble frequency in C mode in equation (3.1).
g	Acceleration due to gravity.
G_B, G_b	Bubble flow rate.
G_f, G_b	Gas flow rate (and Gas flow rate through an orifice).
h	Height above distributor plate in equation (2.36).
h	Bubble nose-to-floor height.
h	Vertical distance between the noses of two bubbles.
h'	Vertical distance between the centres of two bubbles.
h_{cr}	Critical vertical distance behind a bubble beyond which the velocity of a following bubble is not affected.
h_s	Height of a spout or a jet.
H	Height of a fluidised bed.
H_{mf}	Bed height at minimum fluidisation.
j	Jitter time.
K	Constant in equation 4.1.
K_b	Dimensionless constant in the bubble rise velocity equation (2.4), and constant in equation (2.18).
K_d	Constant in equation (2.29).

l	Separation length between the leading and the coplanar probes.
L_b	Bubble vertical axis length in equation (2.27).
m	Wall correction factor in equation (2.9).
n	
n_o, N, N_2	Total number of orifices in a distributor plate.
N_1, n_w	Number of active orifices in a distributor plate, (at a given gas flow rate).
p, P_1, P_2	Constants in different equations.
r, r'	Radial distance.
r_b, R, R_b	Radius of a bubble.
r_w	Radius of the concave bubble base.
S	Distance in Figure (6.1).
t_c	Time taken by a pair of bubbles to coalesce.
T1, T2, T1', T'2	Time delays, in 'B' and 'C' modes.
t_d	Delay between operation of two neighbouring orifices.
t_o	Time for bubble to grow to diameter D_{bc} from a single orifice.
T_d	Time of detachment, equation (2.23).

U_a, U_A	Absolute bubble rise velocity.
U_b, U_B	Bubble rise velocity relative to the particulate phase.
U	Superficial gas velocity.
$U_{b\infty}$	Rise velocity of a bubble in an infinite medium.
U_{mf}	Minimum fluidising velocity.
U_M	Minimum gas velocity at which a distributor could function without any orifice becoming momentarily non-operative, (equation 2.36).
U_E	Emulsion phase velocity vector.
U_{bc}	Velocity of a combined bubble.
V_b, V_B	Volume of a bubble.
V_{bo}	Volume of a primary bubble.
V_S	Volume of a sphere with the same radius as a bubble in equation 4.6.
X, Y, Z	Distances along the X, Y and Z co-ordinates, See page 118.
Z	Vertical distance above the bubbling nozzle.

GREEK LETTERS

α and β	Coefficients in equation (4.2).
δ	Distance in Figure (4.12).
Δp	Pressure drop.
Δt	Time interval.
ε_B	Volume fraction of a section of a bed occupied by bubbles.
$\bar{\varepsilon}_B$	Average bubble voidage.
ε_D	Porosity of dense phase.
θ	Angle in equation (6.1) and Figure (6.1).
θ_w, θ_{w1}, θ_{w2}	Wake angles.
ρ_p	Density of particles.
ρ_g	Density of gas.
ν	Kinematic viscosity.
ϕ	Angle between two coalescing bubbles defined in equation (2.34).

REFERENCES

1. Allahwala, S A., PhD Thesis, Monash University, 1975.

2. Andeen, B R., Glicksman, L R and Bowman, R. "Fluidisation" - Proc. second Eng. Foundation Conference, 1978, Edited by Davidson, J F and Keairns, D L., Cambridge University Press.

3. Argyriou, D T., List. H L and Shinnar, R. A.I.Ch.E. Journal, 1971, 17, No 1, p.122.

4. Baum arten, P K and Pigford, R L., A.I.Ch.E. Journal, 1960. 6, p.115.

5. Burgess, J M., Ph.D. Thesis, Edinburgh University, 1974.

6. Burgess, J M and Calderbank, P H., Chem. Eng. Sci., 30, 1975.
   (a) Part I p.743
   (b) Part II p.1107
   (c) Part III p.1511

7. Botterill, J S M., George, J S and Besford, H. Chem. Eng. Prog. Symp. Ser., 1966, 62. No 62, p.7.

8. Catipovic, N M., Jovanovic, G N., Fitzgerald, T J and Levenspiel, O., "Fluidisation" - Edited by Grace, J R and Matsen, J M., 1980. p.225.

9. Chandran, R., PhD. Thesis, Lehigh University - 1980.

10. Chiba, T., Terashima, K, and Kobayashi, H. Chem. Eng. Sci., 1972, 27, p.965.

11. Chiba, T., Terashima, K and Kobayashi, H. Journal of Chem. Eng. Japan 1973. 6, No 1, p.79.

12. Clift, R and Grace, J R. Chem. Eng. Prog. Symp. Ser., 1970, 66, No. 105, p.14.

13. Clift, R and Grace J R., A.I.Ch.E. Journal, 1971, 17, No 1. p.252.

14. Clift, R and Grace J R., Chem. Eng. Prog. Symp. Ser. 1971, 67, No 116, p.23.

15. Clift, R and Grace J R., Trans. Instn. Chem. Engrs., 1972, 50, p.364.

16. Clift, R. and Grace, J R., Chem. Eng. Sci., 1972, 27. p.2309.

17. Cloete, F L D., Proc. of the Int. Symp. on Fluidisation, 1967, p.305. Netherlands University Press.

18. Collins, R., J. Fluid Mech., 1965, 22, p.763.

19. Collins, R., J. Fluid Mech., 1967, 28, p.97.

20. Darton, R C., Lanauze, R D., Davidson, J F and Harrison, D. Trans. Instn. Chem. Engrs. 1977, 55, p.274.

21. Davidson, J F. and Harrison, D., "Fluidised Particles" - 1963, Cambridge University Press.

22. Davidson, J F., Paul, R C., Smith, M J S., and Duxbury, H A., Trans. Instn. Chem. Engrs., 1959, 37, p.T323.

23. Davidson, J F and Schuler, B. O. G., Trans. Instn. Chem. Engrs., 1960, 38, p.335.

24. Davies, R M and Taylor, Sir Geoffrey, Proc. Roy. Soc. A., 200, p.375.

25. Donsi, G., Massimilla, L., Crescitelli, S and Volpicelli, G. Powder Techn. - 1972. 6, p.217.

26. Dumitrescu, D T., Z Angew, Math. Mech. - 1943, 23, p.139.

27. Fakhimi, S., PhD. Thesis, University of Cambridge - 1969.

28. Fakhimi, S and Harrison, D., Chemeca '70, p.29.

29. Farrokhalaee, T and Clift, R., "Fluidisation" - Edited by Grace, J R and Matsen, J M - 1980. p.135.

30. Freedman, W and Davidson, J F., Trans. Instn. Chem. Engrs. 1969. 47, p.T251.

31. Fryer, C., PhD., Thesis, Monash University, 1974.

32. Gabor, J D., Proc. of the Fifth Int. Symp. of Fluidisation - 1967, Netherlands University Press.

33. Geake, J E and Smalley, C., The Chem. Engr., - p.301, May 1975.

34. Geldart, D., Powder Techn., 1967/68. 1, p.355.

35. Geldart, D., Powder Techn., 1970/71. 4, p.41.

36. Geldart, D., Powder Techn. 1972, 6, p.201.

37. Geldart, D and Kelsey, J R., Inst. Chem. Eng. Symp. Ser., 1968, No 30, p.114.

38. Gelperin, N I., Einstein, V G., and Zaikovski, A V., Inzh. - Fiz. Zh., 1966. 10, p.799.

39. Glass, D H., PhD., Thesis., University of Cambridge, 1967.

40. Glass, D H., and Harrison, D., Chem. Eng. Sci. 1964. 19, p.1001.

41. Godard, K and Richardson, J F., Chem. Eng. Sci. - 1969. 24, p.663.

42. Godard, K and Richardson, J F., Can. Journal Chem. Eng. 1969. 47, p.350.

43. Grace, J R., Chem. Eng. Prog. Symp. Ser. - 1971. 67, No. 116, p.159.

44. Grace, J R and Clift, R., Chem. Eng. Sci. - 1974. 29, p.327.

45. Grace, J R., and Clift, R., Can. Journal Chem. Eng. 1974, 52, p.417.

46. Grace, J R., and Harrison, D., Tripartite Chem. Eng. Conference, Symp. on Fluidisation II, 1968, p.5.

47. Grace, J R., and Harrison, D., Instn. Chem. Engrs. Symp. Ser., No 30, - 1968, p.105.

48. Grace, J R., and Venta, J., Can. Journal Chem. Eng. 1973, 51, p.110.

49. Hamilton, C., Ph.D., Thesis, Monash University, 1970.

50. Harrison, D., A.I.Ch.E., - Instn. Chem. Eng. Symp. Ser., - 1965. 6, (6), p.16.

51. Harrison, D., and Grace, J R., Chapter 13, "Fluidisation", edited by Davidson, J F., and Harrison, D. - 1971.

52. Harrison, D and Leung, L S., Trans. Instn. Chem. Engrs. - 1961, 39, p.409.

53. Harrison, D and Leung, L S., Trans. Instn. Chem. Engrs. - 1962, 40, p.146.

54. Harrison, D and Leung, L S., Interaction between Fluids and Particles - (Instn. Chem. Engrs). 1962, p.127.

55. Hills, J H., Ph.D., Thesis, University of Cambridge, - 1971.

56. Hsiung, T.P. and Grace, J R., Proc. Second Eng. Foundation Conference, 1978, Edited by Davidson, J F., and Keairns, D L., Cambridge University Press.

57. Jin Yong, Yu, Z., Zhang, L., and Wang, Z. "Fluidisation", 1980, Edited by Grace, J R., and Matsen, J M. p.365.

58. Johnson, D S L., Ph.D., Thesis, University of Edinburgh - 1969.

59. Kobayashi, H., Arai, F., and Chiba, T., Kagaku Kogaku (Abridged Edition), 1966, 4, No. 1, p.147.

60. Kramers, H., Chem. Eng. Sci., 1951, 1, p.35.

61. Kunii, D., and Levenspiel, O., "Fluidisation Engineering" - 1969, Wiley.

62. Leung, L S., Powder Techn. 1972, 6, p.189.

63. Leva, M and Wen, C Y., Chapter 14, "Fluidisation", Edited by Davidson, J F., and Harrison D., 1971.

64. Lin, S P., A.I.Ch.E., Journal, 1970, 16, No 1, p.130.

65. Lochiel, A C., Ph.D., Thesis, University of Edinburgh - 1963.

66. Lockett, M J., Davidson, J F and Harrison, D.,
Chem. Eng. Sci. - 1967, 22, p.1059.

67. Masson, H and Jottrand, R., Proc. Second Eng. Foundation
Conference, 1978. Edited by Davidson, J F and Keairns, D L.,
p.1.

68. McGrath, L and Streatfield, H D., Trans. Instn. Chem. Engrs.
- 1971, 49, p.70.

69. Matheson, G L., Herbert, W A and Holt, P H.,
Ind. Eng. Chem., 1949, 41, p.1099.

70. Matsen, J M., A.I.Ch.E. Symp. Ser. - 1973,
69, No 128, p.30.

71. Mendelson, H D., A.I.Ch.E. Journal, 1967, 13, p.250.

72. Morgan, C., Ph.D. Thesis, Cambridge University - 1967.

73. Miwa, K., Mori, S., Kato, T., and Muchi, I.,
Int. Chem. Eng. - 1972. 12, No 1, p.187.

74. Mori, S., and Wen, C Y.,
A.I.Ch.E. Journal, 1975, 21, No 1, p.109.

75. Newby, R A., and Keairns, D L.,
Proc. Second Eng. Foundation Conference, 1978,
Edited by Davidson, J F and Keairns, D L., p.320.

76. Nicklin, D J., Chem. Eng. Sci. - 1962. 17, p.693.

77. Orcutt, J C., and Carpenter, B H.,
Chem. Eng. Sci. - 1971, 26, p.1049.

78. Orcutt, J C., Davidson, J F., and Pigford, R L.,
Chem. Eng. Prog. Symp. Ser. - 1962, 58, No 38, p.1.

79. Park, W H., Kang, W K., Capes, C E., and Osberg, G L.,
Chem. Eng. Sci., 1969, 24, p.851.

80. Park, W H., Lee, N G., and Capes, C E.,
Chem. Eng. Sci. - 1974, 29, p.339.

81. Pereira, J A F R., Ph.D., Thesis, University of Edinburgh - 1977.

82. Pereira, J A F R., and Calderbank, P H., IV Annual Research Meeting, Instn, Chem.Engrs., Swansea, April 1977.

83. Potter, O E., Chapter 7, "Fluidisation", Edited by Davidson, J F., and Harrison, D.

84. Pyle, D L., and Harrison, D., Chem. Eng. Sci. 1967, 22, p.1199.

85. Rajinder, K., and Rao, K., Chem. Techn., 1967, 19, No 12, p.733.

86. Richardson, J F., Khan, A R., and Shakiri, K J., Proc. Second Eng. Foundation Conference, 1978. Edited by Davidson J F., and Keairns, D L., p.351.

87. Rietema, K., and Ottengraf, S P P., Paper presented to Northwestern Branch, Instn, Chem. Engrs. 1969.

88. Rigby, G R., Van Blockland, G P., Park, W H., and Capes, C E., Chem. Eng. Sci. 1970, 25, p.1729.

89. Rippin, D W T., "Fluidised Particles", 1963 by Davidson, J F., and Harrison, D., p.24.

90. Rooney, N., Ph.D. Thesis, Cambridge University, 1975.

91. Rowe, P N., Chem. Eng. Prog. Symp. Ser., 1962. 58, No 38, p.42.

92. Rowe, P N., Chapter 4 in "Fluidisation", Edited by Davidson, J F., and Harrison, D., - 1971.

93. Rowe, P N., and Everett, D J., Trans. Instn. Chem. Engrs. 50, 1972.

(a) Part I p.42

(b) Part II p.49

(c) Part III p.55.

94. Rowe, P N., and Matsuno, R., Chem. Eng. Scie. 1971, 26, p.923.

95. Rowe, P N., and Partridge, B A., Interaction between Fluids and Particles - 1962, Instn. Chem. Engrs., p.135.

96. Rowe, P N., and Partridge, B A., Chem. Eng. Sci. 1964, 19, p.81.

97. Rowe, P N., and Partridge, B A., Trans. Instn. Chem. Engrs., 1965, 43, p.T157.

98. Rowe, P N., Partridge, B A., Cheyney, A G., Henwood, G A., and Lyall, E., Trans. Instn. Chem. Engrs., 1965, 43, p.T271.

99. Rowe, P N., Partridge, B A., and Lyall, E., Chem. Eng. Sci, 1964, 19, p.973.

100. Rowe, P N., and Widmer, A T., Chem. Eng. Sci. 1973, 28, p.980.

101. Singh, B., Ph.D. Thesis., Monash University, 1970.

102. Singh, B., Fryer, C., and Potter, O E., Powder Techn. 1972, 6, p.239.

103. Skinner, D G., "The Fluidised Combustion of Coal", 1971, Mills and Boon Ltd.

104. Staub, F W., and Canada, G S., Proc. Second Eng. Foundation Conference, 1978, Edited by Davidson J F., and Keairns, D L., p.339.

105. Toei, R., and Matsuno, R., Proc. Fifth Int. Symp. on Fluidisation - 1967, p.271. Netherlands University Press.

106. Toei, R., Matsuno, R., Kojima, H., Nagai, Y., Nakagawa, K., and Yu, S., Kagaku Kōgaku, (Abridged Edition), 4, No 1, p.142.

107. Tomita, M., and Adachi, T., Journal Chem. Eng. Japan, 1973, 6, No 2, p.196.

108. Toomey, R D., and Johnstone, H F., Chem. Eng. Progr. 1952, 48, p.220.

109. Uno, S., and Kintner, R C., A.I.Ch.E. Journal, 1956, 2, p.420.

110. Vakhrushev, I A., and Basov, V A., Int. Chem. Eng. 1973, 12, No 2, p.319.

111. Wace, P F., and Burnett, S J., Trans. Instn. Chem. Engrs. 1961, 39, p.168.

112. Watson, P R., and Harrison, D., Proc. Symp. 38, Instn. Chem. Engrs. - 1974.

113. Wen, C Y., Krishnan, R., Khosravi, R., and Dutta, S., Proc. Second Eng. Foundation Conference, 1978, Edited by Davidson, J F., and Keairns, D L., p.32.

114. Werther, J., Proc. Second Eng. Foundation Conference, 1978, Edited by Davidson, J F., and Keairns, D L., p.7.

115. Werther, J., Trans. Instn. Chem. Engrs., 1974, 52.

(a) Part I p.149.

(b) Part II p.160.

116. Werther, J., and Molerus, O., Int. Journal Multiphase Flow, 1973.

(a) Part I p.103.

(b) Part II p.123.

117. Werther, J., and Molerus, O., Paper presented at Chisa Conference, 1972, Prague.

118. Whitehead, A B., and Dent, D C., Proc. Fifth Int. Symp. on Fluidisation, 1967, Netherlands University Press, p.802.

119. Whitehead, A B., Nguyen, H V., and Potter, O E.,
Chem. Eng. Sci. 1979, 34, p.1164.

120. Whitehead, A B., and Young, A D.,
Proc. Fifth Int. Symp. on Fluidisation, 1967.

(a) Part I p.284.

(b) Part II p.294.

121. Wood, R T., Kuwata, M., and Staub, F W.,
Fluidisation, 1980, Edited by Grace, J R., and Matsen, J M.,
p.235.

122. Woollard, I N M., and Potter, O E., A.I.Ch.E. Journal,
1968, 14, p.388.

123. Xavier, A M., and Davidson, J F.,
Proc. Second Eng. Foundation Conference, 1978,
Edited by Davidson, J F., and Keairns, D L., p.333.

124. Yacono, C., and Angelino, H., Proc. Second Eng.
Foundation Conference, 1978.
Edited by Davidson, J F., and Keairns, D L., p.25.

125. Yasui, G., and Johanson, L N., A.I.Ch.E. Journal, 1958,
4, p.445.

126. Yoshida, K., Nakajima, K., Hamatani, N., and Shimizu, F.,
Proc. Second Eng. Foundation Conference, 1978,
Edited by Davidson, J F., and Keairns, D L., p.13.

127. Yue, P L., and Kolaczkowski, J A.,
Trans. Instn. Chem. Engrs., 1982, 60, p.164.

128. Zabrodsky, S S., Tamarin, A I., Dolidovich, A F.,
Palchonok, G I., and Epanov, Yu, G.,
"Fluidisation", Edited by Grace, J R., and Matsen, J M.,
1980, p.195.

129. Levy, Y. and Lockwood, F.C.
A.I.Ch.E. Journal 29, No.6, 1983.